" STEADY - STATE AND TRANSIENT PHENOMENA IN PARAMETRIC SUBHARMONIC OSCILLATORS "

by

Robert Giles Harrison, M.A.(Cantab),

a Thesis submitted for the Degree of

DOCTOR OF PHILOSOPHY

of the

UNIVERSITY OF LONDON.

Department of Electrical Engineering,

Imperial College of Science and Technology,

July, 1964.

ABSTRACT

In this thesis the basic mechanisms underlying the behaviour of parametric subharmonic oscillators are examined in four different ways. The two most successful of these approaches are extended to predict, in detail, the steady-state and transient characteristics of certain types of practical subharmonic oscillators which are suitable for use as fast phase-switching logical elements in digital computers. Particular attention is paid to the strong influence of the more significant parasitic elements upon the performance of these devices. For what is believed to be the first time, analytical techniques have been used to obtain theoretical results which agree quantitatively, rather than merely qualitatively, with reality.

ACKNOWLEDGEMENTS

The author wishes to express his deep gratitude to his supervisor, Dr. A.R.Boothroyd, for his guidance, encouragement and advice throughout the course of the research work described in this thesis. He is indebted to Dr. R.Spence of Imperial College for his valuable criticisms and continued interest in this work.

Thanks are also extended to Drs. D.F.Page, D.M.Caughey and A.Singh-akowinta and to P.Apaydin and J.V.Hanson, all formerly of Imperial College, for many stimulating discussions and criticisms.

The financial support of Associated Electrical Industries, (Manchester) Ltd. and the Ministry of Aviation (U.K.) is gratefully acknowledged.

Table of Contents

	Page
Title	1
Abstract	2
Acknowledgements	3
Table of Contents	4
Location of Figures	11
Location of Tables	11
Symbols	12
List of Appendices	9
CHAPTER ONE	20
1. Introduction	20
1.1 Definition of area of research	20
1.2 Survey of previous work on subharmonic oscillators	21
1.3 Aim of thesis and formulation of problem	26
1.4 Statement of original work	28
CHAPTER TWO	29
2. The Mathematical and Physical Environment of Subharmonic Oscillators	29
2.1 Linear resonators and oscillators	29
2.1.1 Negative damping	31
2.2 Linear systems with periodically time-varying parameters	31
2.3 Nonlinear systems	35

CHAPTER THREE 40

3. Nonlinear Reactive Elements 40

3.1 Physical nonlinear reactive elements. 40

3.1.1 Nonlinear inductive elements. 41

3.1.2 Nonlinear capacitive elements 42

3.2 Characterisation of varactors 44

3.2.1 Nonlinear capacitance 44

3.2.2 Experimental verification of the validity of the assumed capacitance law 47

3.2.3 The representation of the nonlinear capacitance on the basis of its charge-voltage relationship. 49

3.2.4 Note on the mathematical model for the charge-voltage characteristic when $n = \frac{1}{2}$ . . . 53

3.2.5 Nonlinear conductance 53

CHAPTER FOUR 55

4. Preliminary Investigation of Parametric Subharmonic Oscillators 55

4.1 'Evolution' of parametron circuits 55

4.1.1 Introduction. 55

4.1.2 Parametron circuits 56

4.2 First-order quasi-static theory 64

4.3 Piecewise-linear theory 71

4.3.1 The case of zero damping. 74

4.3.1.1 The $Z_1 Z_2$ - mode 75

4.3.1.2 The $Z_1 I_2$ - mode. 75

4.3.1.3 The $I_1 Z_2$ - mode 77

4.3.1.4 The $I_1 I_2$ - mode 77

4.3.1.5 Mode-sequences 78

4.3.1.6 Transient response in the case of zero damping 85

4.3.2 The case of finite damping 85

4.3.2.1 Mode-sequences in the case of finite damping 88

4.3.3 Criticism of the piecewise-linear approach . 93

4.4 Possible ways in which the differential equations of varactor parametrons may be formulated 93

CHAPTER FIVE 100

5. Differential Equations of Balanced Varactor Parametrons . 100

5.1 Introduction. 100

5.2 The derivation of the differential equation of the balanced series parametron (BSP) using the "voltage" representation of the capacitive nonlinearity . . 101

5.3 The derivation of the differential equation of the balanced parallel parametron (BPP) using the "voltage" representation of the capacitive nonlinearity . . 105

5.4 Generalisation of the differential equations. . . 108

5.5 The derivation of the differential equation of the balanced parallel parametron (BPP) using the "charge" representation of the reactive nonlinearity . . . 108

5.5.1 The case n = $\frac{1}{2}$ 110

5.5.2 The case n = 1.0. 113

5.5.3 Comparison of the simplified "charge" equations for n = $\frac{1}{2}$ and n = 1 115

5.6 Discussion of method of solving the differential equations 116

CHAPTER SIX 119

6. Steady-State Phenomena 119

6.1 Introduction 119

6.2 Approximation of the generalised "voltage" differential equation for solution 119

6.2.1 Discussion of the validity of the approximate differential equation 122

6.3 Steady-state solution of the generalised "voltage" equation. 123

6.4 Comparison of the solution of the generalised "voltage" differential equation with experiment 128

6.4.1 Summary and conclusions 138

6.5 Steady-state solution of the differential equations of the large-signal "charge" model 139

6.5.1 Special case 1 144

6.5.2 Special case 2 149

6.5.3 Special case 3 152

6.6 Comparison of the large-signal "charge" theory with experiment 153

6.7 Comments on the steady-state phenomena 158

CHAPTER SEVEN 160

7. Transient Phenomena 160

7.1 Historical background 160

7.2 Introduction. 161

7.3 Transient analysis of generalised voltage model . . 163

7.3.1 Simplification of the generalised "voltage" model for transient solution. 163

7.3.2 Transient solutions for the generalised voltage model 165

7.4 Transient analysis of "charge" model. 177

7.4.1 Intermediate harmonic-balance solution for the case in which R_p dominates the device behaviour 179

7.4.2 Intermediate harmonic-balance solution for the case in which R_L dominates the device behaviour 187

7.4.3 Remarks on the phase-angles of the oscillatory charge and voltage along the nose-locus . . 190

7.4.4 Assessment of the relative merits of the two intermediate solutions 191

7.4.5 Exact transient solutions under conditions of zero damping. 192

7.4.6 Small-signal transient theory in the presence of damping: trajectories and stability. . . 199

7.4.6.1 Explanation of certain anomalous theoretical results 207

7.4.6.2 Typical small-signal (Z,ψ)-trajectories 208

7.4.7 Large-signal trajectories in the presence of damping 214

7.4.7.1 Summary 222

7.4.8 Approximate treatment of real-time transient behaviour 224

7.4.8.1 The approximate transient phase solution in the presence of damping 226

7.4.8.2 The approximate transient amplitude solution in the presence of damping 231

7.4.8.3 Transient amplitude solutions for initiation at critical phase-angles 231

7.4.8.4 Transient amplitude solutions for initiation at arbitrary phase-angles 240

7.5 Experimental investigation of transient phenomena . 248

7.5.1 Introduction 248

7.5.2 Experimental arrangements for measurements on phase-initiated transients 249

7.5.3 Method of measuring instantaneous amplitude and phase 258

7.5.4 Transient measurements 261

CONCLUSIONS 277

APPENDICES 280

A4.1 Piecewise-linear mode-equations for the BSP: the case of finite damping 280

A5.1 Derivation of the differential equation of the BSP using the $C=\mathcal{J}(v)$ representation of the capacitive nonlinearity 283

A5.2 Derivation of the differential equation of the BPP using the $C=\mathcal{J}(v)$ representation of the capacitive nonlinearity 286

A5.3 Derivation of the differential equations of the BPP using the $v=\mathcal{J}(q)$ representation of the capacitive nonlinearity: the case $n = \frac{1}{2}$ 289

A6.1 Approximate solution of the generalised "voltage" differential equation 292

A7.1 Expression of $\tilde{y}(\tau)$ in terms of charge coordinates for the case in which R_p dominates the device behaviour . 294

A7.2 Derivation of the intermediate differential equations for the case in which R_p dominates the device behaviour 295

A7.3 Derivation of approximate expression for $\tilde{y}(\tau)$ in charge coordinates for the case in which R_L dominates . . 297

A7.4 Calculation of expression for curves of constant dimensionless rise- and fall-time 299

A7.5 Transient amplitude solution in detuned case . . . 300

A7.6 Transient amplitude solution in resonant case. . . 303

LIST OF REFERENCES 304

Location of Figures

Figure	Page
2.1	34
2.2	34
3.1	43
3.2	45
3.3	48
3.4	52
4.1	61
4.2	63
4.3	65
4.4	66
4.5	66
4.6	73
4.7	79
4.8	82
4.9	83
4.10	84
4.11	90
4.12	91
4.13	95
5.1	102
5.2	106
5.3	111
6.1	129
6.2	132
6.3	133
6.4	136
6.5	137
6.6	146
6.7	146
6.8	147
6.9	148
6.10	154
6.11	156
6.12	157
7.1	166
7.2	170
7.3	171
7.4	173
7.5	174
7.6	176
7.7	181
7.8	194
7.9	195
7.10	198
7.11	200
7.12	202
7.13	205
7.14	210
7.15	212
7.16	213
7.17	215
7.18	217
7.19	219
7.20	221
7.21	223
7.22	227
7.23	230
7.24	234
7.25	238
7.26	239
7.27	244
7.28	246
7.29	247
7.30	250
7.31	253
7.32	255
7.33	257
7.34	259
7.35	262
7.36	264
7.37	265
7.38	266
7.39	268
7.40	269
7.41	270
7.42	271
7.43	272
7.44	273
7.45	274
7.46	276

Location of Tables

Table	Page
3.1	50
3.2	51
4.1	57
4.2	98

SYMBOLS

Most of the commonly-used symbols have their conventional significance. For example, the upper-case symbols V and I represent the steady (d.c.) values or amplitudes of alternating (a.c.) voltages and currents respectively. The lower-case symbols v and i represent the corresponding instantaneously-varying quantities.

The amplitudes of normalised quantities are usually represented by upper-case Roman letters, their instantaneous values by the corresponding lower-case letters.

With certain exceptions, curly Italic capitals signify nonlinear operators, equations, functions or parameters.

Apart from established usages, such as θ and ψ for angles, τ for normalised time and ν for normalised frequency, the Greek symbols are assigned arbitrarily.

Several symbols have more than one meaning. In those parts of the text where confusion might otherwise arise, the less usual meanings are identified by primes. Primes are never used to indicate differentiation.

Subscripts identify a particular meaning of a more generally-defined parameter, thus:

k = damping parameter; k_L = load damping parameter,

ψ = phase-angle of charge; ψ_c = critical value of ψ.

Notations peculiar to this thesis are:

(1) $\overset{\circ}{y} = \frac{dy}{d\tau}$, the derivative of y with respect to normalised time,

(2) $\tilde{y}$ = the approximate value of y,

(3) $Y(\tau)$ = the value of Y at time τ,

(4) $Y(\infty)$ = the steady-state value of Y at $\tau = \infty$, used only in the chapter on transient phenomena.

LIST OF PRINCIPAL SYMBOLS

Lower-Case Roman Symbols — First used on page

a = (i) { 2 for the Balanced Series Parametron ; 1 for the Balanced Parallel Parametron } . . . 108

(ii) a constant

b = a constant

c = (i) ΔV_o 104

(ii) a constant

d = (i) differential operator

(ii) a constant

e = 2.7182818....., base of Naperian logarithms

f = (i) periodic function of time (f_1, f_2, ...) . . . 32

(ii) frequency

f_o = resonant frequency 65

f_p = pump frequency 56

f_s = subharmonic frequency 56

i = instantaneous current (i_1, i_2, ...) 54

i_p = instantaneous pump current

i_s = instantaneous subharmonic current 75

j = $\sqrt{-1}$

k = damping parameter 21

k_L = $\omega_o L G_L$, damping parameter due to load conductance G_L . . 104

k_p = $\omega_o C_o R_p$, damping parameter due to pump-circuit resistance R_p . 112

k_v = $\omega_o L G_v$, damping parameter due to varactor conductance G_v . 104

ℓ = $\frac{32\, k_p \Gamma^3}{B^2 \nu^4}$, frequency-dependent damping parameter used in 'accurate' transient theory 185

First used on page

m = $\frac{1}{2}\delta Z^2 = \frac{1}{8}k_p(\frac{1}{B} - 1)Z^2$, amplitude-dependent damping parameter used in 'accurate' transient theory . . . 185

n = (i) nonlinear capacitance law exponent 44

(ii) $\frac{4\Gamma^3}{B\nu^3}$, detuning parameter used in 'accurate' transient theory 182

q = instantaneous charge (q_1, q_2, ...) 49

q_e = charge of an electron 54

q_p = charge varying at pump frequency

q_s = charge varying at subharmonic frequency

r = $3(\Gamma^2 - 1) + \frac{5}{32}Z^2$, amplitude-dependent detuning parameter used in 'accurate' transient theory 185

r_o = $3(\Gamma^2 - 1)$, small-signal part of r 203

t = time 21

u = sum of normalised varactor charges 110

v = instantaneous voltage (v_1, v_2, ...) 46

v_p = instantaneous pump voltage 67

v_s = instantaneous subharmonic voltage 67

x = (i) arbitrary forcing function 36

(ii) independent variable

(iii) $\frac{v_p}{V_o}$, normalised instantaneous pump voltage . . . 68

y = (i) arbitrary dependent variable 23

(ii) $\frac{v_s}{V_o}$, normalised instantaneous subharmonic voltage . 68

z = (i) $\frac{q}{C_o V_o}$, normalised charge (z_1, z_2, ...) 50

(ii) difference between normalised varactor charges . . 110

Upper-Case Roman Symbols

		First used on page
A =	a constant (A_1, A_2, ...)	
B =	(i) $\frac{2C_o}{2C_o + C_s}$, stray-capacitance parameter.	104
	(ii) a constant (B_1, B_2, ...)	
C =	(i) capacitance	33
	(ii) a constant . .	
C_o =	$\left(\frac{dq}{dv}\right)_{V_o}$, small-signal varactor capacitance at the bias-point V_o	46
C_s =	total lumped stray capacitance	103
D =	a constant	
E =	a constant	
F =	a constant	
G =	conductance (G_1, G_2, ...)	70
G_L =	load conductance	101
G_v =	linear part of varactor conductance	104
H =	$\frac{2(n\zeta - m)}{(5m + \ell)\zeta + 3n}$, parameter used in construction of Isotan curves.	216
I =	d.c. current	54
I_s =	diode saturation current	54
K =	(i) Boltzmann's constant: 1.38044×10^{-16} erg degree^{-1} .	54
	(ii) constant depending on diode geometry.	44
L =	(i) inductance	44
	(ii) $\Gamma^{-1} = \frac{1 - \nu^2(1 - B)}{B\nu^2}$, detuning parameter . . .	142
M =	(i) mutual inductance.	107
	(ii) $\frac{k_L}{B\nu}$, load damping parameter	142

		First used on page
N =	positive integer	50
O =	zero	
P =	power	69
Q =	'goodness' factor	40
R =	resistance	
R_p =	pump-circuit resistance	74
R_s =	varactor series loss resistance	
R_L =	load resistance	74
S =	parameter used in approximate transient theory	167
S_ρ =	$\frac{2X}{n}\sqrt{1-\rho^2}$	197
S_σ =	$\frac{2X}{3n}\sqrt{1+\sigma^2}$	228
T =	(i) Absolute temperature	54
	(ii) period of oscillation	36
V =	(i) d.c. voltage	42
	(ii) peak amplitude of alternating voltage	
V_B =	d.c. bias voltage	44
V_o =	$V_B + \phi$, total varactor junction voltage	46
V_p =	amplitude of pump voltage	69
V_q =	amplitude of quench pulse	259
V_s =	amplitude of subharmonic voltage	69
X =	$\frac{V_p}{V_o}$, normalised amplitude of pump voltage	23
X_o =	$\frac{V_B}{V_o}$, normalised bias voltage	23
Y =	$\frac{V_s}{V_o}$, normalised amplitude of subharmonic voltage	68
Y_c =	$Y.\cos\theta$, cosine component of Y	117

First used on page

Y_s = $Y.\sin\theta$, sine component of Y 117

Z = normalised amplitude of difference between varactor charges 141

Z_c = $Z.\cos\psi$, cosine component of Z 182

Z_s = $Z.\sin\psi$, sine component of Z 182

Upper-Case Italic Symbols

$\mathcal{A}$ = a constant 241

$\mathcal{C}$ = nonlinear capacitance coefficient 58

$\mathcal{E}[\ ]$ denotes a nonlinear differential equation 112

$\mathcal{F}$ = nonlinear function $(\mathcal{F}_1, \mathcal{F}_2, \ldots\ldots)$ 30

$\mathcal{L}$ = nonlinear inductance coefficient 58

$\mathcal{Y}$ = admittance 68

Lower-Case Greek Symbols

α = (i) $\frac{1}{2}Bn$, first nonlinear capacitance coefficient . . . 121

(ii) $\frac{1}{2}\ c^{j(\nu\tau+\theta)}$ . . . . . .

(iii) a constant 33

β = (i) $\frac{1}{4}Bn(n+1)$, second nonlinear capacitance coefficient . 121

(ii) $M + jL$ 142

(iii) a constant 33

γ = (i) $\frac{1}{4}c^2a^2k_v$, first nonlinear conductance coefficient . . 121

First used on page

γ = (ii) $\frac{1}{2}e^{j(\nu\tau+\psi)}$ 184

δ = (i) $\frac{1}{8}c^3a^2k_v$, second nonlinear capacitance coefficient. . 121

(ii) $\frac{1}{4}k_p(\frac{1}{B}-1)$, a damping parameter 143

ζ = a constant value of $\frac{1}{Z}\cdot\frac{d\psi}{dZ}$ defining an Isotan curve . . 214

θ = phase-angle of subharmonic voltage with respect to pump voltage 68

μ = (i) 'dimensionless rise-time', the number of cycles of subharmonic oscillation for the amplitude to change by a factor 'e' 175

(ii) 'small' parameter 38

ν = $\frac{\omega}{\omega_o}$, frequency normalised to resonant frequency . . . 29

ν' = $\frac{\omega L}{R_p}$, frequency normalised to time-constant 86

ξ = (i) $\frac{2\omega L\, i_s}{V_o}$, a dimensionless current 77

(ii) arc tan $\frac{1}{\sigma}$ 206

ξ' = $\frac{R_p q}{V_o}$, a dimensionless current. 86

π = 3.1415926536.....

ρ = $\frac{r_o}{2X} = \frac{3}{2X}(\Gamma^2 - 1)$ 203

σ = $\frac{l}{2n} = \frac{4k_p}{B\nu}$. 203

τ = $\omega_o t$, time normalised to resonant frequency 23

τ' = $\frac{R_p t}{L}$, time normalised to time-constant. 86

ϕ = junction contact potential 44

ψ = phase-angle of subharmonic charge with respect to pump voltage 141

		First used on page
ψ_c =	critical value of ψ (time-invariant)	209
ω =	angular frequency	68
ω_o =	resonant angular frequency	86

Upper-Case Greek Symbols

Γ =	$L^{-1} = \frac{B\nu^2}{1 - \nu^2(1-B)}$, reciprocal of detuning parameter .	150
Δ =	$3n^2 + m(5m + \ell)$	186
Λ =	$\frac{q_e}{KT} = 38.8$ volts^{-1} at 25°C	54
$\prod$ =	continued product	120
$\sum$ =	summation	117
Φ =	magnetic flux	58
Ω =	(i) arc tg ζ	214
	(ii) ohms	83

CHAPTER ONE

1. Introduction

1.1 Definition of area of research

This thesis is concerned with the behaviour of certain resonant systems governed by nonlinear non-autonomous differential equations. In these systems sustained fundamental, harmonic or subharmonic oscillations can occur only in the presence of a pumping signal. We are primarily interested in the case of subharmonic oscillations of order one-half, (i.e. those taking place at half the pump frequency), although lower orders of oscillation are possible.

Such systems, usually referred to as subharmonic oscillators, but properly subharmonic resonators, are of importance because their steady-state oscillation can have either of two equi-probable phases differing by π radians. If a pumping signal is applied to such a device, then under suitable conditions the oscillation will build up towards a steady state which has one or other of the two possible phases. Phase selection will depend on the phase and amplitude of any residual oscillation existing at the instant of turn-on. In the absence of residual oscillation the phase selection will be governed by noise. It is therefore possible to control the final binary phase-state of the device by means of a very small-amplitude determining signal. This phase-locking signal may be applied shortly before the instant of turn-on, and can be removed soon after the build-up commences.

Devices having the controllable bistable phase property described above have been used as storage elements and majority-logic switching circuits in

digital computers. The detailed theoretical and experimental investigation of subharmonic oscillators suitable for such applications constitutes the chosen area of research.

1.2 Survey of previous work on subharmonic oscillators

The existence of the phenomenon of subharmonic oscillation, or resonance, was recognised as long ago as 1859 when Melde[1] described his now famous experiment on the maintenance of transverse vibrations in a string longitudinally excited by means of a tuning fork. In 1883 Lord Rayleigh[2] explained Melde's results by means of the equation

$$\ddot{\theta} + k\dot{\theta} + \theta(n^2 - 2\alpha \sin 2pt) = 0 \qquad (1.1)$$

in which k and α were assumed to be small. This is a Mathieu equation extended to include the influence of damping. He obtained a solution of the form

$$\theta = A_1 \sin pt + B_1 \cos pt + A_3 \sin 3pt + B_3 \cos 3pt + \ldots, \qquad (1.2)$$

in which the first two terms represent an oscillation at a frequency equal to one-half of the driving frequency 2p. The other terms represent odd harmonics of the subharmonic frequency p. Linear differential equations of this type have formed the basis of much of the subsequent theoretical work.

In 1926 Fallou[3] described a static frequency divider consisting of a series resonant circuit containing a nonlinear iron-cored inductor, and in 1929 and 1936 Rouelle[4,5] published some experimental data on subharmonics in similar ferroresonant circuits. The occurrence of subharmonic oscillations in loudspeakers was discussed by Pederson[6] in 1935, and in 1941 McCrumm[7]

experimentally determined the starting conditions and ranges of voltage and current for which the oscillations can occur. Steady subharmonic oscillations of orders down to the one-seventh in a series circuit were reported by Spitzer[8] in 1945.

Since Rayleigh's time it has been customary to approach the theoretical explanation of subharmonic oscillations by way of one of the classical differential equations known to have subharmonic solutions. These include the Mathieu and Duffing equations. An attempt is usually made to adapt the chosen equation to fit the behaviour of a physical system. This method of attack has probably been used because these differential equations have an extensive mathematical literature[9,10,11,12] which, however, becomes relatively useless when the equations are modified by additional terms in order to account for particular physical phenomena. The differential equation approach has been virtually mandatory because of the close interrelation between the influences of the significant parameters in subharmonic oscillators. A "commonsense" theoretical approach, of a kind which might succeed in the investigation of linear time-invariant systems, would almost inevitably lead to misconceptions and incorrect conclusions. Among the more serious pitfalls is the danger of inadvertantly using the principle of superposition in the analysis of nonlinear systems. In recent years some success has been had with non-differential equation methods, particularly the method of piecewise-linearisation as exemplified by the work of Lavi and Finzi[13], but these have certain limitations which will be discussed in Chapter 4.

In 1949 an approximate subharmonic solution of the forced Duffing equation was obtained by Levenson[14] who used a perturbation method. Ludeke[15] and Hayashi[16], in 1951 and 1953 respectively, both attacked it by means of

the method of harmonic balance. These authors did not compare their results with any experimental data.

Up to this time the subharmonic oscillator had been regarded either as a passive frequency-divider of no more than academic interest, or as an explanation of certain anomalous effects which had been observed in power transmission systems. In 1954, however, von Neumann[17] and Goto[18,19] simultaneously and independently realised that the device could be used for the storage of binary phase-coded information. It was then that Goto coined the term "parametron" to designate subharmonic oscillators intended specifically for use as logical circuit storage elements.

In 1955 Goto[20] discussed the practical application of magnetic parametrons in digital computers. He also treated phase-initiation switching in terms of a Mathieu equation empirically modified by the addition of damping and nonlinear detuning terms.

One-half, one-third and one-fifth-order subharmonic oscillatory solutions of certain variants of the forced Duffing equation were obtained by Hayashi[21] in 1956. The specific equation he investigated for $\frac{1}{2}$th-order subharmonics was

$$\ddot{y} + k\dot{y} + y^3 = X \cos 2\tau + X_o , \qquad (1.3)$$

in which the forcing function contains both steady and oscillatory terms. The initial conditions leading to certain kinds of oscillation were obtained but not compared with any experiment. A similar equation was further investigated by Hayashi, Nishikawa and Abe[22], but again without experimental verification.

Subsequently, certain digital computers utilising magnetic parametrons

were developed in Japan: in 1956 Takahashi and Goto[23] discussed the memory for such a computer and in 1958 Muroga[24], Muroga and Takashima[25] and Goto[26] dealt with the principles of majority logic and system design to be employed therein.

In 1958 Zen'iti, Sekiguti and Takasima[27] described what appears to be the sole example of a parametron using the phenomenon of ferroelectric capacitance. They found its frequency capabilities to be considerably inferior to those of the magnetic parametrons.

The idea of using the depletion layer capacitance of a junction diode as the nonlinear reactive element, (the "varactor"), led to the possibility of very much higher frequencies of operation. Varactor parametrons were described by a number of authors. These include Zen'iti, Fusimi, Kataoka and Yamanaka[28] in 1957, Zen'iti[29] in 1958, Sterzer and Beam[30] and Hilibrand and Beam[31] in 1959.

Since 1957 most of the work published on parametrons has tended to fall into one or other of two categories: the experimental and the theoretical. Wholly experimental work was reported in 1959 by Sterzer and Beam[30] and by Sterzer[32] who constructed an unbalanced stripline varactor parametron which operated satisfactorily at a pump frequency of 4 kMc/s. Without invoking any theory, he discussed how it might be used in a hypothetical microwave computer. Onyshkevych, Kosonocky and Lo[33] covered the same ground in somewhat more detail. In 1961 Abeyta, Borgini and Crosby[34] constructed a computer subsystem using balanced varactor parametrons pumped at 3.7 kMc/s, but without very convincing results. No other systems employing varactor parametrons seem to occur in the literature.

The purely experimental approach suffers from certain disadvantages. So

various and complicated are the phenomena for different physical circuits and even for the same circuit under slightly differing conditions, that it is virtually impossible to arrive at any kind of "optimum" design or to make any progress in understanding the mechanisms involved by means of this method alone.

Theoretical work since 1957 has been concerned primarily with the treatment of idealised and even arbitrary mathematical situations. The stimulus for this seems to have been the parametric amplifier which, as was shown by Bloom and Chang[35], could be treated in terms of idealisations with considerable success. Attempts to apply their ideas to the parametron were less successful and extremely poor correlation between theory and experiment resulted. Hilibrand, Mueller, Stocker and Gold[36] treated such an idealised parametron and attempted to predict its transient behaviour by extrapolation from a small-signal quasi-static analysis which assumed infinitely slowly-varying amplitudes and phases. Since this analysis did not predict even the steady-state phenomena, it is not surprising that the transient solution should be inadequate, apart from the fact that it involved the violation of the quasi-static assumption. By means of a very similar analysis Nethercot[37] treated a parametron in which the phase of oscillation was switched by a large-amplitude over-riding signal of the opposite phase.* This type of switching involves large-amplitude signals, for which the theory does not hold. The paper contains certain mathematical errors, as does that of Rouche.[38]

The "classical" approach reappeared in a paper published in 1960 by

---

* This is the so-called method of Forced Phase Switching.

Hayashi, Nishikawa and Abe[22], who gave an elegant analysis of the $\frac{1}{2}$th-order subharmonic solution of an idealised system obeying a variant of the Duffing equation:

$$\ddot{y} + k\dot{y} + ay + by^3 = X \cos 2\tau + X_o \qquad (1.4)$$

In none of these papers was an attempt made to relate the theory to any physical system and this is understandable in view of the nature of the effects to be explained. Furthermore, it has been usual to restrict attention to those cases in which the pumping frequency is exactly twice the small-signal resonant frequency. This restriction has led to an unrealistic picture of the capabilities of these devices.

Since 1961, the year in which the present investigations were initiated, the subject appears to have been virtually neglected. This is possibly due to pessimistic reports concerning the relative slowness of the transients. These reports may be attributed to concentration on the resonant mode of operation which, as we shall see, is not necessarily the best way of using a parametron. In addition it should be pointed out that the parametron computer, being an R.F. system, requires a much narrower bandwidth than the more usual types of computer in which the frequency spectrum must extend from d.c. up to the highest frequency of interest. It is therefore likely that the parametron will come into its own when computer operation frequencies are increased considerably beyond those possible at the present time.

1.3 Aim of thesis and formulation of problem

We have seen that research on subharmonic oscillators has tended to follow two seldom-intersecting paths: the theoretical and the experimental.

This thesis aims to bring these two paths together and to provide a comprehensive and reasonably accurate background for the understanding of the mechanisms involved in the production of steady-state subharmonic oscillations. In addition it aims to explain the processes governing the manner in which the oscillations build up from a small initial level to their final amplitude. The thesis then attempts to predict the quantitative behaviour of actual parametrons which are known to have fast-transient capabilities and other desirable properties, in order to find the optimum conditions for their use. The investigation treats transient as well as steady-state phenomena, and it is found that practical devices obey neither of the "classical" differential equations, those of Mathieu and Duffing, except as a very gross approximation. As far as transients are concerned, previous work has exhibited a preoccupation with the amplitude transient to the neglect of the phase transient, perhaps for traditional reasons. It will be seen that neither the amplitude nor the phase transient can be considered in isolation, and that the latter is at least as important as the former, particularly since we are dealing here with phase-coded information.

We shall endeavour to obtain our results in the form of algebraic expressions and to eschew analogue, numerical or graphical methods, since these merely verify that a satisfactory model has been chosen to represent the device, i.e. that the initial assumptions made were reasonable ones. Such methods do not, in general, lead to new insights, neither do they give results unobtainable from experiment. Computer methods may be useful in cases where there is no information about the solution, but the parametron can be regarded as its own analogue. Furthermore, if there are more than two independent parameters governing the behaviour of the system, it is

virtually impossible to produce numerical or graphical results to cover all possible combinations. A new set of parameters requires the digital computer programme to be re-run with a new data-tape, or the potentiometers of the analogue computer to be re-set. On the other hand, the end-product of the analytical approach consists of equations which are valid for all combinations of parameters which do not violate the original assumptions. Thus there exists the possibility of optimising the system on the basis of such equations.

One of the objects of the present work is to discover the limits to which analytical methods can reasonably go in the investigation of nonlinear problems of the kind under consideration.

There has been in the past little success in the quantitative or even qualitative prediction of the transient phenomena, so that particular attention is paid to this subject and to the influences on it of the initial conditions and phase-switching mechanisms.

1.4 Statement of original work

Except where specific reference is made to the work of others, the content of this thesis represents the results of original research carried out independently by the author. Particular attention is drawn to the quantitative agreement obtained between the theoretical and experimental results, under both transient and steady-state conditions, and to the fact that devices of practical utility, rather than idealised models, have been considered.

CHAPTER TWO

2. The Mathematical and Physical Environment of Subharmonic Oscillators

2.1 Linear resonators and oscillators

Linear stationary-parameter oscillators and energised resonators are superficially alike since both contain a resonant structure and a source of power. However, they differ in several important respects. In general terms these are:

(i) The resonator must be supplied with alternating power, whereas the oscillator derives energy from a real or virtual negative damping sustained by a d.c. power-supply. The oscillator therefore requires some means for coupling the source of power into its resonant circuit but the directly-energised resonator does not.

(ii) The behaviour of the linear resonator is described by the differential equation

$$\ddot{y} + k\dot{y} + y = x(\tau) = X.\sin\nu\tau \qquad (2.1)$$

This has the sole periodic solution

$$y(\tau) = \frac{X}{\sqrt{(1-\nu^2)^2 + (k\nu)^2}} \cdot \sin(\nu\tau - \varepsilon), \qquad (2.2)$$

where $\operatorname{tg}\varepsilon = \frac{1-\nu^2}{k\nu}$

Multiples or submultiples of the driving frequency ν cannot occur. Thus the frequency of the oscillation induced in a linear time-invariant resonator is always the same as that of the energising source. The solution (2.2) also shows that the amplitude and phase of the oscillation are uniquely determined

by the amplitude X and frequency ν of the forcing function and by the damping k. Equation (2.1) describes an Energised Linear Resonator with Stationary Parameters. This is a non-autonomous system in the sense that the vibrations die away if the excitation $x(\tau)$ is removed. Otherwise a steady-state solution exists. The amplitude of $y(\tau)$ can be infinite for resonance (ν =1) and no damping (k=0), but this is not a physical case, and does not affect the argument. The amplitude and phase of the vibrations in a linear stationary-parameter oscillator, on the other hand, are completely independent of the characteristics of the system. The differential equation of a linear oscillator is independent of the variable (e.g. voltage, current, charge) chosen. It is of the form

$$\ddot{y} - 2k\dot{y} + y = 0. \qquad (2.3)$$

This represents an autonomous system. The phase of y is arbitrary since there is no reference phase, and the amplitude of y increases exponentially without limit. The frequency of oscillation, however, is fixed at

$$\nu = \sqrt{1 - k^2} \qquad (2.4)$$

Thus the linear resonator is a physically realisable system, but the true linear resonator is not. In a real oscillator the amplitude always limits at a value defined by some nonlinearity in the damping, no matter how weak that nonlinearity may be. The canonic model of a real oscillator is the generalised van der Pol equation

$$\ddot{y} + \mathfrak{f}(y).\dot{y} + y = 0. \qquad (2.5)$$

$\mathfrak{f}(y)$ is a nonlinear damping function, negative for small y and positive for large y. This is an autonomous equation and has a steady-state solution of defined amplitude but arbitrary phase.

2.1.1 Negative Damping

The concept of negative damping was found useful by Page[39] in explaining the behaviour of certain oscillators containing negligible nonlinearity, and by Whitehead[40] in treating the transient behaviour of the super-regenerative oscillator. In the latter case the device can be regarded as linear until nonlinear dissipative limiting of the amplitude "suddenly" occurs. In cases such as these, the differential equation will have the form of (2.3), whether the oscillation is due to a real negative resistance, such as a suitably-biassed tunnel diode, or to a virtual negative resistance caused by positive feed-back.

Negative damping has also been invoked to explain the behaviour of sub-harmonic oscillators, but seems to have given rise to misleading ideas in this context. In particular it has not led to a satisfactory explanation of the strong inter-relationship between the amplitude and phase in these devices. In particular, the results so obtained cannot be extrapolated to account for large-signal phenomena.

The possibilities of the concept will be investigated in more detail in Section 4.2, Chapter 4.

Attention will now be directed to linear systems in which non-harmonic oscillation is possible.

2.2 Linear systems with periodically time-varying parameters

In the previous section we have considered linear systems with time-invariant parameters. It was seen that in the case of resonators, the oscillation takes place at the driving frequency, and that in the case of oscillators, the vibrations occur in the vicinity of resonance, $\nu \cong 1.0$.

If the oscillator or resonator contains nonlinear damping, up-harmonics can be excited, but subharmonics can only be obtained in systems having non-constant reactance or restoring force. Two kinds of non-constant restoring force are possible: those which are periodic functions of time

$$f(t) = f(t + T), \quad \text{where } T = \text{one period;}$$

and those which are functions (linear or nonlinear) of the displacement (voltage, current, etc.).

In this Section we consider linear systems with periodically time-varying restoring force, or reactance. The classical example of such a system is the Mathieu equation. For our purposes this may be written in the form*

$$\ddot{y} + y(1 - X.\sin 2\nu\tau) = 0. \qquad (2.6)$$

This equation can have up-harmonic, fundamental or subharmonic oscillatory solutions of order one-half for, roughly speaking, ν less than $\frac{1}{2}$, equal to $\frac{1}{2}$ or near unity, respectively. The exact conditions for oscillation, however, depend on the pump amplitude X as well as the frequency ν. This is shown in Figure 2.1, which indicates the regions of the (ν,X)-plane within which $\frac{1}{2}$th-order subharmonic and harmonic oscillations can occur. The solutions within these regions are unstable in the sense that the amplitude of the oscillation grows without limit as time increases.

---

* Equation (2.6) can be expressed in the canonical form by means of the transformations

$$X = \frac{2q}{a}, \quad \nu = \frac{1}{\sqrt{a}}, \quad \tau = z\sqrt{a}$$

and by replacing sine by cosine, so that (2.6) becomes

$$\frac{d^2y}{dz^2} + (a - 2q \cos 2z)y = 0. \qquad (2.7)$$

As we have remarked above, the solutions of the Mathieu equation are well known, and certain aspects of them are qualitatively similar to the results obtained from experimental balanced parametrons. The only physical devices obeying Mathieu's equation accurately are those in which the "restoring force" is directly controlled by the external force. An example is a resonant circuit containing a capacitor with plate-separation mechanically varied in such a way that the following law is obeyed:

$$C(\tau) = C(0).\ (1 - X \sin 2\nu\tau)^{-1},\quad X < 1. \qquad (2.8)$$

However, the high-frequency parametrons with which this thesis is concerned contain reactances which are essentially functions of the "displacement" and their behaviour can be predicted accurately only when this dependency is taken into account.

Goto[28] has somewhat arbitrarily used the Mathieu equation as a basis for explaining the behaviour of experimental parametrons. The poorness of this approximation becomes evident when Figure 2.1 is compared with Figure 2.2 which shows the regions of instability of a typical experimental parametron. Moreover, since the Mathieu equation is <u>linear</u>, no steady-state oscillatory solution can exist, neither is amplitude hysteresis* predicted. For these reasons Goto has empirically modified the Mathieu equation by the addition of damping and nonlinear terms, resulting in

$$\ddot{y} + k\dot{y} + y(1 + \alpha + \beta y^2 - X.\sin 2\nu\tau) = 0 \qquad (2.9)$$

in order to account for the experimental results. Good agreement was still not obtained.

---

* See Chapter 6, Section 6.4.

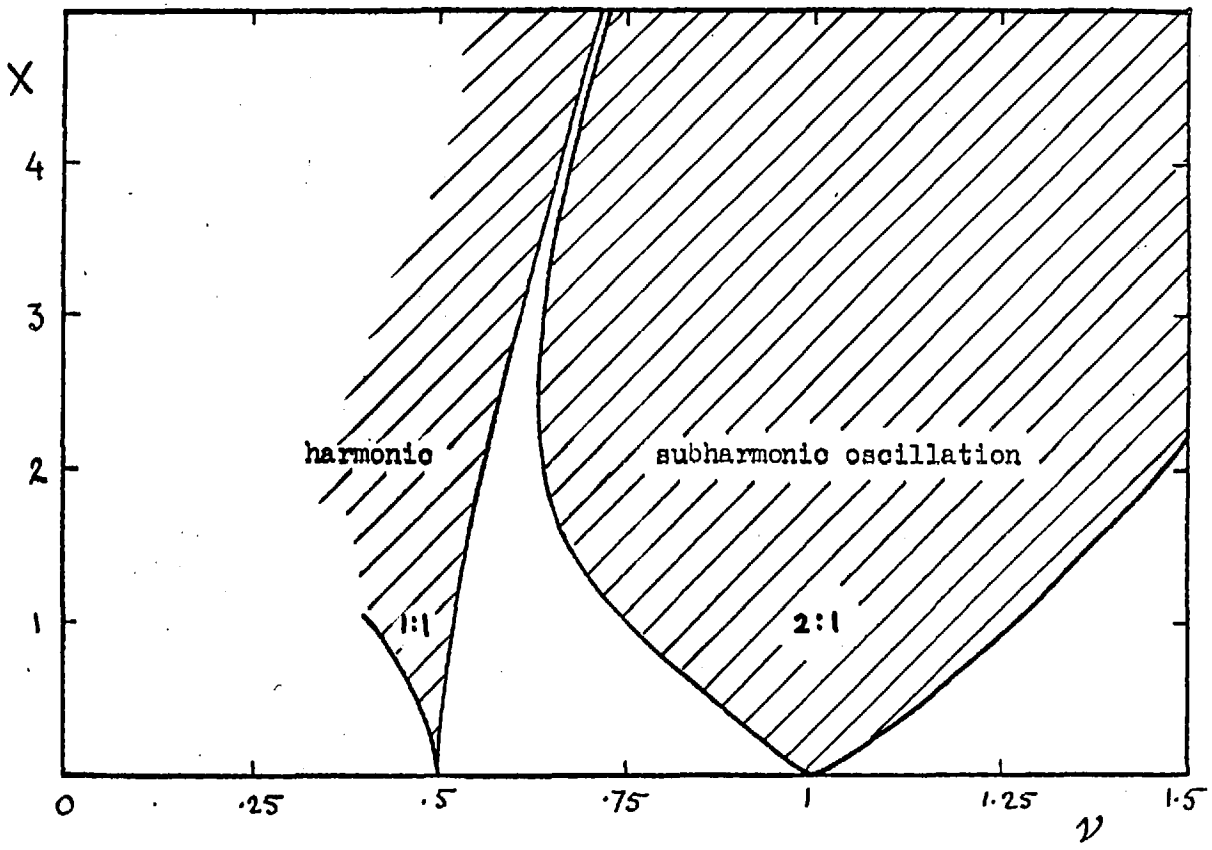


Fig. 2.1 - Regions of instability of Mathieu's Equation, transformed to (ν, X)-coordinates.

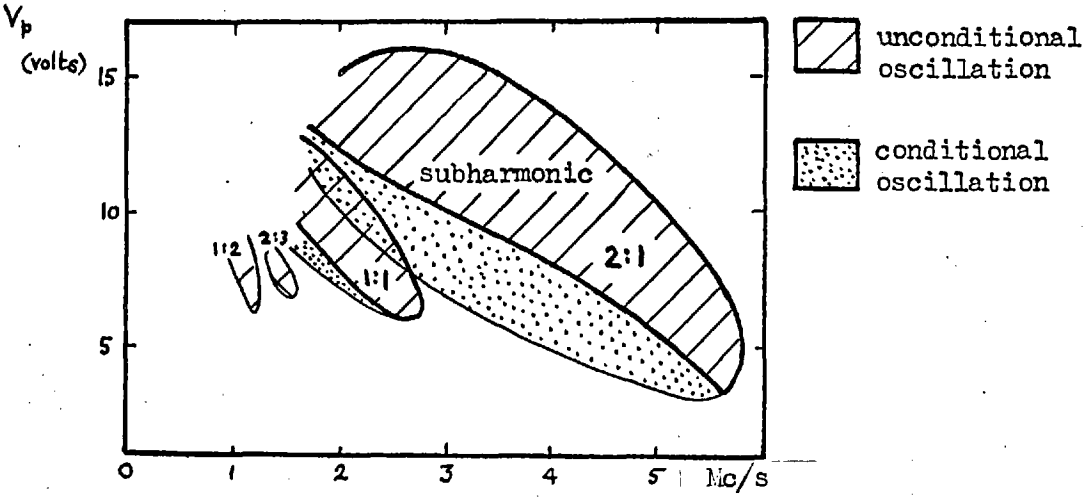


Fig. 2.2 - Regions of instability of a typical experimental parametric oscillator, after Sterzer[32].

The distinction between the oscillator and the externally-excited resonator becomes obscure in a linear system with periodically time-varying parameters. Such a system can be regarded as "a resonator plus a forcing function" or equally well as "a resonator plus virtual negative damping". It resembles a resonator in that the external signal alternates, but differs from it in two ways:

i) the phase angle of the oscillation is related to that of the periodic forcing-function,

ii) the amplitude of the oscillation is not limited and can grow without bound. This behaviour is similar to that of a linear oscillator with constant parameters and negative damping.

Equation (2.6) is a special case of the more general linear differential equation with periodically time-varying coefficients

$$f_1(\tau).\overset{oo}{y} + f_2(\tau).\overset{o}{y} + f_3(\tau).y = 0. \qquad (2.10)$$

The coefficients f_j are all periodic functions of τ :

$$f_j(\tau) = f_j(\tau + T) , \quad j = 1, 2, 3,$$

where T is the period of the forcing function.

We shall see later that some of the nonlinear differential equation models of real parametrons can be expressed in Linear Time-Varying form as a first approximation, but the results of any analysis conducted on this basis will apply only for very small signal amplitudes.

2.3 Nonlinear systems

The parametrons to be investigated in this thesis are all characterised by nonlinear differential equations. At this point it is important to draw

a distinction between true subharmonic oscillation and the so-called "subharmonic oscillation" of autonomous systems. True subharmonic oscillation, or resonance, can occur only in linear or nonlinear non-autonomous systems. The other type of oscillation, however, is due to the synchronisation (or entrainment) of a self-running system to a submultiple of the frequency of an external signal. Confusion between the two phenomena seems to exist in the literature. This may be due to the superficial similarity between them. An example occurs in Hayashi[41].

True subharmonic resonance can only take place in non-autonomous systems of the general type

$$\frac{d^2}{d\tau^2}\left[\mathcal{J}_1(y, x(\tau)) \right] + \frac{d}{d\tau}\left[\mathcal{J}_2(y, x(\tau)) \right] + \mathcal{J}_3(y, x(\tau)) = 0. \tag{2.11}$$

This equation must fulfil the following conditions.

(1) The forcing function must be periodic:

$x(\tau) = x(\tau + \frac{T}{2})$,

where T is the period of the induced oscillation.

(2) The forcing function $x(\tau)$ must be present in at least one of the functions $\mathcal{J}_1$ or $\mathcal{J}_3$.

(3) No sustained oscillation may take place in the absence of the forcing function.

Differential equations which have subharmonic solutions will be of the type (2.11), but it does not follow that <u>all</u> such differential equations necessarily have subharmonic solutions.

It is easy to see that (2.11) includes linear differential equations with time-varying coefficients, of the general type (2.10). A specific example is the modification (2.9) of the Mathieu equation used by Goto, for

which

$$\begin{aligned} \mathcal{F}_1 &= y , \\ \mathcal{F}_2 &= ky , \\ \mathcal{F}_3 &= y(1 + \alpha + \beta y^2 - x(\tau)), \\ T &= \frac{2\pi}{\nu} , \end{aligned}$$

and the three conditions are fulfilled.

A typical nonlinear example is the generalised Duffing equation

$$\ddot{y} + k\dot{y} + \mathcal{F}(y) = x(\tau) \qquad (2.12)$$

where $\mathcal{F}(y)$ is a nonlinear function. In this case

$$\begin{aligned} \mathcal{F}_1 &= y , \\ \mathcal{F}_2 &= ky , \\ \mathcal{F}_3 &= \mathcal{F}(y) - x(\tau) , \end{aligned}$$

and T can again be chosen to fulfil condition (1).

An example of (2.11) which obviously does not have a subharmonic solution is the linear stationary-coefficient differential equation (2.1) for which

$$\begin{aligned} \mathcal{F}_1 &= y , \\ \mathcal{F}_2 &= ky , \\ \mathcal{F}_3 &= y - x(\tau) \end{aligned}$$

and all three conditions can still be satisfied.

The spurious subharmonic oscillation, which is in reality subharmonic synchronisation, occurs in autonomous systems characterised by the generalised van der Pol equation

$$\ddot{y} + \mathcal{F}(y).\dot{y} + y = x(\tau). \qquad (2.13)$$

Here $\mathcal{F}(y)$ is a nonlinear damping function which is negative for certain

values of y. It is evident that condition (2) is violated. Since the damping can be negative, self-oscillation is possible in the absence of $x(\tau)$, so that condition (3) is not fulfilled either.

Subharmonic synchronisation in a system described by a canonical van der Pol equation with forcing function

$$x(\tau) = X.\cos 2\nu\tau + X_o$$

and nonlinear damping

$$\mathcal{F}(y) = -\varepsilon(1 - y^2)$$

has been treated theoretically by Hayashi, Shibayama and Nishikawa[42]. They showed that for the case

$$X_o = 0.5, \quad \varepsilon = 0.2,$$

which implies a rather weak nonlinearity, subharmonic synchronisation of order one-half is possible over a narrow range of requencies near $\nu = 1.0$.

It can be seen that the entrained oscillation will have two possible stable phases, π radians apart, with respect to the phase of the alternating part of $x(\tau)$. Furthermore, if the system parameters are such that self-oscillations just fail to occur, then under certain circumstances they can be "triggered" on by the application of $x(\tau)$. To a certain extent this behaviour does resemble true subharmonic oscillation and could be used for the storage of binary phase-coded information in a similar way. This suggestion might form a basis for further research.

The celebrated and much-quoted paper of Mandelstam and Papalexi[43], despite outward appearances, also deals with subharmonic synchronisation of this kind. It treats the case of a valve feed-back oscillator obeying an equation of the form (2.13) with a nonlinear damping term

$$\mathcal{F}(y) = \mu\left[k - (ay + by^2 + cy^4)\right]$$

which is positive for small y and negative for large values of y. Their paper deals particularly with the case in which the system is not in a state of self-oscillation and is turned on by a synchronising function $x(\tau)$ having the frequency 2ν where ν is near unity.

In subsequent work in this thesis we shall find that the differential equations of practical parametrons all conform to the type (2.11) and obey the associated conditions. In some cases it will be seen that the non-linearity is contained in the function $\mathcal{F}_1$ rather than in $\mathcal{F}_3$.

CHAPTER THREE

3. Nonlinear Reactive Elements

3.1 Physical nonlinear reactive elements

In the previous Chapter it has been remarked that periodically time-varying reactance per se is, in general, inadequate for the construction of high-frequency parametrons. The practical "non-mechanical" parametrons with which this thesis is concerned must contain nonlinear reactance. Nonlinear dissipation may be present also, but is to be regarded as an undesirable parasitic, contributing nothing to the generation of subharmonics. This may be contrasted with the situation in frequency multipliers. Multiplication can be achieved through the use of either nonlinear reactance or nonlinear dissipation, although the efficiency of the frequency conversion will be much reduced in the latter case.[44]

We shall now consider what physical nonlinear reactive elements are possible for use in parametrons and shall discuss factors leading to the choice of a type suitable for use in high-frequency devices.

Subharmonic oscillations can be excited in almost any resonant system containing nonlinear reactance, so long as the system as a whole has a sufficiently high quality factor Q. The magnitude of Q, which is properly a quantity relating to linear systems, and is somewhat ill-defined in nonlinear systems, will set an upper limit to the frequency at which the parametron can be operated.

Practical nonlinear reactive elements are either inductive or capacitive; to a first approximation these can be regarded as duals of one another. To a higher approximation, the duality generally fails, since

infinitely many nonlinear characteristics are possible. First let us consider nonlinear inductive elements.

3.1.1 Nonlinear inductive elements

Inductors which owe their nonlinearity to saturation effects in iron or ferrite cores have been used extensively in Japan. For example the MUSASINO-1 parametron computer described by Goto[26] and others[25] used such inductors wound upon "binocular" two-hole ferrite cores in balanced parametrons. However, although these parametrons proved to be extremely reliable, it was found that the hysteresis losses in the cores limited the maximum usable pumping frequency to about 2 Mc/s, and that the highest computer clock-frequency was about 6 Kc/s. In a later Japanese parametron computer[26] designated PC-2, the corresponding frequencies were 6 Mc/s and 100 Kc/s respectively.

Kaufman and Pfeiffer[45] have reported an inductive parametron in which the coil is wound upon a cylindrical anisotropic thin film of permalloy deposited on a beryllium-copper conductor. The permeability of the film is made to vary in sympathy with an axial pumping current and a time-varying inductance results. If the permeability was a linear function of the pumping current, the device might be expected to obey Mathieu's equation quite closely. However, as in other inductive devices, saturation effects will inevitably introduce nonlinearities, and hysteresis losses will limit the frequency of operation. It was found that a parametron using this kind of inductance could be pumped at 20 Mc/s, making possible a clock frequency of 300 Kc/s. These frequencies are somewhat greater than those possible with the earlier inductive parametrons, but still not as high as those obtainable

in "conventional" computers.

Because of their restricted frequency capabilities, a detailed investigation of parametrons employing nonlinear or time-varying inductors has not been undertaken in the present work.

3.1.2 Nonlinear capacitive elements

One possible kind of nonlinear capacitive reactance is the barium titanate capacitor. This is a "conventional" capacitor which uses a ceramic containing $BaTiO_3$ as the dielectric material. The nonlinearity of the capacitance arises from the dependence of the permittivity of the dielectric upon the applied voltage. These capacitors are very lossy and are not suitable for high-frequency use.[27]

Another type of nonlinear capacitive reactance which has been investigated[46] is the barrier-capacitance of a selenium rectifier. The intrinsic rate of capacity-variation with applied field is reduced by the thin insulating layer in series with the p-n junction, and the device is suitable only for very low-frequency operation since the Q decreases to unity at about 1 Mc/s.

A very much more promising device for use at high frequencies is the depletion-layer capacitance of a reverse biased silicon or germanium p-n junction diode. The theory of these diodes has been given by Shockley[47]. Their behaviour can be described quite accurately by means of the equivalent circuit[48] of Figure 3.1. This consists basically of a parallel combination of voltage-sensitive capacitance C(V) and nonlinear conductance G(V). At high frequencies the series resistance R_s of the semiconductor material and the lead inductance L become significant. At very high frequencies,

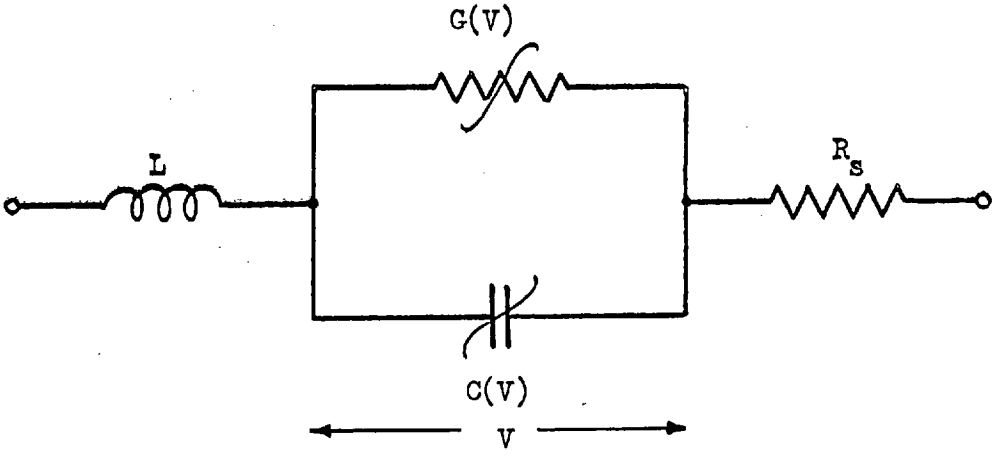


Figure 3.1 -

Equivalent circuit of p-n junction varactor diode.

G(V) is swamped by C(V), and R_s is the only loss element of any importance. The lead inductance L can be minimised by making the diode short and thick. If a suitable varactor is chosen, L can generally be neglected in practice. R_s is usually designed to be as small as possible. For the frequencies employed in the experimental work reported in this thesis its effect may be neglected. On the other hand, we shall see that G(V) can become important at such frequencies, particularly under conditions of heavy pumping, and therefore cannot always be neglected.

In order to be able to treat the varactor as a nonlinear circuit element, mathematical models of the functions C(V) and G(V) are required. The characterisation of varactors in these terms is considered in the next Section.

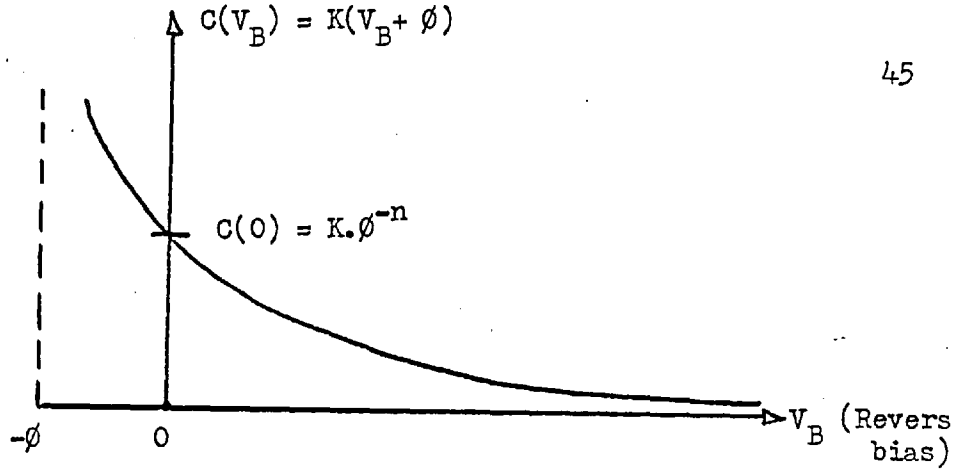
3.2 Characterisation of varactors

3.2.1 Nonlinear capacitance

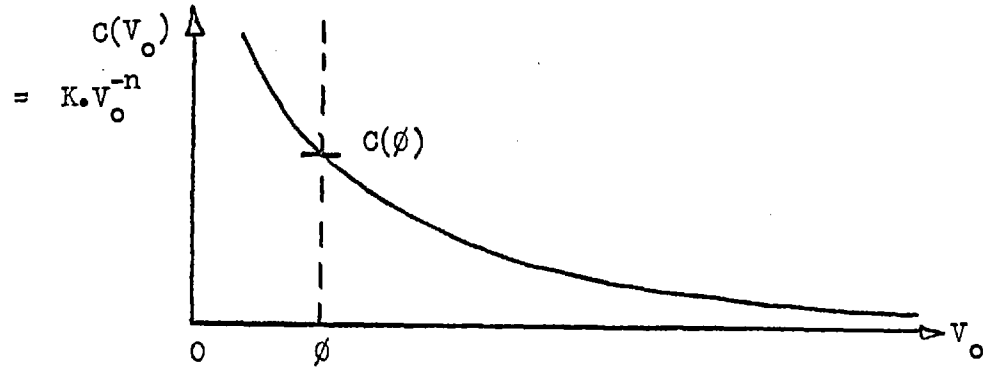
It is well known [36,47] that the voltage-dependence of the depletion-layer capacitance of a junction diode is given quite accurately by

$$C(V_B) = K(V_B + \phi)^{-n} . \qquad (3.1)$$

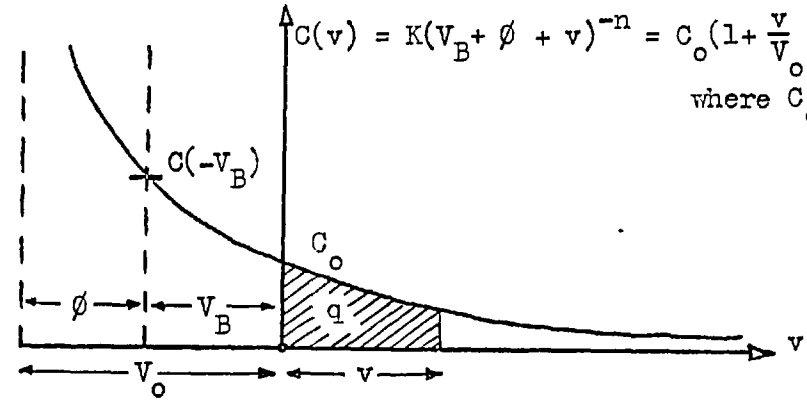
Here V_B is the external reverse bias applied across the diode, ϕ is the "built-in" junction contact potential, n is an exponent between 0 and 1 depending on the grading at the junction and K is a constant governed by the geometry of the device. The curve defined by equation (3.1) is shown in Figure 3.2(a). The capacitance-law expressed in this form is not particularly suitable for comparison with measurements on actual varactor diodes. For that purpose, it is advantageous to write the capacitance law in an



(a) Nonlinear capacitance law referred to the external bias voltage V_B.



(b) Nonlinear capacitance law referred to the total junction bias $V_o = V_B + \emptyset$
This representation is used in varactor measurements.



(c) Nonlinear capacitance law referred to instantaneous external voltage v. This representation is used for analytical purposes.

Figure 3.2 - Representations of the nonlinear capacitance.

alternative second form:

$$C(V_o) = KV_o^{-n} , \tag{3.2}$$

where $V_o = V_B + \phi$ is the total junction bias. The curve defined by this law is shown in Figure 3.2(b). Since $C(\phi) = K\phi^{-n}$, the constant K can be eliminated, yielding

$$C(V_o) = C(\phi) \left[\frac{V_o}{\phi}\right]^{-n} . \tag{3.3}$$

The exponent n is therefore given by

$$n = \frac{\lg \left[\frac{C(V_o)}{C(\phi)}\right]}{\lg \left[\frac{\phi}{V_o}\right]} . \tag{3.4}$$

That is, n can be determined from the slope of the $C(V_o)$, V_o-characteristic plotted on log-log coordinates. If the varactor obeys the law (3.1), then the characteristic is a straight line.

For specifically analytical purposes, a third variant of the nonlinear capacitance law is useful. In this case the origin of the voltage-axis is transferred to the total-bias point V_o, as indicated in Figure 3.2(c). The voltage variable is now considered to be v, the time-varying part of the voltage across the junction, and the law becomes

$$\begin{aligned} C(v) &= K(V_B + \phi + v)^{-n} \\ &= C_o(1 + \frac{v}{V_o})^{-n} , \end{aligned} \tag{3.5}$$

where $C_o = KV_o^{-n}$ is the small-signal capacitance at the total-bias point V_o.

3.2.2 Experimental verification of the validity of the assumed nonlinear capacitance law

The small-signal capacitance $C(V_o)$ of several different types of abrupt-junction varactor diodes has been measured. The measurements were performed on a Boonton R-X meter for $C(V_o) < 25$ pF and on a Marconi Q-meter for $C(V_o) > 25$ pF. The reverse bias voltage V_B was applied externally and the peak-to-peak voltage across the diode was kept as small as was consistent with accurate measurements. This precaution is particularly important under conditions of zero or forward bias, since the incremental capacitance is then a strong function of voltage. If the amplitude of the alternating signal is too great, the measured capacitance will be in excess of the true value. In each case the magnitude of the junction contact potential ϕ was fixed by choosing a value which gave the best fit to a straight line when the $C(V_o), V_o$- information was plotted on logarithmic coordinates. The exponent n could then be found from the slope of this straight line. The value of n is rather strongly dependent on the exact choice of ϕ.

Figure 3.3 shows the measured nonlinear capacitance characteristics of typical examples of a number of different types of varactor diodes. A large number of examples were actually measured: only representative characteristics are shown here. In nearly all cases the assumed law (3.3) is obeyed accurately. The exception is the Transitron SC-1 silicon varactor diode: no value of ϕ could be found which caused the experimental points to lie along a straight line. In addition, for values of V_B less than about 2 volts, and for zero and forward bias, these varactors were found to be very much more lossy than the other types. For these reasons they were not used

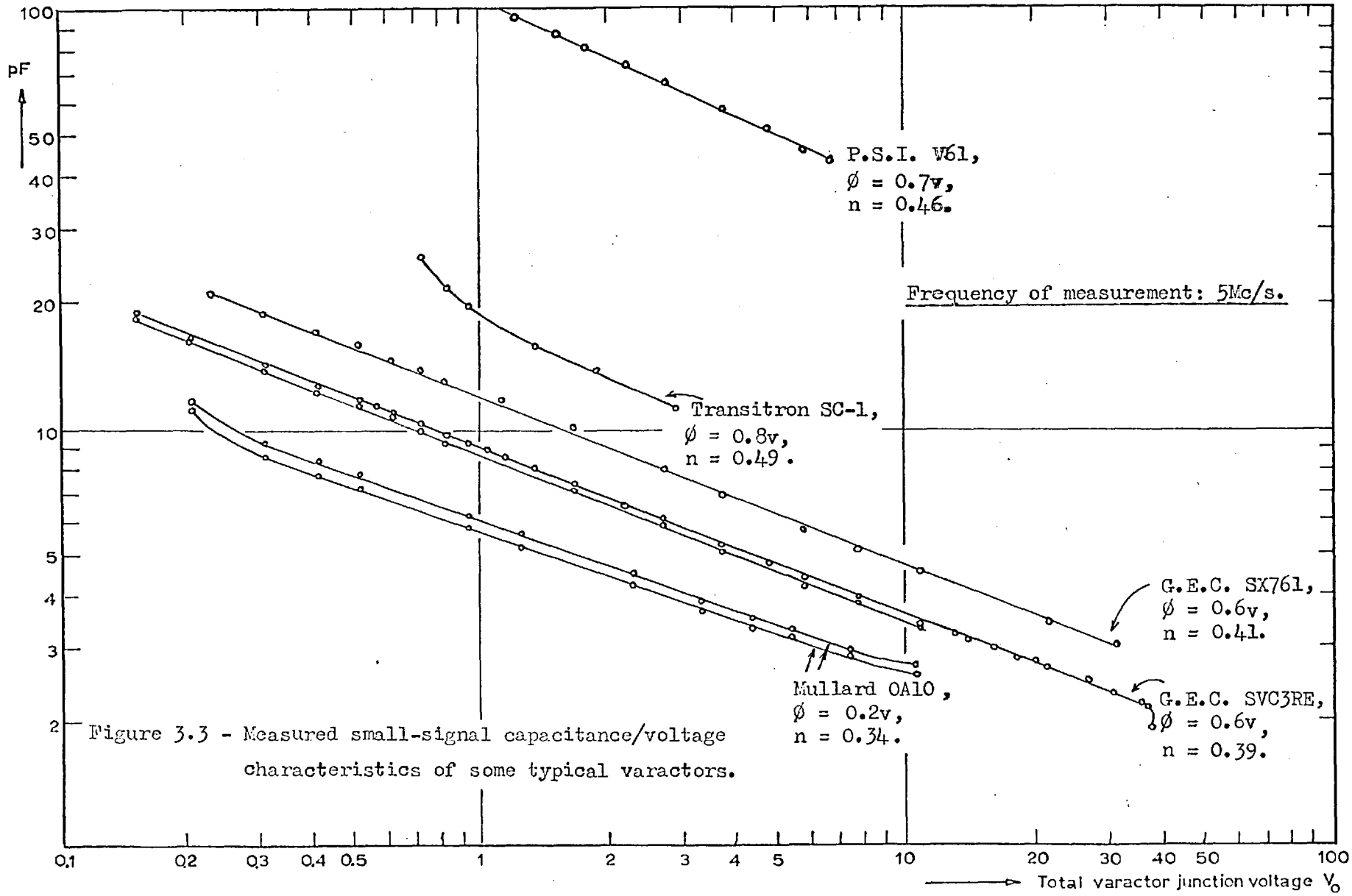


Figure 3.3 - Measured small-signal capacitance/voltage characteristics of some typical varactors.

in experimental work.

As well as diodes specifically designed to be varactors, measurements were also made on a number of Mullard OA-10 germanium junction diodes. These functioned quite well as nonlinear capacitors although their exponents n were only about 0.35. Since parts of the theoretical work (to be given) will assume that n = 0.5, these diodes were also rejected for experimental work.

Most of the experiments have been carried out using the G.E.C. SVC 3 RE silicon varactors. These are relatively high-Q units and obey the assumed law from well into the region of forward bias to the onset of reverse breakdown. Their measured values of n average about 0.4, somewhat less than the theoretical value of $\frac{1}{2}$ for abrupt-junction varactors.[48] In spite of this, good agreement between theory and practice has been obtained.

3.2.3 The representation of the nonlinear capacitance on the basis of its charge-voltage relationship

For certain analytical purposes it will be desirable to characterise the nonlinear capacitance in terms of an instantaneous charge which is a function of the instantaneous voltage. Figure 3.2(c) shows the nonlinear capacitance law referred to the instantaneous external voltage v, with the origin placed at the total bias voltage $V_o = V_B + \phi$. The shaded area under the curve represents the increment of charge on the varactor junction due to a voltage excursion v. It is given by

$$q = \int_o^v C(v)dv = C_o \int_o^v \left(1 + \frac{v}{V_o}\right)^{-n} dv$$

$$= \frac{C_o V_o}{1-n}\left[\left(1 + \frac{v}{V_o}\right)^{1-n} - 1\right] .$$

The inverse of this is

$$v = V_o \left[\left(\frac{1-n}{C_o V_o} \cdot q + 1 \right)^{\frac{1}{1-n}} - 1 \right], \qquad (3.6)$$

which takes particularly simple forms when

$$n = \frac{N}{1+N}$$

where N is a positive integer. Expressions for v for these values of n are given in the following table:

n	v
0	$\frac{q}{C_o}$, a linear capacitor.
$\frac{1}{2}$	$V_o \left[\left(\frac{1}{2} \cdot \frac{q}{C_o V_o} + 1 \right)^2 - 1 \right]$
$\frac{2}{3}$	$V_o \left[\left(\frac{1}{3} \cdot \frac{q}{C_o V_o} + 1 \right)^3 - 1 \right]$
. . .	. . .
1	$V_o \left[\exp \frac{q}{C_o V_o} - 1 \right]$

Table 3.1

If we perform the normalisations:

$$y = \frac{v}{V_o} ,$$

$$z = \frac{q}{C_o V_o} ,$$

then

$$y = \left[(1-n)z + 1\right]^{\frac{1}{1-n}} - 1 , \quad 0 \leqslant n < 1,$$

and the charge-voltage relations become:

n	y
0	z
$\frac{1}{2}$	$z(1 + \frac{1}{4} z)$
$\frac{2}{3}$	$z(1 + \frac{1}{3} z + \frac{1}{27} z^2)$
$\frac{3}{4}$	$z(1 + \frac{3}{8} z + \frac{1}{16} z^2 + \frac{1}{256} z^3)$
⋮	⋮
1	$z(1 + \frac{1}{2} z + \frac{1}{6} z^2 + \frac{1}{24} z^3 + ...)$ $= e^z - 1$

Table 3.2

Some of these nonlinear reactance characteristics are shown in Figure 3.4. They are valid only for certain ranges of z and y. The non-physical parts of the characteristics are shown as broken lines.

The graded-junction varactor diode has a nonlinear capacitance characteristic with n close to $\frac{1}{3}$, which is a value which does not occur in Table 3.2. The abrupt-junction varactor, however, has n close to $\frac{1}{2}$, which is a value leading to the very simple expression for y in the second place

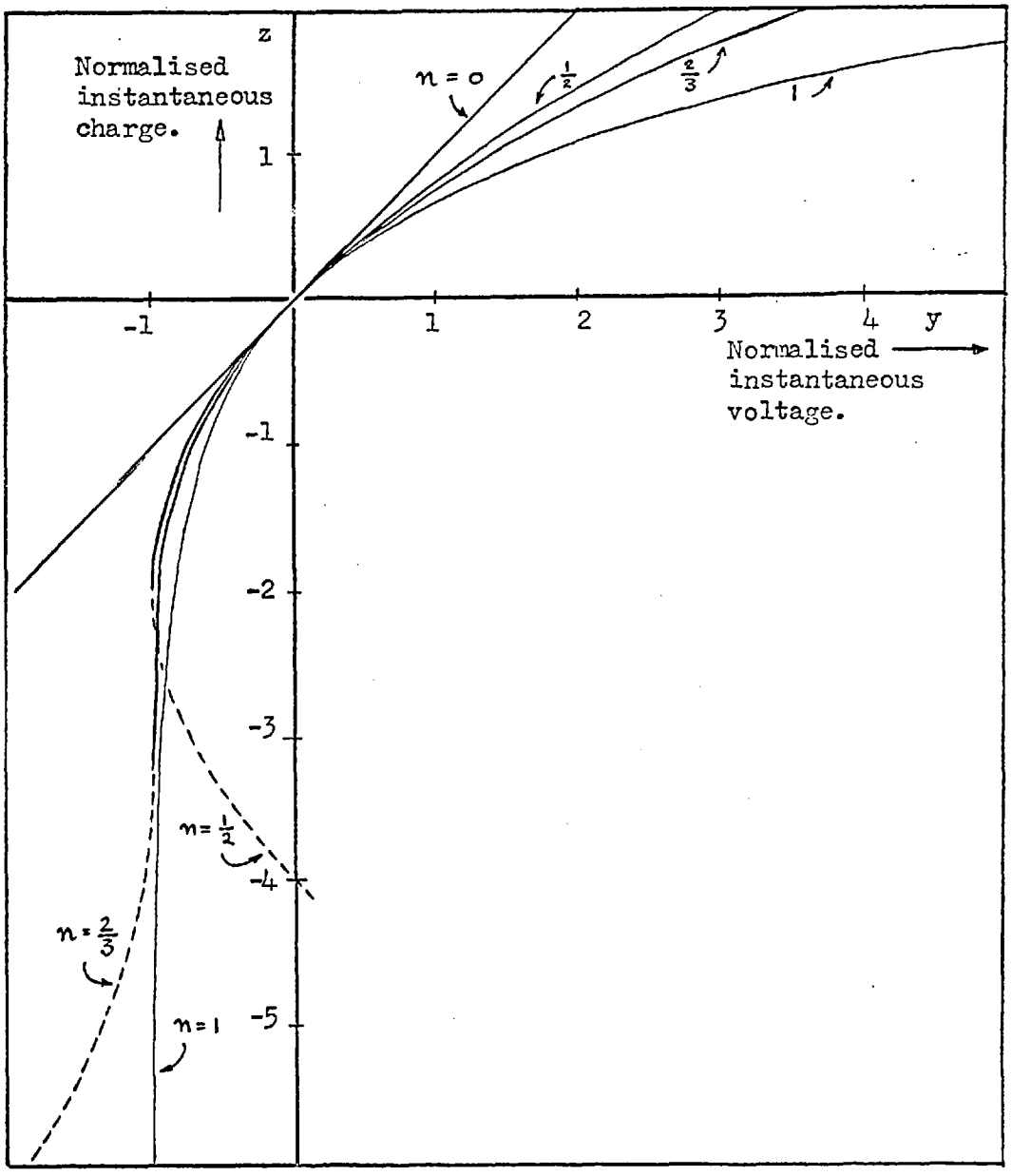


Figure 3.4 -

Theoretical charge/voltage characteristics for varactors with various values of the exponent n.

of the table. It is desirable to use a varactor with the greatest possible nonlinearity: the abrupt-junction varactor affords the largest rate of change of capacitance with voltage readily obtainable at the time of writing. Recently, however, experimental "hyper-abrupt" varactors have been reported,[49] in which n is approximately unity over a certain range of reverse bias voltages. The possibilities of such devices are not explored in detail in this thesis, but suggest an interesting point of departure for further work, as will be indicated in Sub-Sections 5.5.2. and 5.5.3.

3.2.4 Note on the mathematical model for the charge-voltage characteristic when $n = \frac{1}{2}$

The derived normalised charge-voltage relation for the case $n = \frac{1}{2}$ is

$$y = z + \frac{1}{4} z^2 ,$$

so that z is a two-valued function of y. One of the values is physical but the other is not. The non-physical part of the corresponding (y,z)-characteristic is that for which the capacitance $\frac{dq}{dv}$ is negative. When one works in terms of the charge-variable z, it is necessary to reject any theoretical results corresponding to the "forbidden" part of the characteristic. This is indicated in Figure 3.4 by a broken line. At the point $y = -1$, $\frac{dq}{dv}$ becomes infinite, approximating the behaviour of a real varactor.

3.2.5 Nonlinear conductance

Although the voltage-sensitive conductance G(V) is shunted out by the effective parallel capacitance C(V) at sufficiently high frequencies, at lower frequencies and for very large signal levels its influence may be important. It is therefore desirable to be able to treat it mathematically.

The conductance G(V) can be characterised adequately by means of the well known diode law

$$i = I_s(e^{-\lambda(V_B+ v)} - 1) .$$

Here i is the total (direct + instantaneous) current flowing, I_s is the so-called saturation current and V_B and v are respectively the direct external bias voltage and the applied instantaneous voltage, both being defined here as positive for the direction of <u>reverse</u> bias. The quantity λ is the reciprocal voltage $q_e/KT = 38 \text{ volt}^{-1}$ at 25°C, where q_e is the charge on an electron, K is Boltzmann's constant and T is the Absolute temperature.

In subsequent work we shall work in terms of the operating-point voltage

$$V_o = V_B + \phi ,$$

so that the diode law will be written in the form

$$i = I_s(e^{-\lambda(V_o- \phi + v)} - 1). \qquad (3.7)$$

CHAPTER FOUR

4. Preliminary Investigation of Parametric Subharmonic Oscillators

4.1 'Evolution' of parametron circuits

4.1.1 Introduction

Contrary to the situation with linear circuits, little progress can be made in the understanding of nonlinear systems without consideration of specific circuits. A general theory embracing all circuit possibilities, particularly those involving more than one kind of nonlinearity, seems to be out of reach at present. Some elegant general results on the energy relationships in dissipationless nonlinear systems have been obtained by Manley and Rowe[50] and by Manley[51]. Some general theorems concerning the energy and co-energy in nonlinear lossless circuits composed of either capacitors or inductors (but not both) have been given by Cherry[52]. The power dissipated in nonlinear all-resistor circuits has been treated in an analogous way in terms of 'content' and 'co-content' by Millar[53]. Unfortunately, these theorems do not apply to practical systems in which all three kinds of element are present.

An additional complication in the study of non-linear circuits is that parasitic elements can cause a change of kind as well as of magnitude, unlike their behaviour in linear circuits.

The selection of parametrons suitable for use as fast computer elements must therefore be made on the basis of experimental evidence. The complexity of the analysis of individual circuits is such that the effort of treating systems of unknown utility is largely wasted.

4.1.2 Parametron circuits

As indicated in Table 4.1, in which all dissipative elements have been omitted for the sake of simplicity, it is possible to trace the "evolution" of, and the relationships between, various kinds of practical parametron circuits from the starting-point of the Parametric Amplifier. The left-hand column of the Table contains devices which employ nonlinear inductance, while the right-hand column contains those using nonlinear capacitance. These devices will hereinafter be referred to as inductive and capacitive parametrons respectively.

The Parametric Amplifier consists basically of three linear sharply-tuned circuits resonant separately to the pumping frequency f_p, the signal frequency f_s and to the difference frequency $f_p - f_s$ (the so-called idling frequency). These three resonant circuits are coupled together via a nonlinear reactance. If the signal frequency is made exactly half the pumping frequency, then the idling circuit may be omitted since $f_p - f_s = f_s$. If the pumping amplitude is large enough, subharmonic oscillations of order one-half can be excited in the "signal" circuit, resonant to f_s. The result is the high-Q Degenerate Parametric Amplifier. It is referred to in the Table as the Type I Parametron. The external signal can be omitted for the moment: it will reappear later under the guise of the "phase-locking" signal. Because of the sharp tuning, the induced subharmonic oscillations will be reasonably sinusoidal and a small-signal analysis is satisfactory. This fortunate from a mathematical point of view, since the differential equation of the complete parametron is fourth-order nonlinear (equivalent to two simultaneous second-order nonlinear equations), the analysis of which presents severe difficulties.

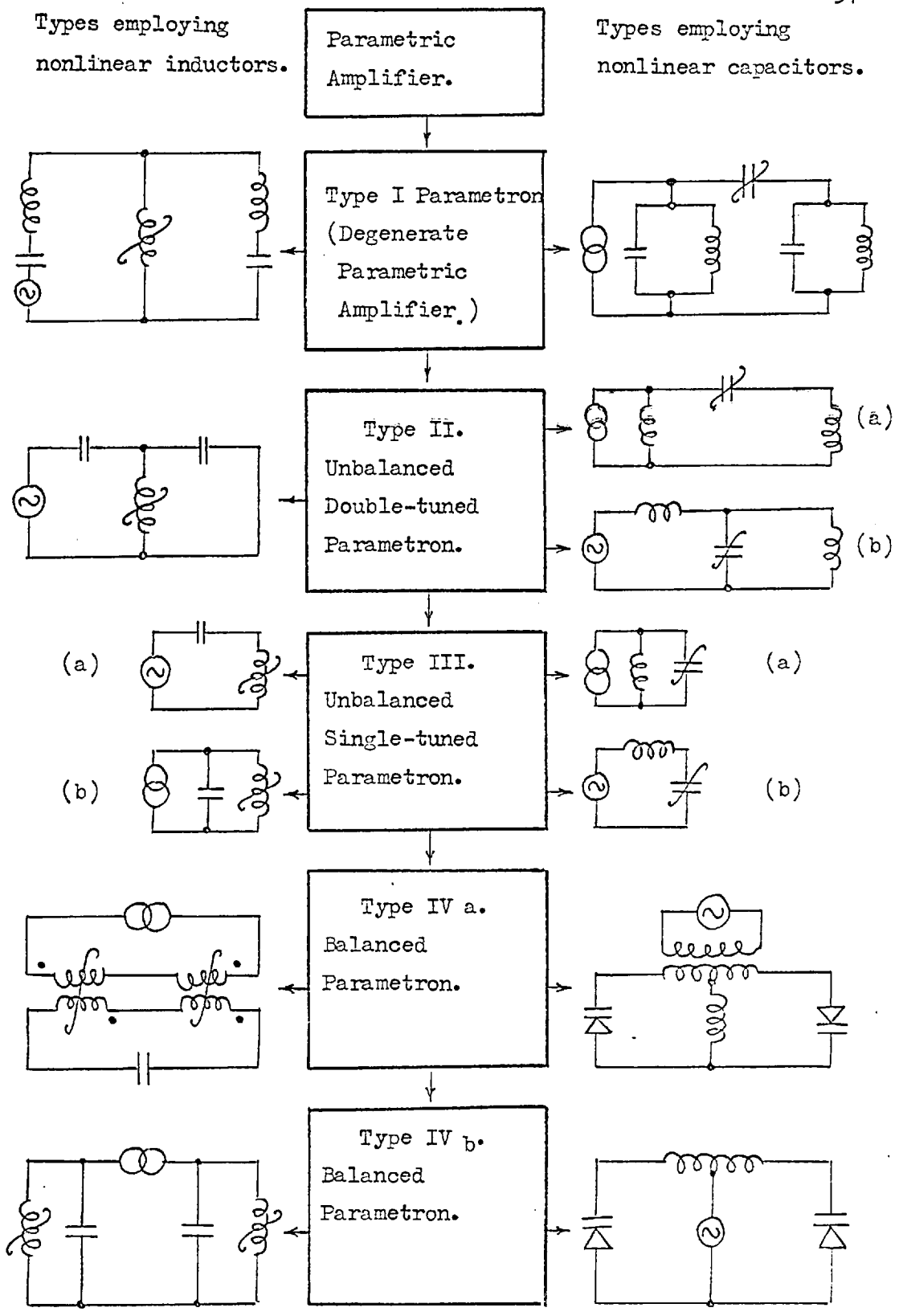


Table 4.1 - Evolution of parametrons.

At this point it may be remarked that certain of the inductive and capacitive parametrons on opposite sides of the Table can be regarded as rough duals of each other. Thus if the nonlinear capacitance can be represented by a series

$$q(v) = C_o v + \mathcal{C}_2 v^2 + \mathcal{C}_3 v^3 + \cdots\cdots\cdots , \qquad (4.1)$$

where q and v are the instantaneous charge and voltage; and the nonlinear inductance by a series

$$\Phi(i) = L_o i + \mathcal{L}_2 i^2 + \mathcal{L}_3 i^3 + \cdots\cdots , \qquad (4.2)$$

where Φ and i are the instantaneous flux and current, then it can be seen that the nonlinear functions are in a sense dual. However, since the nonlinear coefficients $\mathcal{C}_j$ and $\mathcal{L}_j$ are not in general proportional to one another:

$$\mathcal{C}_j \neq \text{const.} \mathcal{L}_j ,$$

the duality will be but approximate.

Bloom and Chang[35] have treated the case of a Type I Inductive Degenerate Parametric Amplifier by a small-signal "high-Q" method, using the power series expansion (4.2) for $\Phi(i)$, truncated at the second term. Their results apply only for signal levels much lower than those encountered in parametrons, furthermore, in order to simplify the calculations, they do not consider the case in which the pump is detuned from resonance.

Hilibrand, Mueller, Stocker and Gold[36], while not being specific about circuits, have in effect studied an identical system, in their case regarded as a Type I capacitive parametron. Their results apply only very approximately to a practical device, and again detuning is not considered.

The Type I Parametrons, which are Degenerate Parametric Amplifiers, can

be made to convert pump power into subharmonic power with good efficiency. However, they suffer from the severe disadvantage that the amplitude of the subharmonic oscillation is able to change only very slowly during a phase-switching operation. This is because of the considerable energy-storage of the sharply-tuned resonant circuits which are needed to suppress practically and analytically undesirable harmonics. Behaviour of this kind is distinctly not what is required of a fast switching element. We are therefore led to consider how the amplitude transient may be speeded up.

The resonant case treated in the references mentioned above is not an optimum condition for the production of fast transients, even in the absence of filters.

The fast-switching requirement leads us to the Type II Unbalanced Double-Tuned Parametrons of the Table, in which some of the non-essential energy-storing reactive elements have been removed. However, the elimination of these elements means that in general a large number of unwanted harmonics will appear because the filtering is now poor. A reasonably accurate analysis will become exceedingly difficult. Nevertheless, Nethercot[37] has used the method of Bloom and Chang to treat a Type II inductive parametron as though it were of Type I. His results do not apply for the circuit considered because it cannot physically fulfil the conditions of the analysis. Thus he assumes that the small-signal part L_o of the nonlinear inductance can, with a suitable pair of capacitances, be used to form two coupled high-Q resonant individually to $2f_s$ and f_s. However, the total inductance can be regarded as linear only for vanishingly small signal levels. Therefore the assumption that an efficient filtering action can be obtained fails for any finite signal level, and the sharp-tuning approximation

is invalid.

A further step in reducing the number of energy-storing elements results in the parametron circuits of Type III in Table 4.1. These consist simply of a nonlinear reactance and a linear reactance of the "opposite" kind, the circuit being "resonant" to one-half the pumping frequency. A Type III(a) inductive parametron has been studied by Hayashi[21] and Type III (b) capacitive parametrons by Aiken and Finzi[52] and by Hedderley[53] although the latter author introduces additional energy-storing reactances into his lossless circuit. The Type III parametrons are extremely difficult to analyse since they suffer from the disadvantages of unbalance and lack of filtering in full measure: the subharmonic output signal is very non-sinusoidal and consists of the pump frequency, the subharmonic frequency and many harmonics of all orders. A typical example of the waveforms encountered in a Type III(b) capacitive parametron in which a varactor is used as the nonlinear reactance is shown in Figure 4.1.

To sum up this far, we conclude that in certain circumstances, unbalanced parametrons may be useful. However, if they are sufficiently sharply-tuned to be amenable to analysis, (Types I and II), then they become relatively useless as switching elements because the transients are so long. They may, however, make excellent frequency dividers, but this aspect does not concern us here. Type III unbalanced parametrons, on the other hand, have fast-transient capabilities, but are not readily treated by analytical methods.

The problem is to obtain a reasonably sinusoidal subharmonic output, and at the same time to have as little energy-storage as possible. A solution is to add together two circuits of Type III in such a way that the

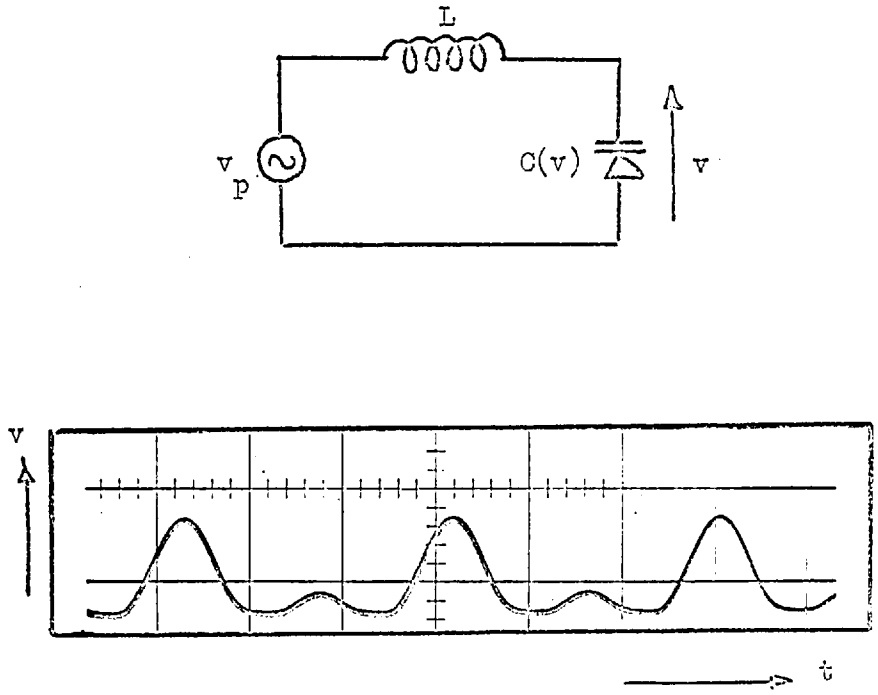


Figure 4.1 - Photograph of varactor voltage waveform in a typical Type III(b) capacitive parametron.

nonsinusoidal subharmonic outputs of each combine to produce an approximate sinusoid. This "adding" process is illustrated diagrammatically in Figure 4.2. Two different ways of adding together a pair of capacitive Type III parametrons are shown, resulting in the Balanced Types IV(a) and IV(b). Note that in these devices the orientation of the nonlinear reactive elements becomes important. We shall refer to the Type IV(a) capacitive device as a Balanced Series Parametron (BSP) because its varactors are in "series", and to the Type IV(b) capacitive circuit as a Balanced Parallel Parametron (BPP) since its varactors are in "parallel".

These balanced parametrons combine the advantages of low energy-storage and reasonably sinusoidal output with several other virtues which will be discussed in Chapter 7. The present thesis is primarily concerned with these types since they afford a good compromise between practical utility and theoretical manageability.

The Type IV(a) inductive parametron has been used[26] as a computer element, but has not been treated theoretically except by Lavi and Finzi[13], who perform a piecewise-linear analysis assuming a square-wave pump. The Type IV(a) capacitive parametron has been used in some experimental investigations[32,33] but no theoretical explanation of the observed phenomena has been given.

Type IV(b) inductive parametrons do not seem to occur in the literature, although the Type IV(b) capacitive parametron has been used in some sketchy experiments[34].

The balanced parametrons have the major advantage that they effectively isolate the pump and subharmonic circuits from each other, so that they interact only via the nonlinear reactances. This means that virtually none

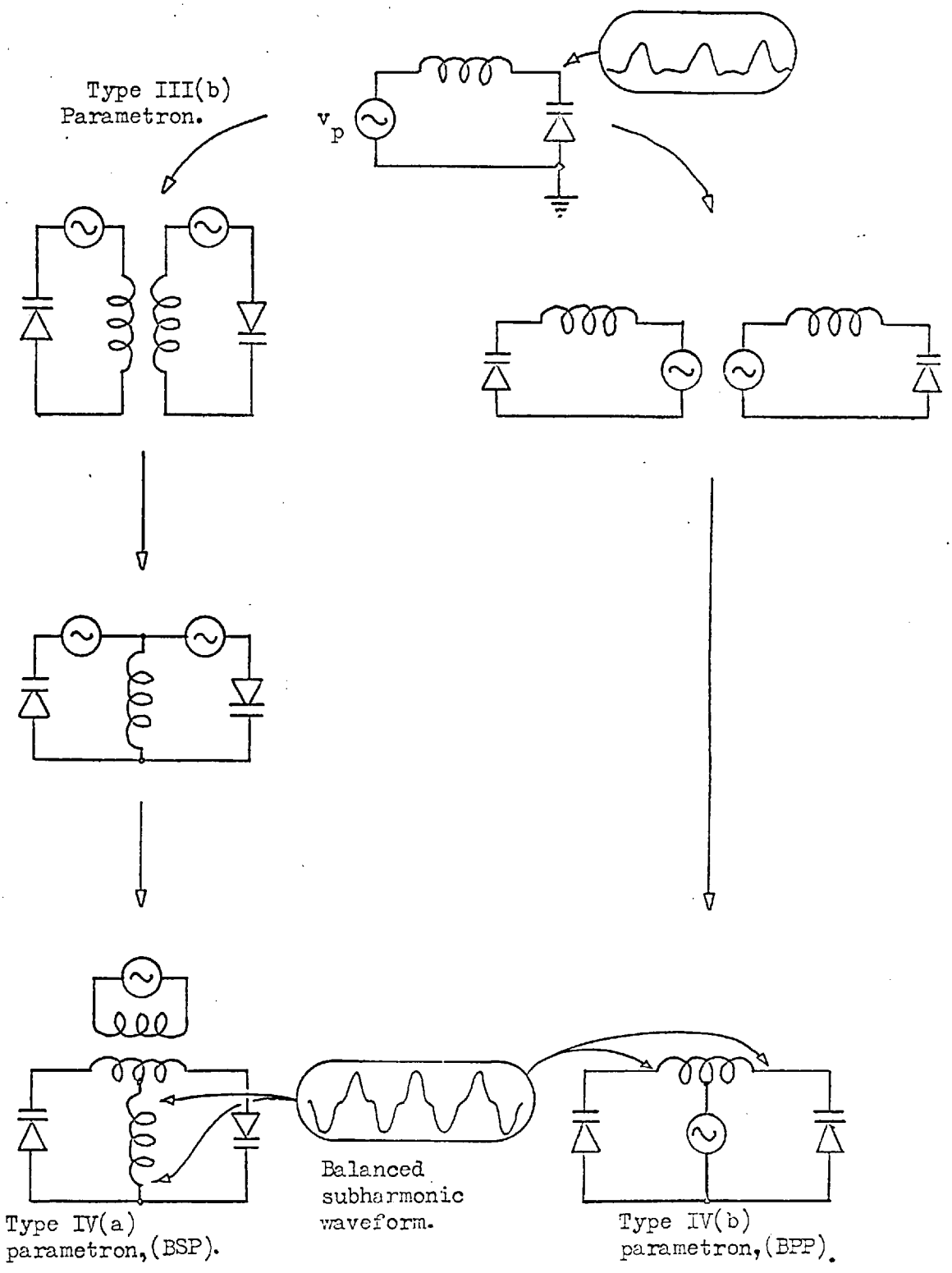


Fig. 4.2 -

Evolution of Type IV capacitive balanced parametrons from two Type III(b) capacitive parametrons.

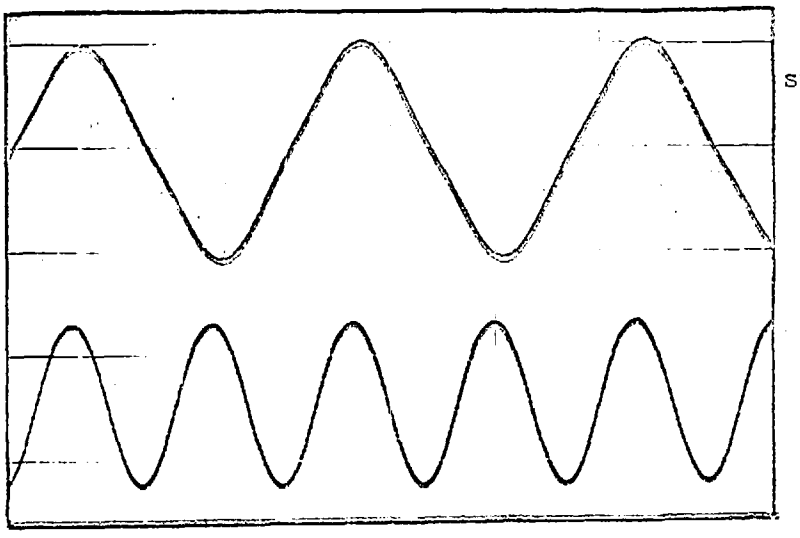
of the pump frequency appears in the output and none of the subharmonic frequency in the input. Thus there is a self-filtering action which does not involve additional energy-storing elements. Furthermore, since the devices are balanced from the point of view of the subharmonic signal, only odd harmonics of the subharmonic frequency occur, thus improving the purity of the output, see for example Figure 4.3.

In practice the balance of the BSP is, in general, somewhat inferior to that of the BPP, primarily because of the different effects of parasitic capacitances. These matters will be discussed in more detail in Chapter 6 which deals with experiments on the steady-state behaviour of the devices. Suffice it to say for the moment that the BPP is inherently the better-balanced of the two parametrons.

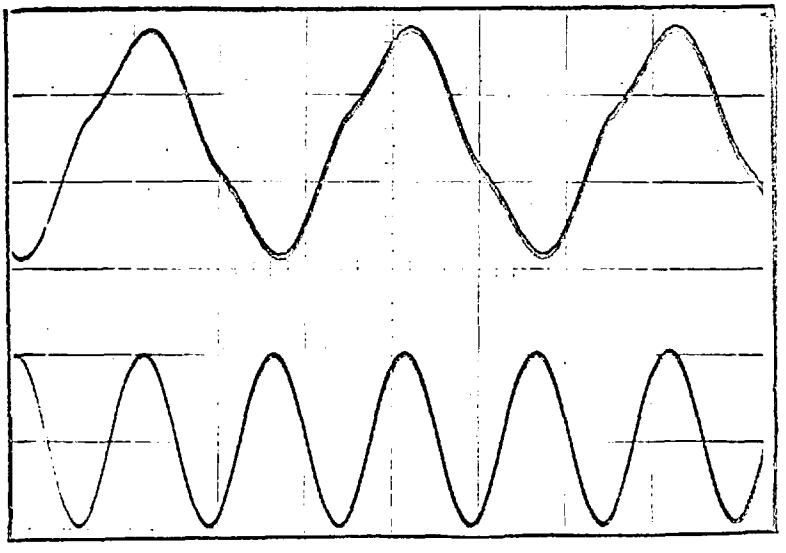
4.2 First-order quasi-static theory

Before we go on to consider parametrons in detail, it will be instructive to treat a typical device by means of an approximate small-signal quasi-static method due to Hilibrand et al[36]. This method by passes the formulation of actual differential equations. The example selected here is the Type IV(a) capacitive parametron, or BSP, the basic circuit of which is given in Figure 4.4.

The method is based on the expansion of the reactive nonlinearity in a power series about the total bias point V_o. Only the first two terms of this series will be retained. This at once restricts the validity of the analysis to small voltage excursions about V_o. By considering the voltages across and the currents flowing in this simplified nonlinear reactance, it will be possible to set up equivalent circuits for the parametron at the



(a) Resonant case: $f_s = f_o = 7.22$ Mc/s, $\nu = 1.0$. $V_p = 0.8$ volt, $V_s = 1.65$



(b) Detuned case: $f_s = 0.9 \cdot f_o = 6.48$ Mc/s, $\nu = 0.9$. $V_p = 1.0$ v, $V_s = 2.02$ v.

Figure 4.3 - Photographs of typical waveforms in BPP.

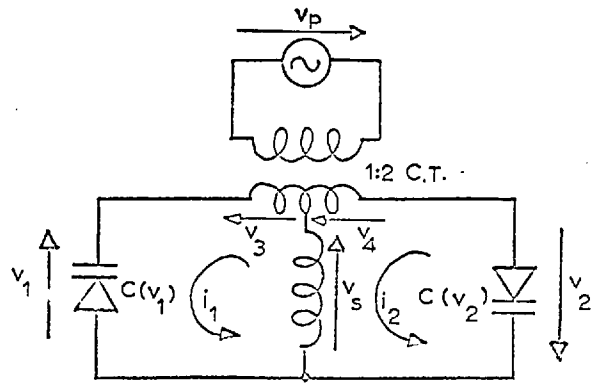


Figure 4.4 - Basic circuit of BSP.

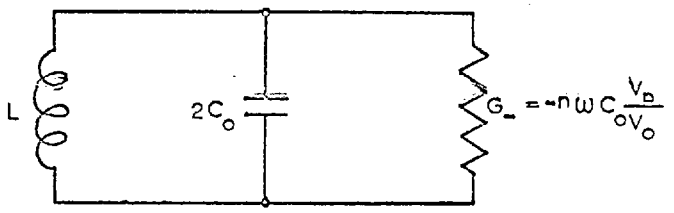


Figure 4.5(a) - Equivalent circuit at frequency ω when $\theta = 0, \pi$.

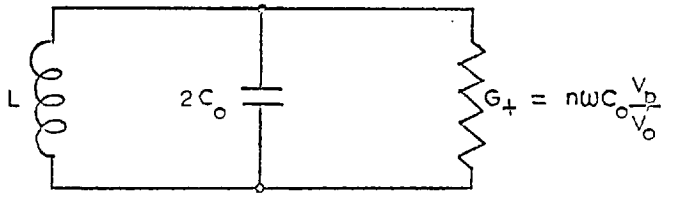


Figure 4.5(b) - Equivalent circuit at frequency ω when $\theta = \pm \frac{\pi}{2}$.

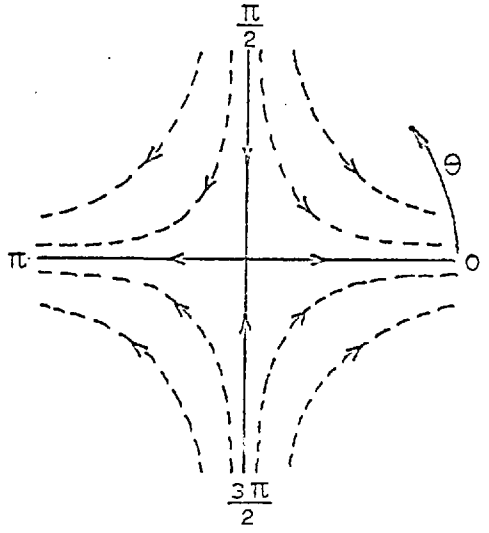


Figure 4.5(c) - Small-signal amplitude-phase relationship.

various frequencies of interest. It will be assumed that the rates of change of amplitude and phase of the subharmonic voltage v_s developed across L are negligibly small: this is the quasi-static assumption. It is not necessarily fulfilled in practice, but will greatly simplify the calculations.

It is assumed that there are no losses, that the transformer is ideal and that its ratio is 1:2 so that

$$v_3 = v_4 = -v_p \ .$$

The "accurate" varactor law is

$$C(v) = C_o(1 + \frac{v}{V_o})^{-n}$$

which is approximated here by its first-order expansion

$$C(v) \cong C_o(1 - n\frac{v}{V_o}). \qquad (4.1)$$

Now C(v) is by definition $\frac{dq}{dv}$, so that the current flowing in a varactor is

$$i = \frac{dq}{dv} \cdot \frac{dv}{dt} = C(v)\dot{v} \ .$$

Therefore $i_1 = C(v_1)\dot{v}_1$

and $i_2 = C(v_2)\dot{v}_2$.

also $v_1 = -v_p + v_s$

$v_2 = -v_p - v_s$,

so that the total varactor current is

$$i = i_2 - i_1 \cong C_o(1 - n\frac{v_2}{V_o})\dot{v}_2 - C_o(1 - n\frac{v_1}{V_o})\dot{v}_1$$

$$= C_o(\dot{v}_2 - \dot{v}_1) + \frac{nC_o}{2V_o}\frac{d}{dt}(v_1^2 - v_2^2)$$

$$= -2C_o\frac{d}{dt}\left[v_s(n\frac{v_p}{V_o} + 1)\right] \ .$$

In terms of the normalised quantities

$$x = \frac{v_p}{V_o} \quad , \quad y = \frac{v_s}{V_o}$$

this reads

$$i \cong -2C_o V_o \frac{d}{dt}\left[y(nx + 1)\right] \quad .$$

Let us define the pump by

$$x = X \sin 2\omega t = -j\tfrac{1}{2}X(e^{j2\omega t} - e^{-j2\omega t})$$

and assume that the subharmonic can be approximated by

$$\tilde{y} = Y \sin(\omega t + \theta) = -j\tfrac{1}{2}(Y_1 e^{j\omega t} - Y_1^* e^{-j\omega t}) \qquad (4.2)$$

where

$$Y_1 = Ye^{j\theta}$$

Then $\tilde{y}(nx + 1) = -j\frac{1}{2}(Y_1 e^{j\omega t} - Y_1^* e^{-j\omega t}) + \frac{1}{4}nX(Y_1 e^{-j\omega t} + Y_1^* e^{j\omega t})$,

in which we have rejected the cross-products $Y_1 e^{j3\omega t}$ and $Y_1^* e^{-j3\omega t}$ since they have been tacitly assumed negligible in (4.2). Differentiation yields the approximate current flowing in the inductor L at the subharmonic frequency ω:

$$\tilde{i} = -2\omega C_o V_o \left[\tfrac{1}{2}(Y_1 e^{j\omega t} + Y_1^* e^{-j\omega t}) + j\tfrac{1}{4}nX(-Y_1 e^{-j\omega t} + Y_1^* e^{j\omega t})\right] \quad .$$

If this is divided by $\tilde{v} = V_o\tilde{y}$, we obtain the approximate equivalent admittance due to the varactors at the subharmonic frequency. This appears in parallel with L and written in the usual notation is

$$Y_\omega = j2\omega C_o - n\omega C_o X \frac{Y_1^*}{Y_1}$$

$$= j2\omega C_o - n\omega C_o \frac{V_p}{V_o} e^{-j2\theta} \quad .$$

The first of these terms represents a capacitance of magnitude $2C_o$ while the second represents an admittance the nature of which depends on θ. Thus it is a pure negative conductance for $\theta = 0, \pi$, a pure positive conductance for $\theta = \pm \frac{\pi}{2}$, and becomes capacitive or inductive for $\theta = \frac{\pi}{4}$, $\frac{-3\pi}{4}$ or $-\frac{\pi}{4}$, $\frac{3\pi}{4}$ respectively.

It is to be noticed that, strictly speaking, the solution obtained by this analysis is neither steady-state nor transient, but applies only to the conditions obtaining shortly after the instant of turn-on when the amplitude of the subharmonic is very small and is changing extremely slowly.

The angle θ can be identified as the phase with which the oscillation is initiated, and upon which subsequent events depend, as we shall now show.

The equivalent circuit at the subharmonic frequency ω, when $\theta = 0$ or π, is shown in Figure 4.5(a). It consists of a tuned circuit in parallel with a negative conductance and therefore gives rise to exponentially growing oscillations. If, on the other hand, $\theta = \pm \frac{\pi}{2}$, then the equivalent circuit is as shown in Figure 4.5(b) and now contains a positive conductance which leads to exponentially decaying oscillations. Such considerations enable us to draw a rough diagram of the way in which the small-signal amplitude may be expected to change with variations in the initial phase angle, as indicated in Figure 4.5(c).

It is possible to determine the net power generated at the frequency ω. It is found that this also depends on θ. For $\theta = 0$ or π, the power generated is

$$P_\omega\Big|_{0,\pi} = + \tfrac{1}{2} n\omega C_o \cdot \frac{V_p V_s^2}{V_o} ,$$

but for $\theta = \pm \frac{\pi}{2}$, power is removed from the subharmonic oscillation:

$$P_\omega\Big|_{\pm\frac{\pi}{2}} = -\tfrac{1}{2}n\omega C_o \cdot \frac{V_p V_s^2}{V_o} \quad .$$

P_ω is zero at the intermediate phases $\pm\frac{\pi}{4}$, $\pm\frac{3\pi}{4}$ for which the device is purely reactive.

It is possible to calculate the current flowing in one of the varactors and hence the admittance of a varactor at the pump frequency. The result is

$$\tfrac{1}{2}Y_{2\omega} = j2\omega C_o + \tfrac{1}{2}n\omega C_o \frac{Y_1^2}{X}$$

$$= j2\omega C_o + \tfrac{1}{2}n\omega C_o \frac{V_s^2}{V_o V_p} \quad ,$$

that is, a capacitance C_o in parallel with a conductance $\frac{1}{2}\ G_{2\omega}$ which is always positive. The power supplied by the pump is therefore

$$P_{2\omega} = \left(\frac{V_p}{\sqrt{2}}\right)^2 \cdot G_{2\omega} = \tfrac{1}{2}\ n\omega C_o \cdot \frac{V_s^2 V_p}{V_o} \quad ,$$

since there are two varactors. This is equal to the power P_ω generated at the subharmonic frequency at the particular phase-angles 0 or π. Power-balance occurs only at these phase angles. Conservation of energy therefore means that the small-signal subharmonic phase angle must tend to one or other of these values.

The nonlinear reactance will generate harmonics of the subharmonic frequency ω. Since the system is balanced, only the odd harmonics will occur. Thus if we include a term $-j\frac{1}{2}(Y_3 e^{j3\omega t} - Y_3^* e^{-j3\omega t})$ in the assumed solution $\tilde{y}$ to account for the third harmonic, the admittance appearing in parallel with L at the frequency ω is found to be

$$Y_\omega = j2\omega C_o - n\omega C_o X \frac{Y_1^* + Y_3}{Y_1} \quad .$$

However, since the amplitude and phase of the third harmonic are not known in relation of those of the subharmonic, the present method does not enable us to discover its effect on the admittance y_ω, and no advantage is to be obtained by its inclusion.

To sum up, the method described here does indicate that the small-signal equivalent circuit of a parametron is, in a sense, a function of the past history of the device. However, it has several serious shortcomings among which may be mentioned the following.

(1) No steady-state solution is predicted.

(2) The solution which is obtained fails to hold rigorously under transient conditions. For example, the equivalent circuit of Figure 4.5(a) suggests an amplitude solution

$$Y(t) = Y(0).e^{+kt} ,$$

but such a solution violates the quasi-static assumption.

(3) Detuned cases are not covered.

It is therefore necessary to investigate other possible methods of attack.

4.3 Piecewise-linear theory

In the previous section the example of the BSP has been analysed by means of a small-signal quasi-static method. The results were found to be of very limited application. In this section the possibilities of the method of piecewise-linearisation will be investigated. For comparative purposes, the problem selected here is the same as the one treated in the last section.

In the piecewise-linear (PWL) method the nonlinearity is represented

by a chain of straight-line elements. The greater the number of elements, the more accurate is the representation and the final result of the analysis. In the present case, the nonlinear charge-voltage characteristic of a varactor will be represented by a highly approximate model consisting of two straight-line elements, as shown in Figure 4.6(a). The varactor is supposed to have two possible states, the Z-state in which the capacitance is zero, and the I-state in which it is infinite. The properties of these states are summarised below.

State	Varactor capacitance	Varactor voltage	Varactor charge
Z	0	$v > -V_o$	$q = 0$
I	∞	$v = -V_o$	$q < 0$

In the Z-state the varactor can have any constant charge without affecting the results. The charge is here assumed to be zero for simplicity. In the following analysis, charge-storage effects are neglected.

The previous section used an approximation, equation (4.1), to the nonlinear capacitance function which consisted of a single straight line on the (C, v)-plane. The slope of this line was a function of the exponent n, and the representation was valid only for very small signal levels. The present two-line representation, on the other hand, will apply only for large signal amplitudes. We shall not specify how large at this point.

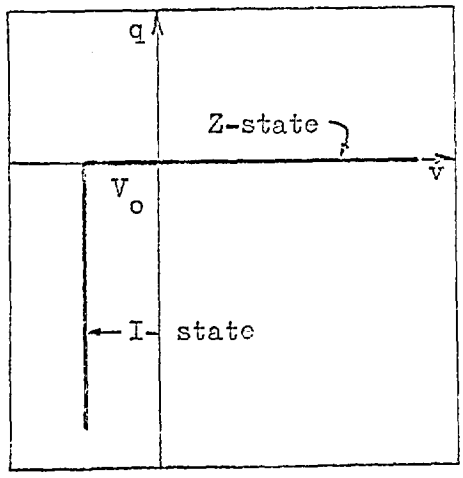


Figure 4.6(a) -

Idealisation of varactor voltage-charge characteristic.

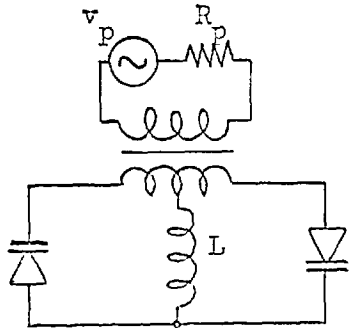


Figure 4.6(b) -

Physical circuit.

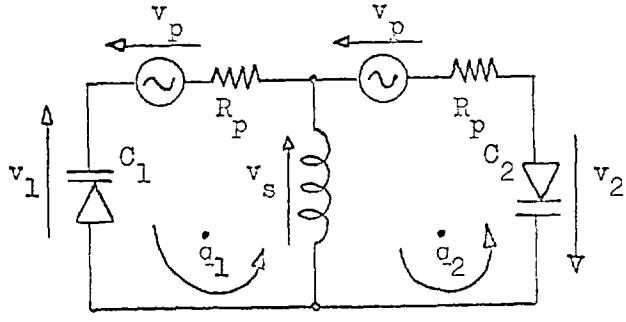


Figure 4.6(c) -

Equivalent circuit for piecewise-linear analysis.

Figure 4.6(b) shows the physical circuit of the BSP to be analysed. It is similar to that of Figure 4.4 but has in addition a series loss element R_p in the pump circuit. It is found that this resistance must be included if the details of the large-signal waveforms are to be explained. A load R_L in parallel with the inductor L is insufficient for this purpose.

The equivalent circuit is given in Figure 4.6(c). R_p appears twice because the input transformer is taken to be ideal and has been eliminated.

The nature of the mechanism of the large-signal subharmonic oscillation will be clarified if at first the influence of the damping is neglected. The following sub-section treats this zero-damped case.

4.3.1 The case of zero damping

Three circuit equations apply for all possible combinations of the varactor states Z and I. The subscripts 1 and 2 will refer to quantities associated with the varactors C_1 and C_2 respectively. The individual varactor voltages are

$$v_1 = v_p + v_s \geqslant -V_o , \tag{4.3}$$

$$v_2 = v_p - v_s \geqslant -V_o , \tag{4.4}$$

while the subharmonic voltage appearing across L is

$$v_s = L(\ddot{q}_2 - \ddot{q}_1) . \tag{4.5}$$

Since there are two varactors, each of which can exist in two states, there are four possible parametron modes. They are:

(1) the $Z_1 Z_2$ - mode in which both varactors are in the zero-capacitance state,

(2) the Z_1I_2- mode } in which the varactors are in

(3) the I_1Z_2- mode } different states and

(4) the I_1I_2- mode , in which both varactors are in the infinite-capacitance state. The behaviour of the parametron will be examined for each mode separately. Mode-sequencies corresponding to physical types of oscillation will then be determined.

The pump will be supposed to be a perfect voltage source except when presented with a short circuit. In that case, zero output voltage will be assumed.

4.3.1.1 The Z_1Z_2- mode

This mode is characterised by $q_1 = 0$ and $q_2 = 0$. It follows that the subharmonic current $i_s = \dot{q}_2 - \dot{q}_1$ is zero. Equation (4.5) shows that the subharmonic voltage v_s is also zero. The system is balanced, so that no power is transferred from the pump to the subharmonic oscillation. The pump voltage is impressed directly across the varactors. Equations (4.3) and (4.4) show that a necessary condition for the mode is

$$v_p > -V_o ,$$

or in terms of the normalisations established in the previous section

$$x > -1 . \qquad (4.6)$$

This means that the negative excursion of the pump oscillation must not exceed the total bias voltage if the mode is to exist.

4.3.1.2 The Z_1I_2- mode

Here the varactor C_1 is in the zero-capacitance state while the varactor C_2 is in the infinite-capacitance state. The parametron is unbalanced and

pump power is transferred to the subharmonic frequency. The varactor voltages are

$$v_1 = v_p + v_s > -V_o , \tag{4.7}$$

$$v_2 = v_p - v_s = -V_o , \tag{4.8}$$

while the varactor currents are

$$\dot{q}_1 = 0 , \tag{4.9}$$

$$\dot{q}_2 \neq 0 . \tag{4.10}$$

Equation (4.8) shows that the subharmonic voltage is

$$v_s = v_p + V_o$$

or in normalised form

$$y = x + 1 .$$

For the particular pumping function

$$x = X \sin 2\omega t$$

used in the previous section, this reads

$$y = X \sin 2\omega t + 1 . \tag{4.11}$$

Elimination of v_s from equations (4.7) and (4.8), followed by normalisation, indicates that the condition for the existence of the $Z_1 I_2$ mode is again

$$x > -1 . \tag{4.12}$$

The subharmonic current i_s during the mode can be found from equation (4.5). Since $q_1 = 0$,

$$v_s = L\ddot{q}_2$$

so that

$$i_s = \frac{1}{L} \int v_s \, dt.$$

In normalised form, the solution of this is

$$\xi = X(1 - \cos 2\omega t) + 2\omega t + \xi(0) \quad , \qquad (4.13)$$

where $\xi = \frac{2\omega L i_s}{V_o}$, the dimensionless subharmonic current and $\xi(0)$ is its value at $t = 0^o$.

4.3.1.3 The I_1Z_2- mode

This is similar to the Z_1I_2- mode, but the rôles of the two varactors are now reversed. Proceeding as before, the subharmonic voltage is found to be

$$y = - X \sin 2\omega t - 1 \qquad (4.14)$$

under the condition

$$x > - 1.$$

The subharmonic current is

$$\xi = - X(1 - \cos 2\omega t) - 2\omega t - \xi(0) \, . \qquad (4.15)$$

4.3.1.4 The I_1I_2- mode

The fourth possibility is the mode in which both varactors are in the infinite-capacitance state. The varactor voltages are both fixed:

$$v_1 = v_p + v_s = - V_o$$

$$v_2 = v_p - v_s = - V_o \, .$$

Addition of these equations shows that

$$v_p = - V_o$$

or $$x = - 1 \qquad (4.16)$$

which means that the pump is presented with a "short-circuiting" voltage-V_o and limits at this value. Subtraction of the equations shows that the

subharmonic voltage v_s is zero. Equation (4.5) then indicates that the subharmonic current i_s is constant during the mode.

4.3.1.5 Mode-sequences

If $X < 1$, no subharmonic oscillation is possible and the behaviour of the parametron is described by the Z_1Z_2- mode. At $X = 1$, oscillation consisting of an alternation of Z_1I_2 and I_1Z_2- modes "suddenly" commences. If $X > 1$, oscillation continues, but now I_1I_2- modes appear interspersed between the Z_1I_2 and I_1Z_2- modes.

Thus the simplest mode-sequence supporting oscillation occurs for $X = 1$. Let us consider this case. Since the system is balanced, it will be sufficient to consider only one subharmonic half-cycle. The other half-cycle will follow by symmetry. In the Z_1I_2 mode, the voltage waveform is given by equation (4.11) and is shown in Figure 4.7(b).

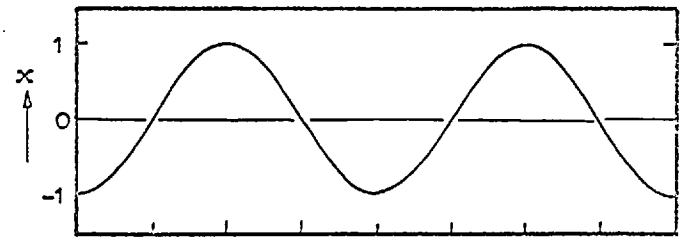
The current waveform is given by equation (4.13) which contains an undetermined constant $\xi(0)$. It is possible to express this constant in terms of t_1, the instant at which the mode commences. To do this, we first notice that the subharmonic voltage must obey the boundary condition

$$y(t_1) = -y(t_1 + \frac{\pi}{\omega}). \qquad (4.17)$$

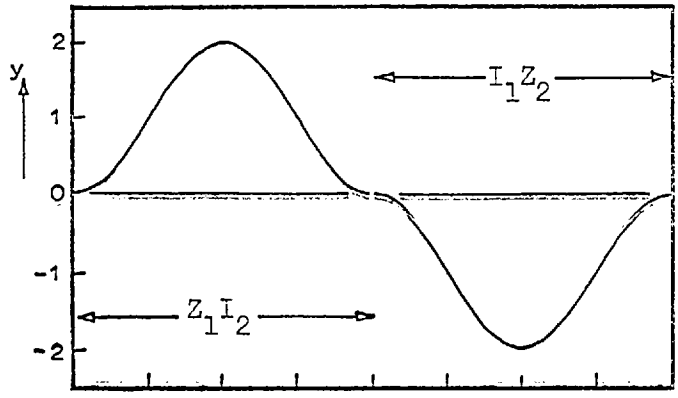
If equation (4.11) is substituted into this, the following expression for t_1 is obtained:

$$\sin 2\omega t_1 = -\frac{1}{X} . \qquad (4.18)$$

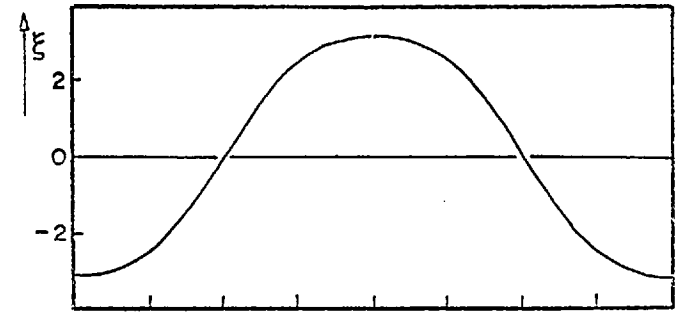
It is evident that t_1 cannot exist for $X < 1$. The next step is to formulate a boundary condition on the subharmonic current. Since this current flows in the inductor L, it cannot be discontinuous. It must therefore obey the



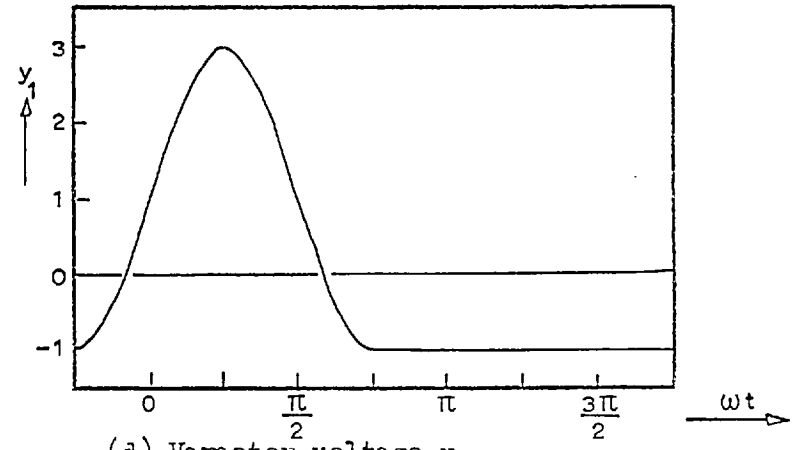
(a) Pump voltage x.



(b) Subharmonic voltage y.



(c) Subharmonic current ξ .



(d) Varactor voltage y_1.

Figure 4.7 - BSP waveforms predicted by the PWL method.
Conditions: zero damping, X = 1.0.

condition

$$\xi(t_1) = -\xi(t_1 + \frac{\pi}{\omega}). \qquad (4.19)$$

This can be used to eliminate $\xi(0)$ from equation (4.13), yielding for the current

$$\xi(t) = X(\cos 2\omega t_1 - \cos 2\omega t) + 2\omega(t - t_1) - \pi . \qquad (4.20)$$

Finally, by putting X = 1 in equation (4.18), we find

$$t_1 = -\frac{\pi}{4\omega} ,$$

so that the solution is

$$\xi(t) = 2\omega t - \cos 2\omega t - \frac{\pi}{2} . \qquad (4.21)$$

The current waveform specified by this expression is shown in Figure 4.7(c). It should be remarked that the amplitude $\frac{\pi V_o}{2\omega L}$ of the un-normalised current is a function of the frequency ω, whereas the amplitude of the voltage is not.

If the pump amplitude X is increased beyond unity, I_1I_2- modes appear between the Z_1I_2 and I_1Z_2- modes. The oscillation is now described by the sequence

$$-Z_1I_2 \; -I_1I_2 \; -I_1Z_2 \; -I_1I_2 \; -Z_1I_2 \; - \text{etc.}$$

Since y is zero during the I_1I_2- modes, the boundary condition (4.17) still applies. Equation (4.18) for the time t_1 at which the Z_1I_2- mode begins therefore remains valid. The current ξ is <u>constant</u> during the I_1I_2- modes, so that the boundary condition (4.19) can no longer be applied to the Z_1I_2- mode. It can be seen by symmetry that ξ must be zero at $t = \frac{\pi}{4\omega}$. Equation (4.13) then gives

$$\xi(t)\Big|_{Z_1I_2} = 2\omega t - X \cos 2\omega t - \frac{\pi}{2} . \qquad (4.22)$$

Figure 4.8 shows the various waveforms in the BSP calculated for the case X = 3.0. The waveforms are very similar to those observed experimentally under conditions of heavy pumping. This may be seen by comparing the predicted voltage and current waveforms of Figure 4.8(b),(c) with the photograph of Figure 4.9.

Figure 4.10 shows the theoretical and experimental relations between the pump amplitude X and the subharmonic amplitude Y. For the present case of zero damping, the theoretical (X,Y)-profile is independent of frequency. In practice, the shape of the profile does depend on the frequency to some extent, particularly near resonance, $\nu = 1.0$. However, resonance implies "small-signal" operation, for which the PWL method is inappropriate. If the subharmonic frequency is detuned sufficiently away from resonance, the shape of the (X,Y)-profile becomes relatively insensitive to frequency variations. The experimental profile in Figure 4.10. was measured for such a detuning, $\nu = 0.6$. It can be seen that the agreement with theoretical predictions is surprisingly good, considering the extreme approximation made concerning the nonlinear reactance characteristic of the varactors. Certain differences between the theoretical and practical curves should be pointed out.

(1) The experimental profile exhibits hysteresis, whereas the theoretical result does not. It is apparently necessary to invoke damping if this phenomenon is to be explained by the PWL method. *

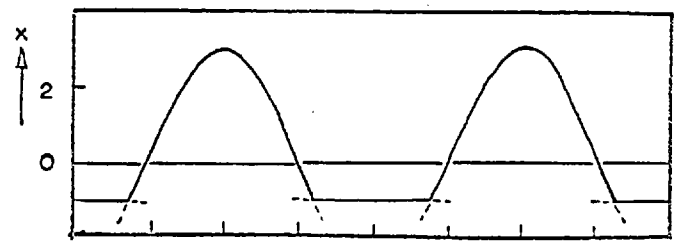
(2) The slopes of the profiles are similar in the range

$$1.0 < X < 2.0 ,$$

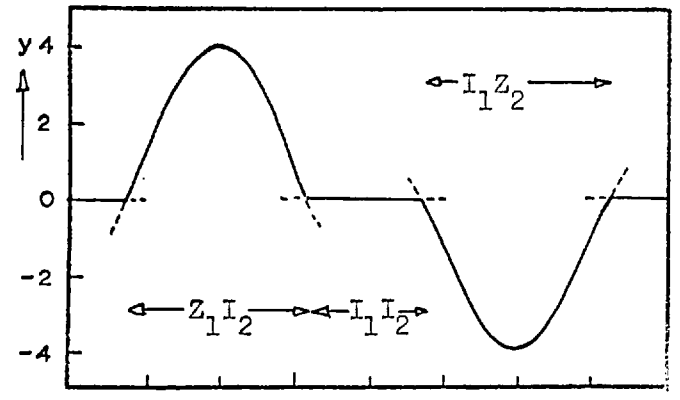
although theory predicts a larger subharmonic voltage amplitude than is

---

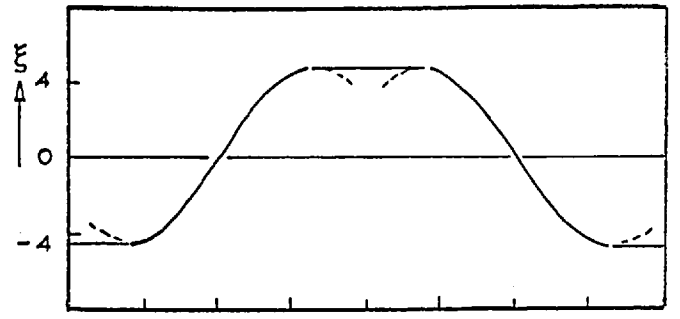
* We shall see in Chapter 6 that another theoretical approach predicts hysteresis even in the lossless case.



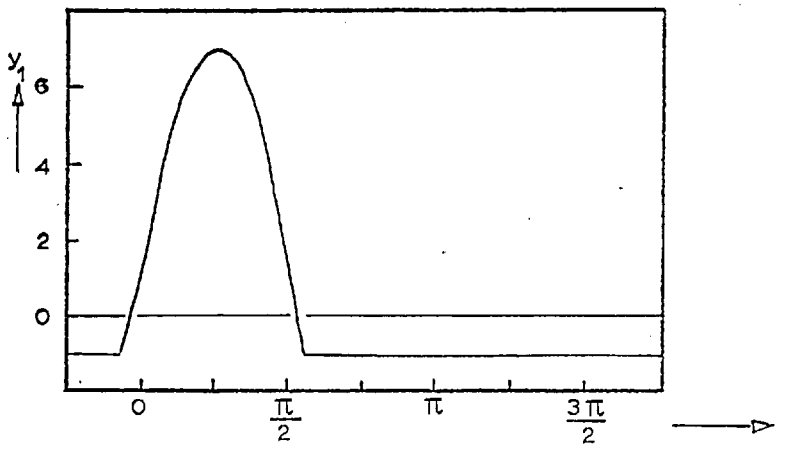
(a) Pump voltage x.



(b) Subharmonic voltage y.



(c) Subharmonic current ξ .



(d) Varactor voltage y_1.

Figure 4.8 -

BSP waveforms predicted by the PWL method.
Conditions: zero damping, X= 3.0.

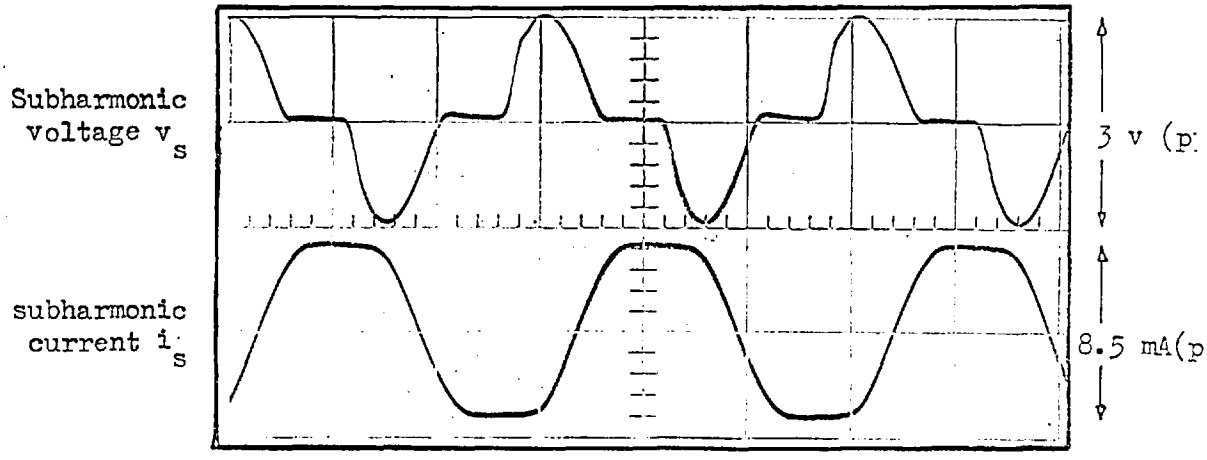


Figure 4.9 -

Subharmonic voltage and current waveforms for a typical practical BSP. (Photograph).

Experimental circuit:

SVC 3RE silicon varactor diodes,

$R_p = 50\ \Omega$,

resonant subharmonic frequency $f_o = 4.67$ Mc/s.

Operating conditions:

Frequency of operation $f_s = 2.8$ Mc/s,

$\therefore f_s/f_o = \nu = 0.6$,

pump voltage amplitude $V_p = 1.0$ volts,

total bias voltage $V_o = 0.7$ volts,

$\therefore X = 1.43$.

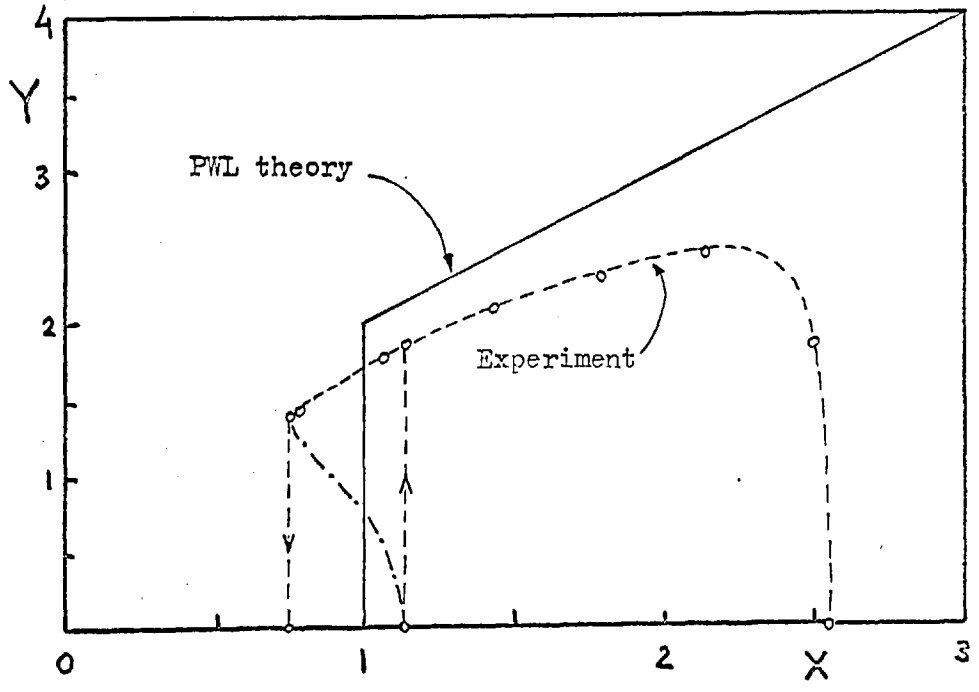


Figure 4.10 -

(X,Y) - profile for typical experimental BSP compared with curve given by PWL theory for the case of zero-damping.

Experimental circuit:

SVC 3RE silicon varactor diodes.

R_p = 50 Ω (internal resistance of pump).

f_o = Resonant subharmonic frequency = 4.67 Mc/s,

f_s = frequency of oscillation = 2.8 Mc/s

$f_s/f_o = \nu = 0.6$.

V_o = 0.7 volt.

observed in practice. The difference can be attributed to degradation of the performance of the physical parametron because of

(1) dissipation and

(2) the use of varactors with a reactance characteristic less nonlinear than was assumed in the theory.

(3) The amplitude Y of the theoretical profile increases linearly as X increases, but the experimental curve falls to zero at X = 2.55. The abrupt cessation of oscillation is caused by dissipation due to forward diode-conduction in the varactors. This nonlinear damping becomes important only for fairly large values of X.

4.3.1.6 Transient response in the case of zero damping

In the present lossless case, theory predicts that if the pump voltage is suddenly applied to the parametron, the oscillation immediately commences at its steady-state amplitude. This is at variance with the experimental observation that several cycles of subharmonic oscillation are required for the amplitude to build up to the steady-state value. It is evident that transient phenomena cannot be explained by the PWL method unless damping is included.

4.3.2 The case of finite damping

In the foregoing sub-section the possibilities of the PWL method have been explored for the lossless case. Several shortcomings were apparent, some of which were due to omission of the damping. Let us now attempt to find the corresponding results when the pump-circuit resistance R_p is not negligible.

The parametron can still exhibit four different modes, as in the lossless case. The no-oscillation Z_1Z_2-mode is unaffected by the introduction of R_p. The unbalanced Z_1I_2 and I_1Z_2-modes, however, become more difficult to treat theoretically because of the appearance of the time-constant L/R_p. The I_1I_2-mode is also influenced by this time-constant, but can be dealt with quite simply because the output terminals are disconnected from the pump in this balanced condition.

The equations corresponding to (4.3) and (4.4) for the varactor voltages are now

$$v_1 = v_p + v_s - R_p \dot{q}_1 \geqslant -V_o , \qquad (4.23)$$

$$v_2 = v_p - v_s - R_p \dot{q}_2 \geqslant -V_o , \qquad (4.24)$$

while equation (4.5) for the inductor voltage remains unchanged.

The calculations will be considerably simplified if time, frequency and current are normalised with respect to the time-constant L/R_p:

$$\tau' = \frac{R_p t}{L} \text{ , a dimensionless time-variable,}$$

$$\nu' = \frac{\omega L}{R_p} \text{ , the dimensionless frequency,}$$

$$\xi' = \frac{R_p \dot{q}}{V_o} \text{ , the dimensionless current.}$$

These three quantities have specialised definitions in this sub-section. For this reason they are primed to distinguish them from the similar, but differently defined, quantities used elsewhere. (Thus τ and ν are defined with respect to the resonant angular frequency ω_o. Such a frequency does not exist in the present case).

The Z_1Z_2-mode equations are the same as in the lossless case, while the equations for the Z_1I_2, I_1Z_2 and I_1I_2- modes are derived in Appendix 4.1.

The complete set of equations is summarised below for convenience.

$Z_1 Z_2$-mode				
Subharmonic voltage	:	y	$= 0.$	(4.25)
Subharmonic current	:	ξ'	$= 0$	(4.26)
Constraint	:	x	> -1	(4.27)

$Z_1 I_2$-mode	
$y = \frac{2\nu' X}{1+4\nu'^2}\left[2\nu' \sin 2\nu'\tau' + \cos 2\nu'\tau'\right] + \left[y(0) - \frac{2\nu' X}{1+4\nu'^2}\right] e^{-\tau'}$	(4.28)
$\xi' = x - y + 1$	(4.29)
$y > -(1 + x)$	(4.30)

$I_1 Z_2$-mode	
$y = -\frac{2\nu' X}{1+4\nu'^2}\left[2\nu' \sin 2\nu'\tau' + \cos 2\nu'\tau'\right] + \left[y(0) + \frac{2\nu' X}{1+4\nu'^2}\right] e^{-\tau'}$	(4.31)
$\xi' = -(x + y + 1)$	(4.32)
$y < 1 + x$	(4.33)

$I_1 I_2$-mode	
$y = y(0)\, e^{-\tau'/2}$	(4.34)
$\xi' = -2y$	(4.35)

The "initial conditions" $y(0)$ in the above expressions are to be interpreted as being defined separately for each mode.

4.3.2.1 Mode-sequences in the case of finite damping

The simplest conceivable mode-sequence leading to subharmonic oscillation is again an alternation of Z_1I_2 and I_1Z_2 modes. Let the Z_1I_2-mode begin at τ_1' and end at $\tau_1' + \frac{\pi}{\nu'}$. At these instants the subharmonic currents must be equal and opposite, giving the following boundary condition on ξ':

$$\xi'(\tau_1') = -\xi'(\tau_1' + \tfrac{\pi}{\nu'}), \tag{4.36}$$

corresponding to (4.19). Substitution of equation (4.29) into this yields

$$x(\tau_1') - y(\tau_1') + 1 = -x(\tau_1' + \tfrac{\pi}{\nu'}) + y(\tau_1' + \tfrac{\pi}{\nu'}) - 1 \tag{4.37}$$

There is a similar boundary condition on y at the beginning and end of the mode:

$$y(\tau_1') = -y(\tau_1' + \tfrac{\pi}{\nu'}). \tag{4.38}$$

If y is eliminated between this and (4.37) there results

$$x(\tau_1') + x(\tau_1' + \tfrac{\pi}{\nu'}) + 2 = 0. \tag{4.39}$$

With the assumed function for $x(\tau')$, this gives for the instant at which the mode starts

$$X.\sin 2\nu'\tau_1' + 1 = 0. \tag{4.40}$$

If $X > 1$, then in one complete pump-cycle there are two possible values of τ_1' which satisfy this equation. Experiment indicates that actual values of τ_1' lie in the range

$$-\frac{\pi}{2\nu'} \leqslant \tau_1' \leqslant -\frac{\pi}{4\nu'}$$

for the particular mode-sequence considered. The least pump amplitude which will support subharmonics is again X = 1.0.

To find the voltage solution, the unknown constant y(0) in equation (4.28) can be expressed in terms of τ_1' by means of (4.38). The complete solution for y during the Z_1I_2-mode is found to be

$$y(\tau') = \frac{2\nu' X}{1+4\nu'^2}\left[2\nu'\sin 2\nu'\tau' + \cos 2\nu'\tau' - \frac{2e^{(\tau_1'-\tau')}}{1+e^{-\pi/\nu'}}(2\nu'\sin 2\nu'\tau_1' + \cos 2\nu'\tau_1')\right], \tag{4.40}$$

starting at the amplitude

$$y(\tau_1') = \frac{2\nu' X}{1+4\nu'^2}(2\nu'\sin 2\nu'\tau_1' + \cos 2\nu'\tau_1')\tanh\frac{\pi}{2\nu'} . \tag{4.41}$$

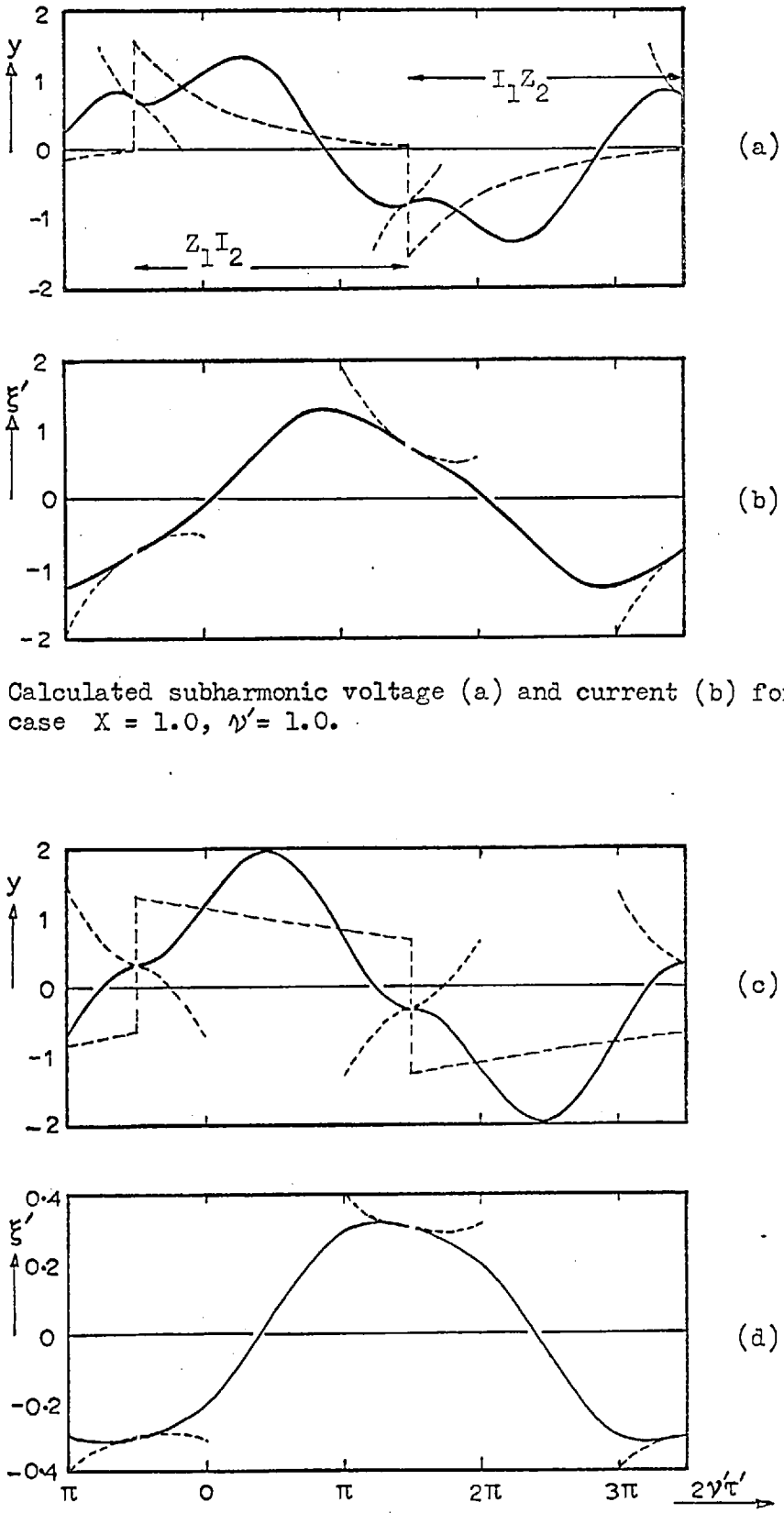
Equation (4.40) is of the form

$$y(\tau') = A.\sin(2\nu'\tau' + \varepsilon) + B.e^{-\tau'} .$$

Thus the voltage waveform is composed of a sequence of segments, each consisting of the sum of a sinusoid and a decaying exponential. The coefficients A and B are such that the boundary conditions are satisfied.

Figure 4.11 contains voltage and current waveforms calculated according to equations (4.40) and (4.29) respectively for two different values of ν'. The smaller value corresponds to heavy damping and/or low frequencies, the larger to light damping and/or high frequencies. The functions $\pm B.e^{-\tau'}$ have been superimposed upon the voltage waveforms in order to clarify the manner in which they are built up. These theoretical waveforms are very similar to those encountered in practice. As an example, Figure 4.12 shows typical experimental voltage and current waveforms for a case in which damping due to R_p is important. This photograph should be compared with the calculated results of Figure 4.11(c) and (d).

Figure 4.11 also illustrates the point that if X is kept constant at the value 1.0, and if the frequency ν is reduced, then the peak amplitude Y of the subharmonic voltage also decreases. This is in accord with



Calculated subharmonic voltage (a) and current (b) for the case X = 1.0, ν' = 1.0.

Calculated voltage (c) and current (d) for the case X = 1.0, ν' = 5.0.

Figure 4.11 - Waveforms in BSP with finite damping. PWL method.

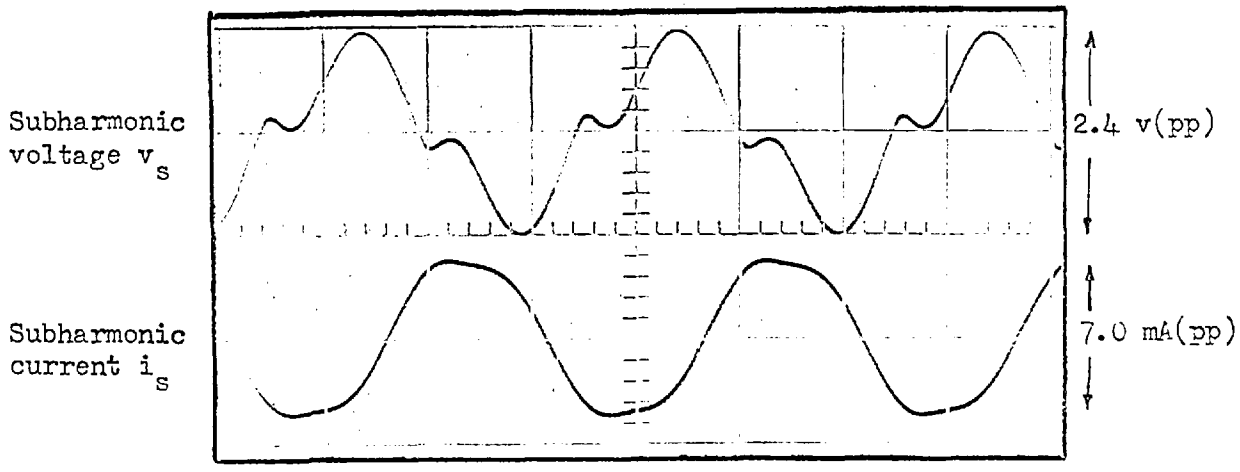


Figure 4.12 -

Subharmonic voltage and current waveforms in a typical BSP under conditions for which the damping due to R_p is important. (Photograph).

Experimental circuit:

Same as for Figure 4.9.

Operating conditions:

Frequency of operation f_s = 2.8 Mc/s,
therefore $f_s/f_o = \nu = 0.6$;
pump voltage amplitude V_p = 0.6 volts,
total bias voltage V_o = 0.7 volts,
therefore X = 0.86.

R_p = 50 Ω, L = 19 μH,
therefore $\nu' = \omega L/R_p = 6.7$.

experimental observations.

The good agreement obtained here is all the more remarkable when it is noticed that the calculated waveforms do not always satisfy the conditions (4.30) and (4.33). The interpretation of this anomaly must be that the initial assumptions upon which the theory is based are not strictly realistic ones. Thus the (q,v)-characteristic of a real varactor is less sharp than has been assumed here, so that in practice the varactor voltage excursions are <u>not</u> abruptly curtailed when the "infinite-capacitance" I-state is reached.

The only way in which mathematical rigour can be achieved in the PWL analysis of a lossy parametron is to specify that the oscillation must always consist of the mode-sequence

$$- Z_1 I_2 - I_1 I_2 - I_1 Z_2 - I_1 I_2 - \text{etc.}$$

It was found in the lossless case that the duration of the $I_1 I_2$-mode decreased to zero as X was reduced towards unity. In the present case, however, it is necessary for these modes to persist even for X = 1.0.

The ensuing calculations are complicated by the fact that the starting-times of two different modes must now be determined (instead of just τ_1'). Indeed, it is found that the relevant times can be calculated only by solving a pair of simultaneous trancendental equations.* This would require

---

* The equations in question are

$$-1 - x(\tau_1') = (1+x(\tau_o')) \, e^{-\frac{1}{2}(\tau_1' - \tau_o')}$$

and

$$2(1+x(\tau_o')) e^{-(\tau_1' - \tau_o')} = \left[\frac{2\nu' X}{1+4\nu'^2}(2\nu' \sin 2\nu'\tau_1' + \cos 2\nu'\tau_1') + 1 + x(\tau_1')\right]\left[e^{-\pi/\nu'} - 1\right],$$

where τ_o' is the starting-time of an $I_1 I_2$-mode and τ_1' of a $Z_1 I_2$-mode. Were it not for the factor $\frac{1}{2}$ in the exponent of the first equation, the solution would be a comparatively simple matter.

the use of graphical or numerical (computer) techniques. Since the object of the present work is to find purely algebraic explanations of the mechanism of subharmonic oscillation, this line of attack has been discontinued.

4.3.3 Criticism of the piecewise-linear approach

The primary advantage of the PWL approach is its ability to predict complicated waveforms. However, the nature of the mathematics associated with the method is such that it does not afford a suitable basis for the formulation of a more general or more accurate theory. In particular, there seems to be little prospect of the emergence of a useful treatment of the transient phenomena.

4.4 Possible ways in which the differential equations of varactor parametrons may be formulated

Up to this point, the mechanism of subharmonic oscillation has been investigated by two quite different approaches. The first, an essentially small-signal method, led to equivalent circuits for the various frequencies of interest. These circuits gave a useful intuitive picture of how the oscillations arise, but not to quantitatively realistic results. The second method, which was applicable only to the investigation of large-signal phenomena, gave remarkably good results for the steady-state waveforms and for the detuned (X,Y)-profile in the case of a lossless parametron. However, when dissipation was introduced, the method was not entirely satisfactory, and quickly led to analytical difficulties.

Neither approach gave any prospect of an adequate treatment of the

transient phenomena. In the first method, the limitation was the quasi-static assumption. The second method gave no useful information about the transient response in the lossless case. In the dissipative case cycle-by-cycle transients would have to be computed numerically, a laborious and uninformative process. An analytical solution would certainly not be possible.

The inevitable conclusion is that the problem must be attacked by means of the solution of differential equations. Attention will now be directed to this end. In order to establish a secure foundation on which to base more exact calculations, we shall in this section derive and discuss the differential equations of certain simple unbalanced parametrons. In the next Chapter, these will be extended to include the more useful balanced types.

All parasitic (i.e. non-essential) elements will, for the moment, be omitted. They are important only when accurate results are required, and tend to complicate the simplicity sought at this stage.

Contrary to the situation in a linear system, the nature of the differential equation of a nonlinear system depend on the way in which it is formulated.[54] Certain forms of the equation may be very much more amenable to reasonably accurate analysis than others. This point may be illustrated by referring to the simple nonlinear-capacitance parametron, Type III(b) of Table 4.1.

For convcience, the circuit of this device is re-drawn in more detail in Figure 4.13. The instantaneous pump-voltage is v_p and the voltage across the linear tuning inductor L is v_L. The instantaneous current $\dot{q}$ is the rate of change of the charge on the nonlinear capacitor C(v). For the sake of a concrete example, this capacitor is taken to be a varactor, oriented as

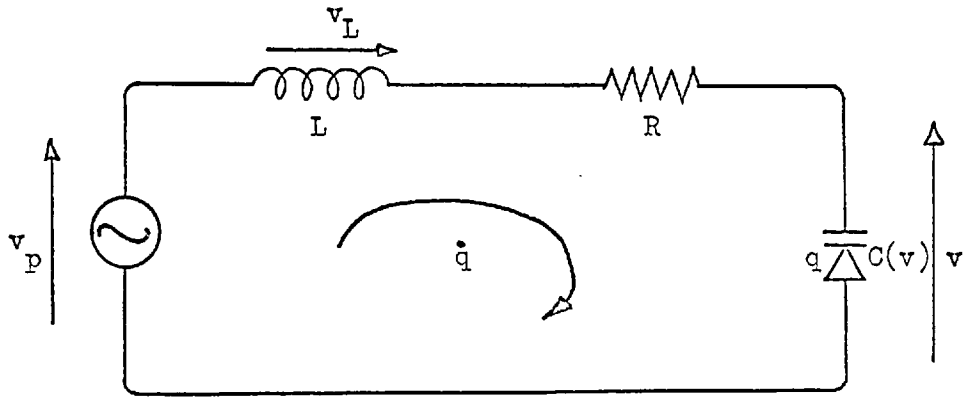


Figure 4.13 -

Idealised Type III(b) Varactor Parametron.

indicated by the diode symbol. The instantaneous voltage across the varactor is v. Finally, the circuit contains a series loss-resistance R to account for resistance in the pump source and other parts of the parametron.

The following discussion will use the normalisations x, y and z for the pump voltage, subharmonic voltage and varactor charge respectively, as defined previously.

By summing the voltages around the loop:

$$L\,C_o\,\ddot{z} + R\,C_o\,\dot{z} + y = x. \qquad (4.42)$$

Now let us put $L\,C_o = 1/\omega_o^2$, $\omega_o C_o R = k$, and normalise the time-variable:

$$\tau = \omega_o t,$$

then

$$\frac{d^2z}{d\tau^2} + k\,\frac{dz}{d\tau} + y = x\,, \qquad (4.43)$$

which can be written

$$\overset{oo}{z} + k\overset{o}{z} + y = x, \qquad (4.44)$$

where the circles signify differentiation with respect to the normalised time. This equation superficially resembles a linear equation, but only because an explicit nonlinear relation between the varactor voltage y and charge z has not yet been introduced. This may be done in three different ways.

(1) Let us take the varactor law in the form of equation (3.5), Chapter 3:

$$C(v) = C_o\,(1 + \frac{v}{V_o})^{-n}\,, \qquad (4.45)$$

Let the variable for the differential equation be the varactor voltage v. Then since $\frac{dq}{dv} = C(v)$,

$$\dot{q} = C(v)\,\dot{v},$$

$$\text{or} \quad \dot{z} = (1+y)^{-n}\,\dot{y},$$

so that the First Form of the differential equation is

$$\boxed{\frac{d}{d\tau}\left[(1+y)^{-n}\,\dot{y}\right] + k(1+y)^{-n}\,\dot{y} + y = x(\tau)} \qquad (4.46)$$

where, for example, $x(\tau) = X \cdot \sin 2\nu\tau$ for $\frac{1}{2}$th-order subharmonic oscillations.

(2) A second possibility is to take the same form of the nonlinear reactance law, but to let the main variable be the voltage across the inductor, $v_L = v - v_p$. Then a Second Form of the differential equation is

$$\frac{d}{d\tau}\left[(1+x+y)^{-n}\,(\dot{x}+\dot{y})\right] + k(1+x+y)^{-n}\,(\dot{x}+\dot{y}) + y = 0,$$

where now $y = \dfrac{v_L}{V_o}$. This can be written more simply:

$$\boxed{\frac{1}{1-n}\cdot\frac{d^2}{d\tau^2}\left[(1+x+y)^{1-n}\right] + \frac{k}{1-n}\cdot\frac{d}{d\tau}\left[(1+x+y)^{1-n}\right] + y = 0.} \qquad (4.47)$$

Notice that the pumping function x is now imbedded in the nonlinear parts of the equation.

(3) The third and most interesting result is obtained when one works in terms of the variable q, the charge on the varactor junction. To this end we use the $v = \mathcal{J}(q)$ representation of the varactor, as derived in Sub-Section 3.2.3, Chapter 3:

$$v = V_o\left[\left(\frac{1-n}{C_o V_o}\cdot q + 1\right)^{\frac{1}{1-n}} - 1\right], \qquad (4.48)$$

so that a Third Form of the differential equation is immediately

$$\boxed{\ddot{z} + k\dot{z} + \left[(1-n)\,z + 1\right]^{\frac{1}{1-n}} - 1 = x(\tau)}, \qquad (4.49)$$

which is a special case of the generalised Duffing equation (2.12), Chapter 2, and which is valid for $0 \leqslant n \leqslant 1$. If $n = 1$, as is possible in certain recently reported varactors[49], then the $v = \mathcal{J}(q)$ law must be written (see Table 3.1, Chapter 3)

$$v = V_o\left[e^{\frac{q}{C_o V_o}} - 1 \right] , \qquad (4.50)$$

which results in the differential equation

$$\boxed{\overset{\circ\circ}{z} + k\overset{\circ}{z} + e^{z} - 1 = x(\tau)} \quad . \qquad (4.51)$$

Following the remarks of Sub-Section 3.2.3, Chapter 3, equation (4.49) becomes particularly simple for

$$n = \frac{N}{1+N} \quad , \quad N \text{ a positive integer.}$$

Thus if $n = \frac{1}{2}$, which is approximately the value for an abrupt-junction varactor, we get the equation

$$\overset{\circ\circ}{z} + k\overset{\circ}{z} + z + \frac{1}{4} z^2 = x(\tau) \qquad (4.52)$$

which is in the canonical form of the Duffing equation.

Similarly, one can construct a table of differential equations for the various special values of n:

N	n	
0	0	$\overset{\circ\circ}{z} + k\overset{\circ}{z} + z = x(\tau)$
1	$\frac{1}{2}$	$\overset{\circ\circ}{z} + k\overset{\circ}{z} + z + \frac{1}{4} z^2 = x(\tau)$
2	$\frac{2}{3}$	$\overset{\circ\circ}{z} + k\overset{\circ}{z} + z + \frac{1}{3} z^2 + \frac{1}{27} z^3 = x(\tau)$
⋮	⋮	⋮
∞	1	$\overset{\circ\circ}{z} + k\overset{\circ}{z} + z + \frac{1}{2!} z^2 + \frac{1}{3!} z^3 + \ldots = x(\tau)$ or $\overset{\circ\circ}{z} + k\overset{\circ}{z} + e^{z} - 1 = x(\tau)$

Table 4.2

The case $n = \frac{1}{2}$ gives the simplest nonlinear equation in this Table. It is also the most important practically, since abrupt-junction varactors have n near 0.5 and give the greatest nonlinearity readily available.

The two different "voltage" forms of the differential equation, equations (4.46) and (4.47), can be treated analytically only if the nonlinear functions are approximated by their truncated power-series expansions. This immediately restricts attention to small-signal operation because the approximation will fail as soon as the relevant normalised variable approaches unity (i.e. as soon as the voltage concerned approaches V_o). However, the Third Form of the equation in terms of the charge variable z can be treated exactly (for the special values of n), and since no approximation need be invoked, the analysis will hold for large-signal operation with $v \gg V_o$.

Whatever may be the exact parametron configurations selected for detailed study, the considerations of this section will apply to the extent that several different but equally valid differential equations can be obtained for a single system, some of which may be more useful than others.

CHAPTER FIVE

5. Differential Equations of Balanced Varactor Parametrons

5.1 Introduction

It has been remarked in Sub-Section 4.1.2 of the previous chapter that balanced parametrons have several practical and theoretical advantages over the unbalanced types. The rest of the thesis will therefore be devoted to a detailed study of certain balanced varactor parametrons which have been found by experiment to have good transient characteristics.

It was indicated in Table 4.1 that two basic types of balanced varactor parametron exist. They were referred to there as the Types IV(a) and IV(b) capacitive parametrons. Following the nomenclature of Sub-Section 4.1.2, they will henceforward be referred to as the BSP and BPP respectively.

In the first part of this chapter, differential equations will be derived for both types of parametron, assuming the $C = \mathcal{F}(v)$, or "voltage" representation for the reactive nonlinearities. In order to predict the quantitative behaviour of actual parametrons, it will be necessary to include the effects of parasitic elements. These elements are primarily linear, although forward diode-conduction in the varactors constitutes a nonlinear parasitic and is difficult to treat. Subsequently, it will be shown that the two differential equations are sufficiently similar in form to be assimilated into a single, more general, mathematical model. This generalised "voltage" equation will contain nonlinear functions which must be replaced by approximations before analytical solution can be undertaken. For this reason, the second part of the chapter is concerned with the derivation of mathematical models based on the $v = \mathcal{F}(q)$, or "charge" representation of the

nonlinear reactive characteristic of the varactor. It will be seen that under certain conditions this representation gives rise to differential equations in which the nonlinear functions do not require approximation before solution is attempted. The chapter ends with a discussion of methods for solving the derived differential equations.

5.2 The derivation of the differential equation of the balanced series parametron (BSP) using the "voltage" representation of the capacitive nonlinearity

The physical circuit of the BSP is shown in Figure 5.1(a). The pumping voltage v_p is coupled via the transformer T to a resonant circuit consisting of the two varactors C_1 and C_2 and the inductance L. G_L is the load conductance and V_B is the bias voltage external to the varactors.

In order to construct an equivalent circuit suitable for analysis, the following five assumptions are made.

(1) The pump generator v_p is taken to be an approximately zero-impedance source.

(2) The transformer T is assumed to be ideal with 1:2 turns ratio and centre-tapped secondary, so that v_p appears twice in the equivalent circuit of Figure 5.1(b).

(3) A varactor is represented by a parallel combination of a nonlinear capacitance and a nonlinear conductance defined by the laws (3.5) and (3.7) discussed in Chapter 3:

$$C(v) = C_o\left(1 + \frac{v}{V_o}\right)^{-n} \qquad (5.1)$$

and

$$I(v) = I_s\left(e^{-\lambda(V_B + v)} - 1\right), \qquad (5.2)$$

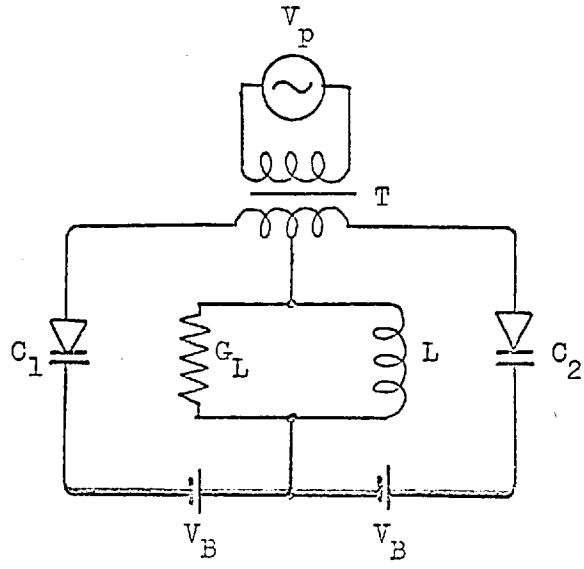


Figure 5.1(a) - Physical circuit of BSP.

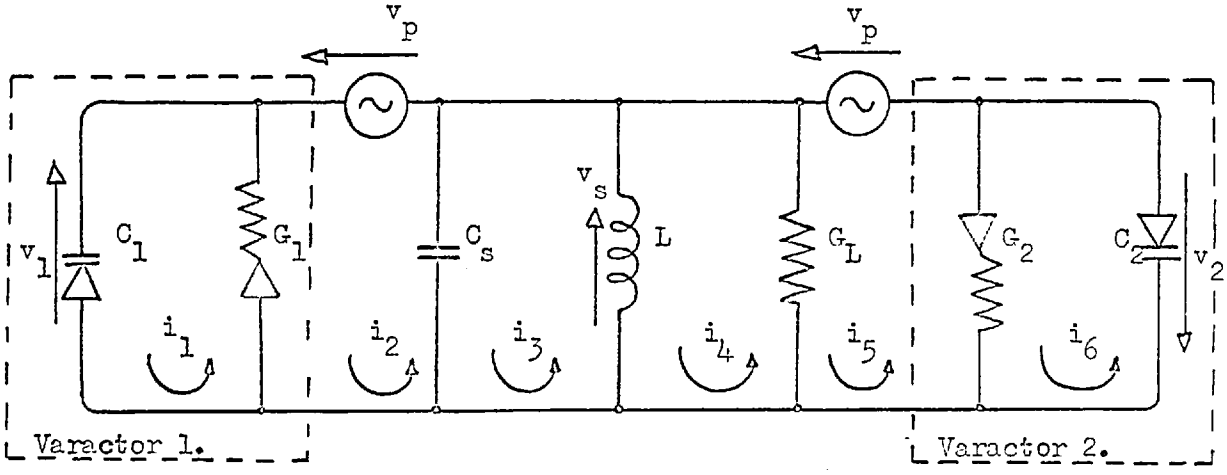


Figure 5.1(b) - Equivalent circuit of BSP for analysis.

respectively, where

$C(v) = \frac{dq}{dv}$, the incremental nonlinear capacitance,

C_o is the small-signal capacitance at the total bias point $V_o = V_B + \phi$,

$I(v)$ = the nonlinear diode current,

I_s = the saturation current and

$\Lambda = \frac{q_e}{KT}$, where q_e is the charge of an electron, K is Boltzmann's constant, and T is the Absolute temperature.

(4) The stray capacitances, which for moderately high-frequency operation have a pronounced influence upon the behaviour of the device, are lumped as a single capacitance C_s in parallel with L and G_L.

(5) The storage of minority carriers in the varactor junctions is assumed to be negligibly small.

These assumptions are concerned only with the process of setting up an adequate mathematical model of the device, and must be distinguished from the further assumptions which will have to be made when the resulting differential equations are to be solved.

The nonlinear capacitance is defined by

$$C(v) = \frac{dq}{dv} \quad , \tag{5.3}$$

so that the instantaneous current flowing in a varactor is

$$i = \frac{dq}{dt} = C(v) . \frac{dv}{dt} \quad . \tag{5.4}$$

If the variables are normalised thus:

$$y = \frac{v_s}{V_o} \quad , \quad x = \frac{v_p}{V_o} \quad , \quad \tau = \omega_o t \quad , \tag{5.5}$$

then, as is shown in Appendix 5.1, it is possible to write the complete differential equation of the BSP in the following form:

$$(1 - B)\ddot{y} + k_L \cdot \dot{y} + y + \pm\frac{B}{2(1-n)} \cdot \frac{d^2}{d\tau^2}\left[(1+x+y)^{1-n} - (1+x+y)^{1-n}\right] + 2k_v \cdot \frac{d}{d\tau}\left[e^{-cx} \cdot \sinh cy\right] = 0 \quad (5.6)$$

This equation is valid for $0 \leqslant n \leqslant 1$. Here

$$\omega_o = \frac{1}{\sqrt{L(2C_o + C_s)}} \quad (5.7)$$

is the small-signal resonant angular frequency,

$$B = \frac{2C_o}{2C_o + C_s} \quad (5.8)$$

is a parameter to account for the effect of the stray capacitance,

$$k_v = \frac{\omega_o L I_s}{V_o} \cdot e^{-\Lambda V_B} \quad (5.9)$$

is a damping parameter due to the conductance of a varactor diode,

$$k_L = \omega_o L G_L \quad (5.10)$$

is a damping parameter due to the load conductance and

$$c = \Lambda V_o = \frac{qV_o}{KT} \quad (5.11)$$

is a normalised voltage parameter appearing in the nonlinear conductance function. The first three terms of the differential equation (5.6) correspond to a damped resonator consisting of the linear elements in the parametron: C_o, C_s, L and G_L. The fourth term is caused by the nonlinear reactances, and appears in a form analogous to the corresponding part of the unbalanced equation (4.47), Chapter 4. The fifth term is a nonlinear damping

function to account for the varactor conductances G(v). This function consists of two parts. The unsymmetrical part e^{-cx} occurs because the nonlinear conductances are in series from the point of view of the pump. The subharmonic, on the other hand, sees these conductances in parallel, hence the presence of the antisymmetrical part sinh cy.

As far as the generation of subharmonics is concerned, the pumping function $x(\tau)$ is coupled to the tuned circuit only via the nonlinear reactances. This can easily be seen by setting n equal to zero in equation (5.6). This has the effect of linearising the reactances. The fact that x remains in the nonlinear damping term is of no consequence here, since nonlinearities in the damping cannot give rise to subharmonic oscillations.

The essential difference between the differential equations of balanced and unbalanced parametrons now becomes clear: it lies in the nonlinear terms containing the subharmonic voltage variable y. These terms are unsymmetrical functions of y in the unbalanced parametrons but antisymmetrical functions in the balanced devices.

5.3 The derivation of the differential equation of the balanced parallel parametron (BPP) using the "voltage" representation of the capacitive nonlinearity

The physical circuit of the BPP is shown in Figure 5.2(a). The varactors C_1 and C_2 are now both connected in the same polarity. The pump v_p and the bias voltage V_B are connected in series to the centre-tap of the tuning inductance L, across which is the load R_L. It is possible to use two separate inductors instead of L, but in general this leads to poor balance.

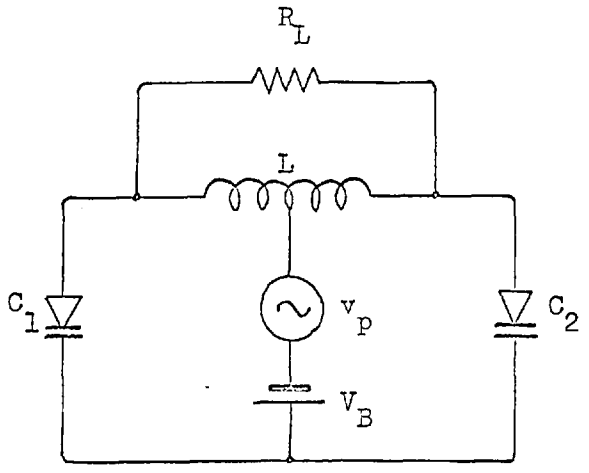


Figure 5.2(a) -
Physical circuit of BPP.

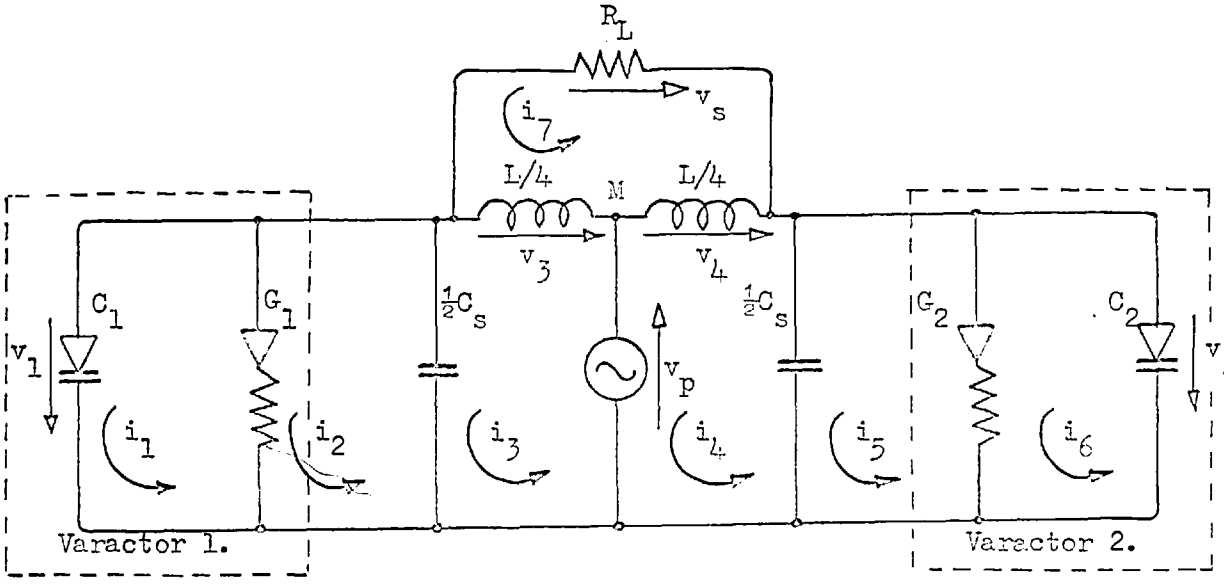


Figure 5.2(b) -
Equivalent circuit of BPP for "voltage" analysis.

If L is a bifilar* winding upon a toroidal ferrite core, very good balance can be obtained. Furthermore, there will be close-coupling between the two halves of L, which, although not essential for the operation of the circuit, will enable a considerable simplification of the theory to be made.

The equivalent circuit of Figure 5.2(b) results from the following assumptions.

(1) The pump source has zero internal impedance.

(2) The two halves of L are perfectly coupled, so that $M = \frac{1}{4} L$.

(3) As in the case of the BSP, each varactor is represented by a parallel combination of a nonlinear capacitance and a nonlinear conductance.

(4) The stray capacitance C_s is lumped in two equal halves across the two varactors.

By making the same normalisations as were used in the previous section**, it is shown in Appendix 5.2 that the complete differential equation of the device is

$$(1 - B)\overset{\circ\circ}{y} + k_L.\overset{\circ}{y} + y + \frac{B}{1-n} \cdot \frac{d^2}{d\tau^2}\left[(1+x+\tfrac{1}{2}y)^{1-n} - (1+x-\tfrac{1}{2}y)^{1-n}\right] + k_v.\frac{d}{d\tau}\left[e^{-cx}\sinh\tfrac{1}{2}cy\right] = 0 \qquad (5.12)$$

which is again valid for $0 \leqslant n \leqslant 1.0$.

---

* Two wires are wound together on a ferrite toroid, the turns being spaced evenly around its circumference.

** Except that the resonant frequency is here $\omega_o = \frac{2}{\sqrt{L(2C_o + C_s)}}$, (see Appendix 5.2).

5.4 Generalisation of the differential equations

If the differential equations (5.6) and (5.12) for the two kinds of balanced parametron are compared, it can be seen that they differ only in minor details. They can therefore be assimilated into the following single differential equation covering both types

$$(1 - B)\overset{\circ\circ}{y} + k_L\overset{\circ}{y} + y + \frac{B}{a(1-n)} \cdot \frac{d^2}{d\tau^2}\left[(1+x+\tfrac{1}{2}ay)^{1-n} - (1+x-\tfrac{1}{2}ay)^{1-n}\right] + ak_v \cdot \frac{d}{d\tau}\left[e^{-cx}\sinh \tfrac{1}{2}acy\right] = 0 \quad , \tag{5.13}$$

where $\begin{cases} a = 2 & \text{for the BSP,} \\ a = 1 & \text{for the BPP.} \end{cases}$

This is of the general form of equation (2.11):

$$\frac{d^2}{d\tau^2}\left[\mathcal{J}_1(x,y)\right] + \frac{d}{d}\left[\mathcal{J}_2(x,y)\right] + \mathcal{J}_3(x,y) = 0$$

discussed in Section 2.3, Chapter 2, with

$$\mathcal{J}_1(x,y) = (1-B)y + \frac{B}{1-n}\left[(1+x+\tfrac{1}{2}ay)^{1-n} - (1+x-\tfrac{1}{2}ay)^{1-n}\right] ,$$

$$\mathcal{J}_2(x,y) = k_L y + k_v e^{-cx} \cdot \sinh \tfrac{1}{2}acy ,$$

$$\mathcal{J}_3(x,y) = y,$$

and is of the type for which true subharmonic resonance can occur.

5.5 The derivation of the differential equation of the balanced parallel parametron (BPP) using the "charge" representation of the reactive nonlinearity

The analysis based on the $v = \mathcal{J}(q)$ representation of the nonlinear

capacitance characteristic of the varactor is considerably more complicated than that based on the $C = \mathcal{J}(v)$ representation. This, together with the fact that in practice the BPP is a more useful device than the BSP, suggests that it is advisable to restrict the detailed large-signal "charge" analysis to the case of the BPP. The corresponding analysis of the BSP follows very similar lines but does not lead to any new insights.

The practical utility of the BPP resides largely in its very fast turn-off capability. This can be achieved by simultaneously biassing both the varactors into forward conduction with a sufficiently sharp-edged pulse. The Q of the circuit is then reduced to the point where the subharmonic oscillations are quenched within about one cycle.* This will be discussed further in Section 7.5, Chapter 7 which deals with quantitative measurements on the transient phenomena and related practical details.

We shall now derive a differential-equation model for the equivalent circuit of Figure 5.2b, based on the $v = \mathcal{J}(q)$ representation of the non-linear reactances.

It is found that the expressions become exceedingly unwieldy if the nonlinear part G(v) of the varactor conductance is included in the theoretical model. It is therefore assumed that the parametron is never operated under conditions of appreciable forward conduction, and this is justified on the practical grounds that such conduction leads to excessive consumption of pump power, to distortion of the pump waveform and in particular to the degradation of the transient response. The presence of resistance R_p in series with the pump helps to inhibit the first two of there undesirable effects, since then the pump never sees a short circuit. Neglecting the

---

* see, for example, Figure 7.33.

nonlinear varactor conductance does, however, mean that the cessation of subharmonic oscillation at pump amplitudes which are large (compared with the bias voltage V_o) will not be predicted.

In the course of the following derivation, use will be made of the fact that the $v = \mathcal{J}(q)$ expression becomes particularly simple if the exponent n is $\frac{1}{2}$, as has been seen in Section 3.2.2. In a subsequent section, the corresponding mathematical model for the case n = 1 will be obtained, since this gives the largest possible nonlinearity for a varactor, and may be of importance in the future.

5.5.1 The case $n = \frac{1}{2}$

The complete equivalent circuit to be analysed appears in Figure 5.3. In terms of normalised charges and voltages, the reactance characteristics of the two varactors for the case $n = \frac{1}{2}$ are

$$y_1 = z_1 \left(\tfrac{1}{4} z_1 - 1 \right) \qquad (5.14)$$

and $$y_2 = z_7 \left(\tfrac{1}{4} z_7 + 1 \right) . \qquad (5.15)$$

The subscripts correspond to those used in the Figure for the un-normalised quantities. It is shown in Appendix 5.3 that if there is perfect coupling between the two sections of the tuning inductor, then by working in terms of the sum of the varactor charges

$$u = z_7 - z_1 \qquad (5.16)$$

and the difference between them

$$z = z_7 + z_1 , \qquad (5.17)$$

the following three equations are obtained:

$$u = -4 \left(1 + \frac{y}{z} \right) , \qquad (5.18)$$

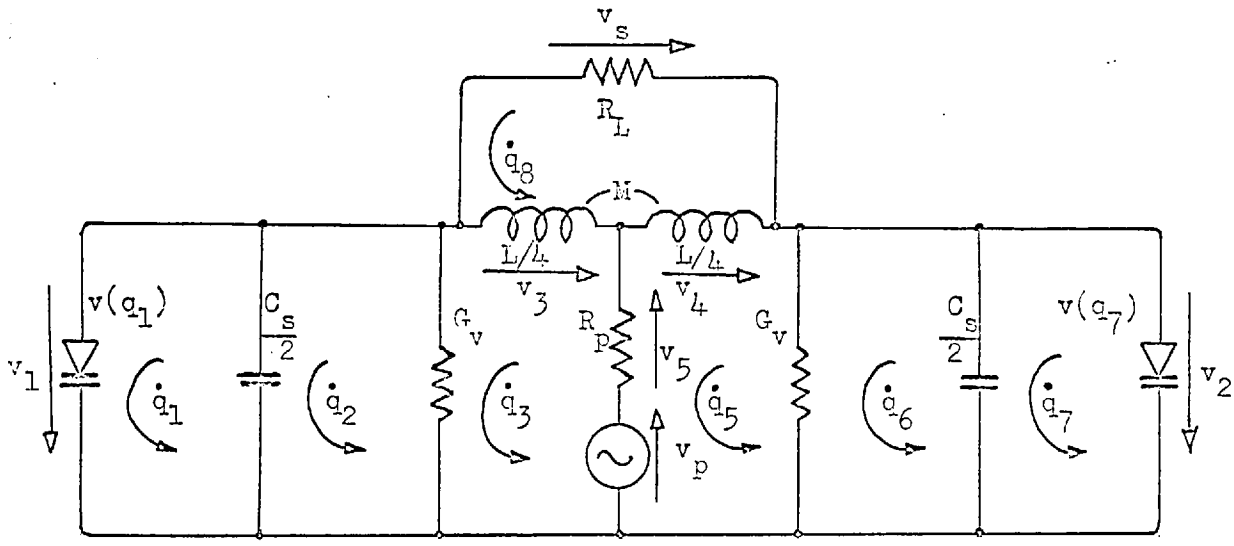


Figure 5.3 -
Equivalent circuit of BPP for "charge" analysis.

$$(1-B).\overset{oo}{y} + (\tfrac{1}{2}k_v + k_L)\overset{o}{y} + y = B.\overset{oo}{z} \qquad (5.19)$$

and

$$k_p.\overset{o}{u} + B.x + \tfrac{1}{8}k_p(1-B).\frac{d}{d\tau}(z^2+u^2)+\tfrac{1}{2}(B+k_vk_p)\left[\tfrac{1}{8}(z^2+u^2)+u\right] = 0. \qquad (5.20)$$

The parameters here are:

$\omega_o = \sqrt{\dfrac{4}{L(2C_o + C_s)}}$, the small-signal resonant angular frequency,

$B = \dfrac{2C_o}{2C_o + C_s} = \tfrac{1}{2}\omega_o^2 L C_o$, the stray-capacitance parameter,

$k_p = \omega_o C_o R_p$, the pump-circuit damping parameter,

$k_v = \omega_o L G_v$, the linearised damping parameter due to the varactor conductances,

$k_L = \omega_o L G_L$, the load damping parameter.

By eliminating u, the sum of the varactor charges, between equations (5.18) and (5.20), it is possible to obtain a differential equation in the inductor voltage y and the difference z between the varactor charges:

$$k_p\left\{\tfrac{1}{4}(1-B)z^4\overset{o}{z} + 4\left[(1-B)y-Bz\right]\cdot(z\overset{o}{y}-y\overset{o}{z})\right\} + Bz^3x + (B+k_vk_p)(\tfrac{1}{16}z^5-z^3+y^2z) \equiv \mathfrak{E}\left[x,y,z\right] = 0. \qquad (5.21)$$

Equations (5.19) and (5.21) constitute the "charge" mathematical model for the BPP in the case where $n = \frac{1}{2}$. Ideally, it would be desirable to

eliminate the charge variable z between these equations. Unfortunately, this is not possible, and the pair must be solved simultaneously. Equation (5.19) is second-order linear, and prescribes the relationship between the charge and the voltage, while (5.21) is first-order nonlinear, and contains the reactance characteristic of the parametron in a non-approximated closed form.

For a reasonable reverse bias voltage V_B,

$$G_v = \frac{I_s}{V_o} e^{-\Lambda V_B} \ll \omega_o L,$$

so that the damping parameter k_v can be neglected for conditions under which forward varactor conduction is avoided.

The advantage of expressing the differential equations in the "charge" form (5.19) with (5.21), rather than in the "voltage" form (5.13), is that in the former case only simple integral powers of the variables occur and not fractional or irrational powers. For example, if $n = \frac{1}{2}$, a practical value for abrupt-junction varactors, equation (5.13) contains the nonlinear reactance function $\sqrt{1+x+\frac{1}{2}ay} - \sqrt{1+x-\frac{1}{2}ay}$, which leads to analytical difficulties unless expressed in approximate form.

5.5.2 The case n = 1.0

In the previous sub-section we have obtained the detailed "charge" mathematical model for a practical BPP in which the varactors are characterised by the exponent $n = \frac{1}{2}$. We have remarked earlier that "hyper-abrupt" junction varactors have been realised in which n is approximately unity over a certain range of reverse bias voltages V_B. Parametrons utilising varactors with this degree of nonlinearity may become important in the future since they should be both more efficient and have faster switching capabilities

than those employing varactors with $n = \frac{1}{2}$.

The "charge" differential equation for the simplest of the unbalanced parametrons, Type III(b) of Table 4.1, has already been derived for the case $n = 1$. It appears at the foot of Table 4.2 and is

$$\overset{oo}{z} + k.\overset{o}{z} + e^{z} - 1 = x(\tau) ,$$

where k is a series damping parameter and $x(\tau)$ is the pumping function.

Turning now to the complete BPP, it is found that in place of equations (5.14) and (5.15), we have for the varactor voltages

$$y_1 = e^{-z_1} - 1$$

$$y_2 = e^{+z_7} - 1$$

so that the equations for the sum and difference of the varactor voltages are respectively

$$y_1 + y_2 = 2(e^{\frac{u}{2}} \cosh \tfrac{z}{2} - 1) \qquad (5.22)$$

and $$y_1 - y_2 = y = -2\, e^{\frac{u}{2}} \sinh \tfrac{z}{2} , \qquad (5.23)$$

where u is the sum of and z is the difference between the varactor charges, as before. The result is that the first-order differential equation corresponding to (5.20) is now

$$k_p\left[B\overset{o}{u} + 2(1-B)\frac{d}{d\tau}\left(e^{\frac{u}{2}} \cosh \tfrac{z}{2}\right)\right] + Bx + (B+k_v k_p)\left(e^{\frac{u}{2}} \cosh \tfrac{z}{2} - 1\right) = 0, \qquad (5.24)$$

while the linear equation (5.19) remains unchanged. By eliminating u between equations (5.23) and (5.24) we finally obtain

$$\boxed{k_p\left[2B\left(\frac{\overset{o}{y}}{y} - \frac{\overset{o}{z}}{2}\coth\tfrac{z}{2}\right) - 2(1-B)\left(\frac{\overset{o}{y}}{2}\coth\tfrac{z}{2} + \frac{1}{4}y\overset{o}{z}\cdot(1-\coth^2\tfrac{z}{2})\right)\right] + Bx - (B+k_v k_p)(1 + \frac{y}{2}\coth\tfrac{z}{2}) = 0.} \qquad (5.25)$$

This, together with equation (5.19), constitutes the mathematical model of the BPP for the case n = 1. If (5.25) is compared with (5.21), certain similarities will become apparent. However, the former is so much more complicated than the latter that its solution will not be attempted here. It is included for the sake of completeness.

5.5.3 Comparison of the simplified "charge" equations for n = ½ and n = 1

The essential differences between the mathematical models for the cases n = ½ and n = 1 become clearer if a simplification is made. Suppose the stray capacitance and pump-circuit damping are negligible, so that B = 1 and $k_p = 0$. Then equations (5.21) and (5.25) become respectively

$$y^2 + \frac{1}{16}.z^2 + z^3x - z^2 = 0 \quad , \quad \text{for } n = \tfrac{1}{2}$$

and $$-\frac{y}{2} \cdot \coth\frac{z}{2} + x - 1 = 0 \quad , \text{ for } n = 1 \, .$$

If, in addition, the dampings due to the load and varactor conductances are neglected, so that k_v and k_L are zero, then the linear equation (5.19) is just

$$y = \overset{oo}{z} \, .$$

This makes it possible to express the simplified equations in terms of the charge variable z only:

$$\boxed{(\overset{oo}{z})^2 + \frac{1}{16}.z^2 + z^2(x - 1) = 0} \qquad \text{for } n = \tfrac{1}{2}$$

and

$$\boxed{-\tfrac{1}{2}\,\overset{oo}{z} \cdot \coth\frac{z}{2} + (x - 1) = 0} \qquad \text{for } n = 1 \, .$$

Both of these belong to the general type (2,11). In the first case the relevant functions are

$$\mathcal{J}_1 = z, \quad \mathcal{J}_2 = 0, \quad \mathcal{J}_3 = \pm z\sqrt{\tfrac{1}{16} z + x - 1}$$

and in the second case

$$\mathcal{J}_1 = z, \quad \mathcal{J}_2 = 0, \quad \mathcal{J}_3 = -2(x-1).\tanh \tfrac{z}{2} .$$

5.6 Discussion of method for solving the differential equations

In the absence of an exact solution, there are many ways in which a nonlinear differential equation might be attacked. The number of possibilities is sharply reduced by the following requirements.

(1) The solutions should be algebraic. Thus graphical or numerical solutions are to be rejected unless absolutely unavoidable.

(2) Transient solutions as well as steady-state solutions are sought.

For example the classical method of Poincaré[55] is applicable only to the discovery of periodic solutions of differential equations of the type

$$\ddot{y} + y = x(\tau) + \mu\mathcal{J}(y,\dot{y}),$$

where $x(\tau)$ is a forcing function and μ is a "small" parameter attached to the nonlinear and damping terms. The periodic solutions correspond to steady-state conditions. Under transient conditions, however, the solutions are non-periodic, so that methods of this kind must be rejected.

The only simple approach which fulfils all the requirements is the method of slowly-varying amplitude and phase, also known as the method of Harmonic Balance. This involves the assumption that the solution can be written as a Fourier series of harmonic terms

$$y = \sum_{N=0}^{\infty} Y_N(\tau).\sin\left[N\nu\tau + \theta_N(\tau)\right] \qquad (5.26)$$

$$= \sum_{N=0}^{\infty}\left[Y_{sN}(\tau).\sin N\nu\tau + Y_{cN}(\tau).\cos N\nu\tau\right], \qquad (5.27)$$

where the amplitudes $Y_N(\tau)$ and phases $\theta_N(\tau)$ are unknown functions of time to be determined. This solution is substituted into the original differential equation. The coefficients of $\sin N\nu\tau$ and $\cos N\nu\tau$ are then equated separately to zero, resulting in a set of equations in Y_{sN} and Y_{cN} and their derivatives and powers. The slowly-varying amplitude and phase assumption is that

$$\dot{Y}_N \ll N\nu\,, \quad \dot{\theta}_N \ll N\nu\,.$$

This means that the rate of change of the amplitude and phase of each term is small compared with the associated frequency. Consequently all derivatives of order higher than the first, and all products of first-order derivatives are to be neglected. The result is a set of first-order equations for the rates of change of amplitude and phase:

$$\begin{aligned}\dot{Y}_N &= \mathcal{F}_{1N}\,(\,Y_1, Y_2, \ldots\ldots, \theta_1, \theta_2, \ldots\ldots)\\ \dot{\theta}_N &= \mathcal{F}_{2N}\,(\,Y_1, Y_2, \ldots\ldots, \theta_1, \theta_2, \ldots\ldots)\end{aligned} \qquad (5.28)$$

where $N = 1, 2, 3, \ldots$.

In principle this (infinite) set of equations is soluble for the amplitudes and phases of the frequency components.

In practice it is not possible to retain an infinite number of terms in the assumed solution. If it is known in advance (e.g. from experimental evidence) that the solution is nearly sinusoidal, then a few terms or even a single term of the Fourier series may be sufficient. If such an approximation is made, all cross-product terms in frequencies greater than the highest frequency in the assumed solution must be neglected.

In general the original differential equation will contain "arbitrary" nonlinearities. An example is equation (5.13). In order to apply the method of Harmonic Balance it is necessary to expand such nonlinear functions into power series. Mathematical feasibility usually demands that these series be truncated after a few terms. This approximation leads to errors unless the signal level is very small. In certain cases, however, for example equation (5.21), the nonlinearities appear as simple powers and since no series approximation is required, solutions can be found for large signal levels.

The forms (5.26) and (5.27) of the assumed solution are inconvenient when the differential equations to be solved are at all complicated. Mathematical simplicity is achieved by writing the solution in the form

$$y = \sum_{N=0}^{\infty} -jY_N(\tau).(\alpha_N - \alpha_N^*) ,$$

where $$\alpha = \tfrac{1}{2}e^{j(N\nu\tau + \theta_N(\tau))} .$$

Instead of equating the coefficients of $\sin N\nu\tau$ and $\cos N\nu\tau$ separately to zero, the same result is obtained with much less effort by equating the coefficients of $(\alpha_N + \alpha_N^*)$ and $j(\alpha_N - \alpha_N^*)$ separately to zero.

Equations (5.28) for the rates of change of the amplitudes and phases of the frequency-components of the solution will be referred to as the Intermediate Solution. The steady-state solution is found by equating all the time-derivatives to zero. In order to find the transient solutions, however, the set (5.28) must be solved as it stands. Since the functions $\mathcal{F}_{1N}$ and $\mathcal{F}_{2N}$ are generally nonlinear, exact solution is seldom possible and further approximate methods must be invoked.

CHAPTER SIX

6. Steady-State Phenomena

6.1 Introduction

This Chapter is concerned with the steady-state solutions of differential equations of real balanced parametrons. It begins by approximating the nonlinear functions in the generalised "voltage" equation to the point where analytical treatment becomes possible. The solution of the equation is then obtained and compared with measurements on typical balanced parametrons. The possibilities and limitations of this small-signal result are discussed. Next, the detailed "charge" differential equation is solved. No approximation of the mathematical model is required in this case. The Chapter ends with an investigation of the improved accuracy of the result, with particular reference to large-signal operation.

6.2 Approximation of the generalised "voltage" differential equation for solution

It has been pointed out in the previous Chapter that the analysis of parametron-models based on the $C = \mathcal{J}(v)$ representation of the nonlinear capacitances involves the use of two different kinds of approximation. Firstly, there are the approximations concerned with the simplification of the "exact" differential equations to the point where it is feasible to use the chosen method of analysis. This stage of approximation is not always essential. In certain cases the nonlinear functions may already exist in the form of simple integral powers. Again, they may be of a type suitable for direct treatment by, for example, the Ritz-Galerkin method.[56] Secondly,

there is the approximation which is introduced when particular assumptions are made about the nature of the solution. Such assumptions always have to be made unless the nonlinear differential equation in question can be solved exactly. This is seldom possible. The errors due to these separate causes tend to be multiplicative, producing drastically incorrect results for conditions under which they are both important.

The generalised "voltage" differential equation describing the behaviour of both the BSP and the BPP, which was derived in Section 5.4, must now be reduced to a suitable approximate form. If the analysis is restricted to the case of small-signal oscillations about the total bias voltage V_o, then it is possible to replace the nonlinear functions by their truncated power-series expansions about V_o. The results obtained by this procedure will apply only when the relevant variables of expansion are less than unity, otherwise the power series will fail to converge and the approximations will not hold. The nonlinear reactance function appearing in equation (5.13) can be expanded as follows:

$$(1 + x + \tfrac{1}{2} ay)^{1-n} - (1 + x - \tfrac{1}{2} ay)^{1-n} =$$

$$= \sum_{r=1}^{\infty} \frac{1}{r!} \left[(x+\tfrac{1}{2}ay)^r - (x-\tfrac{1}{2}ay)^r \right] \cdot \prod_{s=1} (2-n-s) =$$

$$= ay - nxay + \tfrac{1}{2}n(n+1)\left[x^2 ay + \frac{1}{12}(ay)^3\right] - \tfrac{1}{6}n(n+1)(n+2)\left[x^3 ay + \frac{1}{4}x(ay)^3\right] + \ldots, \qquad (6.1)$$

where a = 2 for the BSP and a = 1 for the BPP.

The nonlinear damping function can be expanded in the following manner:

$$e^{-cx} \sinh \tfrac{1}{2} cay =$$

$$= \sum_{r=0}^{\infty} \sum_{s=0}^{\infty} \frac{(-cx)^r (\frac{1}{2} cay)^{2s+1}}{r!\,(2s+1)} =$$

$$= \tfrac{1}{2}c \left\{ ay - cxay + \tfrac{1}{2}c^2 \left[x^2 ay + \frac{1}{12}(ay)^3 \right] - \tfrac{1}{6}c^3 \left[x^3 ay + \tfrac{1}{4} x (ay)^3 \right] + \cdots\cdots \right\}. \tag{6.2}$$

It is interesting to observe that the expansions (6.1) and (6.2) of the reactive and resistive nonlinear functions differ only in their coefficients. If they are both terminated somewhat arbitrarily at the third power, so as to avoid excessive mathematical complication, the following approximate nonlinear differential equation is obtained:

$$\ddot{y} + k_o \dot{y} + y + 2 \frac{d^2}{d\tau^2} \left[\alpha\, xy + \beta(x^2 y + \frac{1}{12} a^2 y^3) \right] + 2 \frac{d}{d\tau} \left[\gamma\, xy + \delta(x^2 y + \frac{1}{12} a^2 y^3) \right] = 0, \tag{6.3}$$

which is valid so long as the conditions

$$|x| < 1$$

$$|\tfrac{1}{2} ay| < 1$$

are both fulfilled.

The constants appearing in this equation are defined below.

The coefficient

$$k_o = k_L + \tfrac{1}{2} c\, a^2 k_v = \omega_o L (G_L + \tfrac{1}{2} a^2 \Lambda\, I_s e^{-\Lambda V_B})$$

is a parameter containing (a) the effects of the load damping $k_L = \omega_o L G_L$ and (b) the component of the nonlinear varactor damping due to the bias voltage V_B, namely, $k_v = \omega_o L \frac{I_s}{V_o} e^{-\Lambda V_B}$. The parameters

$$\alpha = \tfrac{1}{2} Bn \quad , \quad \beta = \frac{1}{4} Bn\,(n+1)$$

are coefficients of the nonlinear reactance function, while

$$\gamma = \frac{1}{4} c^2 a^2 k_v, \quad \delta = \frac{1}{8} c^3 a^2 k_v$$

are coefficients of the nonlinear damping function.

The first three terms of equation (6.3) relate to the linear oscillatory system which results when all the nonlinearities and time-varying parameters are eliminated. The first square bracket contains the approximate reactive nonlinearity; the second the approximate resistive nonlinearity. The sign of x has been changed in (6.3). This is permissible since x has not yet been defined.

It may be remarked in passing that if the voltage variable y is sufficiently small, the terms in y^3 may be neglected, so that equation (6.3) becomes linear with time-varying coefficients:

$$\frac{d^2}{d\tau^2}\left[(1 + 2\alpha x + 2\beta x^2)\, y\right] + \frac{d}{d\tau}\left[(k_o + 2\gamma x + 2\delta x^2)\, y\right] + y = 0, \qquad (6.4)$$

which is a practical example of the form given in equation (2.10), discussed in Section 2.2, Chapter 2.

6.2.1 Discussion of the validity of the approximate differential equation

From the point of view of the output signal, the resistive nonlinearity is a hyperbolic-sine function of voltage. It is therefore a much more 'violent' function than is the reactive nonlinearity. This means that the nonlinear resistance does not become important until the voltage excursion is quite large, but then "suddenly" dominates the device behaviour. Thus

it can be seen that the truncated series approximation to the resistance function will, in general, be considerably less valid than the approximation to the nonlinear reactance function. If the signal-level is small enough, the approximation to the resistance function can be regarded as satisfactory. However, the influence of the nonlinear resistance will be slight under such conditions. Moreover, for moderate values of reverse bias voltage V_B, the nonlinear resistance may be neglected altogether, since then k_v, which is proportional to $e^{-\Lambda V_B}$, becomes extremely small.

6.3 Steady-state solution of the generalised "voltage" equation

In finding an approximate solution of equation (6.3) for the case of subharmonics of order one-half, the requirements of the section relating to the transient response (Section 7.3) will be anticipated. It will be assumed that the normalised voltage y can be approximated by

$$\tilde{y} = Y(\tau).\sin(\nu\tau + \theta(\tau)), \qquad (6.5)$$

where the amplitude $Y(\tau)$ and phase $\theta(\tau)$ are unknown functions of time, the phase being referred to that of the normalised pumping voltage

$$x = X.\sin 2\nu\tau \qquad (6.6)$$

which is taken to have zero phase-angle.

In order to solve (6.3) by the Harmonic Balance method, it is necessary to calculate the following nine quantities:

$\tilde{y}$	$\tilde{\tilde{y}}^{o}$	$\tilde{\tilde{y}}^{oo}$
-	$(x\tilde{y})^{o}$	$(x\tilde{y})^{oo}$
-	$(x^2\tilde{y})^{o}$	$(x^2\tilde{y})^{oo}$
-	$(\tilde{y}^3)^{o}$	$(\tilde{y}^3)^{oo}$

(6.7)

This can be done in terms of conventional trigonometrical Cartesian coordinates

$$Y_s(\tau) = Y(\tau).\sin\theta(\tau)$$

and $$Y_c(\tau) = Y(\tau).\cos\theta(\tau)\ ,$$

so that (6.5) is

$$\tilde{y} = Y_s(\tau).\cos\nu\tau + Y_c(\tau).\sin\nu\tau\ .$$

However, the use of these coordinates leads to extremely long and tedious calculations. Considerable simplification of the process results if complex-polar coordinates are employed.

Thus (6.5) becomes

$$\tilde{y} = -j\,Y(\tau)(\alpha - \alpha^*)\ , \qquad (6.8)$$

where $\alpha(\tau) = \frac{1}{2}\,e^{j(\nu\tau + \theta(\tau))}$,

and the pumping function (6.6) is now given by

$$x = -j2X(\alpha^2 e^{-j2\theta} - \alpha^{*2}\,e^{j2\theta})\ . \qquad (6.9)$$

The nine quantities indicated in (6.7) are calculated using (6.8) and (6.9) and the following quantities are rejected:

(1) α^3, α^{*3}, α^5, α^{*5}, because they correspond to harmonics 3ν and 5ν, which are assumed by (6.8) not to occur;

(2) $\overset{\circ\circ}{Y\theta}$, $\overset{\circ\circ}{\theta}$, $\overset{\circ\circ}{Y}$, $\overset{\circ}{\theta}^2$, $\overset{\circ}{Y}^2$, because it is assumed that the amplitude and phase of y change slowly with time, so that all second derivatives and products of first derivatives are negligible. The conditions for this are

$$\left|\frac{\overset{\circ}{\theta}}{\nu}\right| \ll \nu \quad \text{and} \quad \left|\frac{\overset{\circ}{Y}}{Y}\right| \ll \nu\ ,$$

and experiment indicates that these should be fulfilled for the turn-on transients in practical parametrons.

It is shown in Appendix 6.1 that if the resultant nine quantities (6.7) are substituted into equation (6.3), and the coefficients of $(\alpha + \alpha^*)$ and $j(\alpha - \alpha^*)$ are separately equated to zero, then the following pair of equations is obtained:

$$2\nu\frac{\dot{Y}}{Y}\left[1+\beta\left(X^2+\frac{3a^2}{8}\cdot Y^2\right)\right] + (\nu+\dot{\theta})\left[k_o+\delta\left(X^2+\frac{a^2}{8}\cdot Y^2\right)\right] + \\ + X_*\left[\alpha\nu(2\dot{\theta}-\nu)+\gamma\frac{\dot{Y}}{Y}\right]\cos 2\theta + X_*\left[2\alpha\nu\cdot\frac{\dot{Y}}{Y}+\gamma(\nu-\dot{\theta})\right]\sin 2\theta = 0, \tag{6.10}$$

and

$$\frac{\dot{Y}}{Y}\left[k_o+\delta\left(X^2+\frac{3a^2}{8}Y^2\right)\right] - \nu(\nu+2\dot{\theta})\left[1+\beta\left(X^2+\frac{a^2}{8}Y^2\right)\right] + 1 + \\ + X_*\left[\alpha\nu(2\dot{\theta}-\nu)+\gamma_*\frac{\dot{Y}}{Y}\right]\sin 2\theta - X\left[2\alpha\nu\frac{\dot{Y}}{Y}+\gamma(\nu-\dot{\theta})\right]\cos 2\theta = 0\ . \tag{6.11}$$

The immediate objective is attained by setting the time-derivatives $\dot{Y}$ and $\dot{\theta}$ equal to zero, so that the equations for the steady-state solution are

$$\nu k_o + \nu\delta\left(X^2+\frac{a^2}{8}Y^2\right) - \nu^2\alpha X_*\cos 2\theta + \nu\gamma X_*\sin 2\theta = 0\ , \tag{6.12}$$

$$\text{and } (\nu^2-1)+\nu^2\beta\left(X^2+\frac{a^2}{8}Y^2\right)+\nu^2\alpha X_*\sin 2\theta - \nu\gamma X_*\cos 2\theta = 0, \tag{6.13}$$

which are of the form

$$-A_*\cos 2\theta + B_*\sin 2\theta + C = 0,$$

$$A_*\sin 2\theta - B_*\cos 2\theta + F = 0,$$

Elimination of θ gives the steady-state amplitude solution

$$A^2 + B^2 = C^2 + F^2\ , \tag{6.14}$$

while the steady-state phase-solution is

$$\text{tg } 2\theta = \frac{AF - BC}{CA - BF}\ . \tag{6.15}$$

In terms of the quantities in equations (6.12) and (6.13), equation (6.14) gives:

$$(\nu X)^2\left[(\alpha\nu)^2+\Upsilon^2\right]=\left[(\nu^2-1)+\beta\nu^2\left(X^2+\frac{a^2}{8}Y^2\right)\right]^2+\nu^2\left[k_o+\delta\left(X^2+\frac{a^2}{8}Y^2\right)\right]^2 . \tag{6.16}$$

This can be solved for Y to yield

$$Y^2=\frac{8}{a^2}\left[\frac{\beta(1-\nu^2)-\delta k_o}{(\beta\nu)^2+\delta^2}-X^2\pm\sqrt{X^2\left[\frac{(\alpha\nu)^2+\Upsilon^2}{(\beta\nu)^2+\delta^2}\right]-\frac{1}{\nu^2}\left[\frac{\beta\cdot k_o\nu^2+\delta(1-\nu^2)}{(\beta\nu)^2+\delta^2}\right]^2}\right], \tag{6.17}$$

which applies for both the Balanced Series Parametron and the Balanced Parallel Parametron. The "Frequency Characteristic", or the boundary of the region on the (ν,X)-plane within which half-order subharmonics are possible, is given by putting $aY = 0$ in equation (6.16):

$$(\nu X)^2\left[(\alpha\nu)^2+\Upsilon^2\right]=\left[(\nu^2-1)+\beta\nu^2X^2\right]^2+\nu^2\left[k_o+\delta X^2\right]^2 . \tag{6.18}$$

This expression is independent of "a" and therefore applies for both BSP and BPP as it stands, although it must be remembered that the three damping parameters k_o, Υ and δ will not be the same in the two cases. Equation (6.18) yields the following rather complicated explicit expression for $X(\nu)$:

$$X^2=\frac{\frac{1}{2}\left[(\alpha\nu)^2+\Upsilon^2\right]-\left[\beta(\nu^2-1)+k_o\delta\right]}{(\beta\nu)^2+\delta^2}\pm\sqrt{\left\{\frac{\frac{1}{2}\left[(\alpha\nu)^2+\Upsilon^2\right]-\left[\beta(\nu^2-1)+k_o\delta\right]}{(\beta\nu)^2+\delta^2}\right\}-\frac{1}{\nu^2}\left[\frac{(\nu^2-1)^2+(\nu k_o)^2}{(\beta\nu)^2+\delta^2}\right]} . \tag{6.19}$$

A reasonably simple phase solution does not occur unless the nonlinear damping terms Υ and δ are small (i.e. the varactors are not driven into forward conduction), in which case $A=\nu^2\alpha X$ and $B = 0$, so that

$$\text{tg } 2\theta = \frac{F}{C} ,$$

or making use of the amplitude solution, which is now $A^2 = C^2 + F^2$,

$$\text{tg } 2\theta = \pm \sqrt{\left(\frac{A}{C}\right)^2 - 1}$$

$$= \pm \sqrt{\left(\frac{\nu\alpha X}{k_o}\right)^2 - 1} \quad , \qquad (6.20)$$

which is independent of "a" and Y. A corresponding Y-independent expression for the phase can be obtained for γ and δ not small, but is very much more complicated than this. Rearrangement of equation (6.20) shows that the curves of constant steady-state phase-angle on the (ν, X)-plane are the rectangular hyperbolae

$$\nu X = \pm \frac{k_o}{\alpha} \cdot \sec 2\theta \, . \qquad (6.21)$$

If the nonlinear damping terms γ, δ are neglected, the following expression for the (ν, X, Y) amplitude-solution is obtained in place of (6.17):

$$Y^2 = \frac{8}{a^2} \left\{ \frac{1}{\beta} \left[\left(\frac{1-\nu^2}{\nu^2}\right) \pm \sqrt{(\alpha X)^2 - \left(\frac{k_o}{\nu}\right)^2} \right] - X^2 \right\} , \qquad (6.22)$$

while the (ν, X) Frequency Characteristic (6.19) becomes

$$X^2 = \frac{1-\nu^2}{\beta\nu^2} + \frac{1}{2}\left(\frac{\alpha}{\beta}\right)^2 \pm \left(\frac{\alpha}{\beta}\right) \sqrt{\frac{1-\nu^2}{\beta\nu^2} + \frac{1}{4}\left(\frac{\alpha}{\beta}\right)^2 - \left(\frac{k_o}{\alpha\nu}\right)^2} \, . \qquad (6.23)$$

The results obtained above may be expected to agree with practical measurements when the following three conditions are simultaneously fulfilled.

(1) The pump amplitude must be limited: $|X| < 1$.

(2) The subharmonic voltage amplitude must also be restricted: $|Y| < \frac{2}{a}$.

(3) The subharmonic frequency must be near the resonant frequency of the parametron: $\nu \cong 1$.

6.4 Comparison of the steady-state solution of the generalised "voltage" differential equation with experiment

The parametrons investigated in this thesis have been designed to have resonant frequencies in the vicinity of 5 Mc/s. The choice of such a frequency means that the inductive components are physically small and easily constructed. At the same time the complications of operation at much higher frequencies are avoided. The present theory should apply equally well to parametrons operated at higher frequencies so long as the circuits can be regarded as being composed of lumped elements.

In all cases the inductive elements consist of evenly-spaced turns upon half-inch diameter Ferroxcube toroids. Accurately centre-tapped inductors are obtained by using bifilar windings, that is, the two wires are wound together around the toroid.

The steady-state theory developed in the previous section has been compared with measurements on a typical experimental BSP, the circuit of which is shown in Figure 6.1. The balance of this type of parametron is somewhat impaired by the presence of distributed capacitance between the windings of the unbalance-to-balance input transformer. The result is the appearance of a component at the pump-frequency in the output voltage across L. Considerable improvement could be effected by adding a trimming capacitance as indicated in the Figure. An alternative procedure would be to interpose a grounded screen between the two windings, but this is not easily provided in the case of toroidally-wound transformers.

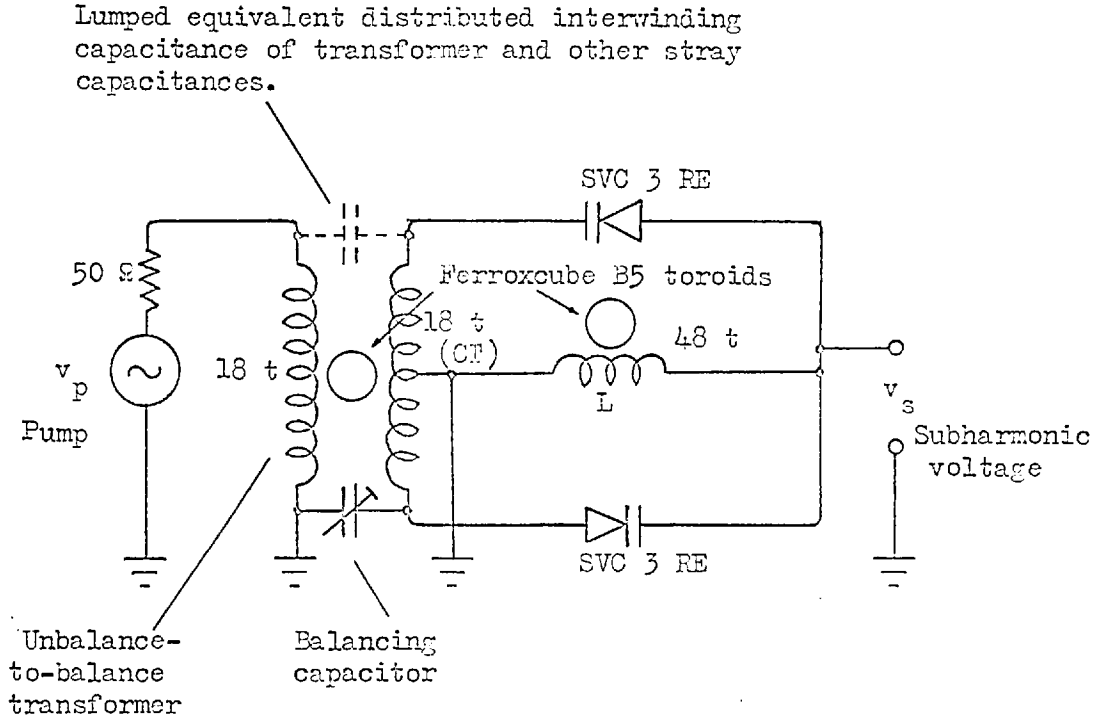


Figure 6.1 -
Circuit of experimental BSP with method of neutralising stray capacitances.

The varactors used were G.E.C. type SVC 3 RE silicon junction diodes. The transformer was 18:18 turns quadrifilar wound (both primary and secondary were centre-tapped) on a Ferroxcube B5 toroid, while the inductor L consisted of 48 turns on a similar toroid.

The directly-measurable parameters of the device were:

V_B = 0, zero external bias voltage,

V_o = ϕ = 0.7 volt for silicon,

C_o = 13.4 pF, approximately the same for both varactors,

L = 18.7 μH,

f_o = 4.39 Mc/s, measured by finding the frequency at which the least pump voltage was needed for sustained subharmonic oscillation and

G_L = 20 μ mho.

The stray capacitance C_s, which has to account for all the strays in the circuit, could not be measured directly. However, it is easily calculated from

$$C_s = \frac{1}{(2\pi f_o)^2 L} - 2C_o = 42.8 \text{ pF}.$$

This is considerably greater than 2 C_o, so that the stray capacitance parameter is

$$B = \frac{2C_o}{2C_o + C_s} = 0.385 .$$

The nonlinear capacitance-law exponent n was approximately 0.44 for each varactor.

From the above circuit parameters, it is possible to calculate the following quantities which will be required in the computation of the theoretical solution:

k_o = 0.0102, the linear damping parameter,

α = 0.0846, the first nonlinear capacitance coefficient,

β = 0.0610, the second nonlinear capacitance coefficient.

Figure 6.2(a) shows, for a considerable range of frequency ν and pump amplitude X,

(1) the measured region of unconditional (soft) subharmonic oscillation of order one-half (the Frequency Characteristic) and

(2) the corresponding theoretical region calculated according to equation (6.23). The two regions are dissimilarly shaded. The agreement is good for frequencies within ± 4% of resonance and for pump amplitudes X up to about 0.8. This region of agreement can be seen more clearly in Figure 6.2(b). For $X > 0.8$, the truncated series approximation to the nonlinear reactance function begins to fail. Furthermore, the onset of forward conduction in the varactor diodes, which has been neglected here, would cause the 'large-X' limit of oscillation to occur at a smaller pumping amplitude (for a given value of ν) than the present theory predicts. For values of ν less than about 0.95, the disagreement between theory and practice becomes quite severe, largely because of the approximate nature of the differential equation (6.3) upon which the theory is based.

Figure 6.2(a) also shows he 'small-X' limit of unconditional (soft) oscillation as predicted by the piecewise-linear theory of Section 4.3, Chapter 4. A combination of this result for $\nu < 0.95$ and the present theory for $\nu > 0.95$ affords a reasonable approximation to the actual behaviour of the device.

For a fixed value of ν, equation (6.22) defines a curve on the (X,Y)-plane which is referred to here as the (X,Y)-profile. Figure 6.3(b) shows

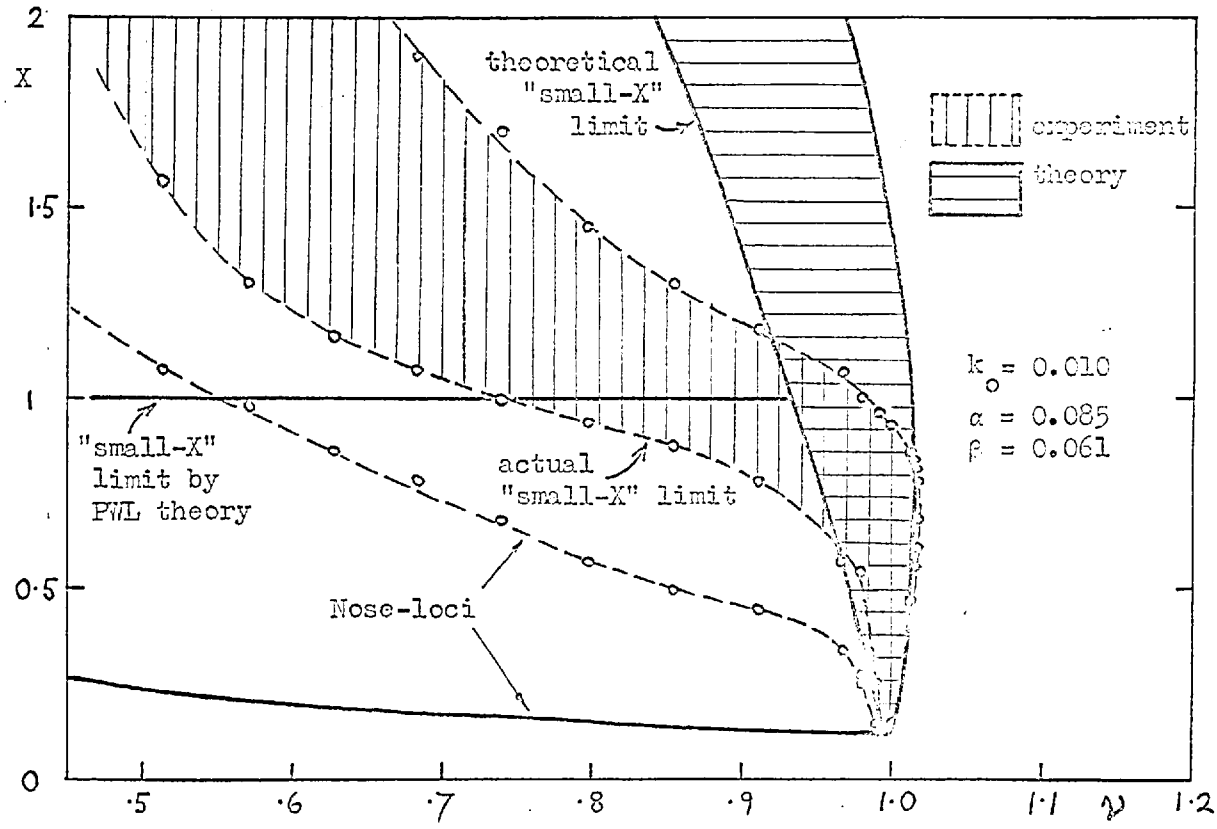


Figure 6.2(a) - Experimental and theoretical frequency characteristics and nose-loci for BSP.

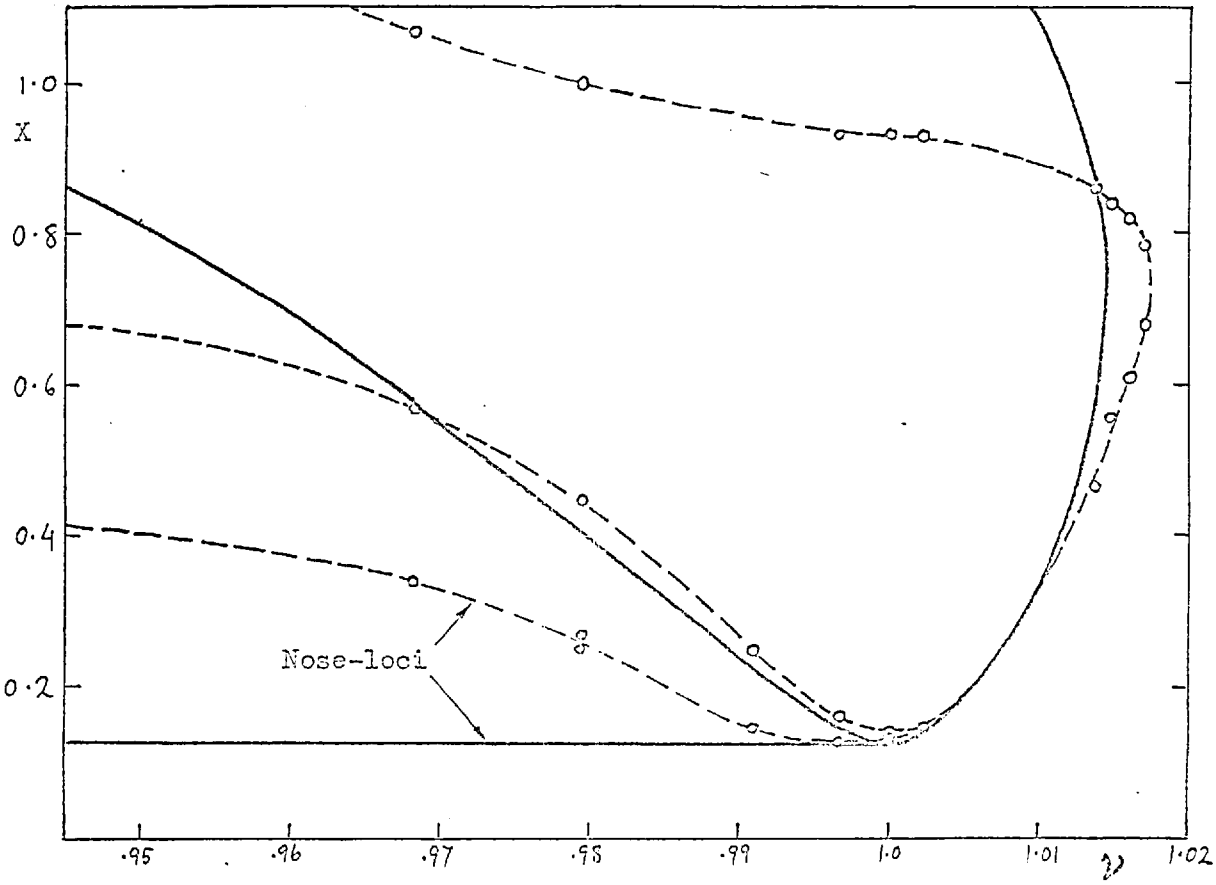


Figure 6.2(b) - Magnified portion of Fig. 6.2(a).

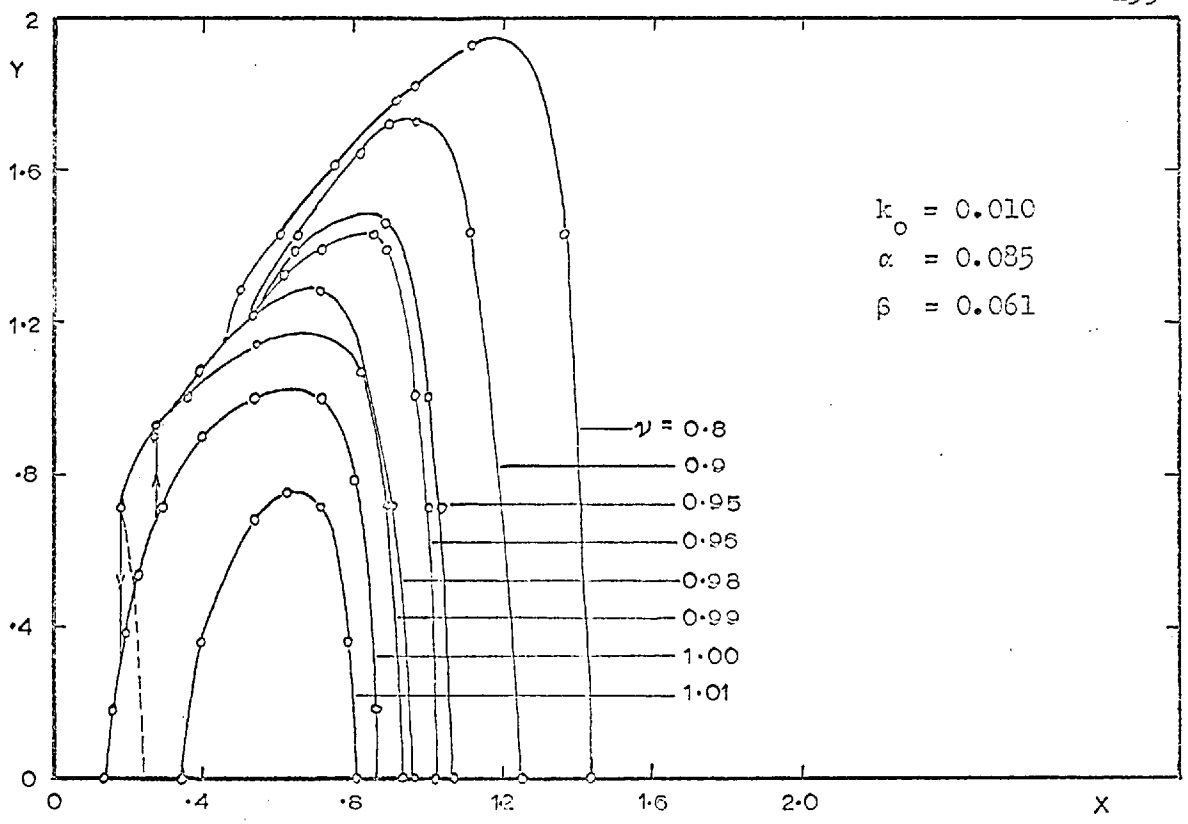


Figure 6.3(a) - Measured (X,Y)-profiles for experimental BSP.

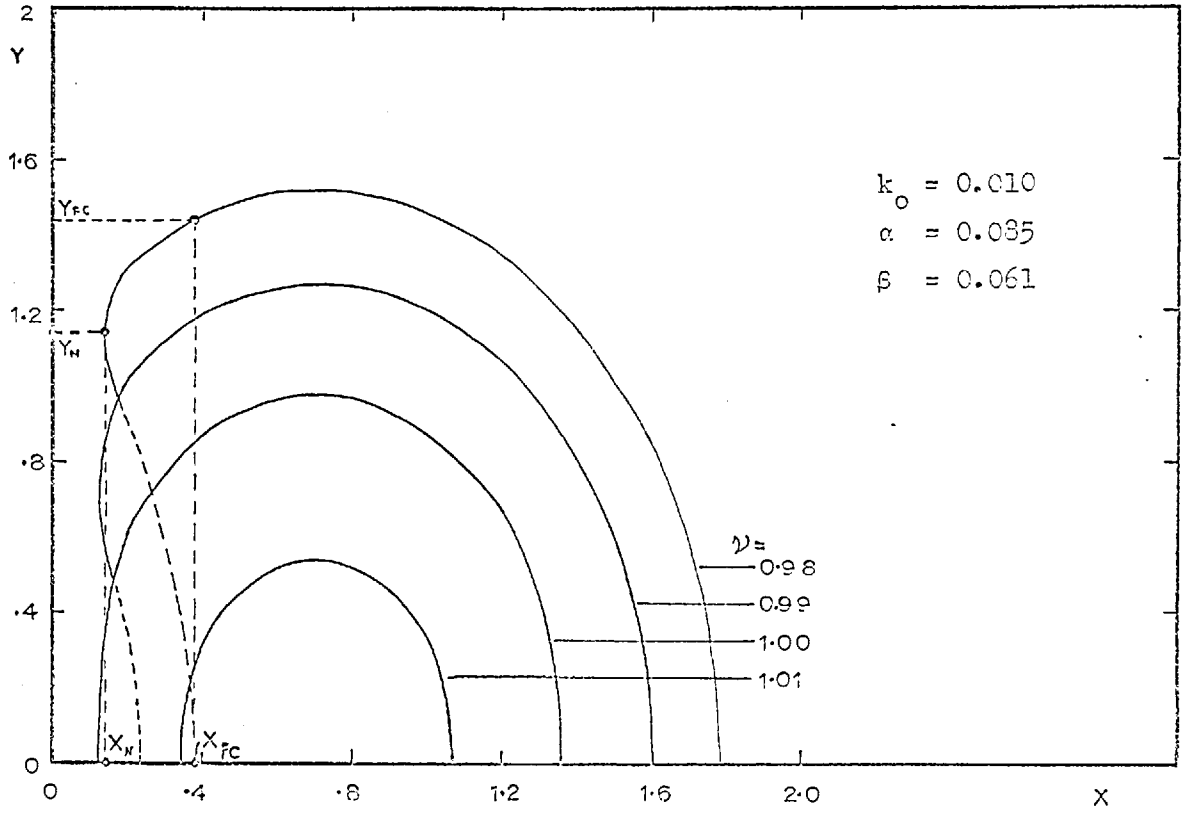


Figure 6.3(b) - Calculated (X,Y) -profiles for the same case.

such profiles, calculated for the same BSP as before. It can be seen that if $\nu < 1.0$, the profiles are double-valued in Y for a certain range of X. Let us consider, for example, the particular profile for $\nu = 0.98$. If X is slowly increased from zero, there is no oscillation at all until the value X_{FC} lying on the Frequency Characteristic is reached. At this point oscillation suddenly commences and the amplitude jumps to $Y = Y_{FC}$. For larger values of X, Y remains on this stable upper part of the profile, which corresponds to the positive internal root of equation (6.22). If X is increased sufficiently, Y decreases to zero again and remains zero no matter how large X becomes. If, on the other hand, X is steadily decreased, the upper part of the profile is re-traced until the "nose" (X_N, Y_N) is reached. The amplitude then abruptly drops to zero. The part of the profile beneath the "nose" is given by the negative internal root of (6.22).

Thus in the range

$$X_N < X < X_{FC} ,$$

amplitude hysteresis occurs, a common phenomenon in nonlinear systems.

Figure 6.3(a) shows the measured (X,Y)-profiles. It can be seen that hysteresis occurs as predicted. Quantitative agreement between the theoretical and actual profiles is obtained only in the region

$$X < 0.75$$
$$Y < 0.80,$$

although they are qualitatively similar outside this region.

The path traced out in (ν, X, Y)-space by the points (X_N, Y_N) of the profiles will be called the 'nose-locus'. The equation of this curve can be found by setting the root in equation (6.22) equal to zero. The projection of the locus on the (ν, X)-plane is therefore the curve

$$X^2 = \left(\frac{k_o}{\alpha\nu}\right)^2 .$$

Theoretical and experimental projections of the nose-loci are shown in Figures 6.2(a) and 6.2(b). In general, Y is large along a nose-locus, so that the agreement between the predicted and actual curves is good only near resonance ($\nu = 1$).

Three-dimensional (ν,X,Y)-surfaces for the amplitude response are given in Figures 6.4(a) and 6.4(b). In these diagrams the range of has been restricted to those values for which reasonable agreement between theory and practice is obtained. At lower frequencies the actual (X,Y)-profiles tend towards the shape predicted by PWL theory. See for example Figure 4.10, Chapter 4. The surfaces of Figure 6.4 are remarkably similar in shape, particularly in the vicinity of resonance. The nose-loci are indicated by heavy dashed lines.

Figure 6.5(a) shows experimental curves of constant steady-state subharmonic phase-angle θ. Phase angles were measured by observing the separation of the positive-going zero-crossings of the pump and subharmonic voltage waveforms displayed on an oscilloscope. The measurements are somewhat difficult to make at the experimental frequencies. This is particularly true for operating conditions which cause the subharmonic waveform to depart from the sinusoidal. The procedure adopted here was to judge the phase-position of the fundamental component of the subharmonic waveform as accurately as possible by eye. The results of a number of independent readings were then averaged.

The corresponding theoretical curves of constant θ are shown in Figure 6.5(b). They were calculated from equation (6.21) and are in fact portions

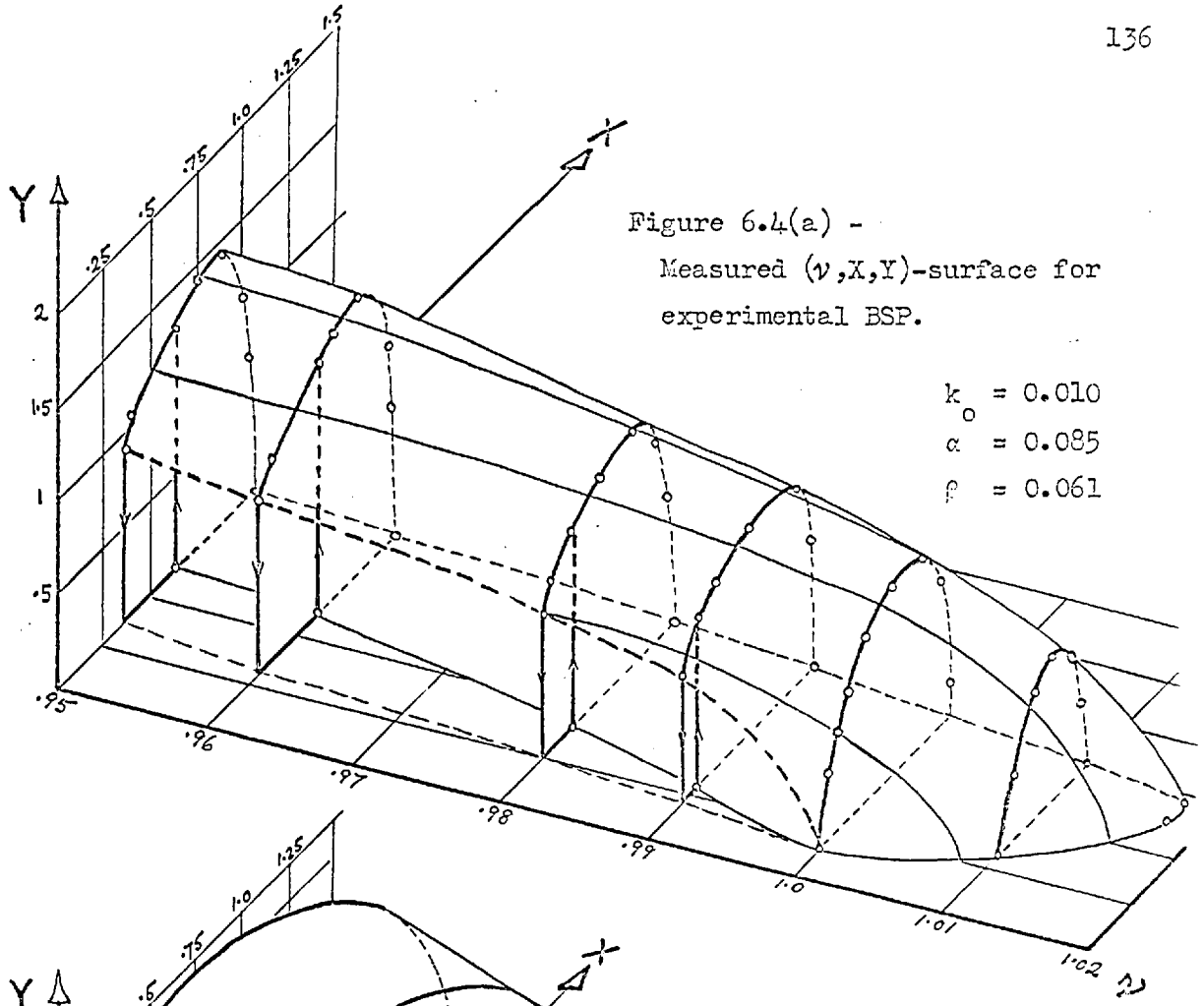


Figure 6.4(a) -
Measured (ν, X, Y)-surface for experimental BSP.

$k_o = 0.010$
$\alpha = 0.085$
$\beta = 0.061$

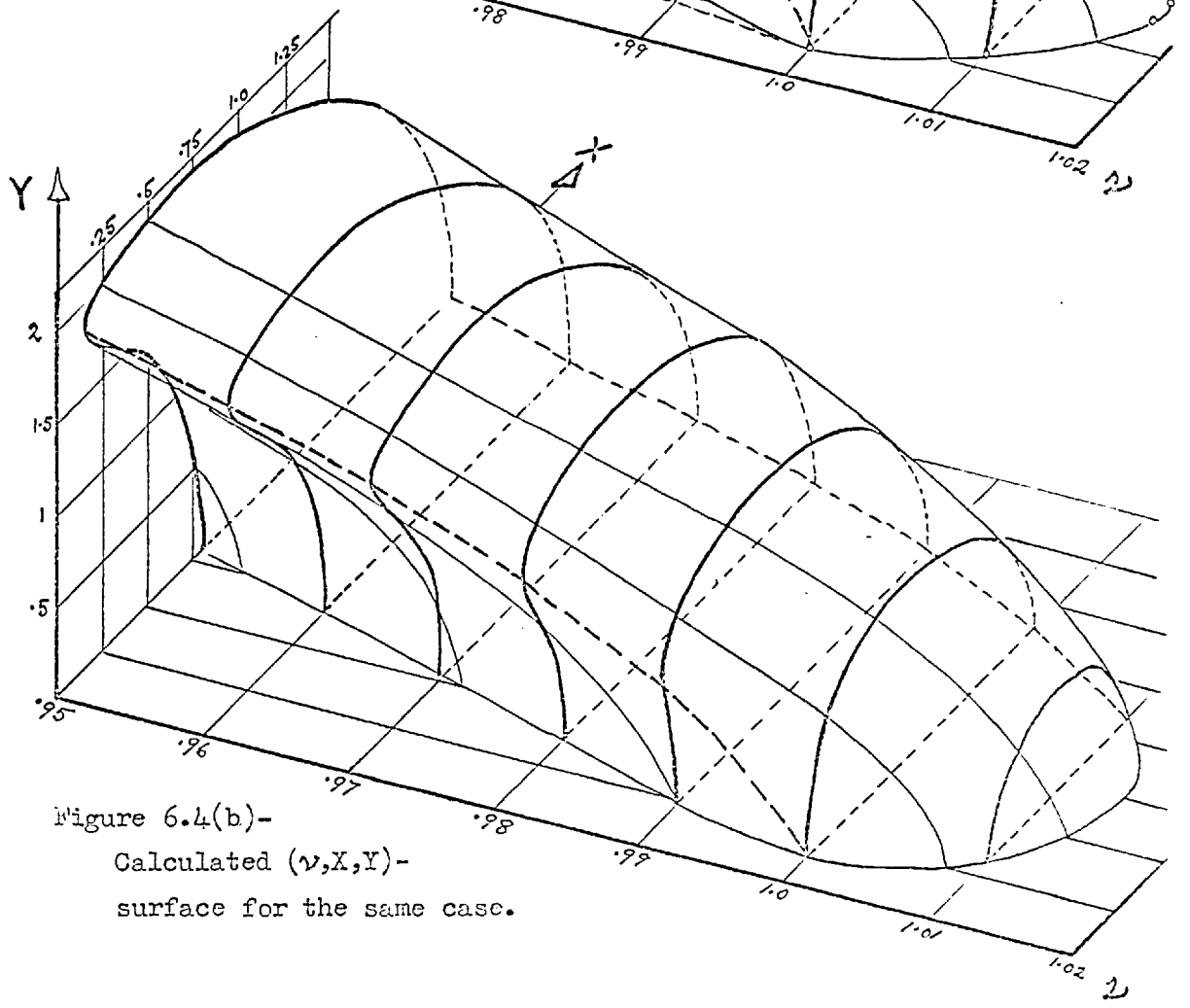


Figure 6.4(b)-
Calculated (ν, X, Y)-surface for the same case.

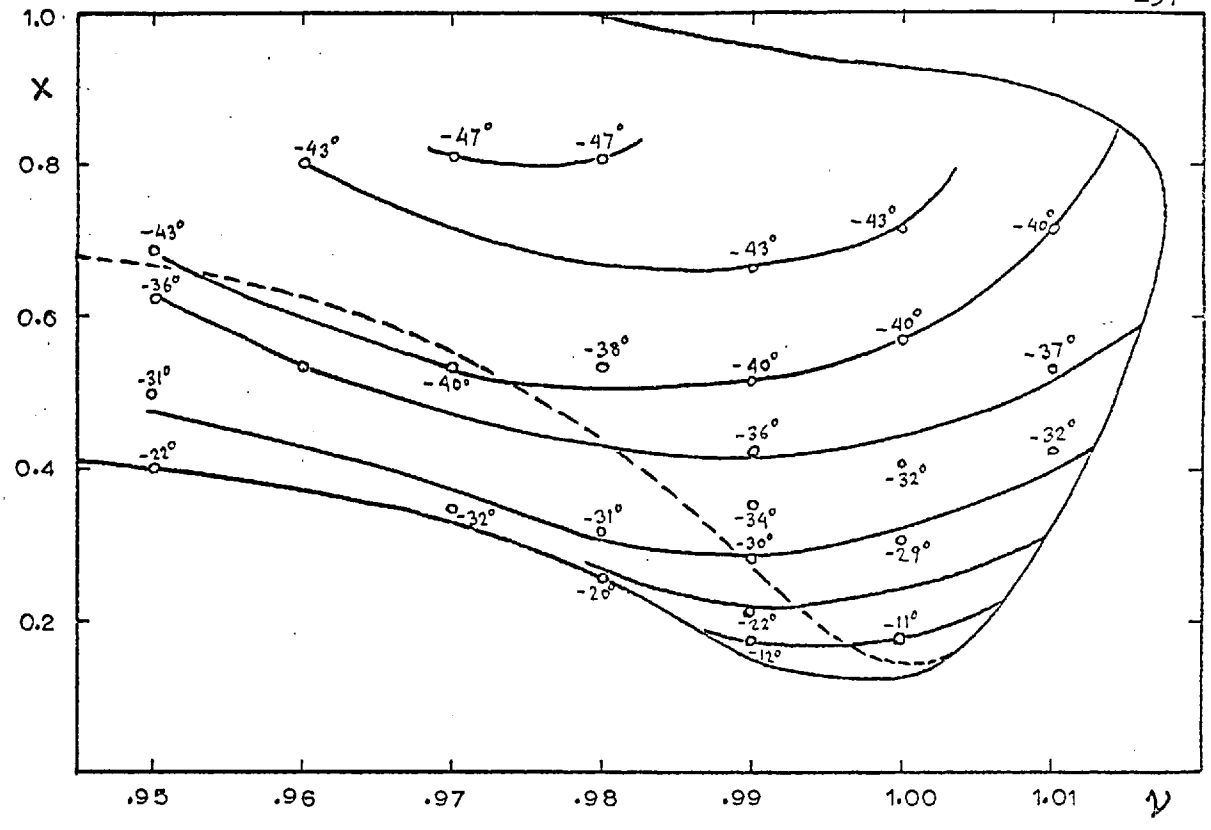


Figure 6.5(a) - Measured curves of constant steady-state phase-angle θ for BSP. Parameters as for figure 6.4.

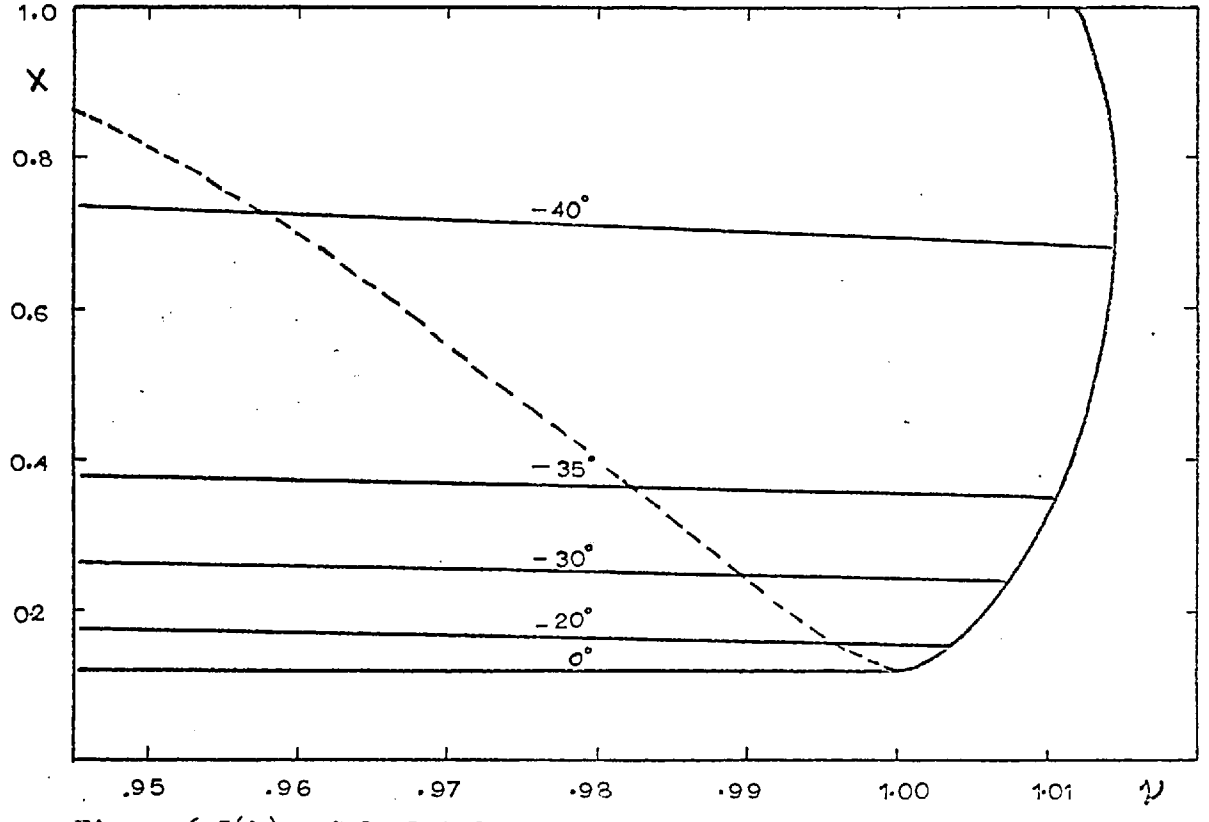


Figure 6.5(b) - Calculated curves of constant steady-state phase-angle for the same case.

of rectangular hyperbolae. The predicted phase angles are in close agreement with experiment in the small-signal region. Elsewhere the agreement is reasonable.

6.4.1 Summary and conclusions

The potentialities of the approximate "voltage" differential-equation approach have been investigated in some detail for a typical practical parametron. Good quantitative agreement between theory and practice has been obtained for operating conditions which did not violate any of the assumptions and approximations subsumed during the process of solution. Even when some of the constraints were exceeded, the solution was still qualitatively satisfactory.

The theoretical results have been computed without taking into account the influence of the nonlinear damping coefficients γ and δ. If they are included, the calculations become much more complicated than is considered reasonable in view of the small margin of improvement which may be expected. Thus, that part of the theoretical Frequency Characteristic which corresponds to large values of X would agree more nearly with the experimental curve. This would be so because the varactors support large-amplitude voltages at the pump frequency under such conditions. Therefore the influence of the nonlinear damping coefficient e^{cx} (and hence the influence of the coefficients γ and δ) comes into play.

The disagreement between theory and practice for values of ν less than 0.95 and for values of X greater than about 0.8 is primarily due to the small-signal validity of the approximate differential equation (6.3). Had we been able to solve (5.13) directly, large-signal agreement might have

been obtained.

The relative success of the above analysis acts as a powerful encouragement to develop a theory based on solutions of the "charge" differential equations (5.19) and (5.21), and to discover to what extent the range of validity is increased. Since these equations can be solved in the large-signal case without further approximation, better agreement can be expected so long as the varactors are not driven into forward conduction. This is because inclusion of the nonlinear damping complicates the "charge" model to an intolerable degree. The steady-state solution of these "charge" equations constitutes the substance of the remainder of this chapter.

6.5 Steady-state solution of the differential equations of the large-signal "charge" model

It was shown in Section 5.4 that the differential-equation models for the two basic kinds of balanced varactor parametron were sufficiently similar to be treated simultaneously when the $C = \mathcal{J}(v)$, or "voltage", representation of the varactors was employed. It is reasonable to suppose that this is also the case when the $v = \mathcal{J}(q)$, or "charge" representation is used.

The Balanced Parallel Parametron (BPP) has been chosen for detailed analysis because, as indicated in Section 5.5, it is the more practically useful of the two devices. The analysis of the BSP follows very similar lines, but since no new phenomena arise, it is not treated here by the "charge" method.

The somewhat complicated derivation of Section 5.5 led to the following pair of differential equations for the "charge" model; a second-order

linear equation relating the instantaneous normalised voltage y to the instantaneous normalised differential charge z:

$$(1-B)\overset{oo}{y} + (\tfrac{1}{2}k_v + k_L)\overset{o}{y} + y = B\overset{oo}{z}, \qquad (6.24)$$

and a first-order nonlinear equation in y and z containing the nonlinear charge-voltage law in non-approximated form:

$$k_p\left\{\tfrac{1}{4}(1-B)z^4\overset{o}{z} + 4\left[(1-B)y-Bz\right](z\overset{o}{y}-y\overset{o}{z})\right\} + Bz^3x + (B+k_vk_p)(\tfrac{1}{16}z^5-z^3+y^2z)$$
$$\equiv \mathfrak{F}\left[x,y,z\right] = 0. \qquad (6.25)$$

If the damping parameters k_v and k_L (due to the varactor conductance and to the loading respectively) are negligibly small, and if there is no stray capacitance C_s, so that B = 1, then equation (6.24) becomes simply

$$y = \overset{oo}{z} \qquad (6.26)$$

which can be substituted into (6.25) to give a single equation in z only:

$$4k_p(\overset{oo}{z}\overset{o}{z} - z\overset{ooo}{z}) + (\overset{oo}{z})^2 + \frac{1}{16}z^4 + z^2(x-1) = 0, \qquad (6.27)$$

which, by rejecting the term in k_p and $\frac{1}{16}z^4$, may be seen to be related to a "squared" Mathieu equation. However, we shall not, for the moment, treat this simple case, but rather equations (6.24) and (6.25) simultaneously with the proviso that forward diode conduction is not involved, so that the parameter k_v may be neglected.

In accordance with the terminology employed in the "voltage" analysis, we again assume that the pump is defined by

$$x = X.\sin 2\nu\tau \qquad (6.28)$$

where X is the amplitude, and no phase-angle need be included because the phases of all other signals will be defined with reference to the pumping signal. We shall also continue to use the method of harmonic balance so that our steady-state results, although approximate, will be consistent with

the transient results, which do not seem to be analytically obtainable by any other simple method.

Since the system is balanced, the waveform of the voltage appearing across the inductance and also the differential charge waveform may be assumed to be predominantly sinusoidal; only odd harmonics occur, and experiment indicates that they do not become important until quite large values of detuning ($\nu \ll 1$) are reached. These assumptions are further justified by the degree to which the results approximate reality.

Accordingly, the normalised subharmonic voltage is assumed to be

$$\tilde{y} = Y \sin(\nu\tau + \theta), \tag{6.29}$$

and a similar assumption is made concerning the normalised subharmonic differential charge

$$\tilde{z} = Z \sin(\nu\tau + \psi), \tag{6.30}$$

in which the amplitudes Y and Z and the phases θ and ψ are for the moment taken to be non-time-varying quantities. The reason for this is that a general analysis valid for the transient as well as the steady-state case (i.e. including the time-derivatives $\dot{Y}$, $\dot{\theta}$, etc.), which was possible when the approximate "voltage" representation was used, becomes so complicated as to be impracticable. Therefore the steady-state will be treated with both k_p and k_L present, but the transient response will be investigated separately for the two important cases:

(1) when the pump-circuit damping k_p is the dominant loss parameter and

(2) when the load damping k_L dominates.

Substitution of (6.29) and (6.30) into the linear differential equation (6.24) yields, when integrated twice:

$$\tilde{z} = -Y\left[L \sin(\nu\tau + \theta) + M \cos(\nu\tau + \theta)\right], \tag{6.31}$$

where $L = \frac{1 - \nu^2(1-B)}{B\nu^2}$ and $M = \frac{k_L}{B\nu}$. (6.32)

In place of (6.25), we now form the approximate nonlinear differential equation

$$\mathcal{E}\left[x, \tilde{y}, \tilde{z}\right] = 0, \tag{6.33}$$

where $\tilde{y}$ and $\tilde{z}$ are given by (6.29) and (6.31) respectively and x is given by (6.28). Because of the complexity of (6.25), it is advantageous to write x, y, and z in the forms:

$$x = -j2X(\alpha^2 e^{-j2\theta} - \alpha^{*2} e^{j2\theta}), \text{ where } \alpha = \tfrac{1}{2}e^{j(\nu\tau+\theta)}, \tag{6.34}$$

$$\tilde{y} = -jY(\alpha - \alpha^*), \tag{6.35}$$

$$\tilde{z} = -Y(\alpha\beta^* + \alpha^*\beta), \text{ where } \beta = M + jL. \tag{6.36}$$

Having formed (6.33), and rejected the terms α^3, α^{*3}, α^5, α^{*5}, corresponding to frequencies higher than ν (because of the approximation (6.29) that they are not important), we equate the coefficients of $(\alpha + \alpha^*)$ and $-j(\alpha - \alpha^*)$ separately to zero. This procedure is equivalent to, but much simpler than, a harmonic-balance calculation in terms of trigonometric functions.

Omitting the damping parameter k_v, which is due to varactor conductance, one obtains the following pair of equations defining the steady-state behaviour of the BPP:

$$Y^2(L^2+M^2)^2\alpha\alpha^*(2M\nu\delta - \tfrac{5}{8}L) + 3L(L^2+M^2-1) - 4M\sigma +$$
$$-X\left[M(3L^2+M^2)\cos 2\theta + 2L^3 \sin 2\theta\right] = 0 \tag{6.37}$$

and

$$-Y^2(L^2+M^2)^2\alpha\alpha^*(2\nu L\delta + \tfrac{5}{8}M) + M(3(L^2+M^2) - 1) - 4M\sigma.\nu k_L$$
$$+ X\left[-L(3M^2+L^2)\cos 2\theta + 2M^3 \sin 2\theta\right] = 0 \tag{6.38}$$

where

$$\delta = \frac{1}{4} k_p \left(\frac{1}{B} - 1\right) \tag{6.39}$$

$$\sigma = \frac{4k_p}{B\nu}$$

$$\alpha\alpha^* = \frac{1}{4}$$

The corresponding solution for the subharmonic charge can be found from the steady-state relations

$$Z^2 = (L^2 + M^2)Y^2$$

and $$\psi = \theta.$$

Equations (6.37) and (6.38) are of the form

$$\begin{aligned} A.\cos 2\theta + B.\sin 2\theta + C = 0 \\ D.\cos 2\theta + E.\sin 2\theta + F = 0 \end{aligned} \tag{6.40}$$

whence the steady-state amplitude of the subharmonic voltage, Y, is given by

$$(AE - BD)^2 = (AF - CD)^2 + (BF - CE)^2 \tag{6.41}$$

and the corresponding phase-angle θ by

$$\operatorname{tg} 2\theta = \frac{AF - CD}{CE - BF} . \tag{6.42}$$

After some rearrangement, equation (6.41) turns out to be

$$4X^2(L^2 + M^2)^4 = (LC + MF)^2 + 4(MC - LF)^2 \tag{6.43}$$

where

$$\left.\begin{aligned} C &= (L^2 + M^2)^2 Y^2 \left(\tfrac{1}{2}M.\nu\,\delta - \frac{5}{32}L\right) + 3L(L^2 + M^2 - 1) - 4M\sigma, \\ F &= -(L^2+M^2)^2 Y^2 \left(\tfrac{1}{2}L.\nu\,\delta + \frac{5}{32}M\right) + M(3(L^2+M^2) - 1) = 4M\sigma.\nu k_L, \end{aligned}\right\} \tag{6.44}$$

Written in full, equation (6.43) is

$$\begin{aligned} &4X^2(L^2 + M^2)^4 = \\ &= \left[\frac{5}{32}(L^2 + M^2)^3 Y^2 + M^2 + 3(L^2 - (L^2 + M^2)^2) + 4M\sigma(M.\nu k_L + L)\right]^2 + \\ &+ 4\left[\tfrac{1}{2}\nu\,\delta.(L^2 + M^2)^3 Y^2 - 2LM + 4M\sigma(L.\nu\, k_L - M)\right]^2 . \end{aligned} \tag{6.45}$$

It is possible to invert this equation in order to obtain an explicit expression for Y, but the result is somewhat unwieldy.

Equation (6.42) for the phase angle is

$$\text{tg } 2\theta = \frac{L(L^2 + 3M^2).C - M(M^2 + 3L^2).F}{2(L^3.F + M^3.C)} \qquad (6.46)$$

which does not lend itself to further simplification unless k_L is the only damping parameter of importance.

There is an ambiguity in the interpretation of equation (6.46). Physically, it is known that the stable subharmonic oscillation can have either of two fixed phase angles 180° apart. However, since

$$\tan 2\theta = \tan 2(\theta \pm \frac{N\pi}{2}),$$

where N is an integer, equation (6.46) permits the existence of another pair of steady-state phase angles oriented at 90° to the first pair. Selection between the two possibilities will follow from the stability considerations of Chapter 7, Sub-Section 7.4.6.

In order to gain some insight into the significance of these complicated solutions, certain special cases will be considered.

6.5.1 Special Case 1

The simplest form of the solution is obtained when all the circuit damping is absent and there is not stray capacitance:

$$k_p = 0, \quad k_v = 0, \quad k_L = 0, \quad B = 1.$$

This special case corresponds to an idealised conservative system described by the simultaneous equations

$$\left.\begin{aligned} &z^2(x-1) + \frac{1}{16}\, z^4 + y^2 = 0 \\ \text{and}\quad &y = \overset{oo}{z}. \end{aligned}\right\} \qquad (6.47)$$

These reduce to the single equation

$$(\overset{oo}{z})^2 + \frac{1}{16}\, z^4 + z^2(x-1) = 0. \qquad (6.48)$$

The solution of this equation is obtained by putting M and δ equal to zero, so that (6.45) gives

$$4X^2 = \left[\frac{5}{32} \cdot \frac{1}{\nu^4} \cdot Y^2 + 3(\nu^4 - 1)\right]^2 \qquad (6.49)$$

for the amplitude, while (6.46) gives simply

$$\text{tg } 2\theta = \infty \qquad (6.50)$$

for the phase. Thus, in this case, the phase angle is always $\pm 45^\circ$ regardless of the operating point (ν,X). This is no longer true when there is any kind of damping in the system.

Equation (6.49) for the subharmonic amplitude defines a three-dimensional surface in (ν,X,Y)-space, "inside" which lie the corresponding surfaces for real non-conservative systems. The intersection of the surface with the (ν,X)-plane is the Frequency Characteristic shown in Figure 6.6. The (ν,Y) and (ν,X)-profiles are given in Figures 6.7 and 6.8 respectively. The solid curves correspond to stable values of the amplitude Y; the broken curves to unstable values.* Two perspective drawings of the complete (ν,X,Y)-surface appear in Figure 6.9.

It can be seen that this idealised model predicts the persistence of subharmonic oscillation down to zero frequency, and down to zero pump amplitude at all frequencies less than $\nu = 1.0$. This behaviour differs

---

* The question of stability is discussed in Section 7.4.6. Chapter 7.

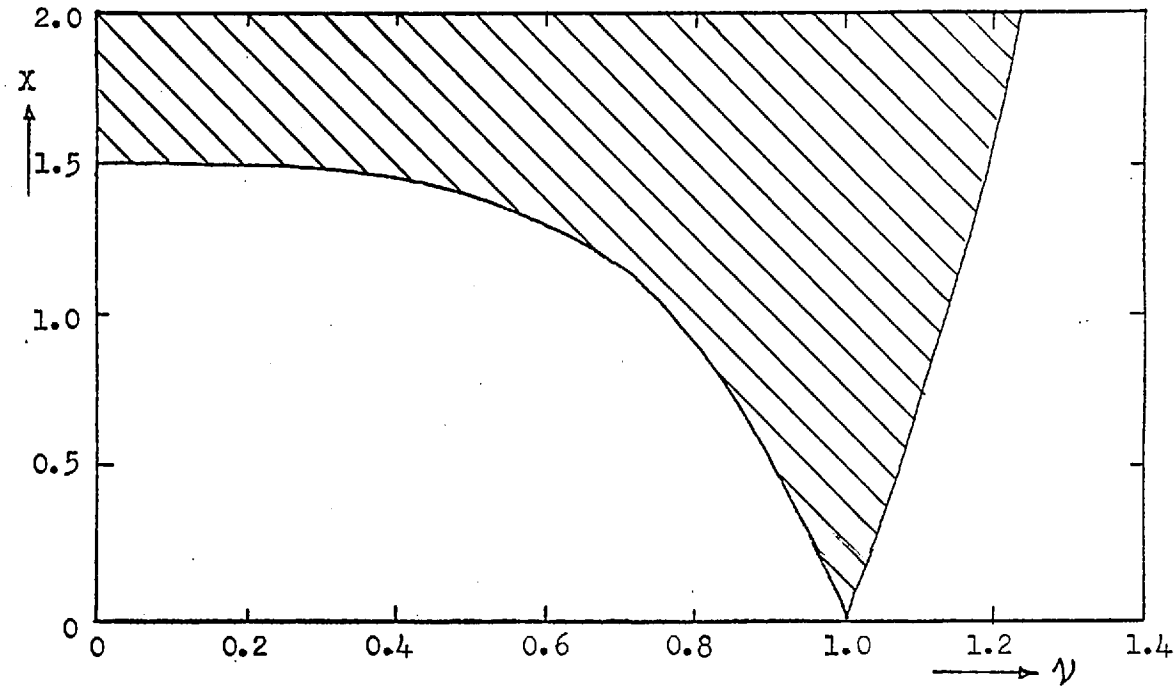


Figure 6.6 - Frequency Characteristic for the BPP: no damping or stray capacitance.

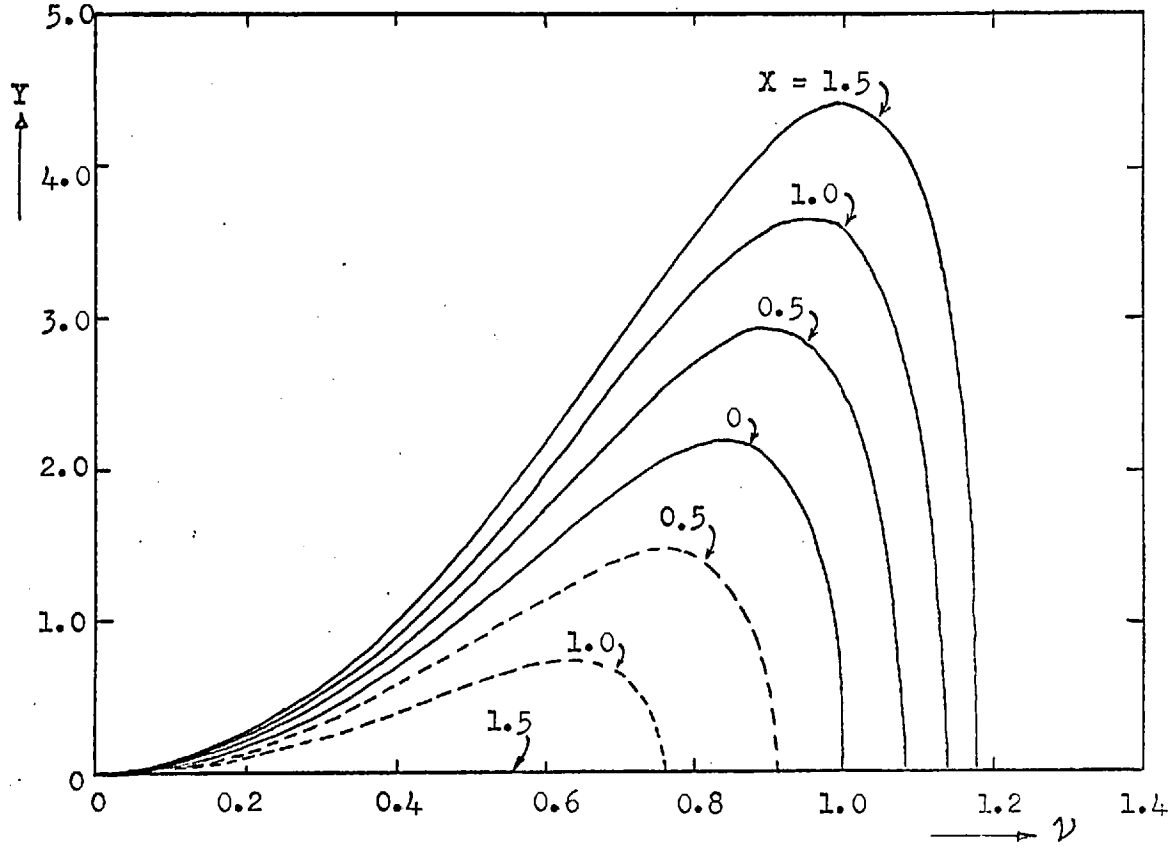


Figure 6.7 - (ν,Y) frequency-amplitude profiles for the same case.

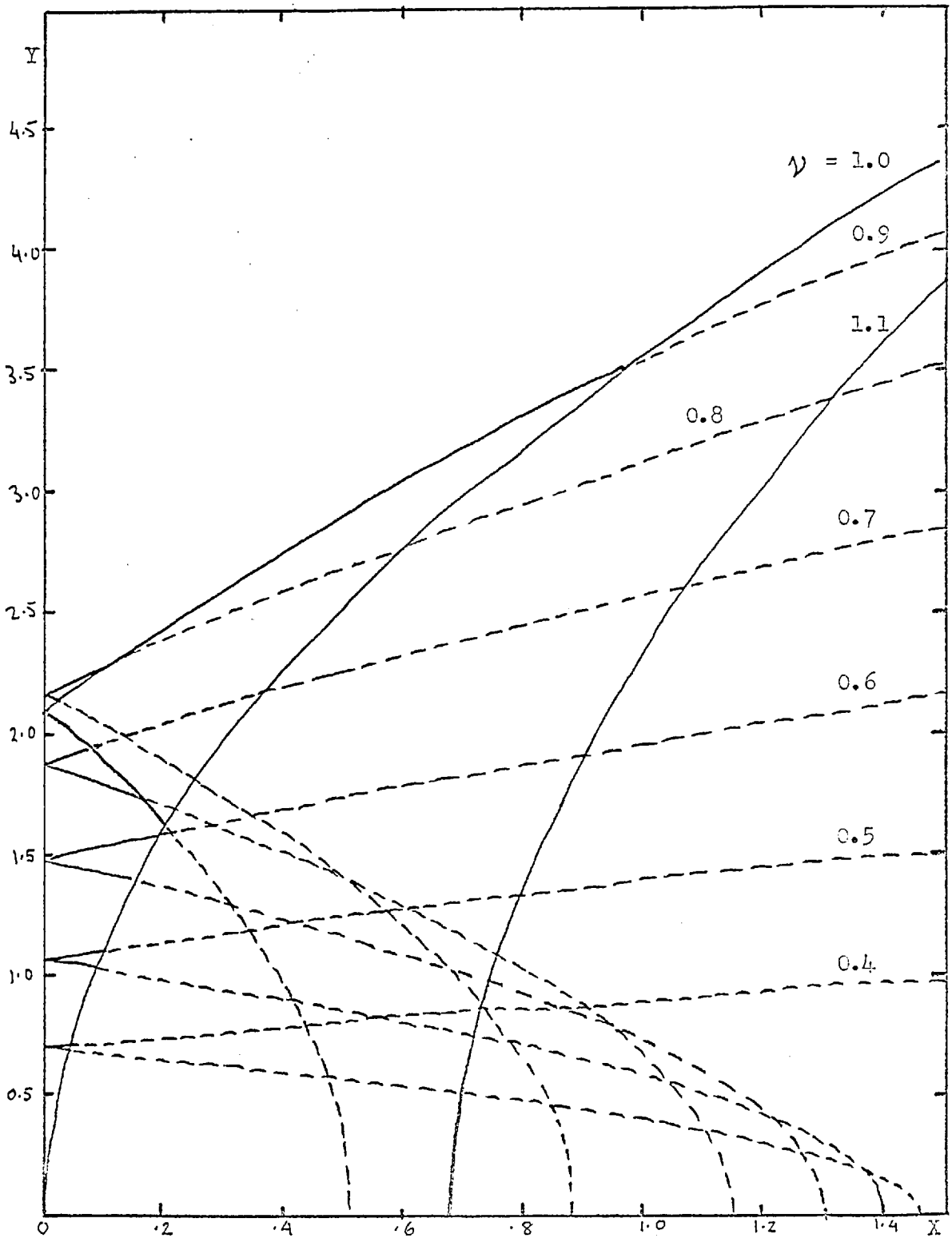


Figure 6.8 - (X,Y)-profiles for the case of no damping and no stray capacitance.

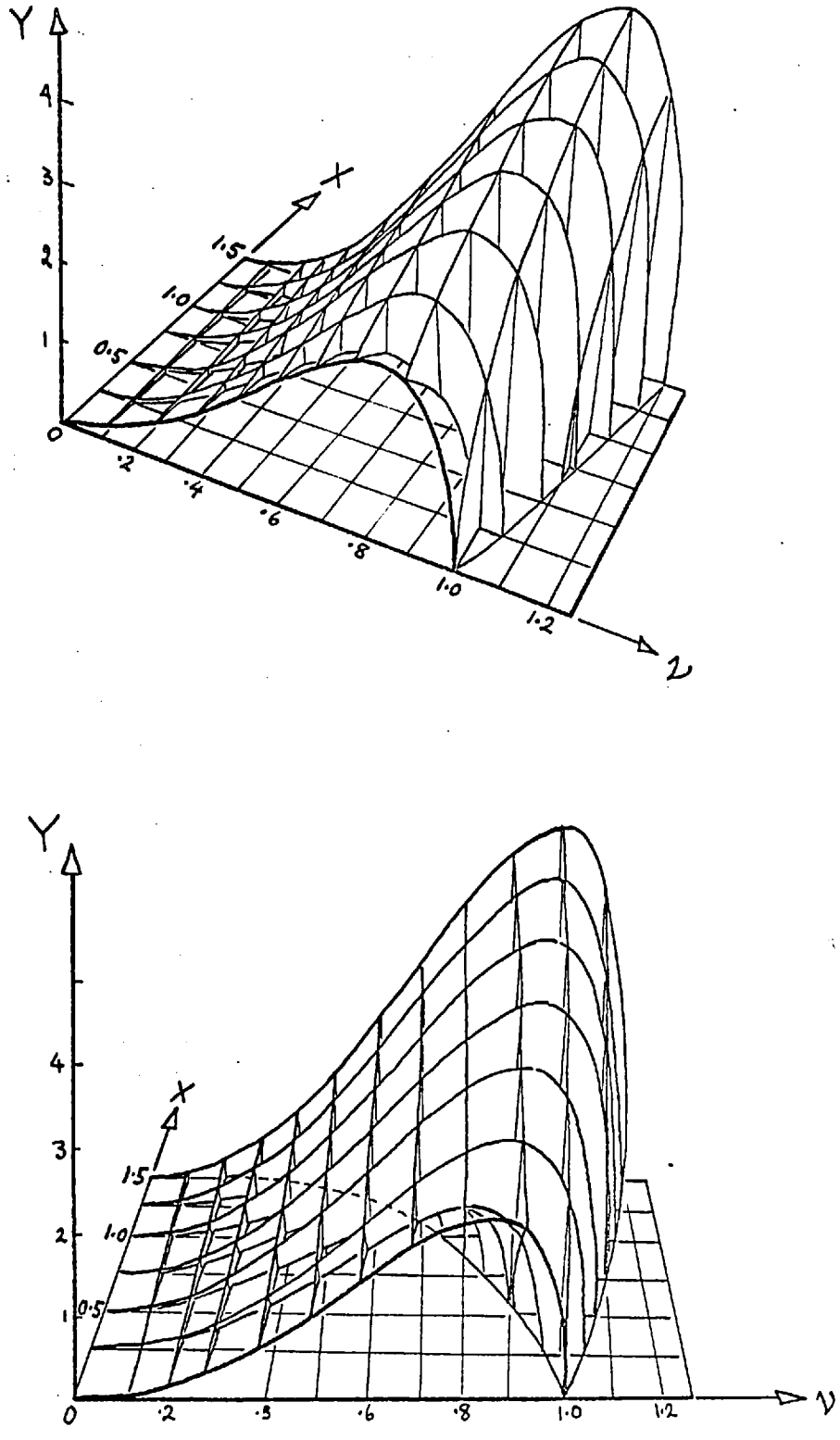


Figure 6.9 - Two aspects of the 'exoskeletal' (ν,X,Y) - surface for Special Case 1.

somewhat from that of a real parametron, but the general characteristics of this "exoskeletal" surface are consistent with practical measurements.

Most of the deviations between this solution and reality are accounted for by the various damping parameters. The parameters k_p and k_L, due to the pump-circuit resistance and the load conductance respectively, have rather different effects. It will be convenient to consider them separately. The next sub-section considers a device in which k_p is the only damping parameter of importance.

6.5.2 Special Case 2

The steady-state behaviour of a real parametron can be predicted quite accurately if one includes in the theory the effects of the source resistance R_p and the stray capacitance C_s. The following conditions are assumed to apply:

$$k_p \geqslant 0, \quad k_v = 0, \quad k_L = 0, \quad B \leqslant 1$$

The conditions

$$k_v = \omega_o L\, G_v = 0$$

and $$k_L = \omega_o L\, G_L = 0$$

mean that the load conductance G_L and the varactor conductance G_v are negligible. Thus typical values are

$$R_p = 500\ \Omega, \qquad f_o = 5\ \text{Mc/s},$$

$$R_v = 100\ \text{K}\Omega, \qquad C_o = 20\ \text{pF},$$

$$R_L = 100\ \text{K}\Omega, \qquad L = 20\ \mu\text{H}.$$

so that $k_p = 0.3$ and $k_v = k_L = 0.012$, giving $k_p \gg (k_v \text{ or } k_L)$.

The amplitude equation (6.43) is now

$$4X^2 = \left[\frac{5}{32}(LY)^2 + 3\cdot(\Gamma^2 - 1)\right]^2 + (\nu\,\delta)^2(LY)^4 \,, \quad (6.51)$$

where $\Gamma = L^{-1}$, and the phase equation (6.46) becomes

$$\text{tg } 2\theta = \frac{\frac{5}{32}(LY)^2 + 3(\Gamma^2 - 1)}{\nu\delta\,(LY)^2} \quad (6.52)$$

Equation (6.51) for the amplitude resembles that obtained in Special Case 1, but now the parameters L and δ appear, due to the stray capacitance C_s and to the damping k_p. It is interesting to observe that if C_s is zero, then B=1 so that the damping term δ containing k_p vanishes. This illustrates the importance of including parasitic elements in the analysis of systems of this kind.

The equation (6.52) for the phase-angle shows that θ depends on both the detuning and the subharmonic amplitude Y, except in the resonant case $\nu = 1$, for then $\Gamma = 1$ and

$$\text{tg } 2\theta = \frac{5}{32}\cdot\frac{1}{\nu\delta} \,, \quad (6.53)$$

independently of Y.

The Frequency Characteristic is obtained by putting Y = 0 in (6.51). The result is similar to Special Case 1 in that the characteristic goes to X = 0 at $\nu = 1$, but now the <u>shape</u> of the curve is modified by the influence of the stray capacitance parameter B, although it is not affected by the damping parameter k_p. Stray capacitance has the effect of narrowing the range of frequencies for which subharmonic oscillation is possible at a given pump amplitude.

The explicit solution for the subharmonic amplitude can be found from

(6.51):

$$Y^2 = \Gamma^{-2}\left\{\left[\frac{\frac{15}{32}(1-\Gamma^2)}{(\frac{5}{32})^2+(\nu\delta)^2}\right] \pm \sqrt{\left[\frac{\frac{15}{32}(1-\Gamma^2)}{(\frac{5}{32})^2+(\nu\delta)^2}\right]^2 - \left[\frac{9(1-\Gamma^2)^2-4X^2}{(\frac{5}{32})^2+(\nu\delta)^2}\right]}\right\}. \qquad (6.54)$$

If this is compared with the corresponding result for the approximate "voltage" solution, equation (6.22), certain similarities become apparent. A significant difference is the absence in (6.54) of the term in X^2 outside the radical. This means that the (ν,X,Y).-surface will not go to zero at large values of X.

As in the case of the "voltage" analysis, the coordinates (X_N,Y_N) of the nose-locus are found by equating the interior of the root in (6.54) to zero:

$$X_N = \frac{3}{2} \cdot \frac{\nu\delta(1-\Gamma^2)}{(\frac{5}{32})^2+(\nu\delta)^2}, \qquad (6.55)$$

$$Y_N = \Gamma\sqrt{\frac{\frac{15}{32}(1-\Gamma^2)}{(\frac{5}{32})^2+(\nu\delta)^2}}. \qquad (6.66)$$

It can be shown that the phase-angle θ_N along the nose-locus is given by

$$\operatorname{tg} 2\theta_N = -\frac{32}{5}\cdot\nu\delta, \qquad (6.57)$$

a function of ν, k_p and B only. This result should be compared with (6.53) for the phase angle at resonance.

The subharmonic phase angle predicted by (6.52) is in close agreement with experimental values measured in the vicinity of resonance. However, as the frequency is reduced below resonance, the present theory predicts that θ decreases, whereas in practice it increases. The considerations of Sub-Section 7.4.6.1, Chapter 7, will show that $\operatorname{sgn}(k_p)$, and hence $\operatorname{sgn}(\delta)$, should

be reversed for all frequencies ν less than unity: the theoretical results are then in accord with experiment.

The comparison of these results with experimental measurements will be deferred until a third Special Case has been dealt with: that in which the predominant source of circuit damping is the load resistance R_L.

6.5.3 Special Case 3

The conditions corresponding to those assumed in the analysis by means of the "voltage" model are

$$\boxed{k_p = 0,\quad k_v = 0,\quad k_L \geqslant 0,\quad B \leqslant 1} \quad .$$

The amplitude and phase equations now become more complicated than in Special Case 2. They are given by (6.45) and (6.46) respectively, where now

$$\left.\begin{aligned} C &= -\frac{5}{32} L(L^2+M^2)^2Y^2 + 3L(L^2+M^2-1) , \\ F &= -\frac{5}{32} M(L^2+M^2)^2Y^2 + M(3L^2+M^2-1) . \end{aligned}\right\} \quad (6.58)$$

The amplitude equation is therefore

$$4X^2(L^2+M^2)^4 = \left[\frac{5}{32}(L^2+M^2)^3Y^2 + M^2 + 3(L^2 - [L^2+M^2]^2)\right]^2 + 16(LM)^2 . \quad (6.59)$$

An explicit solution for Y can be obtained from this:

$$Y^2 = \frac{3\left[(L^2+M^2)^2 - L^2\right] - M^2 \pm 2\sqrt{X^2(L^2+M^2)^4 - 4(LM)^2}}{\frac{5}{32}(L^2+M^2)^3} \quad (6.60)$$

The coordinates (X_N, Y_N) of the nose are again given by equating the internal root to zero:

$$X_N = \frac{2LM}{(L^2+M^2)^2} \quad , \quad (6.61)$$

$$Y_N = \frac{1}{(L^2+M^2)} \cdot \sqrt{\frac{3\left[(L^2+M^2)^2 - L^2\right] - M^2}{\frac{5}{32}(L^2+M^2)}} \quad . \tag{6.62}$$

The steady-state phase-angle is given by (6.46) with C and F as specified by (6.57). The resulting expression is Y-dependent and complicated. However, it will be shown in Sub-Section 7.4.2, Chapter 7 that a Y-independent result for θ can be found by working in terms of the charge phase-angle ψ. Further, it will be shown in Sub-Section 7.4.3 that the phase-angle along the nose-locus is given by the simple expression

$$\text{tg } \theta_N = - \frac{M}{L} .$$

6.6 Comparison of the large-signal "charge" theory with experiment

The circuit of a typical experimental Balanced Parallel Parametron is given in Figure 7.33(b). The measured parameters of such a device were

$$V_B = 0,$$
$$V_o = \phi = 0.7 \text{ volt},$$
$$C_o = 16.3 \text{ pF},$$
$$L = 26.95 \ \mu\text{H},$$
$$f_o = 7.295 \text{ Mc/s},$$
$$R_p = 350 \ \Omega ,$$

from which the following quantities were calculated:

$$B = \tfrac{1}{2} \omega_o^2 L C_o = 0.46,$$
$$k_p = \omega_o C_o R_p = 0.26.$$

Figure 6.10 shows the measured Frequency Characteristic for the parametron described above. The curve is compared with the theoretical characteristics calculated for two values of B from equation (6.51) of

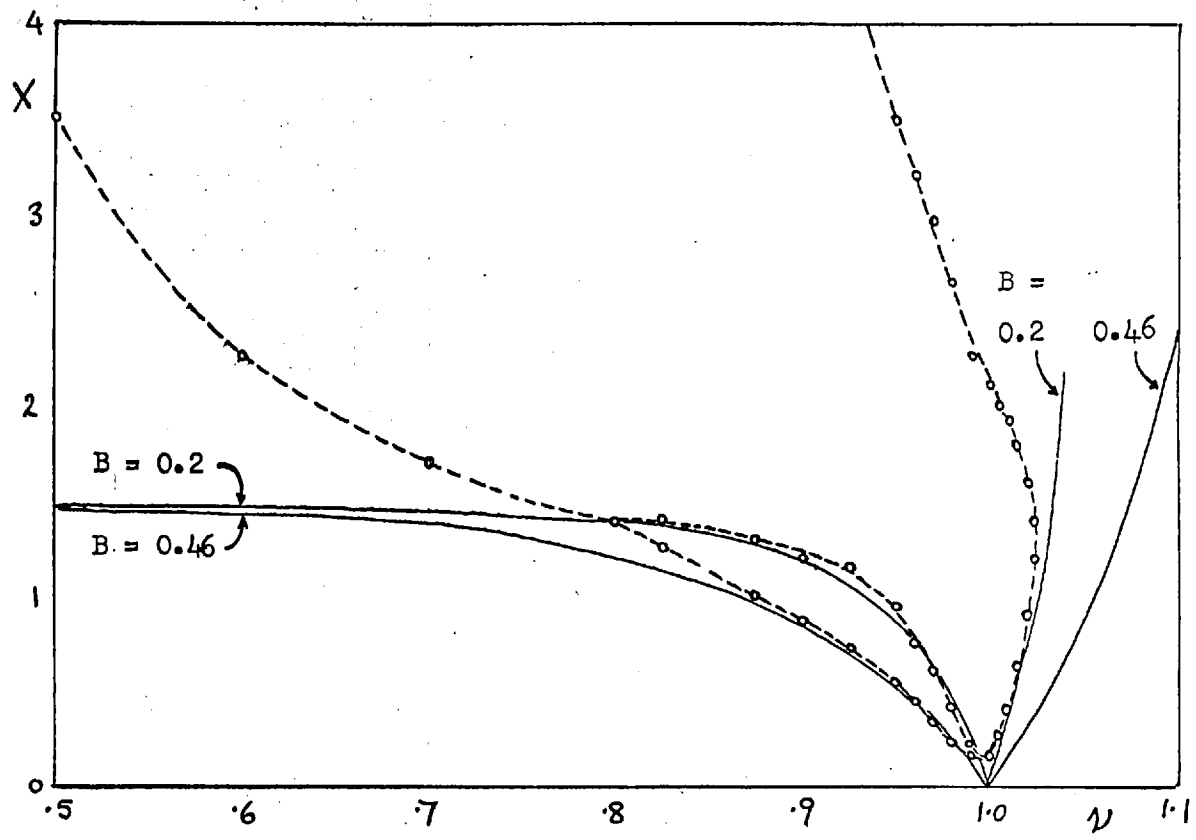


Figure 6.10 -

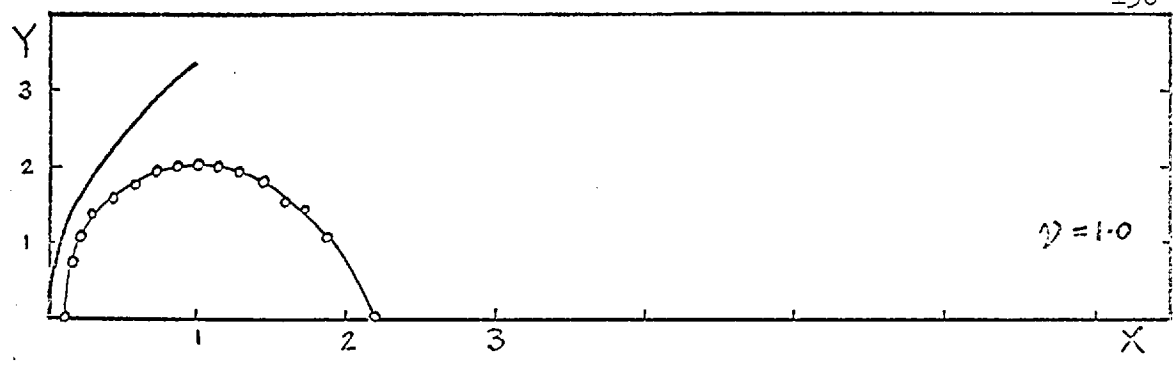
Measured frequency characteristic and nose locus for an experimental BPP compared with theoretical characteristics calculated for the indicated values of B.

$k_p = 0.26$, k_L assumed zero.

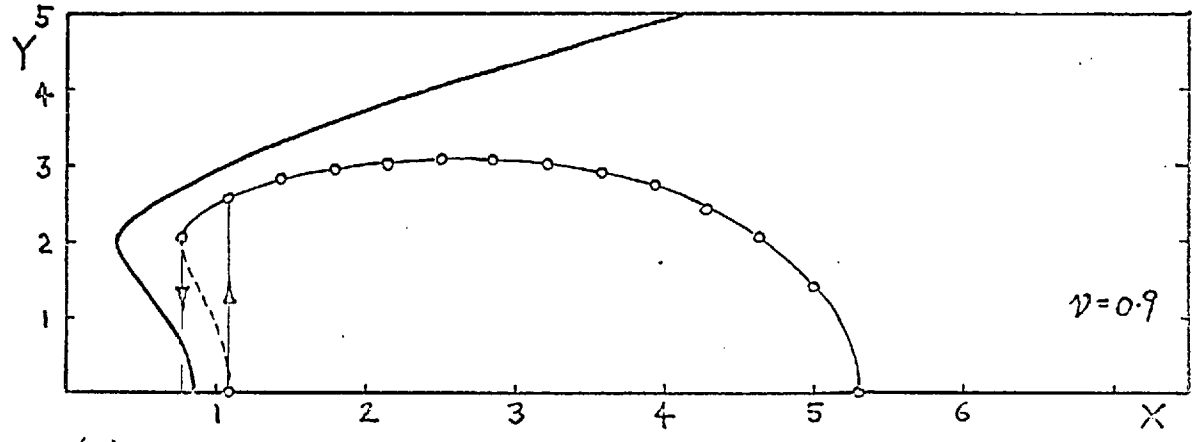
Special Case 2, in which the influence of k_L is neglected. The characteristics agree over a large range of frequencies if B = 0.2. If the calculated value B = 0.45 is used, the agreement is less good, but for large detuning is still superior to the corresponding result given by the "voltage" theory. It is interesting that the theoretical characteristics go to X = 0 at $\nu = 1.0$, unlike the measured curve. The reason for this is that the Frequency Characteristic specified by equation (6.51) is independent of the damping parameter δ and hence of k_p. If the complete expression (6.45) is used, it is found that the characteristic is actually dependent on both k_p and k_L, and that it no longer goes to X = 0 at $\nu = 1$. However, the accuracy obtained by the use of the simpler theory of Special Case 2 is considered adequate for most practical purposes.

Theoretical and experimental (X,Y)-profiles for three values of ν are shown in Figure 6.11. The large-signal agreement is much better than was obtained by the "voltage" method. In particular, in the strongly-detuned case $\nu = 0.8$, the calculated and measured curves are similar even for values of X in excess of 7.0, a very large-signal condition. At such values of detuning and pump amplitude, the subharmonic voltage waveform becomes very "spiky" since its harmonic content is high. The voltages were therefore measured with a true-RMS voltmeter, and the readings subsequently converted to equivalent peak values for comparison with the theory.

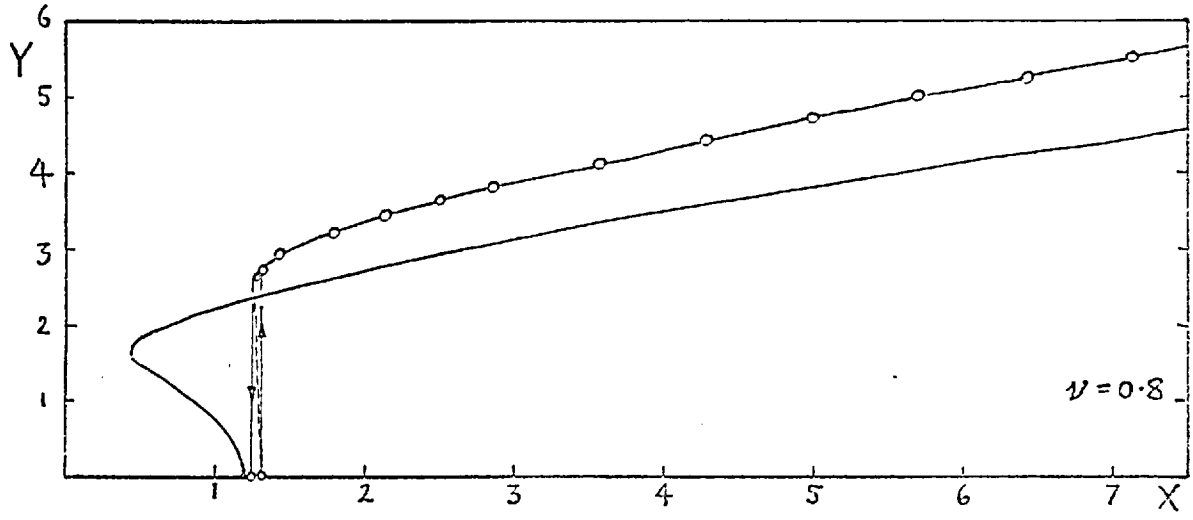
If the load-damping parameter k_L dominates the response, the theoretical frequency characteristic and nose-locus present an appearance considerably different from that of the corresponding curves when the pump-circuit damping parameter k_p dominates. As an example, Figure 6.12 shows the curves calculated from equations (6.59) and (6.61) of Special Case 3 for the



(a) Resonant case: ν = 1.0.



(b) Detuned case: ν = 0.9.



(c) Detuned case: ν = 0.8.

Figure 6.11 - Theoretical and experimental (X,Y) - profiles for a Balanced Parallel Parametron with k_p = 0.26 and B = 0.46.

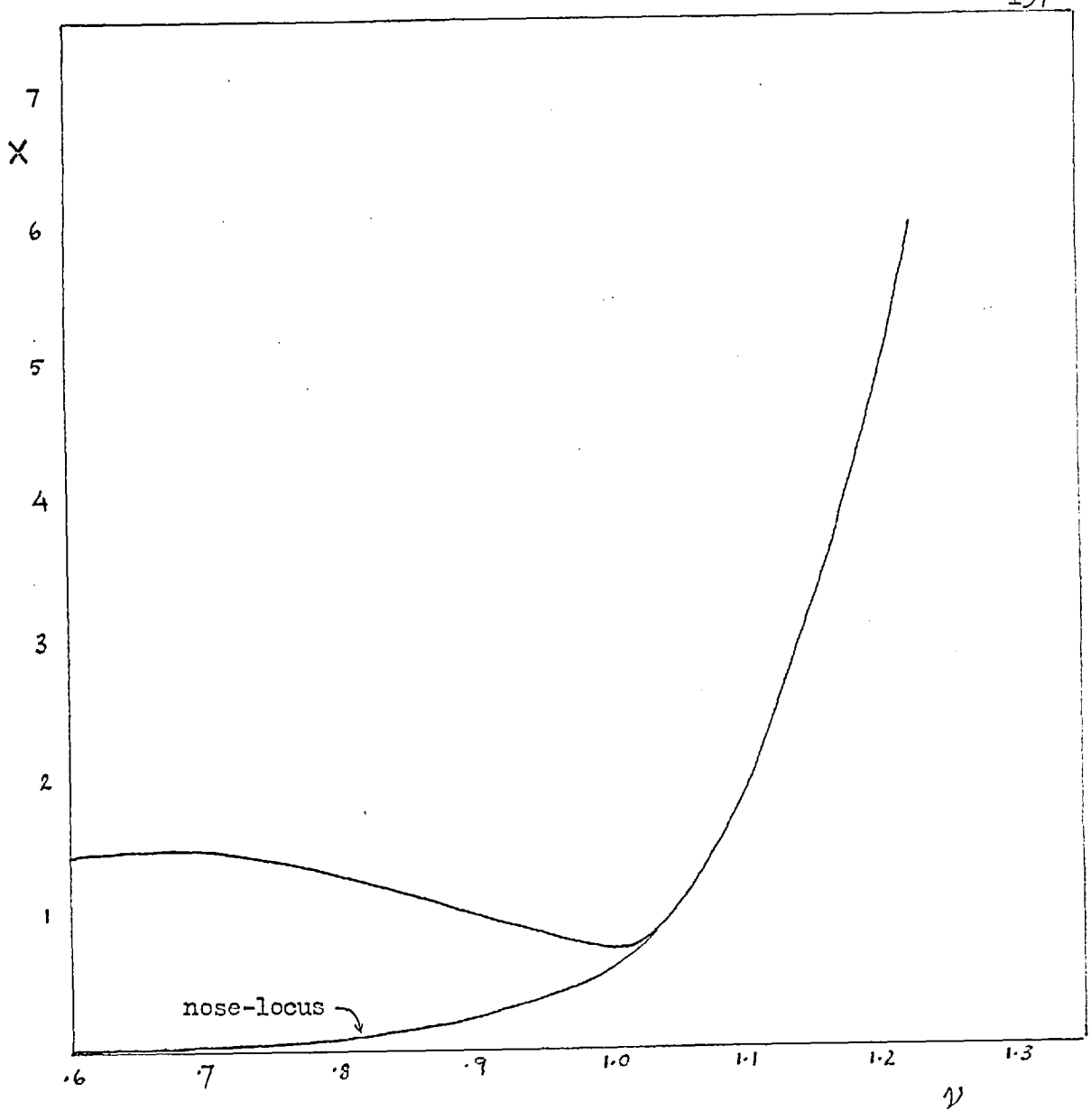


Figure 6.12 -

Theoretical Frequency Characteristic and Nose-Locus for the case:

$k_p = 0$,
$k_L = 0.2$,
$B = 0.45$.

following set of parameters:

$$k_p = 0$$
$$k_L = 0.2$$
$$B = 0.45.$$

This set characterises a BPP with zero pump impedance, typical stray capacitance and a heavy load R_L. As might be expected, these curves superficially resemble those of the approximate "voltage" analysis. For moderate detunings away from resonance, it can be seen that the frequency characteristic and the nose-locus both rapidly approach the curves for the zero-damped case. This indicates that the parameter k_L is of little importance except near resonance.

6.7 Comments on the steady-state phenomena

An accurate prediction of the small-signal steady-state phenomena in the immediate vicinity of resonance has been obtained on the basis of the approximate "voltage" analysis. The accuracy became less good for large signals and significant detuning. The "charge" analysis offers considerable improvement for large signals and detuned cases. The price paid for this is an increase in the complexity of the analysis, particularly when the influences of both the significant damping parameters are included. It should be pointed out that the "voltage" analysis took into account the parameter k_L only; it is probable that the frequency characteristic would have been predicted more accurately had k_p been included also, but little improvement in the large-signal agreement could be expected.

In order to understand the results of the "charge" analysis clearly, three special cases have been considered. It was found that even when all

the parasitic damping and stray-capacitance elements were neglected, (Special Case 1), the predicted steady-state response was in better overall agreement with reality than that given by the previous analysis. The subsequent Special Cases 2 and 3 examined the different effects of k_p and k_L respectively. It was found that engineering accuracy was obtained when all the damping was ascribed to k_p.

Thus, to sum up, the theory described in Special Case 2 has been found to be in adequate agreement with theory over a large part of the (ν,X)-plane if the following conditions are fulfilled:

(1) nonlinear diode-conduction in the varactors must be avoided,

(2) the loading due to R_L must not be too great.

Since the algebraic expressions of Special Case 2 are not unduly complicated, the level of approximation used therein will be adopted for the major part of the transient theory to be described in the next Chapter.

CHAPTER SEVEN

7. Transient Phenomena

7.1 Historical background

Theoretical work on the transient behaviour of parametrons is scarce in the literature, and there has been very little success in the quantitative, or even qualitative, predictions of transient phenomena.

Hilibrand and his co-workers[36] have obtained an approximate exponential solution for the small-signal amplitude transient by means of a quasi-static analysis*. This procedure begins by neglecting all the time-derivatives. Since the transients must therefore be extremely slow, the value of their results is open to question. The influence of the initial conditions upon the subsequent transient behaviour was not considered, neither was an expression derived for the phase transient. In a system which operates on, and is operated by phase-coded information, the phase transient is at least as important as the amplitude transient.

Nethercot[37] has treated Forced Phase Switching on the basis of very similar small-signal quasi-static assumptions. His results are even less valid, since this type of switching is essentially a large-signal operation, involving the overriding of an existing subharmonic oscillation by one of large amplitude and opposite phase.

Hayashi et al[21,22] have investigated the stability of certain theoretical unbalanced parametric oscillators obeying differential equations of the Duffing type. They obtained some results concerning the initial conditions

---

* For a discussion of this method see Section 4.2, Chapter 4.

which lead to various kinds of oscillation, but did not treat the actual time-transients.

7.2 Introduction

We have seen in the previous chapter that calculations based on the "voltage" model for the balanced parametrons do not give a particularly accurate account of the steady-state phenomena, except for small-signal operation near resonance. It follows that transient analyses of the "voltage" model will also be inaccurate. However, in order to illustrate some features of the transient phenomena, the next section contains a simplified version of such an analysis. This retains only the essential stray-capacitance and detuning parameters, and combines mathematical brevity with a reasonable qualitative prediction of the behaviour of experimental devices. The insights gained will serve as guides later in the chapter where the involved but more accurate treatment in terms of the "charge" model is undertaken.

In the following work it will be assumed that the subharmonic phase angle is to be switched by the method of Phase Initiation[32]. This means that the oscillation is first quenched, either by modulating the pumping signal with a rectangular pulse, or by forward-biassing the varactors so that the effective Q of the parametron is rapidly reduced to a small value. The latter variation of the method enables very fast quenching to be achieved, but can only be applied to the BPP. In either case a small locking signal of appropriate phase is then injected into the parametron, and finally by removing the quenching signal, oscillatory conditions are restored. The amplitude and phase of the ensuing subharmonic oscillation will then change

with time until they eventually settle down to their steady-state values. The final amplitude is unique, but there are two possible ultimate phases differing by π radians. The selection between these two possibilities depends, in general, on both the initial phase and the initial amplitude established by the locking signal.

It will be assumed that the amplitude of the phase-locking signal is sufficiently small to be neglected once the transient has begun. It is found in practice that this assumption is fulfilled even if the amplitude is almost as large as that of the steady-state oscillation. Normally, however, much smaller initial amplitudes would be employed. This would enable a single oscillating parametron to determine the ultimate phase of a considerable number of others, yielding a large fan-out factor[32]. In the absence of a definite phase-initiation signal, the final phase-angle and the form of the transient depend on the residual noise in the parametron at the instant at which the quenching is removed. The investigation of noise-initiated transients lies outside the scope of this thesis.

In Forced Phase Switching, however, quenching is not involved. The parametron is pumped continuously and a large overriding signal is applied to force the oscillation into the new phase. This case should properly be treated by an analysis which includes the presence of the forcing signal, but the resulting expressions are even more complicated than those given in the present work. Nevertheless, the detailed transient theory which follows does apply to the case of Forced Phase Switching if the forcing signal is removed as soon as suitable unambiguous large-amplitude initial conditions have been established and the transient is then allowed to proceed. The method has the disadvantage that poor fan-out factors are usually obtained.

7.3 Transient analysis of the generalised voltage model

7.3.1 Simplification of the generalised "voltage" model for transient solution

It is possible to derive small-signal solutions for the instantaneous transient phase and amplitude from the first-order differential equations (6.10) and (6.11) of Section 6.3 by neglecting the coefficients of the terms nonlinear in Y and integrating. The complexity of the resulting expressions is such that their utility is severely limited. Moreoever, as we have already seen, the steady-state solutions derived for these equations were not remarkable for their accuracy, even when the nonlinear terms were included. This was due to the approximations introduced by the use of truncated series expansions of the nonlinear functions. It is evident that little is to be gained by performing transient calculations on such an involved basis.

It will, however, be instructive to obtain the transient solutions of a simplified form of equations (6.10) and (6.11). To do this, we shall neglect the second-order nonlinear reactance parameter β and all the damping parameters k, γ and δ. Only the first-order nonlinear reactance parameter α will be retained. This contains the exponent n and the stray-capacitance parameter B. These simplifications mean that the device must be operated under conditions which ensure that

(i) the subharmonic voltage amplitude is small ($Y \ll 1$),

(ii) the pump voltage X is small enough to avoid nonlinear varactor conduction and

(iii) the linear damping is negligible.

The influence of the linear damping can, of course, be considered here, but

it affects the <u>form</u> of the small-signal results so little that its inclusion was not considered justifiable. Furthermore, it causes the argument to be obscured by the complication of the ensuing calculations.

Equations (6.10) and (6.11) are reduced to the following pair:

$$\left.\begin{aligned} &2\dot{Y} + \alpha\, XY(2\dot{\theta} - \nu).\cos 2\theta + 2\,\alpha\, X\dot{Y}.\sin 2\theta = 0, \\ \text{and}\quad &Y - \nu Y(2\dot{\theta} + \nu) + \nu\alpha XY(2\dot{\theta} - \nu).\sin 2\theta - 2\nu\alpha X\dot{Y}.\cos 2\theta = 0. \end{aligned}\right\} \quad (7.1)$$

The parameter a, which accounted for the differences between the BSP and the BPP, does not appear at this level of approximation. It is associated only with the terms nonlinear in Y, which have been neglected.

The corresponding simplified differential equation for the instantaneous subharmonic voltage y may be written

$$\frac{d^2}{d\tau^2}\left[(1 + 2\alpha x)y\right] + y = 0. \quad (7.2)$$

This is reminiscent of, but different from, the Mathieu equation, which, in a similar notation, is

$$\frac{d^2y}{d\tau^2} + (1 + 2\alpha x)y = 0, \text{ with } x = X\begin{pmatrix}\sin\\ \cos\end{pmatrix} 2\nu\tau\,.$$

Like the Mathieu equation, (7.2) is linear with a time-varying coefficient, and will have no non-zero steady-state solution, (see Section 2.2, Chapter 2). We shall, however, be able to treat the initial part of the transient for which the amplitude is small.

The boundary of the region of oscillation can be found by equating the time derivatives $\dot{Y}$ and $\dot{\theta}$ in (7.1) to zero. Elimination of Y and θ then gives

$$\left[\frac{1 - \nu^2}{\nu^2}\right]^2 = (\alpha X)^2 \quad (7.3)$$

This curve on the (ν, X)-plane is the Frequency Characteristic. It is shown

in Figure 7.1, in which the unstable region is shaded. As might be expected, this is a less accurate result than was obtained in Section 6.4, but will nevertheless be adequate for a qualitative treatment. The dashed line $\alpha X = 1$ indicates the upper limit of validity of the truncated series approximation to the nonlinear reactance function.

Equations (7.1) give the following expressions for the rates of change of amplitude and phase with time:

$$\frac{\overset{\circ}{Y}}{Y} = \frac{\alpha X(2\nu^2 - 1)}{2\nu(1 - (\alpha X)^2)} \cdot \cos 2\theta \qquad (7.4)$$

and $$\overset{\circ}{\theta} = \frac{(1-\nu^2[1 + (\alpha X)^2]) + \alpha X (1 - 2\nu^2).\sin 2\theta}{2\nu(1 - (\alpha X)^2)} . \qquad (7.5)$$

These two solutions can be written in a concise matrix form which is suitable for comparison with more accurate results to be obtained later:

$$\begin{bmatrix} 1 & 0 \\ 0 & 1 \end{bmatrix} \begin{Bmatrix} \frac{\overset{\circ}{Y}}{Y} \\ -\overset{\circ}{\theta} \end{Bmatrix} = \begin{Bmatrix} B.\ \cos 2\theta \\ A + B.\ \sin 2\theta \end{Bmatrix} \qquad (7.6)$$

where

$$A = \frac{\nu^2 (1 + (\alpha X)^2) - 1}{2\nu (1 - (\alpha X)^2)} \qquad (7.7)$$

and

$$B = \frac{\alpha X (2\nu^2 - 1)}{2\nu (1 - (\alpha X)^2)} . \qquad (7.8)$$

Solutions of the equations (7.6) will be obtained in the following sub-section.

7.3.2 Transient solutions for the generalised voltage model

The first-order differential equation for the phase-transient can be

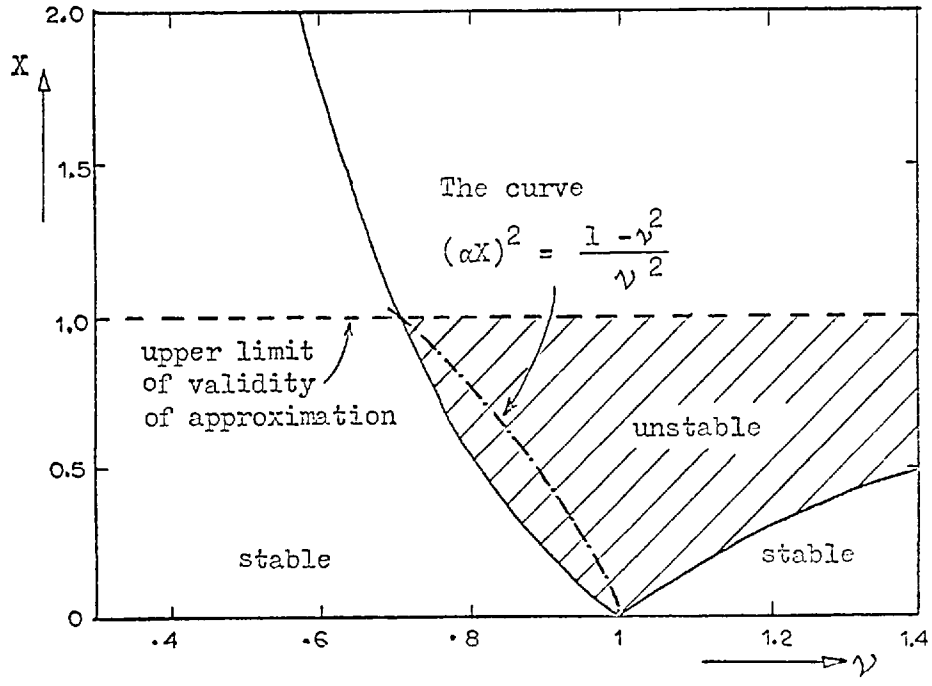


Figure 7.1 -

The Frequency Characteristic for the simplified generalised "voltage" model.

integrated at once:

$$\int d\tau = -\tfrac{1}{2} \int \frac{d(2\theta)}{A + B.\sin 2\theta} \quad . \tag{7.9}$$

The form of the solution depends on whether A is greater or less than B. In the region of soft oscillation in which we are interested, we have the condition

$$(\alpha X)^2 > \left(\frac{1-\nu^2}{\nu^2}\right)^2 \tag{7.10}$$

which is contained within the condition

$$B > A \tag{7.11}$$

so that

$$2\tau = \frac{-1}{\sqrt{B^2 - A^2}} \ln \left(\frac{A.\mathrm{tg}\,\theta + B - \sqrt{B^2 - A^2}}{A.\mathrm{tg}\,\theta + B + \sqrt{B^2 - A^2}} \right) + \text{constant.} \tag{7.12}$$

The constant can be expressed in terms of the initial phase angle $\theta(0)$ at the time $\tau = 0$. With a certain amount of rearrangement the transient phase is then given by

$$\mathrm{tg}\,\theta(\tau) = \frac{S.\mathrm{tg}\,\theta(0) - [A + B.\mathrm{tg}\,\theta(0)] \tanh S\tau}{S + [A.\mathrm{tg}\,\theta(0) + B] \tanh S\tau}, \tag{7.13}$$

where $S = \sqrt{B^2 - A^2}$ (7.14)

The amplitude transient is given by

$$\overset{\circ}{Y}/Y = B.\cos 2\theta \tag{7.15}$$

This equation cannot be integrated as it stands. If, however, the phase solution (7.12) is substituted into it, it becomes homogeneous. Integration then yields

$$\frac{Y(\tau)}{Y(0)} = \frac{1}{S}\sqrt{A\left[2B.\sin 2\theta(0).\sinh^2 S\tau - A\right] + B\left[S.\cos 2\theta(0).\sinh 2S\tau + B.\cosh 2S\tau\right]} \tag{7.16}$$

This shows that the amplitude transient depends on both of the initial conditions $Y(0)$ and $\theta(0)$, whereas the phase transient depends only on the initial phase angle $\theta(0)$. Thus, in the present approximation, the phase-time relation is independent of the subharmonic amplitude, and the amplitude-time relation can be normalised with respect to the initial amplitude $Y(0)$. Equation (7.15) contains trigonometrical functions of $2\,\theta(0)$. This implies that the amplitude phenomena due to an initial phase angle $\theta(0)$ are the same as those due to an initial angle $\theta(0) + \pi$.

Since this is a preliminary investigation of the transient behaviour, it is appropriate to look for a particularly simple case. Such a case is afforded by putting $A = 0$. This implies that our attention is confined, for the moment, to points on the (ν, X)-plane which lie on the curve

$$(\alpha X)^2 = \frac{1 - \nu^2}{\nu^2} \qquad (7.17)$$

which* is indicated in Figure 7.1. It is now found that the instantaneous phase and amplitude are given by

$$\text{tg}\,\theta(\tau) = \text{tg}\,\theta(0)\left[\frac{1 - \tanh S\tau}{1 + \tanh S\tau}\right] = e^{-2S\tau}\,\text{tg}\,\theta(0) \qquad (7.18)$$

and

$$Y(\tau) = Y(0)\sqrt{\cos 2\theta(0).\sinh 2S\tau + \cosh 2S}\ , \qquad (7.19)$$

respectively, where

$$S = \tfrac{1}{2}\sqrt{1 - \nu^2}\ . \qquad (7.20)$$

The (Y,θ)-curves obtained by eliminating the time are, in this particular case, the rectangular hyperbolae

$$Y^2 \sin 2\theta = Y^2(0).\sin 2\theta(0)\ . \qquad (7.21)$$

---

* This is <u>not</u> the curve defining the Frequency Characteristic: see equation (7.3).

An example of these curves for the special case A = 0 is shown in Figure 7.2.

A given pair of initial conditions Y(0), θ(0) define a point such as P on the (Y,θ)-plane. The phase and amplitude of the oscillation will then simultaneously change with time in the manner described by the trajectory passing through the point P, time increasing in the direction of the arrow. The actual variations of phase and amplitude with time must be determined from equations (7.12) and (7.15) respectively. Inspection of equation (7.15) shows that if θ(0) = 0 or π, then

$$Y(\tau) = Y(0).e^{+S\tau}$$

which is the maximum possible rate of rise. Similarly if $\theta(0) = \frac{\pi}{2}$ or $\frac{3\pi}{2}$, then

$$Y(\tau) = Y(0).e^{-S\tau}$$

leading to monotonic decay from the starting amplitude Y(0).

We can show how the initial part of the transient oscillation envelope depends upon the choice of initial condition by plotting equation (7.15) for various values of the initial phase-angle θ(0). The result is shown in Figure 7.3. It is interesting to see that for certain values of θ(0), the amplitude decreases and then increases again.

Such behaviour can be observed in practice when the initial amplitude Y(0) is sufficiently greater than noise-level at $\tau = 0$. Monotonic decay, however, cannot occur in a real system, since residual noise will always eventually trigger oscillation into one phase or the other, in a random manner.

It is noteworthy that quite a large deviation of θ(0) away from the values giving the fastest rates of rise does not delay the turn-on

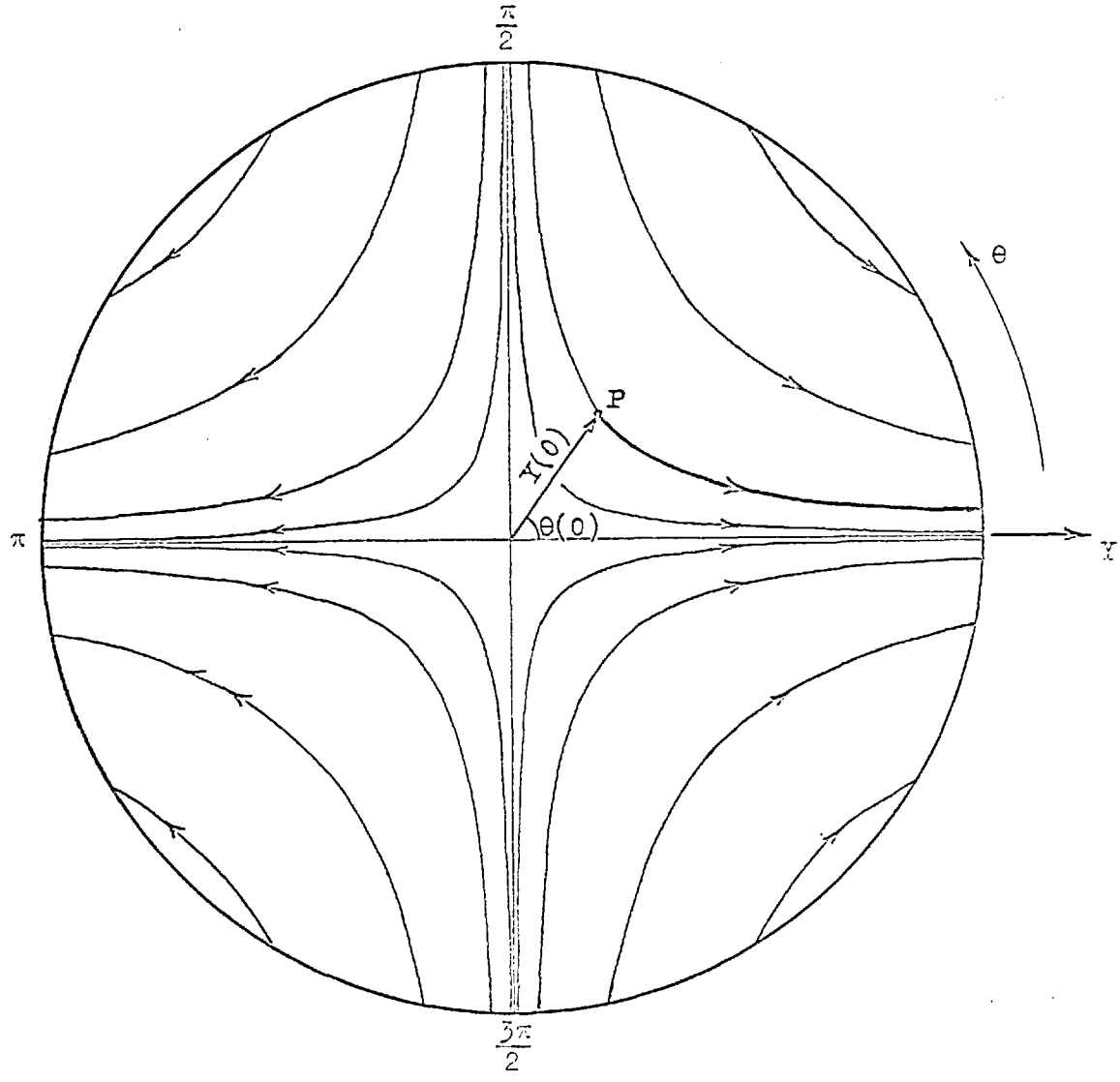


Figure 7.2 - (Y,θ)-trajectories for the special case A = 0.

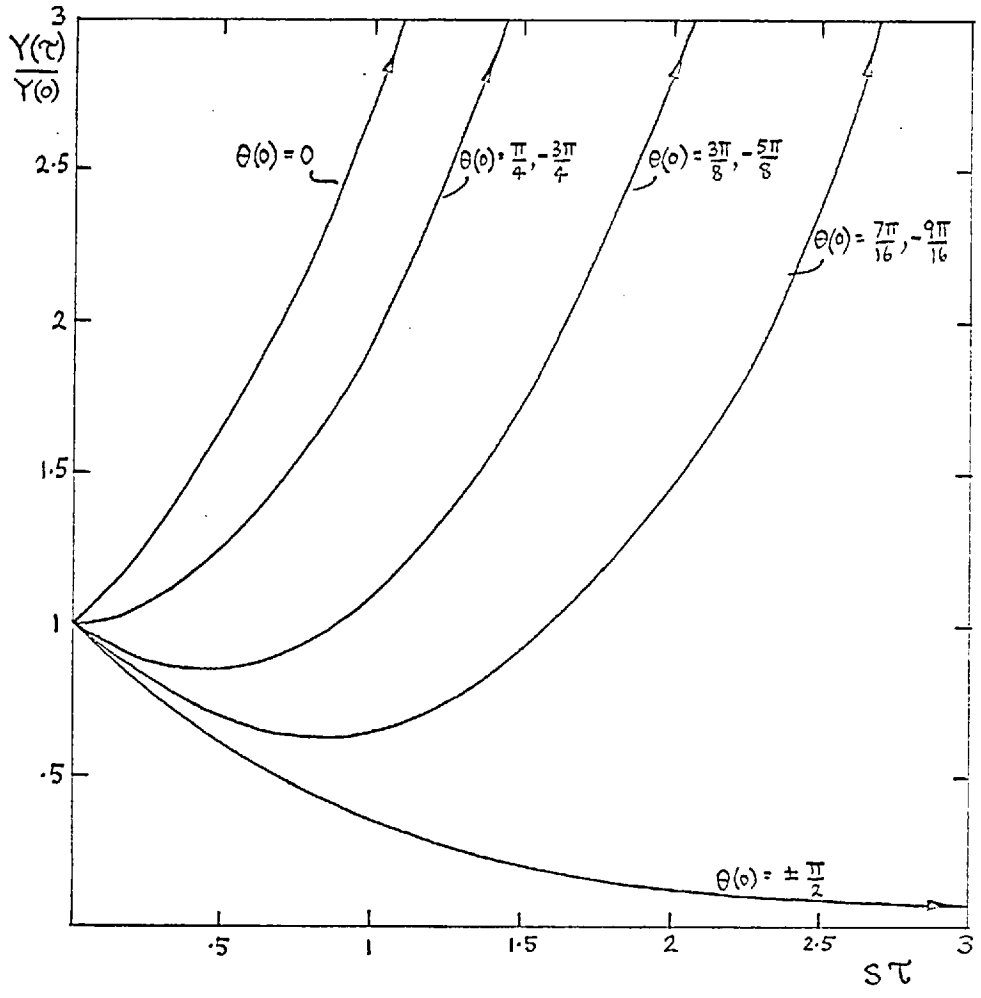


Figure 7.3 -

Approximate transient amplitude solutions: effect of varying the initial phase angle.

significantly: large delay occurs only for narrow ranges of $\theta(0)$ in the vicinity of $\frac{\pi}{2}$ and $-\frac{\pi}{2}$.

Figure 7.4 shows phase-time curves given by equation (7.18) for various values of $\theta(0)$. The curves are all of the same shape, and are merely displaced along the τ-axis. In the present approximation they are independent of $Y(0)$.

Since it is difficult to visualise how the vector $\underline{Y}$ changes in phase and amplitude as time increases, Figure 7.5 shows this variation in (Y,θ,τ)-space for a constant initial amplitude $Y(0)$, (the exact value of which is of no consequence) and for various values of $\theta(0)$. This is a pseudo-perspective drawing in that magnitudes and angles maintain their true values. It can be seen that even for $\theta(0)$ near $\frac{\pi}{2}$, $\theta(\tau)$ is close to 0 or π by the time $S\tau = 3$. This three-dimensional diagram will help us to understand the complicated phenomena we shall encounter in more accurate treatment of the transients in Section 7.4.

A quantity of considerable interest is the number of cycles of sub-harmonic oscillation necessary for the amplitude $Y(\tau)$ to increase by a factor "e". This quantity has been named the "dimensionless risetime" by Hilibrand and his co-workers[36]; it evidently has meaning only when the oscillation envelope is a pure increasing exponential, i.e. one should consider only those initial conditions which lead to a maximum rate of rise. The general condition for pure exponential envelopes is that the initial phase angle be given by

$$\tan\theta(0) = \frac{\pm S - B}{A}$$

where the upper sign corresponds to growing and the lower sign to decaying

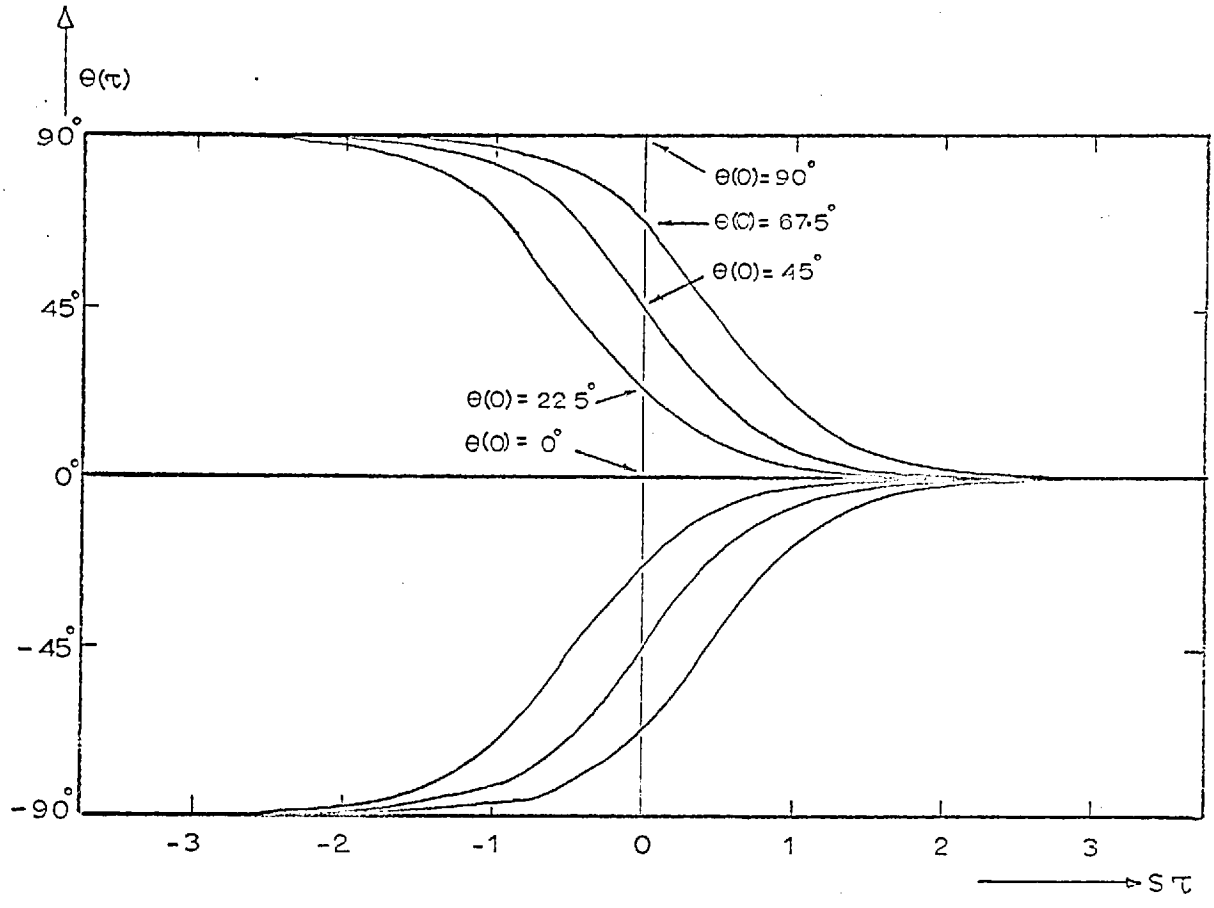


Figure 7.4 -

Approximate phase transient solutions: effect of varying the initial phase angle θ(0).

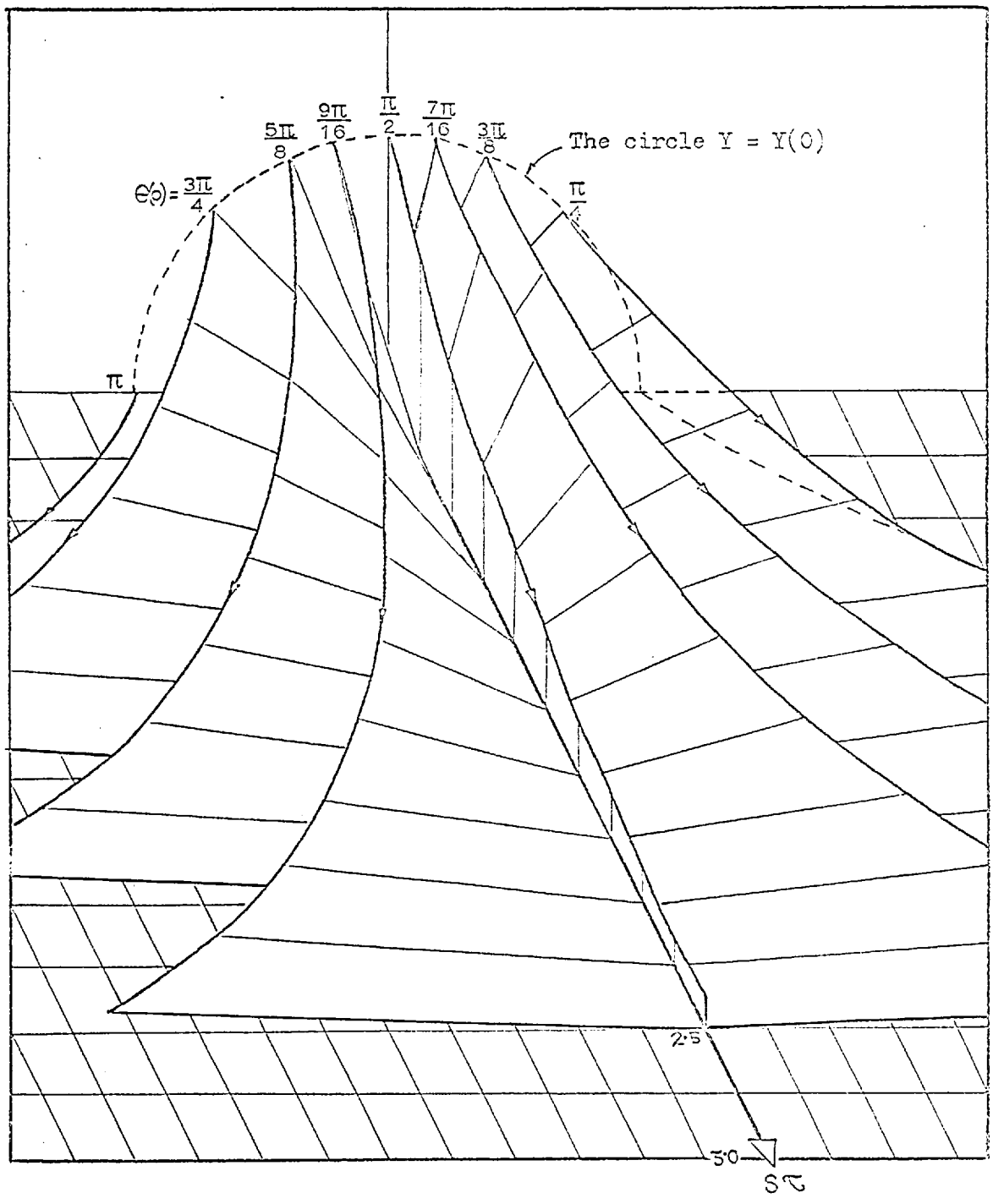


Figure 7.5 - Approximate phase-amplitude-time transients in (Y,θ,τ)-space for a constant initial amplitude $Y(0)$ and for various initial phase angles $\theta(0)$.

oscillations. This may be verified by substituting

$$\sin 2\theta(0) = -\frac{A}{B} \quad , \quad \cos 2\theta(0) = \pm \frac{S}{B}$$

into equation (7.15), which then yields

$$Y(\tau) = Y(0).e^{\pm S\tau} \quad .$$

Note that these remarks are true for all values of A, so that we can calculate the dimensionless risetime anywhere within the shaded region of Figure 7.1.

Let us call the dimensionless risetime μ. Then

$$\mu = \frac{\nu}{2\pi S} \quad , \tag{7.22}$$

where

$$S^2 = B^2 - A^2 = \frac{(1-\nu^2)^2 - \nu^4(\alpha X)^2}{4\nu^2((\alpha X)^2 - 1)} \quad . \tag{7.23}$$

Hence curves of constant dimensionless maximised risetime are given by

$$(\alpha X)^2 = \frac{(\mu\pi)^2 . \left(\frac{1-\nu^2}{\nu^2}\right)^2 + 1}{(\mu\pi)^2 + 1} \quad . \tag{7.24}$$

As $\mu \rightarrow \infty$, $(\alpha X)^2 \rightarrow \left(\frac{1-\nu^2}{\nu^2}\right)^2$, that is, the dimensionless risetime becomes infinitely long at the boundary of the region of oscillation, as might be expected.

Curves of constant μ on the (ν, X)-plane are shown in Figure 7.6. If this diagram is compared with the experimental result for a typical EPP, see Figure 7.46 , it will be seen that there is very rough agreement for $\nu = 1$ and for sufficiently small X. The theoretical curves of constant μ are not two-valued functions of ν. This is due to the extreme approximation of the nonlinear reactance and also to the neglect of the influence of forward varactor conduction at large X.

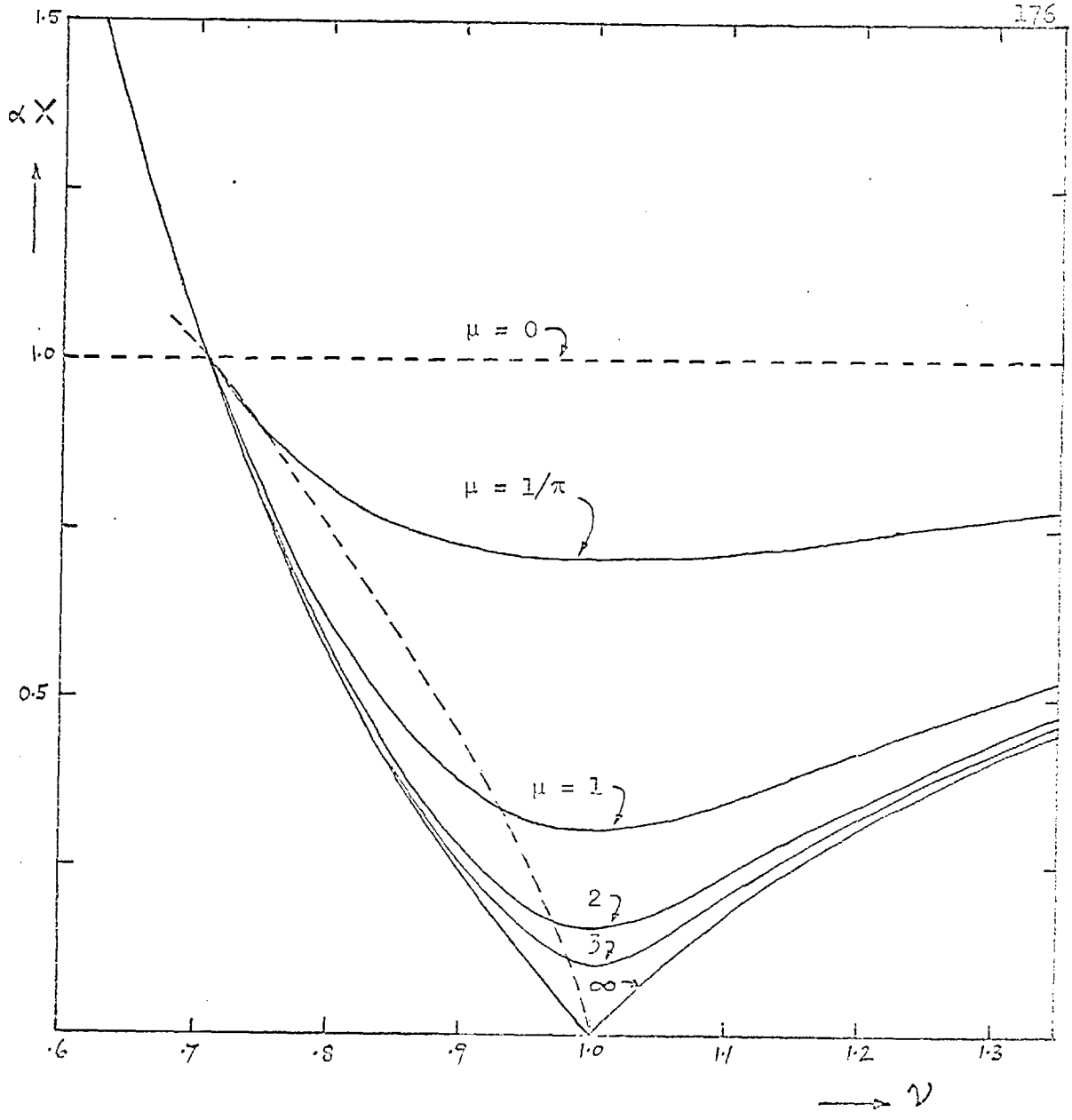


Figure 7.6 -

Approximate curves of constant dimensionless risetime μ on the (ν, X)-plane.

The effect of dissipation in the parametron is to reduce S, thus slow-ind down the maximum rate of rise of the oscillations. The nonlinear dissipation leads to complete cessation of oscillation for sufficiently large X.

The present theory gives $\mu = 0$ for $\alpha X = 1$, i.e. it predicts zero risetime for this value of αX, which is clearly nonphysical and outside the range of approximation.

7.4 Transient analysis of "charge" model

We shall now attempt a considerably more accurate analysis of the transient behaviour of the balanced parametron in response to an initiation signal of given phase $\theta(0)$ and amplitude $Y(0)$. As in the case of the detailed steady-state analysis, attention will again be restricted to the case of the Balanced Parallel Parametron (BPP). That this is a reasonable restriction will be seen in Section 7.5 which deals with experiments on the transient phenomena. It is shown there that this is the device of greatest practical utility. For example, the BPP can be completely quenched in less than one subharmonic cycle, whereas in the case of the BSP, the oscillations must be allowed to decay slowly at a rate determined by the natural "Q" of the device: this can be a very slow process. The BPP has the further advantages that it is inherently well-balanced if a bifilar-wound inductor is employed, and no input transformer is required, thus simplifying its construction.

It has been shown in Section 5.4 that the "voltage" differential equations for the two kinds of balanced varactor parametron differ only in minor

details, and experiment confirms that the behaviour of the two differs only in magnitude and not in kind. A generalised "charge" theory able to predict the behaviour of both types is feasible, but the extra complication is not considered justifiable in a work of this nature.

As was found to be the case in the detailed steady-state analysis, the treatment of the transient response will be much facilitated by the choice of the difference between the charges on the two varactors as the main variable.

The complete simultaneous differential equations describing the behaviour of this "charge" model are (5.19) and (5.21). Following the procedure established in Section 7.3, it is necessary to substitute into these equations assumed solutions for the voltage and the charge. These solutions will have unknown time-varying amplitudes and phases. By using the method of harmonic balance with the "slowly-varying amplitude and phase" approximation, it will then be possible to find a pair of first-order nonlinear differential equations for $\dot{Y}$ and $\dot{\theta}$. However, the transient analysis is exceedingly complicated if all three of the damping parameters k_p, k_v, k_L due to pump circuit resistance, varactor conductance and load conductance respectively, are included in equations (5.19) and (5.21). The analysis does, however, become feasible if the two important damping parameters k_p and k_L are considered separately. The steady-state analysis has shown that inclusion of the sole damping parameter k_p is sufficient to account quite closely for the experimental amplitude phenomena, but that an accurate treatment of the resonant phenomena requires that k_L be included also.

In the next Section the relevant first-order differential equations will be obtained for a BPP in which k_p is the dominant damping parameter. In a

subsequent Section, the process will be repeated for a device in which k_L dominates. The relative possibilities of these intermediate solutions for further analysis will then be considered.

7.4.1. Intermediate harmonic-balance solution for the case in which R_p dominates the device behaviour.

In the case in which the pump-circuit resistance R_p dominates the device behaviour, the differential equations (5.19) and (5.21) become

$$(1 - B)\ddot{y} + y = B\ddot{z}, \tag{7.25}$$

and

$$k_p\left\{\frac{1}{4}(1-B)z^4\dot{z} + 4\left[(1-B)y - Bz\right](z\dot{y} - y\dot{z})\right\} + B\left\{z^3(x-1) + \frac{1}{16}z^5 + y^2z\right\} = \\ = \mathcal{E}\left[x,y,z\right] = 0\ , \tag{7.26}$$

respectively.

This means that

(1) the linearised varactor conductances G_v are negligible, so that $k_v = 0$,

(2) the load conductance G_L is very small, so that $k_L = 0$ and

(3) only the damping parameter k_p due to pump-circuit resistance R_p is retained.

Further, as in the corresponding steady-state case, it is assumed that the parametron is not operated under conditions in which nonlinear losses due to forward diode conduction in the varactors are of importance. This restriction is also a practical requirement in that such losses are exponential functions of voltage and lead to excessive consumption of pump power and undesirably slow transients.

The equivalent circuit which results from these simplifications is shown

in Figure 7.7. It contains only the two ideal varactors $q_1(v)$ and $q_2(v)$, the closely-coupled tuning inductance L, the stray capacitance C_s, the pump generator v_p and the pump-circuit resistance R_p.

We now require the intermediate (and incidentally the steady-state) solution of the pair of differential equations (7.25) and (7.26) relating to this equivalent circuit. It is again assumed that both the instantaneous voltage and the instantaneous charge can be approximated by sinusoidal functions of time, but now with amplitudes and phases which are unspecified functions of time. Thus the approximate normalised subharmonic voltage is taken to be

$$\tilde{y}(\tau) = Y(\tau).\sin\left[\nu\tau + \theta(\tau)\right], \qquad (7.27)$$

and the approximated normalised subharmonic differential charge to be

$$\tilde{z}(\tau) = Z(\tau).\sin\left[\nu\tau + \psi(\tau)\right], \qquad (7.28)$$

where $\tau = \omega_o t$ is the normalised time.

It has been shown in Section 6.5 that the steady-state voltage and charge amplitudes are related by

$$Y^2(\infty) = \Gamma^2 Z^2(\infty),$$

and that the corresponding phase angles are indistinguishable

$$\theta(\infty) = \psi(\infty).$$

This leads us to enquire whether the voltage and charge coordinates may not preserve these particularly simple relationships to a reasonable degree of accuracy under transient conditions, and if so, whether or not a simplification of the process of analysis may be expected.

If the expressions (7.27) and (7.28) are substituted into equation (7.25), the coefficients of $\sin \nu\tau$ and $\cos \nu\tau$ are equated separately to

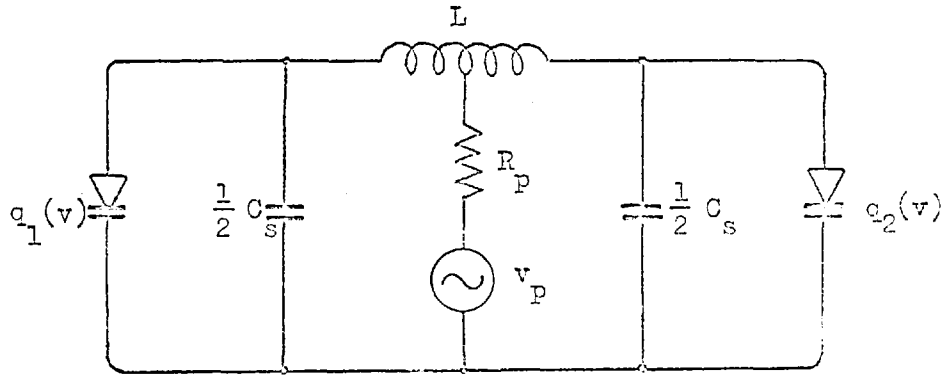


Figure 7.7 - Equivalent circuit of BPP when R_p dominates the device behaviour.

zero, and all second derivatives with respect to τ are neglected, then one finds that

$$\left.\begin{aligned} Y_s + \nu(1-B)(2\dot{Y}_c - \nu Y_s) &= + B\nu(2\dot{Z}_c - \nu Z_s) \\ \text{and}\quad Y_c - \nu(1-B)(2\dot{Y}_s + \nu Y_c) &= - B\nu(2\dot{Z}_s + \nu Z_c), \end{aligned}\right\} \tag{7.29}$$

where a circle above a symbol has its usual meaning of $d/d\tau$, and

$$\left.\begin{aligned} Y_c &= Y.\cos\theta\ , \quad Y_s = Y.\sin\theta\ , \\ Z_c &= Z.\cos\psi\ , \quad Z_s = Z.\sin\psi\ . \end{aligned}\right\} \tag{7.30}$$

If equations (7.29) are differentiated and the second τ-derivatives are again neglected, there results

$$\left.\begin{aligned} \dot{Y}_s &= - \Gamma\, \dot{Z}_s\ , \\ \text{and}\quad \dot{Y}_c &= - \Gamma\, \dot{Z}_c\ , \\ \text{where}\quad \Gamma &= \frac{B\nu^2}{1-\nu^2(1-B)}\ , \end{aligned}\right\} \tag{7.31}$$

as in the steady-state analysis.

Elimination of $\dot{Y}_c$ and $\dot{Y}_s$ between (7.29) and (7.31) yields

$$Y_s = \left(\frac{2\Gamma^2}{B\nu^3}\right)\cdot \dot{Z}_c - \Gamma Z_s\ , \tag{7.32}$$

$$\text{and}\quad Y_c = -\left(\frac{2\Gamma^2}{B\nu^3}\right)\cdot \dot{Z}_s - \Gamma Z_c\ . \tag{7.33}$$

If these expressions are squared and added, and the products of derivatives are neglected since they are assumed to be small, one obtains a simple expression for Y in terms of the charge variables Z and ψ:

$$Y^2 = Z^2(\Gamma^2 + n\dot{\psi}), \tag{7.34}$$

$$\text{where}\quad n = \frac{4\Gamma^3}{B\nu^3}\ .$$

Equation (7.34) is valid under both steady-state and transient conditions. If $\dot{\psi}$ is small compared with ν, which is generally the case, then

$$\frac{\Gamma^2}{n} = \frac{1}{4}\nu\left[1 - \nu^2(1-B)\right] \gg \dot{\psi},$$

so that $$Y^2 = \Gamma^2 Z^2. \qquad (7.35)$$

This means that in the present case, the particularly simple steady-state relation quoted above does apply approximately to the transient case. Thus it is possible to investigate the voltage transient in terms of the charge variables with negligible loss of accuracy. This is a considerable advantage, because it is found that if one attempts to carry out the transient analysis in terms of the voltage variables, the expressions become very much more involved and intractable.

If one is to work in terms of the charge coordinates Z and ψ only, it is necessary to find, in place of (7.27), an expression for $\tilde{y}$ in terms of Z and ψ which is valid under transient conditions. Such an expression can be obtained from the linear differential equation (7.25), and it, together with the assumed solution (7.28) for $\tilde{z}$, must then be substituted into the nonlinear differential equation (7.26). Finally, one will obtain a pair of first-order differential equations of the form

$$\dot{Z}(\tau) = \mathcal{F}_1(Z(\tau), \psi(\tau)),$$
$$\dot{\psi}(\tau) = \mathcal{F}_2(Z(\tau), \psi(\tau)),$$

which describe the way in which the (hitherto unknown) amplitude and phase of the subharmonic charge change with time. Although the functions $\mathcal{F}_1$ and $\mathcal{F}_2$ will in general be nonlinear, these equations will be very much simpler than the equivalent equations for the time-derivatives of the amplitude and phase of the subharmonic voltage, $\dot{Y}$ and $\dot{\theta}$ respectively. This is apparently due to

the fact that the capacitive nonlinearity is defined here as a function of charge and not as a function of voltage. If this pair of nonlinear differential equations can subsequently be solved for $Z(\tau)$ and $\psi(\tau)$, it is then a relatively simple matter to find $Y(\tau)$ and $\theta(\tau)$ - to a good approximation - by means of

$$Y^2(\tau) \approx \Gamma^2 Z^2(\tau) \quad ,$$

and $$\theta(\tau) \approx \psi(\tau) \, .$$

The necessary mathematical operations will again be much facilitated by working in terms of complex polar coordinates. Thus the assumed charge solution (7.28) is written

$$\tilde{z} = -jZ(\gamma - \gamma^*) \, , \qquad (7.36)$$

where $$\gamma = \tfrac{1}{2} e^{j(\nu\tau + \psi(\tau))} \, ,$$

and, as shown in Appendix 7.1, the required expression for $\tilde{y}$ in terms of charge coordinates is, from equations (7.32) and (7.33),

$$\tilde{y} = a\dot{Z}(\gamma + \gamma^*) + jZ(a\dot{\psi} + \Gamma)(\gamma - \gamma^*) \, , \qquad (7.37)$$

where $$a = \frac{2\Gamma^2}{B\nu^3} \, .$$

As before, the pumping function is taken to be

$$x = X.\sin 2\nu\tau,$$

and in terms of the present symbols this reads

$$x = -j2X(\gamma^2 e^{-j2\psi} - \gamma^{*2} e^{+j2\psi}) \, . \qquad (7.38)$$

The next step is to form instead of equation (7.26), the approximate differential equation

$$\Sigma\left[x, \tilde{y}, \tilde{z}\right] = 0 \qquad (7.39)$$

in which $x, \tilde{y}$ and $\tilde{z}$ are given by (7.38), (7.37) and (7.36) respectively.

Because of the assumption that the variables $\tilde{y}$ and $\tilde{z}$ are pure sinusoids, the quantities γ^3, γ^{*3}, γ^5 and γ^{*5}, corresponding to the harmonic frequencies 3ν and 5ν , must be rejected in (7.39). Further, because of the slowly-varying amplitude and phase assumption, all the second-order-small time derivatives are to be rejected. These matters are set out in detail in Appendix 7.2. It is shown there that the following pair of first-order equations in Z and ψ is obtained:

$$\tfrac{1}{8}k_p\left(\tfrac{1}{B} - 1\right)Z^2(\nu + \dot{\psi}) + X.\cos 2\psi - 2a\Gamma\frac{\dot{Z}}{Z} = 0, \tag{7.40}$$

$$\tfrac{5}{8}k_p\left(\tfrac{1}{B} - 1\right)Z^2.\frac{\dot{Z}}{Z} + 16k_p a\nu\left(\left[\tfrac{1}{B} - 1\right]\Gamma + 1\right)\frac{\dot{Z}}{Z} + 2\,X.\sin 2\psi - 3 + \\ + \frac{5}{32}Z^2 + 3\Gamma(\Gamma + 2a\dot{\psi}) = 0\,. \tag{7.41}$$

If one puts

$$\ell = 16k_p a\nu\left(\left[\tfrac{1}{B} - 1\right]\Gamma + 1\right) = \frac{32k_p\Gamma^3}{B^2\nu^4},$$

$$m(Z) = \tfrac{1}{8}k_p\left(\tfrac{1}{B} - 1\right)Z^2,$$

$$n = 2a\Gamma = \frac{4\Gamma^3}{B\nu^3},$$

$$r(Z) = 3(\Gamma^2 - 1) + \frac{5}{32}Z^2,$$

then the equations read simply

$$m(Z)\cdot(\nu + \dot{\psi}) + X.\cos 2\psi - n\frac{\dot{Z}}{Z} = 0, \tag{7.42}$$

$$(5m(Z) + \ell)\frac{\dot{Z}}{Z} + 2X.\sin 2\psi + r(Z) + 3n\dot{\psi} = 0. \tag{7.43}$$

In matrix form they are

$$\begin{bmatrix} n, & m(Z) \\ -(5m(Z)+\ell), & 3n \end{bmatrix}\begin{Bmatrix} \frac{\dot{Z}}{Z} \\ -\dot{\psi} \end{Bmatrix} = \begin{Bmatrix} \nu.m(Z) + X.\cos 2\psi \\ r(Z) + 2X.\sin 2\psi \end{Bmatrix}, \tag{7.44}$$

from which it is easily seen that the explicit equations for $\mathring{Z}$ and $\mathring{\psi}$ are

$$\frac{\mathring{Z}}{Z} = \frac{1}{\Delta}\left[\, 3n(\nu.m(Z) + X.\cos 2\psi) - m(Z).(r(Z) + 2X.\sin 2\psi)\,\right],$$

$$\mathring{\psi} = -\frac{1}{\Delta}\left[(5m(Z) + \ell)(\nu.m(Z) + X\cos 2\psi) + n(r(Z) + 2X.\sin 2\psi)\right],$$

where

$$\Delta = \begin{vmatrix} n, & m(Z) \\ -(5m(Z)+\ ), & 3n \end{vmatrix} = 3n^2 + m(5m + \ell).$$

The square matrix in (7.44) contains parameters relating specifically to the transient response, its column multiplier contains the rates of change of phase and amplitude, while the right-hand column matrix contains the steady-state amplitude and phase solutions.

The pair of first-order nonlinear differential equations (7.44) constitute the sought "intermediate solution" for the case in which k_p dominates the parametron behaviour. It can easily be verified that they give the correct steady-state results by putting $\mathring{Z}$ and $\mathring{\psi}$ equal to zero. The amplitude is then given by

$$4X^2 = r^2 + 4(m\nu)^2 \qquad (7.45)$$

or in full

$$4X^2 = \left[3(r^2 - 1) + \frac{5}{32}.Z^2(\infty)\right]^2 + \left[\nu\delta.Z^2(\infty)\right]^2 , \qquad (7.46)$$

while the steady-state phase angle is given by

$$\operatorname{tg} 2\psi(\infty) = \frac{r}{2m\nu} = \frac{3(r^2 - 1) + \frac{5}{32}.Z^2(\infty)}{\nu\delta.Z^2(\infty)} . \qquad (7.47)$$

The (∞) in these equations implies that sufficient time has elapsed for steady-state conditions to have been attained. If we use (7.46) and (7.47) to find the solutions for the steady state voltage amplitude $Y(\infty)$ and phase $\theta(\infty)$ by means of equation (7.35)

$$Z^2(\infty) = (L.Y(\infty))^2 ,$$

we obtain again equations (6.51) and (6.52) which were previously found in Section 6.5. Comparison of the phase equations confirms that in the present case

$$\psi(\infty) = \theta(\infty) .$$

In the next section, the "intermediate solution" will be obtained for the case in which k_L dominates the behaviour of the device.

7.4.2 Intermediate harmonic-balance solution for the case in which R_L dominates the device behaviour *

The transient solution for the case in which the load resistance R_L is the sole source of loss in a BPP must be based on the following pair of simultaneous differential equations, which are obtained by putting $k_p = 0$ and $k_v = 0$ in equations (5.19 and (5.21), Section 5.5.1:

$$(1 - B)\overset{oo}{y} + k_L\overset{o}{y} + y = B\overset{oo}{z} , \qquad (7.48)$$

and

$$z^3(x - 1) + \frac{1}{16} z^5 + y^2 z = 0. \qquad (7.49)$$

The first step is to find an approximate expression for y in terms of z from equation (7.48). This expression for y must be substituted in (7.49), which can then be solved for z. We shall again use the following expressions for x, y and z:

$$x = X.\sin 2\nu\tau$$

$$\tilde{y} = Y(\tau).\sin(\nu\tau + \theta(\tau)),$$

$$\tilde{z} = Z(\tau).\sin(\nu\tau + \psi(\tau)),$$

---

* The steady-state solutions corresponding to this case have been found in Special Case 3, Section 6.5, Chapter 6.

or in complex form

$$\tilde{y} = -jY(\alpha - \alpha^*) \quad , \quad \text{where } \alpha = \tfrac{1}{2}\, e^{j(\nu\tau + \theta)} \quad ; \qquad (7.50)$$

$$z = -jZ(\gamma - \gamma^*), \quad \text{where } \gamma = \tfrac{1}{2}\, e^{j(\nu\tau + \psi)} \quad . \qquad (7.51)$$

It is shown in Appendix 7.3 that the required approximate expression for y, in terms of the amplitude and phase of the charge, is

$$\boxed{\tilde{y} = (aZ\dot{\psi} - b\dot{Z} + cZ)(\gamma + \gamma^*) - j(a\dot{Z} + bZ\dot{\psi} - dZ)(\gamma - \gamma^*)} \quad , (7.52)$$

where

$$\left.\begin{aligned} a &= \frac{1}{\nu(L^2+M^2)^2}\left[4\left(\frac{1-B}{B}\right) LM + M(3L^2 + M^2)\right] , \\ b &= \frac{1}{\nu(L^2+M^2)^2}\left[2\left(\frac{1-B}{B}\right)(M^2 - L^2) - 2L^3\right] , \\ c &= \frac{M}{L^2 + M^2} \quad , \\ d &= \frac{L}{L^2 + M^2} \quad , \end{aligned}\right\} \qquad (7.53)$$

and L and M have their usual values. Following the method used before, substitution of equation (7.52) for $\tilde{y}$ and equation (7.51) for $\tilde{z}$ into equation (7.49) and rejection of the terms in γ^3 and γ^{*3}, corresponding to the third harmonic of the subharmonic frequency, finally yields the following pair of first-order equations for the amplitude and phase transient behaviour:

$$\left.\begin{aligned} 2(ac + bd)\frac{\dot{Z}}{Z} - 2(ad - bc)\dot{\psi} &= 2cd - X.\cos 2\psi \quad , \\ 2(3ad + bc)\frac{\dot{Z}}{Z} - 2(ac - 3bd)\dot{\psi} &= c^2 + 3(d^2-1) + \frac{5}{32}Z^2 + 2X.\sin 2\psi. \end{aligned}\right\} \qquad (7.54)$$

These can be written shortly:

$$\begin{bmatrix} 2(ac + bd) , & 2(ad - bc) \\ 2(3ad + bc), & 2(ac - 3bd) \end{bmatrix} \begin{Bmatrix} \frac{c}{Z}\dot{Z} \\ -\dot{\psi} \end{Bmatrix} = \begin{Bmatrix} 2cd - X.\cos 2\psi \\ c^2+3(d^2-1)+ \frac{5}{32}.Z^2+2X.\sin 2\psi \end{Bmatrix} \tag{7.55}$$

Equations (7.55) should be compared with (7.44) which is the corresponding result when all the damping is ascribed to the source resistance R_p. It can be seen that the two equations are of the same form, but that (7.55) is more complicated. It is interesting that the only nonlinear term in (7.55) is the $\frac{5}{32} Z^2$ in the column matrix on the right. Unfortunately, this circumstance does not enable us to find an exact transient solution.

The steady-state behaviour is given by setting the time-derivatives equal to zero. For the amplitude we obtain

$$16(cd)^2 + (c^2 + 3(d^2-1) + \frac{5}{32} Z^2)^2 = 4X^2 , \tag{7.56}$$

which is identically equation (6.58), Section 6.5, as may be seen by using equation (7.53) and the relation between the charge and voltage amplitudes

$$Z^2 = (L^2 + M^2)Y^2$$

which results from the steady-state version of (7.52). The equation for the steady-state charge phase angle is

$$\text{tg } 2\psi = - \left\{ \frac{c^2 + 3(d^2-1) + \frac{5}{32} Z^2}{4cd} \right\} ,$$

from which Z^2 can be eliminated by means of (7.56) to give

$$\text{tg } 2\psi = \pm \sqrt{\frac{X^2(L^2 + M^2)^4}{4(LM)^2} - 1} . \tag{7.57}$$

It must be pointed out that, unlike the case in which the source damping k_p dominates, the phase angles of charge and voltage can no longer be regarded as approximately equal; they are related by either of the equations

$$\text{tg } \theta = \frac{L.\text{tg}\psi - M}{L + M.\text{tg}\,\psi}$$

$$\text{or} \quad \text{tg } 2\theta = \frac{(M^2 - L^2).\text{tg } 2\psi + 2ML}{(M^2 - L^2) - 2ML.\text{tg } 2\psi} \qquad (7.58)$$

which can be derived from equation (A7.6) of Appendix 7.3, and are valid under both steady-state and transient conditions.

A Y-independent expression for the voltage phase angle can be obtained from (7.57) and (7.58):

$$\text{tg } 2\theta = \frac{\dfrac{2ML}{M^2 - L^2} \pm \sqrt{\dfrac{X^2(L^2 + M^2)^4}{4(LM)^2} - 1}}{1 \mp \dfrac{2ML}{M^2 - L^2}\sqrt{\dfrac{X^2(L^2+M^2)^4}{4(LM)^2} - 1}}$$

This is much more complicated than (7.56), and is a further indication of the advantages of working in terms of the charge variables.

7.4.3 Remarks on the phase-angles of the oscillatory charge and voltage along the nose-locus

In the case in which k_p is the major damping parameter, the phase-angles of the steady-state charge and voltage oscillations at the nose of the (X,Y)-profile are the same. They are given by equation (6.56), Section 6.5, Chapter 6.

In the other case considered, where k_L dominates, the charge and voltage phase-angles at the nose are no longer the same. Since, by equation

(6.60), Section 6.5, Chapter 6, the X-coordinate of the nose-locus is

$$X_N = \frac{2LM}{(L^2 + M^2)^2} ,$$

it follows from equation (7.57) that

$$tg\ 2\psi_N = 0.$$

This means that in this case the phase-angle ψ_N of the oscillatory charge is constant along the nose-locus. Equation (7.58) shows that the corresponding voltage phase-angle θ_N is given by

$$tg\ 2\theta_N = \frac{2LM}{M^2 - L^2}$$

$$\text{or} \qquad tg\ \theta_N = -\frac{M}{L} .$$

This is not constant, but is a function of the frequency ν, the load damping k_L and the stray-capacitance parameter B.

7.4.4 Assessment of the relative merits of the two intermediate solutions

As they stand, neither of the intermediate solutions (7.44) or (7.55) can be solved exactly. In the case of zero-damping they both reduce to the same intermediate solution. Under certain conditions exact integration is then possible. This case is treated in the next Section, 7.4.5. If the damping is not negligible, it is found that both of the intermediate solutions (7.44) and (7.55) can be integrated for

$$Z \ll 1,$$

but the resulting algebraic equations are very much simpler for (7.44). For this reason, the k_p-dominated case has been selected for detailed investigation later in the Chapter.

7.4.5 Exact transient solutions under conditions of zero damping

It is possible, under certain conditions, to find exact transient solutions for conservative (lossless) parametrons, corresponding to the "exoskeletal" steady-state solutions of Section 6.5, Special Case 1. Such transient solutions do not relate to practical devices, but will give some useful insights into the mechanism of their transient behaviour. In general, equations such as (7.44) and (7.55) cannot be integrated exactly. However, if all damping is neglected, they both reduce to the following pair of equations

$$\begin{bmatrix} n & 0 \\ 0 & 3n \end{bmatrix} \cdot \begin{Bmatrix} \dot{Z} \\ -\dot{\psi} \end{Bmatrix} = \begin{Bmatrix} X \cdot \cos 2\psi \\ 3(\Gamma^2-1) + \frac{5}{32} \cdot Z^2 + 2X \cdot \sin 2\psi \end{Bmatrix}, \quad (7.59)$$

which are exactly integrable under certain conditions.

First, let us eliminate the time-variable τ. We obtain a single equation which relates the instantaneous amplitude and phase:

$$Z \cdot \frac{d\psi}{dZ} = - \cdot \frac{3(\Gamma^2-1) + \frac{5}{32} \cdot Z^2 + 2X \cdot \sin 2\psi}{3X \cdot \cos 2\psi} \quad . \quad (7.60)$$

If this is written in the form

$$\frac{d\psi}{dZ} = - \cdot \frac{P(Z,\psi)}{Q(Z,\psi)} \quad , \quad (7.61)$$

then in order to integrate, we require an integrating factor μ such that Euler's criterion

$$\frac{\partial(\mu P)}{\partial \psi} = \frac{\partial(\mu Q)}{\partial Z} \quad (7.62)$$

is satisfied. Such a factor is

$$\mu = Z^{1/3} \quad (7.63)$$

and the resulting equation for trajectories on the (Z, ψ)-plane is

$$C.Z^{-4/3} + \frac{3}{2}(\Gamma^2-1) + \frac{1}{32}Z^2 + X.\sin 2\psi = 0 , \qquad (7.64)$$

where C is a constant for a particular trajectory. Examples of these curves are shown in Figure 7.8 for a case of soft oscillation, and in Figure 7.9 for a case of hard oscillation. The singularities, which are indicated in the diagrams by open circles, correspond to points on the steady-state (ν,X,Z)-surface. In the case of soft oscillation there are three singularities, of which the outer two correspond to the two stable phases of oscillation. The central one corresponds to the absence of oscillation and it will be seen that the amplitude increases infinitely slowly from this point. In the case of hard oscillation there are five singularities, of which two, identified by (u,u) in Figure 7.9 , correspond to unconditionally unstable points on the "underneath" of the (ν,X,Z)-surface.

We shall now seek solutions for the variation with time of $Z(\tau)$ and $\psi(\tau)$. To do this, we use equations (7.64) and (7.59) to form the homogeneous first order nonlinear differential equations

$$\begin{aligned} \overset{\circ}{Z} &= \mathcal{F}_1(Z) \\ \overset{\circ}{\psi} &= \mathcal{F}_2(\psi) \end{aligned} \qquad (7.65)$$

which apply for zero damping. In principle these are integrable.

Thus, under the conditions $k_p = 0$, $k_L = 0$, the equation for $\overset{\circ}{Z}$ is from (7.59)

$$\frac{\overset{\circ}{Z}}{Z} = \frac{X}{n} . \cos 2\psi \qquad (7.66)$$

which can be homogenised by means of (7.64) to give

$$\frac{\overset{\circ}{Z}}{Z} = \frac{1}{n}\sqrt{X^2 - \left[\frac{3}{2}(\Gamma^2-1) + \frac{1}{32}Z^2 + C.Z^{-4/3}\right]^2} \qquad (7.67)$$

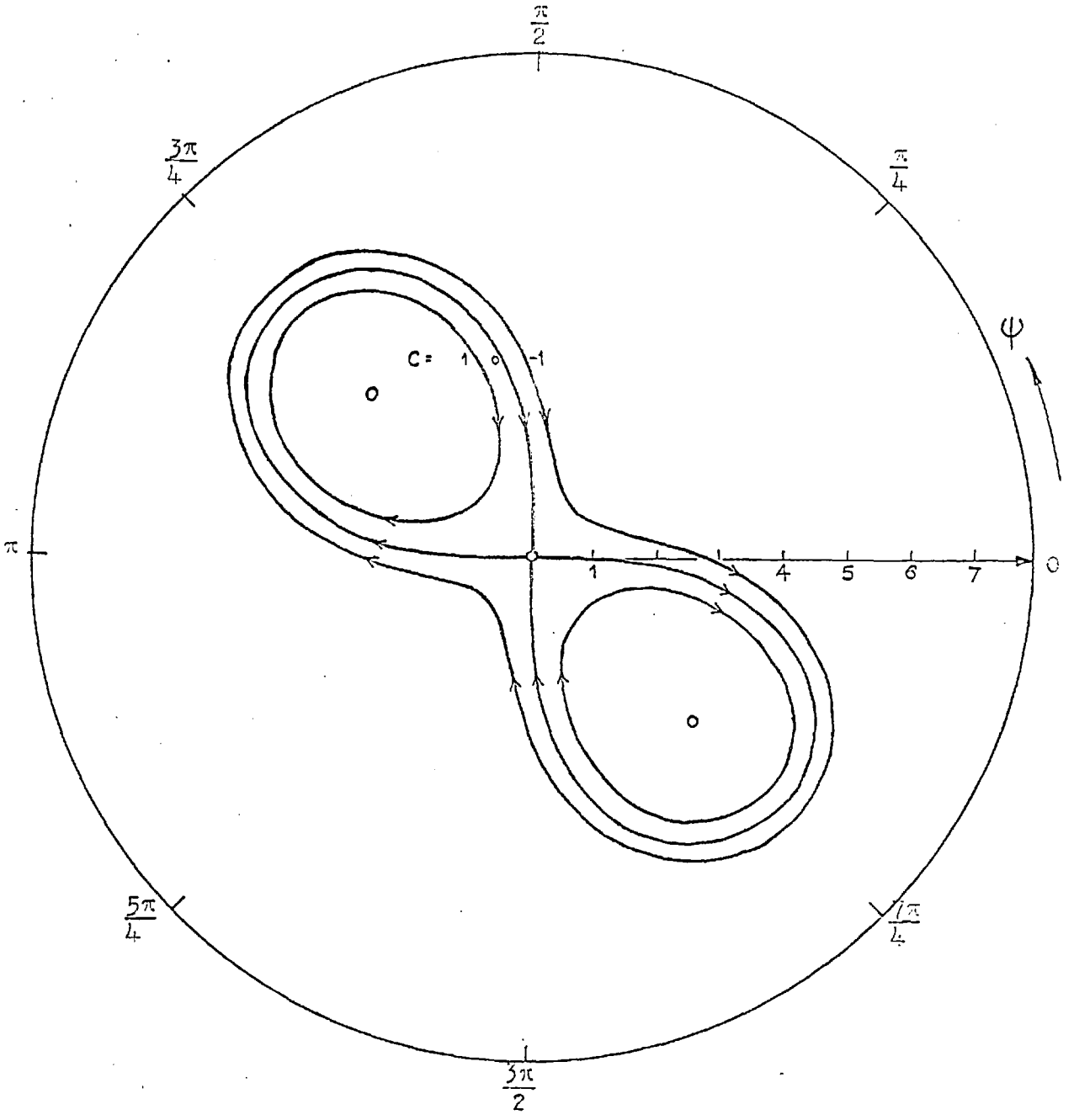


Figure 7.8 - Exact zero-damped trajectories for a case of soft oscillation. The parameters are

$\nu = 1.0$

$X = 1.0$

$k_p = 0$

$B = 1.0$

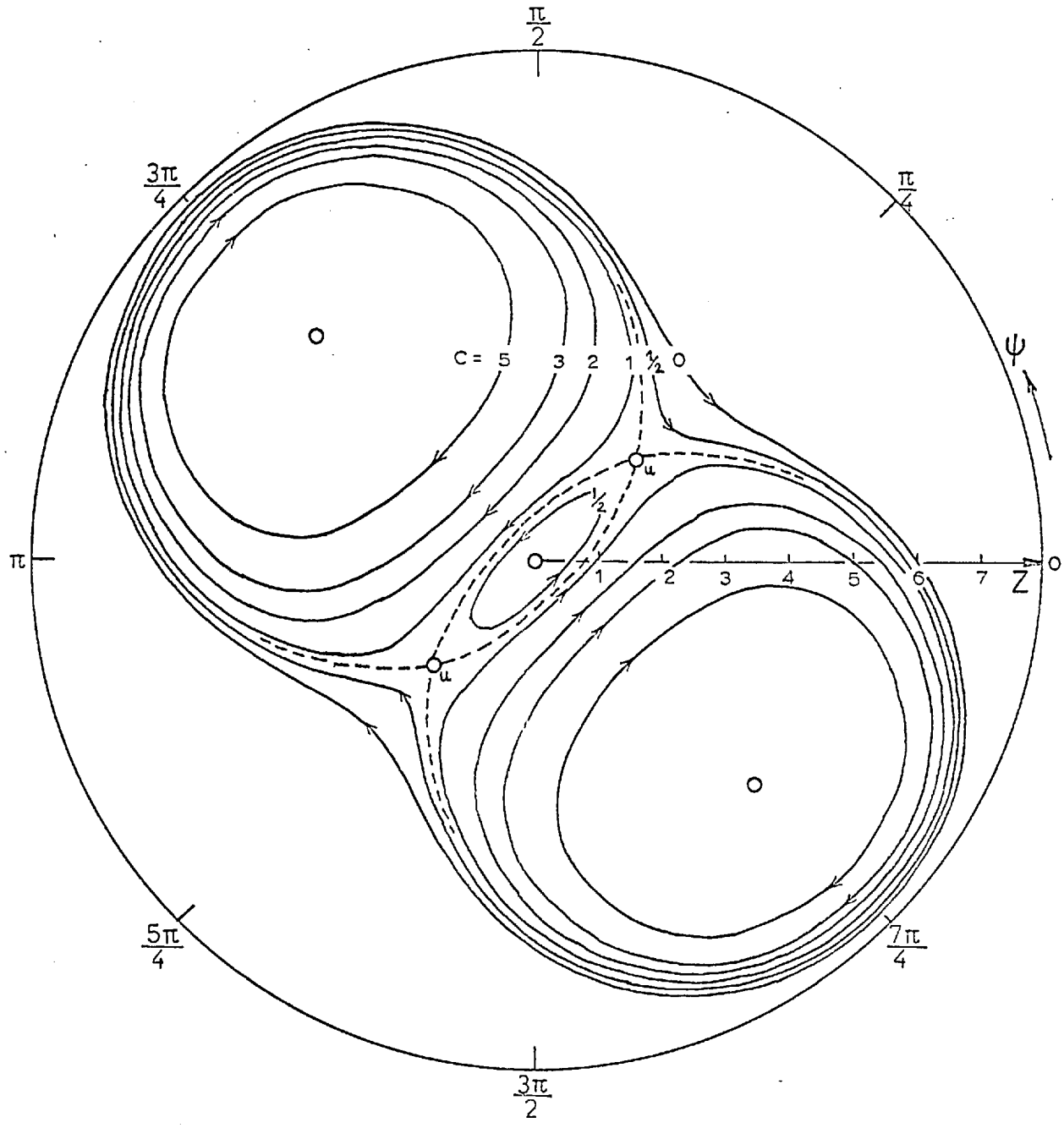


Figure 7.9 - Exact zero-damped (Z,ψ)-trajectories for a case of hard oscillation.

Parameters: $\nu = 0.70$

$X = 0.75$

$k_p = 0$

$B = 1.0.$

This is integrable only for C = 0, in which case the differential equation for the amplitude transient is

$$\boxed{\frac{\dot{Z}}{Z}\bigg|_{C=0} = \frac{1}{n}\sqrt{X^2 - \left[\frac{3}{2}(\Gamma^2-1) + \frac{1}{32}Z^2\right]^2}} \qquad (7.68)$$

The equation for $\dot{\psi}$ is, from (7.59),

$$\dot{\psi} = -\frac{1}{3n}\left[r_o(Z) + 2X.\sin 2\psi\right] \qquad (7.69)$$

If Z^2 is eliminated from this by means of (7.64) we obtain

$$\dot{\psi} = \frac{1}{3n}\left[\frac{9}{2}(\Gamma^2-1) + 3X.\sin 2\psi + 5C.Z^{-4/3}\right] \qquad (7.70)$$

which is homogeneous only for C = 0, and is then integrable:

$$\boxed{\dot{\psi}\bigg|_{C=0} = \frac{1}{2n}\left[3(\Gamma^2-1) + 2X.\sin 2\psi\right]} \qquad (7.71)$$

Equation (7.68) for the transient charge amplitude can be integrated at once, the form of the result depending on whether $\left|\frac{3}{2X}(\Gamma^2-1)\right| = |\rho|$ is greater or less than unity. This criterion determines whether or not soft (unconditional) subharmonic oscillation takes place. Soft oscillation occurs for

$$|\rho| < 1$$

in which case the transient amplitude solution* for trajectories passing through the origin of the (Z,ψ)-plane is

$$e^{S_\rho \tau} = \left(\frac{Z}{Z(0)}\right)^2\left[\frac{\sqrt{1-\rho^2}\sqrt{1-(\rho+aZ^2(0))^2} + 1 - \rho^2 - a\rho Z^2(0)}{\sqrt{1-\rho^2}\sqrt{1-(\rho+aZ^2)^2} + 1 - \rho^2 - a\rho Z^2}\right]. \qquad (7.72)$$

---

* An explicit solution for $Z(\tau)$ is obtainable but is more cumbersome.

where $a = \frac{1}{32X}$,

$$S_\rho = \frac{2X}{n}\sqrt{1-\rho^2} \quad ,$$

and $Z(0)$ is the value of Z at $\tau = 0$.

This shows that if the initial amplitude $Z(0)$ is zero, then the rise-time is infinitely long, i.e. the origin of the (Z,ψ)-trajectory diagram for the case of soft oscillation is stable.

A simple solution occurs for the case of resonance, for which $\rho = 0$, and

$$e^{\frac{2X}{n}\cdot\tau} = \left(\frac{Z}{Z(0)}\right)^2\left[\frac{\sqrt{1-a^2Z^4(0)}+1}{\sqrt{1-a^2Z^4}+1}\right] . \qquad (7.73)$$

Generality is not lost by choosing the initial condition

$$Z^2(0) = \frac{1}{a} = 32X \quad ,$$

which makes

$$e^{\frac{2X}{n}\cdot\tau} = \frac{Z^2}{32X+\sqrt{(32X)^2-Z^4}} . \qquad (7.74)$$

This curve is shown in Figure 7.10(a). The amplitude of the envelope of the subharmonic oscillation increases to a maximum at $\tau = 0$, and then decreases again. In this zero-damped case and for the present definition of the time-origin, the transient amplitude solution is independent of $\mathrm{sgn}(\tau)$.

Equation (7.71) can be integrated to give a solution for the transient behaviour of the phase angle ψ. In the region of soft oscillation, which is defined by $|\rho| < 1$, the solution is

$$e^{S_\rho\tau} = \left[\frac{\rho+\sin 2\psi}{\rho+\sin 2\psi(0)}\right]\cdot\left[\frac{1+\rho\cdot\sin 2\psi(0)+\sqrt{1-\rho^2}\cos 2\psi(0)}{1+\rho\cdot\sin 2\psi+\sqrt{1-\rho^2}\cos 2\psi}\right], \qquad (7.75)$$

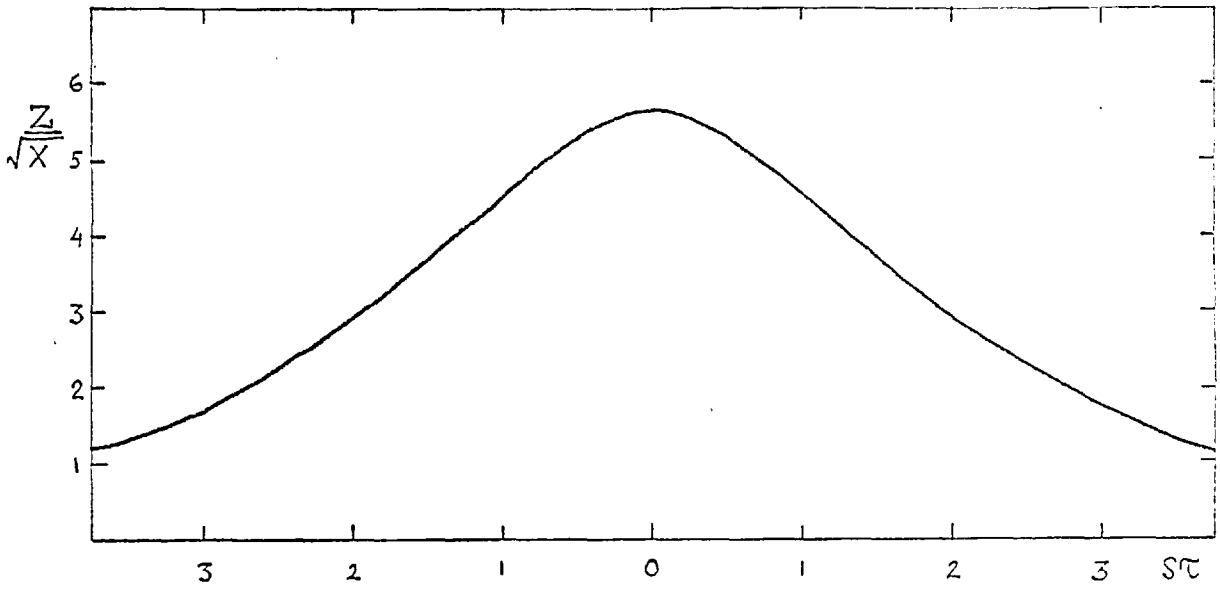


Figure 7.10(a) - Exact zero-damped amplitude transient for the resonant case and for C = 1.0.

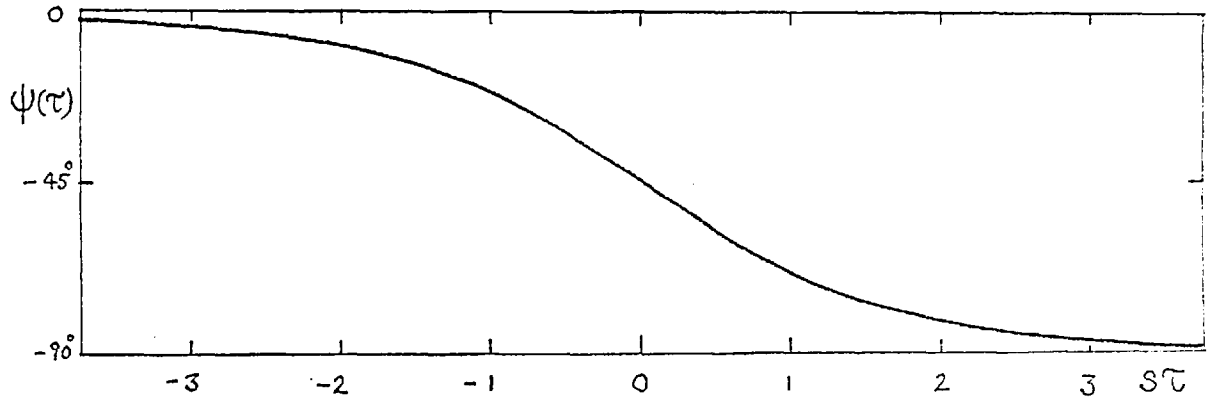


Figure 7.10(b) - Corresponding exact zero-damped phase transient.

where $\psi(0)$ is the initial phase angle at $\tau = 0$, and ρ and S_ρ have the meanings previously defined. In the special case of resonance, and for the choice of initial condition $\psi(0) = -\frac{\pi}{4}$ (corresponding to $Z(0) = \sqrt{32X}$), this result reduces to just

$$e^{S_\rho \tau} = - \text{tg } \psi(\tau). \qquad (7.76)$$

This transient phase solution is shown in Figure 7.10(b), and the composite phase-amplitude-time response in (ψ, Z, τ)-space is illustrated for the case C=0 in Figure 7.11. This diagram gives one a visual picture of the nature of the transients to be investigated.

The amplitude and phase solutions (7.72) and (7.75) each contain only one initial condition. This is a consequence of the constraint C=0. For trajectories which do not pass through the origin of the (Z, ψ)-plane, C is not zero, and the corresponding amplitude and phase solutions (if we were able to obtain them) would each contain two initial conditions, $Z(0)$ and $\psi(0)$.

We shall now turn to the case in which the damping is not zero and is attributed to the parameter k_p.

7.4.6 Small-signal transient theory in the presence of damping : trajectories and stability

The first-order differential equations describing the transient behaviour of the subharmonic phase and amplitude, such as equations (7.44) or (7.55), are both nonlinear and inhomogeneous. They cannot be integrated exactly. We shall therefore make use of an approximate method. This is based on certain experimental observations. Under most conditions of

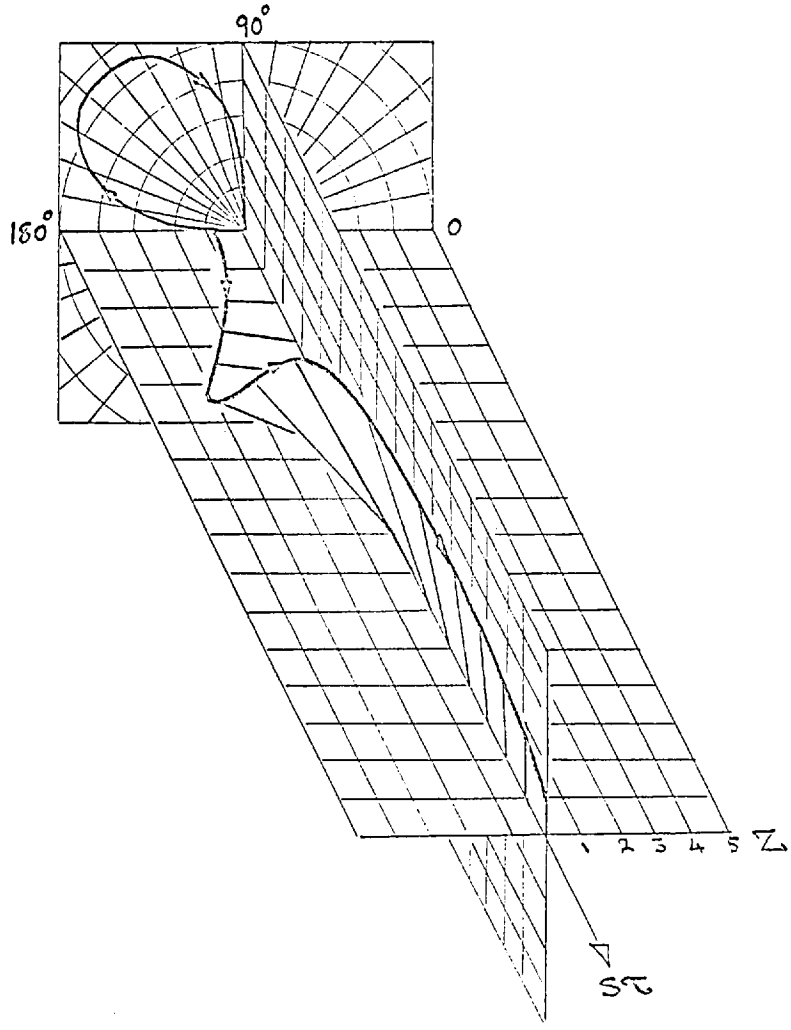


Figure 7.11 - Composite phase-amplitude-time response for the zero-damped resonant case and for C = 0.

practical interest, that is, within the region of soft oscillation, and with certain restrictions on the initial phase-angle, the greater part of the oscillation-envelope of the growing subharmonic voltage V_s is an approximately exponential function of time. As the oscillation grows, nonlinearities eventually cause the amplitude to limit at the steady-state value $V_s(\infty)$. A typical practical example of such an amplitude-transient is shown in the photograph of Figure 7.12. It can be seen that the only part of the envelope which is not approximately exponential is the region near the steady-state value $V_s(\infty)$.

This behaviour suggests that the initial part of the transient, upon which the remainder thereof is highly dependent, could be treated by putting

$$Z \ll 1$$

in the transient theory and neglecting Z^2. It would then be possible to approximate the final part of the transient by terminating the rising amplitude at the steady-state value $Z(\infty)$. This value can, of course, be calculated without assuming $Z \ll 1$.

The equations determining the transient behaviour under the domination of the loss-parameters k_p and k_L are (7.44) and (7.55) respectively. The approximation $Z \ll 1$ results in a much greater simplification of the first than of the second. Fortunately, most of the dissipation in a practical parametron can be ascribed to k_p. The major part of the detailed transient theory will therefore be based on equation (7.44).

The conditions

$$k_v = 0, \quad k_L = 0, \quad Z \ll 1$$

will be imposed. They mean that the conductances of the varactors and of the load are negligible and that the oscillatory differential charge is small

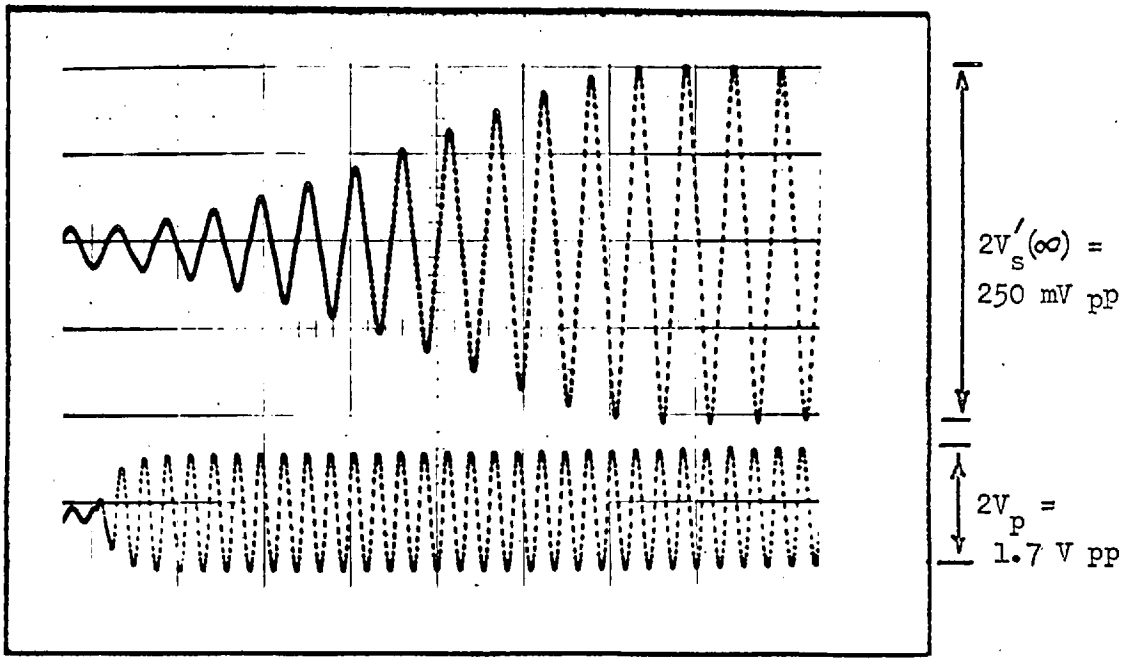


Figure 7.12 - Photograph illustrating approximately exponential behaviour of initial part of amplitude transient.

Conditions: $V_s'(0) = 13$ mV,

$V_B = 0$,

$\nu = 1.0$,

$\theta(0) = -22^\circ$.

Modulated pump (q.v.).

compared with the static varactor charge. It is now possible to find equations for the transient amplitude and phase from (7.44). Without any restrictions on ν, X, k_p or B these equations are

$$\frac{\dot{Z}}{Z} = \frac{X}{n} \cdot \cos 2\psi \qquad (7.77)$$

and

$$\dot{\psi} = -\frac{1}{3n^2}\left[\ell X.\cos 2\psi + n(r_o + 2X.\sin 2\psi) \right], \qquad (7.78)$$

respectively, where

$$r_o = 3(\Gamma^2 - 1).$$

Elimination of τ between these two equations gives a first-order equation relating the instantaneous amplitude and phase of the oscillatory charge:

$$\frac{1}{Z} \cdot \frac{dZ}{d\psi} = - \frac{3nX. \cos 2\psi}{\ell X.\cos 2\psi + 2nX.\sin 2\psi + n.r_o} \qquad (7.79)$$

This will be written shortly

$$\frac{dZ}{Z} = -\frac{3}{4} \cdot \frac{\cos 2\psi \cdot d(2\psi)}{\sigma. \cos 2\psi + \sin 2\psi + \rho}, \qquad (7.80)$$

where

$$\rho = \frac{r_o}{2X} = \frac{3}{2X}(\Gamma^2 - 1) \qquad (7.81)$$

and

$$\sigma = \frac{\ell}{2n} = \frac{4k_p}{B\nu}. \qquad (7.82)$$

Equation (7.80) can be integrated to yield a relation between $Z(\tau)$ and $\psi(\tau)$ for sufficiently small Z. However, before this is done, it is worth noticing that the ranges of ψ which correspond to positive and negative values of Z can be found from (7.77). Thus it can be determined whether $Z(\tau)$ increases or decreases with time. Hence the direction of traversal of the trajectories can be predicted. This small-signal information will ultimately enable us to find the stability of the singularities without recourse to a formal stability analysis. Such an analysis would be difficult

in view of the complexity of (7.44).

It follows from (7.77) that since n, X and Z are all positive,

$$\dot{Z} > 0 \text{ for } \left\{ \begin{array}{lll} -\frac{\pi}{4} & < \psi < & \frac{\pi}{4} \\ \frac{3\pi}{4} & < \psi < & \frac{5\pi}{4} \end{array} \right\} \quad \text{and}$$

$$\dot{Z} < 0 \text{ for } \left\{ \begin{array}{lll} \frac{\pi}{4} & < \psi < & \frac{3\pi}{4} \\ \frac{5\pi}{4} & < \psi < & \frac{7\pi}{4} \end{array} \right\} \quad .$$

The two sets of conditions determine the sign of $\dot{Z}$. They are summarised in Figure 7.13, in which $|Z|$ increases in the shaded and decreases in the unshaded regions. The conditions apply not only for the initial conditions $Z(0)$, $\psi(0)$ but also for the ensuing trajectories, provided $Z \ll 1$. If there is no damping, the latter proviso is redundant, as may be seen by referring to Figures 7.8 or 7.9.

The form of the solution of (7.80) depends on

$$\text{sgn } (1 + \sigma^2 - \rho^2).$$

At first sight it might be supposed that the curve on the (ν, X)-plane defined by

$$\rho^2 = 1 + \left(\frac{4k_p}{B\nu} \right)^2 = 1 + \sigma^2$$

would coincide with the steady-state boundary between the region of hard oscillation and the region of no oscillation. This boundary has already been identified as the projection of the (ν, X, Y) nose-locus on to the (ν, X)-plane. However, the supposition is incorrect since the projection of the nose-locus is given by

$$\rho^2 = 1 + \left(\frac{5}{8} \cdot \frac{1}{\nu k_p} \cdot \frac{B}{1-B} \right)^2 = 1 + \left(\frac{5}{32} \cdot \frac{1}{\nu\delta} \right)^2 .$$

The practically interesting part of the (ν, X)-plane is that for which

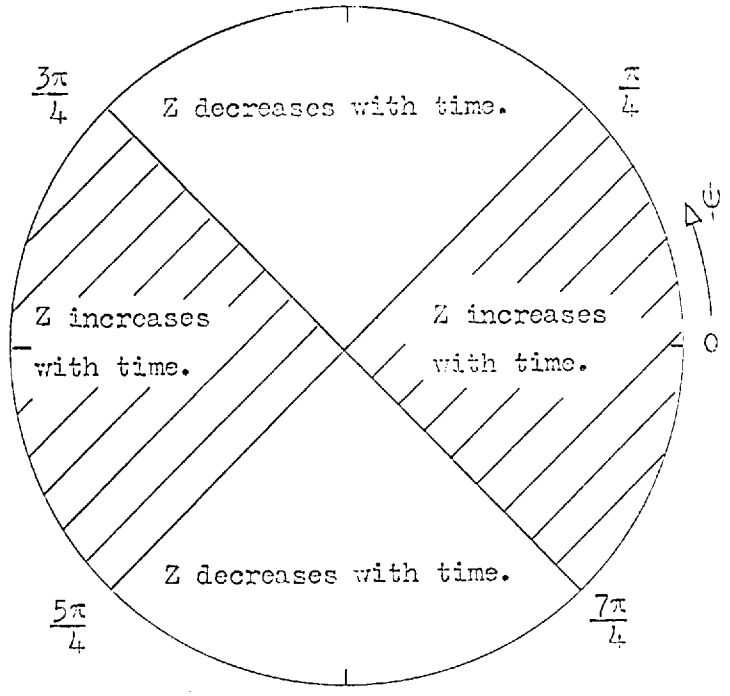


Figure 7.13 - Diagram indicating the phase angles which are associated with growing or decaying oscillations. For zero damping the diagram is valid for all Z, for non-zero damping it is valid for $Z \ll 1$.

soft (unconditional) oscillation occurs. It is defined by

$$\rho^2 < 1.$$

This region is contaimed within the larger domain

$$\rho^2 < 1 + \sigma^2 .$$

The various regions mentioned are indicated in Figure 7.23, and their significance will become apparent in the associated Sub-Section 7.4.8.

The solution of (7.80) for $\rho^2 < 1 + \sigma^2$ is

$$D.Z^{-\frac{4}{3}(1+\sigma^2)} + e^{\sigma(2\psi - \xi)}\left[\rho+\sqrt{1+\sigma^2}\,.\cos(2\psi - \xi)\right].$$

$$\cdot\left[\frac{\rho+\sqrt{1+\sigma^2}.\cos(2\psi - \xi)}{\sqrt{1+\sigma^2}+\rho.\cos(2\psi-\xi)+\sqrt{1+\sigma^2-\rho^2}.\sin(2\psi-\xi)}\right]^{\frac{\sigma\rho}{\sqrt{1+\sigma^2-\rho^2}}} = 0 \quad , \tag{7.83}$$

where $tg\,\xi = \frac{1}{\sigma}$,

and D is a constant defining a particular trajectory.

In the case of resonance ($\nu = 1$) this becomes simply

$$D.Z^{-\frac{4}{3}(1+\sigma^2)} + e^{\sigma(2\psi-\xi)}\cos(2\psi - \xi) = 0, \tag{7.84}$$

since $\rho = 0$.

It is interesting to notice that at resonance the <u>shape</u> of the trajectories is independent of the pump amplitude X. This is because ρ is the only function of X in (7.83).

If the damping parameter k_p is zero, so that $\sigma = 0$, then the solution (7.83) reduces to

$$C.Z^{-4/3} + \frac{3}{2}(r^2 - 1) + X.\sin 2\psi = 0 \tag{7.85}$$

where C = D.X. This can at once be identified as equation (7.64) which was

derived under the zero-damping assumption, except that here $\frac{1}{32} Z^2$ is absent because of the small-signal assumption. In the region $\rho^2 > 1 + \sigma^2$, which lies "outside" that of immediate interest, the trajectories take on a different form:

$$D.Z^{-\frac{4}{3}(1+\sigma^2)} + \left[\rho + \sqrt{1+\sigma^2} \cdot \cos(2\psi - \xi)\right] \cdot \exp\left[\sigma(2\psi - \xi) - \frac{2\sigma\rho}{\sqrt{\rho^2-1-\sigma^2}} \cdot \text{arc tg} \left\{\frac{(\rho-\sqrt{1+\sigma^2}) \text{ tg } \frac{1}{2}(2\psi - \xi)}{\sqrt{\rho^2 - 1 - \sigma^2}}\right\}\right] = 0. \quad (7.86)$$

7.4.6.1 Explanation of certain anomalous theoretical results

Although the "charge" theory so far developed gives a satisfactory explanation of

(1) the steady-state amplitude phenomena and

(2) the transient phenomena under conditions of zero damping,

certain anomalies occur when the steady-state phase-angle and the transient behaviour in the presence of finite damping are to be predicted. It is found that the anomalous theoretical results are only obtained for frequencies below resonance. Careful interpretation of the damping parameter k_p is necessary if physically possible results are to be obtained. It was seen in Chapter 3 that for the case $n = \frac{1}{2}$, the varactor charge q was a two-valued function of the voltage v. Thus, referring to Figure 3.4, $\frac{dq}{dv} = \frac{dz}{dy}$ can be either positive or negative at $v = 0$ $(y = 0)$. Hence the small-signal varactor capacitance

$$C_o = \left.\frac{dq}{dv}\right|_{v=0}$$

can have, as far as the theory is concerned, a positive or a negative sign, the latter being non-physical.

Further, since

$$k_p = \omega_o C_o R_p ,$$

this damping parameter can also be either positive or negative. It is therefore to be expected that certain non-physical theoretical results may be encountered corresponding to negative values of k_p.

It is found that theory is in accord with experiment over a large range of operating conditions if the sign of k_p is reversed for all values of ν less than unity.

These considerations affect the following parameters, all of which contain k_p as a coefficient:

$$\ell = 32k_p\Gamma^3/B^2\nu^4,$$

$$m = \frac{1}{8}k_p(\frac{1}{B} - 1)Z^2 ,$$

$$\delta = \frac{1}{4}k_p(\frac{1}{B} - 1) ,$$

$$\sigma = 4k_p/B\nu .$$

The parameter S, which contains σ^2, is unaffected by $\mathrm{sgn}(k_p)$. For simplicity, all the quantities mentioned above are given in the text with positive signs. The calculated results have been obtained with the appropriate sign of k_p.

7.4.6.2 Typical small-signal (Z,ψ)-trajectories

(Z,ψ)-trajectories have been calculated according to the small-signal equations for a typical practical parametron with the measured parameters

$$k_p = 0.28 , \quad B = 0.45.$$

Figure 7.14 shows trajectories computed from equation (7.84) for resonance. In this particular case, Z is proportional to X for a given phase-angle ψ, so that the curves are all the same shape. Hence neither a radial scale nor a particular value for X need be given. The directions of the arrows, which indicate the motion of the tip of the (Z, ψ)-vector as time increases, have been established by referring to the conditions of Figure 7.13.

Figure 7.14 illustrates several important points:

(1) The trajectories are not, in general, even approximately hyperbolic.

(2) There are two pairs of critical phase-angles for which the phase remains time-invariant. Critical angles leading to growing oscillations will be referred to as $\psi_c +$, those leading to decaying oscillations as $\psi_c -$. The time-invariance obtains for small amplitudes only. We shall see later that for large amplitudes of Z, the corresponding trajectories eventually depart from straight lines.

(3) In the resonant case, the angle between $\psi_c +$ and $\psi_c -$ is 90°. It will be seen that in non-resonant cases this angle differs from 90°.

(4) The quantity $\frac{d\psi}{dZ}$ is zero at the critical phase angles $\psi_c \pm$. This means that in a sufficiently small time-interval the amplitude changes while the phase remains constant. All the trajectories except those corresponding to $\psi_c -$ (here 56° or 236°), eventually depart from the origin and tend towards one of the other pair of critical angles $\psi_c +$ (here -34° or 146°).

(5) The quantity $\frac{dZ}{d\psi}$ is zero at the angles

$$\psi = N \cdot \frac{\pi}{4}$$

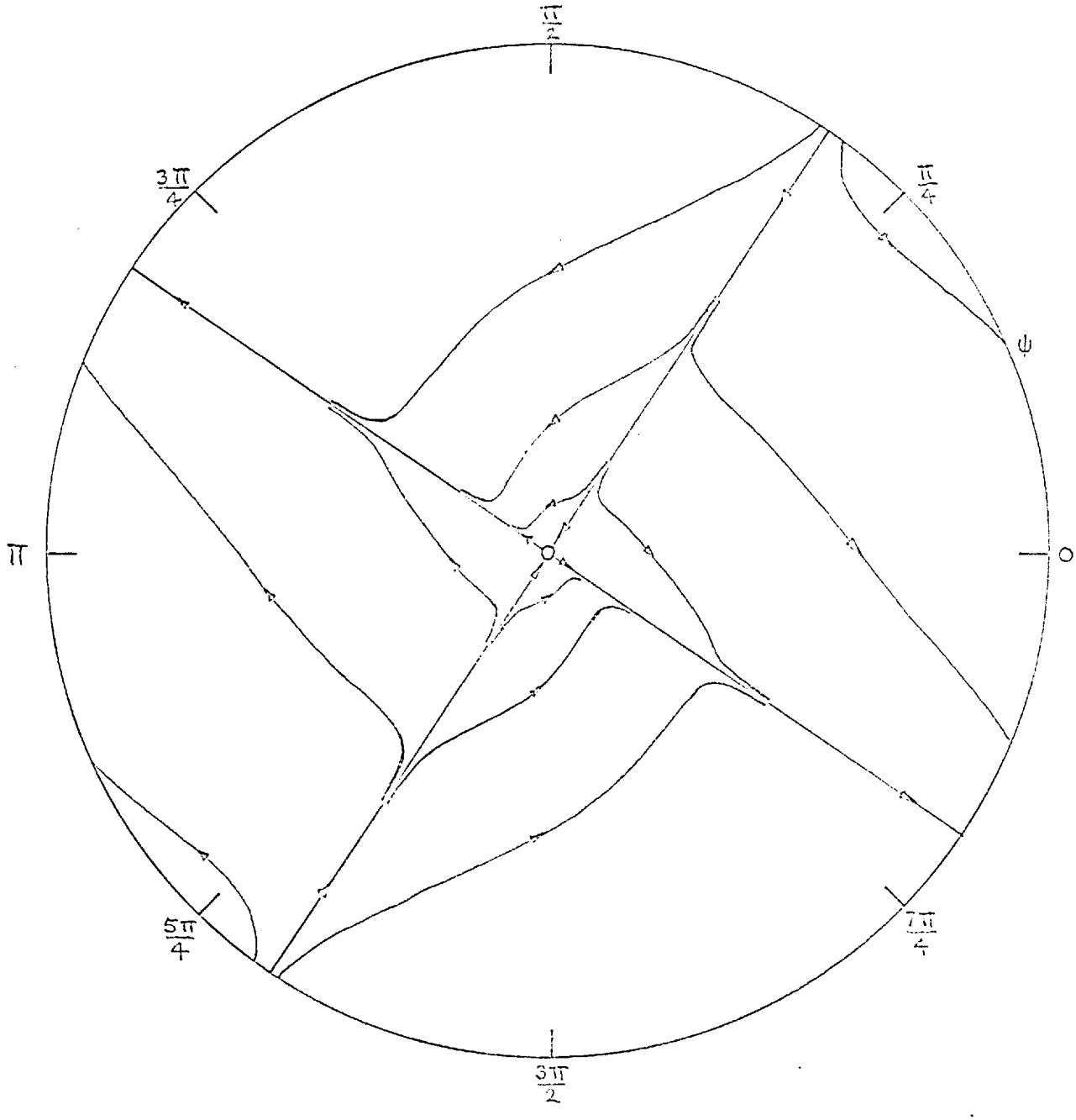


Figure 7.14 - (Z,ψ)-trajectories calculated according to the small-amplitude approximation for the typical practical parameters

$\nu = 1.0$

$k_p = 0.28$

$B = 0.45$.

The curves are independent of X and Z.

where N is an integer. At these particular phase-angles the phase changes while the amplitude remains constant. This is true for all values of tuning, resonant or non-resonant.

Figure 7.15 illustrates some (Z,ψ)-trajectories computed according to the $Z \ll 1$ approximation for a set of typical practical conditions giving rise to hard oscillation:

$$\nu = 0.9$$

$$X = 0.5$$

$$k_p = 0.28$$

$$B = 0.45.$$

Note that the considerations of Sub-Section 7.4.6.1 relating to $\mathrm{sgn}(k_p)$ were taken into account in computing these curves. The diagram shows that for small signal amplitudes, all the trajectories tend ultimately towards the origin as time increases. For certain ranges of ψ, however, the amplitude Z can increase before it finally decreases. This rather unusual behaviour has been observed in practical parametrons initiated with small-amplitude signals in the region of hard oscillation.

It can be shown that for extremely large values of the damping parameter σ, the trajectories tend towards the form indicated in Figure 7.16. The trajectories now consist of circular arcs for all phase angles except for the critical angles $\psi_c \pm$, which are $\pm \frac{\pi}{4}$ and $\pm \frac{3\pi}{4}$. If this diagram is compared with Figure 7.8 for the corresponding zero-damped case, it can be seen that the trajectory-diagrams encountered in practice fall somewhere between these two extremes.

The infinitely-heavily damped trajectories of 7.16, cannot, of course, be related to any physical situation. The steady-state amplitude tends to

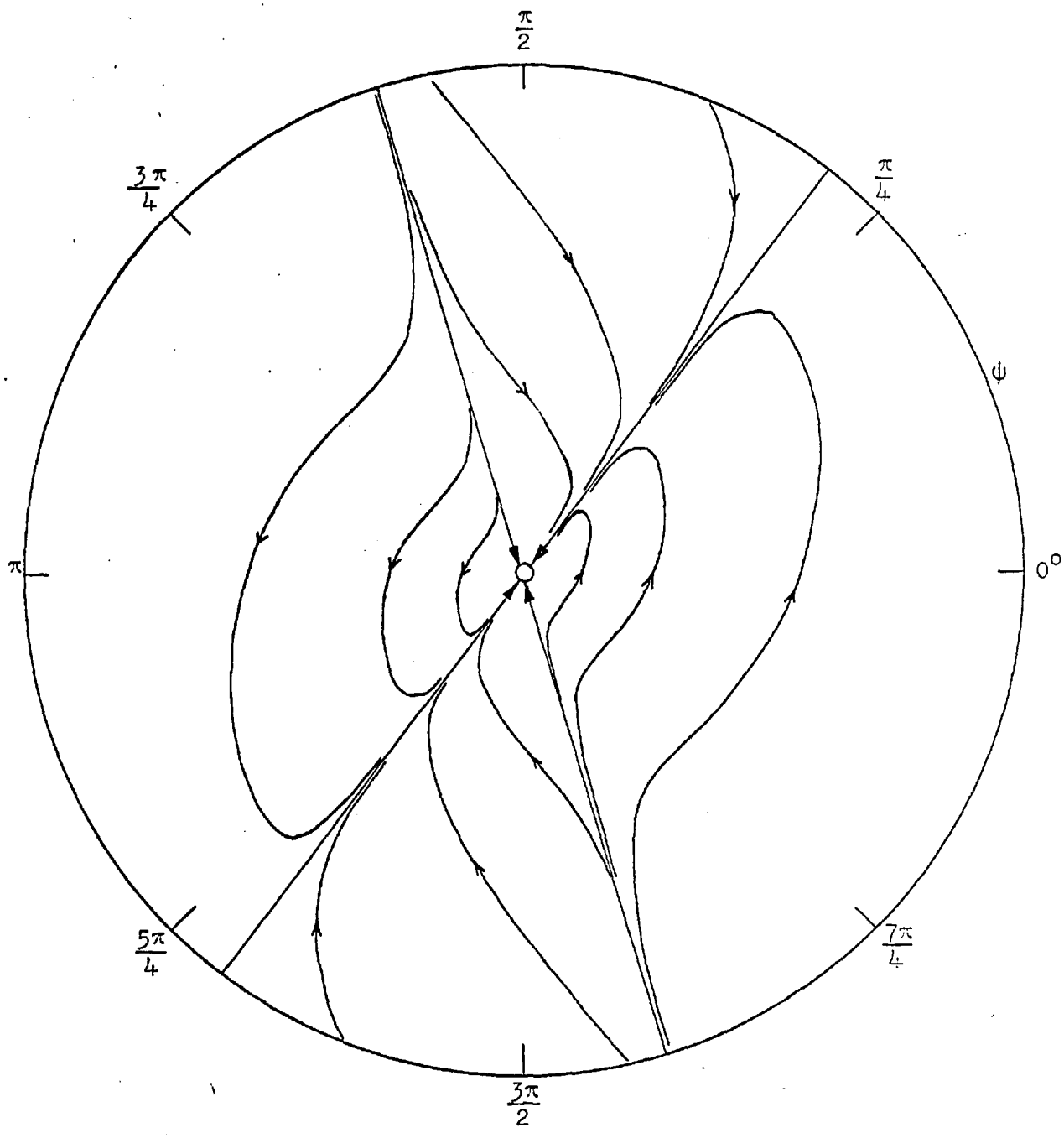


Figure 7.15 - (Z,ψ)-trajectories computed according to the small-amplitude approximation for a case of hard oscillation. The parameters are: ν = 0.9, X = 0.5, k_p = 0.28, B = 0.45. The shape of the curves is independent of Z.

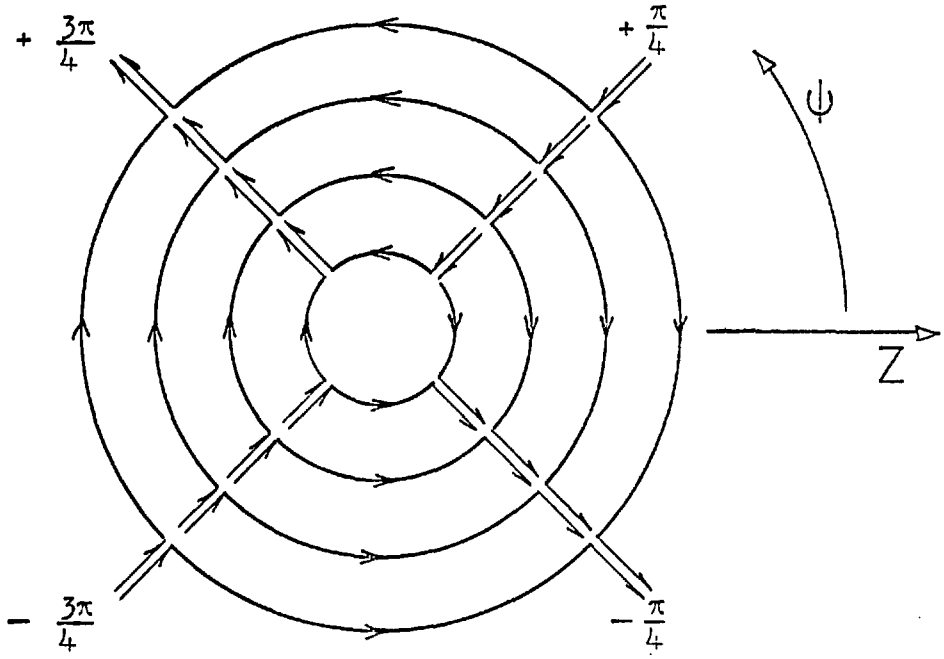


Figure 7.16.-

The form assumed by the small-signal (Z,ψ)-trajectories in the limit $\sigma \longrightarrow \infty$.

zero as the damping increases towards infinity, so that the diagram merely indicates the end-point of a trend.

7.4.7. Large-signal trajectories in the presence of damping

In the presence of the damping parameter k_p, the differential equation for the large-signal (Z,ψ)-trajectories is given by eliminating the time-variable τ between the pair of equations (7.44), Section 7.4.1. The result is

$$\frac{1}{Z}\cdot\frac{dZ}{d\psi} = -\cdot\frac{3n[\nu.m(Z)+ X.\cos 2\psi] - m(Z)[r(Z)+ 2X.\sin 2\psi]}{[5m(Z) + 2][\nu.m(Z)+ X\cos 2\psi] + n[r(Z)+ 2X.\sin 2\psi]}\ , \tag{7.87}$$

where $r(Z)$ and $m(Z)$ are functions of Z^2. It is not possible to integrate this exactly, so that we shall resort to an adaptation of the isocline method in order to obtain the integral curves*. The above equation is of the form

$$\frac{1}{Z}\cdot\frac{dZ}{d\psi} = \mathcal{F}(Z,\psi)$$

where $\mathcal{F}$ is a nonlinear function of Z and ψ. Now consider the curves

$$\frac{1}{Z}\cdot\frac{dZ}{d\psi} = \zeta = \text{constant}.$$

As indicated in Figure 7.17, the trajectory which passes through a point P of such a curve makes a constant angle $\frac{\pi}{2} + \Omega$ with the direction of the Z-vector, where

$$\text{tg}\ \Omega = \zeta$$

---

* Even if we were able to integrate this expression exactly, it is probable that the result would be transcendental, requiring graphical solution, so that one might as well use graphical procedures throughout.

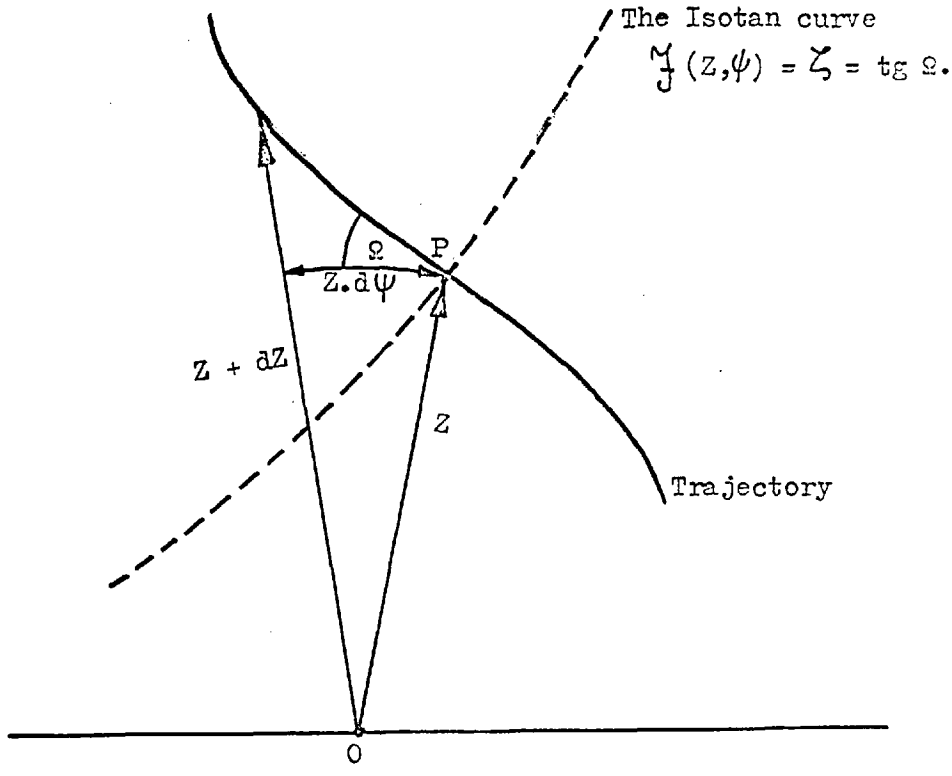


Figure 7.17 - Construction of Isotan curves.

The curves $\mathcal{F}(Z,\psi) = \zeta$ are <u>not</u> isoclines in the usual sense, but their polar equivalent; they will be referred to as "Isotan curves". The concrete example of equation (7.87) leads to the following expression for Isotan curves:

$$\left[n\zeta - m\right]\left[r + 2X.\sin 2\psi\right] + \left[3n + (5m + \ell)\zeta\right]\left[m\nu + X.\cos 2\psi\right] = 0$$

which for convenience in calculation may be written

$$2\psi = \text{arc tg } H + \text{arc cos}\left[-\left\{\frac{m\nu + \frac{1}{3}Hr}{X\sqrt{1 + H^2}}\right\}\right], \quad (7.88)$$

$$= \text{arc tg } H + \text{arc cos}\left[-\left\{\frac{\rho + \frac{Z^2}{2X}(\nu\delta + \frac{5}{32}H)}{\sqrt{1 + H^2}}\right\}\right] \quad (7.89)$$

where $H = \dfrac{2(n\zeta - m)}{(5m + \ell)\zeta + 3n}$.

In order to construct a family of (Z,ψ)-trajectories for a specified set of conditions (ν, X, k_p, B), it is necessary to plot Isotan curves for a range of values of the constant ζ, such as -1, 0, +1, ∞. Then line-segments making an angle $\left(\frac{\pi}{2} + \text{arc tg } \Omega\right)$ with the direction of the Z-vector must be drawn at intervals along the Isotan curves. Finally, the trajectories can be constructed by connecting together the line-segments.

Some (Z,ψ)-trajectories for the typical practical case

$\nu = 1.0$

$X = 0.5$

$k_p = 0.3$

$B = 0.5$

have been calculated according to the above procedure and are illustrated in Figure 7.18. The conditions are similar to those used in the calculation of

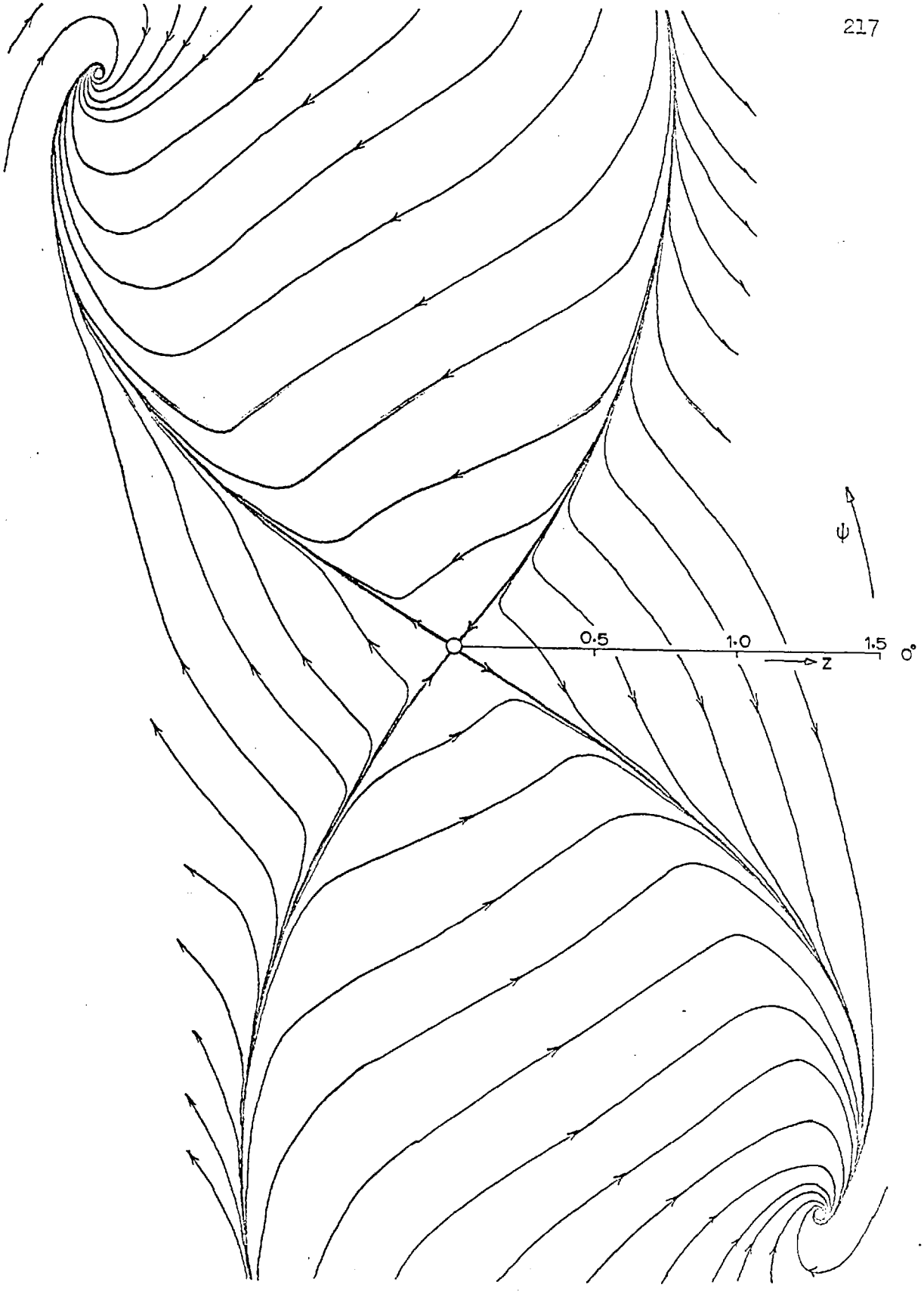


Figure 7.18 - Large-signal (Z,ψ)-trajectories given by the Isotan method for the case $\nu = 1.0$, X = 0.5, $k_p = 0.3$, B = 0.5.

Figure 7.14. If the two diagrams are compared, it will be seen that the trajectories are of the same shape near the origin Z = 0. The present large-signal diagram shows that those trajectories which pass through the origin progressively deviate from straight lines as Z increases. Furthermore, for large values of Z the loci of $\frac{dZ}{d\psi} = 0$ deviate from the straight lines $\psi = \pm \frac{\pi}{4}$ and become the "figure-of-eight" curves $\zeta = 0$.

These integral curves show an interesting phenomenon: there is a strong tendency for the trajectories to approach the S-shaped "backbone" curve, which we shall refer to as the S-curve, much more quickly than they approach the singularities (indicated by open circles). This means that the phase approaches its steady-state value $\psi(\infty)$ much more rapidly than the amplitude approaches $Z(\infty)$. This is an important conclusion when phase-initiation is required, for it means that the parametron can be operated in a "linear" mode (analogously to a method sometimes applied to the super-regenerative oscillator)* in which the oscillation is quenched <u>before</u> the steady-state amplitude $Z(\infty)$ is reached. This enables the parametron switching to be accomplished much faster than would otherwise be possible, leading to increased computing speeds.

Figure (7.18) indicates the further interesting possibility that phase-switching can be accomplished merely by altering the amplitude Z(0) of the initiating signal, the phase $\psi(0)$ thereof being kept <u>constant</u>. To see how this unusual situation can occur, consider Figure (7.19). This diagram shows only the trajectories which pass through the origin of the (Z, ψ)-plane. One of these connects the singularities S_π and S_0, corresponding to

---

* See, for example, Page[39] or Whitehead[40].

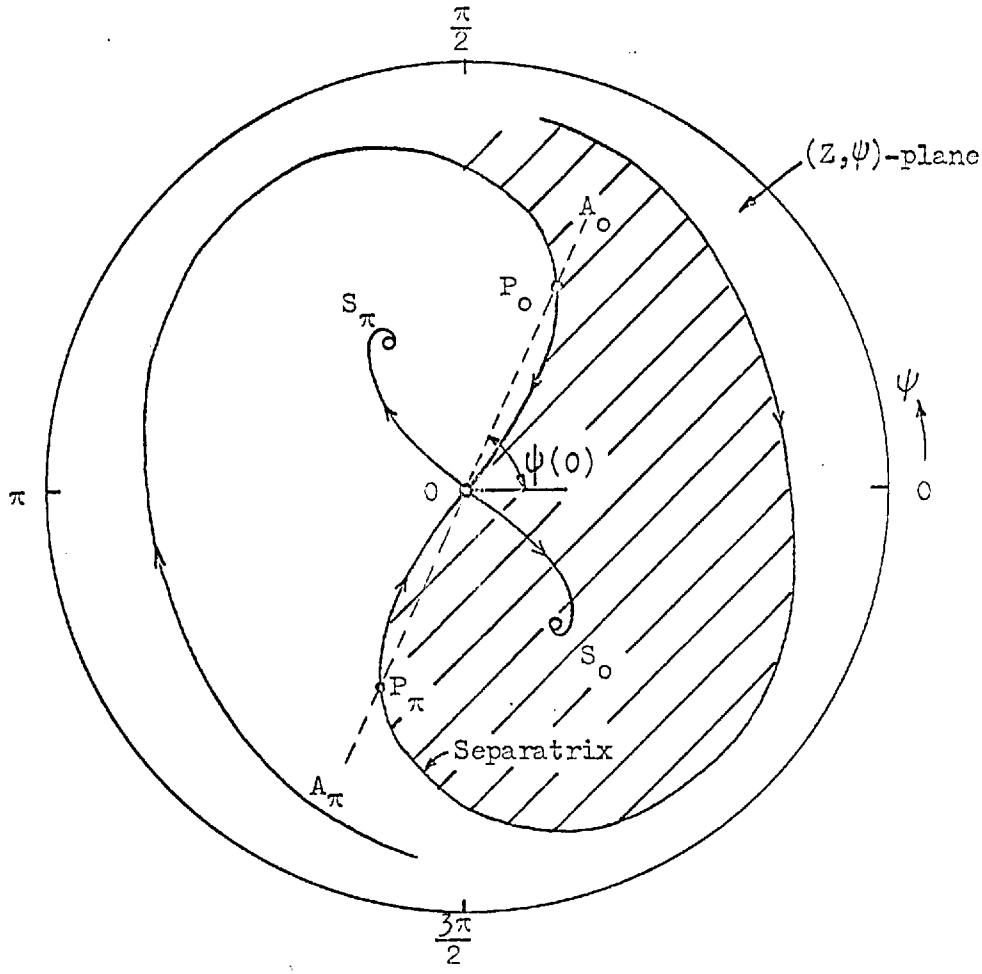


Figure 7.19 - Diagram illustrating phase-switching by amplitude-variation.

stable phases "π" and "0" respectively. The other trajectory, the separatrix, divides the plane into two regions: initial conditions lying in the unshaded region lead ultimately to the singularity S_π, those lying in the shaded region lead to S_o. Now consider the line (A_o, A_π) which cuts the separatrix in the three points P_o, 0, P_π. Suppose the initial conditions are constrained to lie along this line, that is, $\psi(0)$ is fixed and Z(0) is varied. Then if

$$0 < Z(0) < P_o$$

or

$$P_\pi < Z(0) < A_\pi ,$$

the stable phase "π" will be initiated; whereas if

$$0 < Z(0) < P_\pi$$

or

$$P_o < Z(0) < A_o ,$$

the stable phase "0" will be initiated. Thus it is evident that if initial conditions "near" the separatrix are required, the exact magnitude of Z(0) becomes critical if reliable phase-initiation is to be achieved.

Figure 7.20 illustrates some large-signal trajectories constructed by the Isotan method for a point on the (ν, X)-plane below resonance and lying within the region of hard oscillation. The conditions for this diagram are

$$\nu = 0.90 ,$$
$$X = 0.50,$$
$$k_p = 0.28,$$
$$B = 0.90,$$

and are the same as those of Figure 7.15, which shows the corresponding small-Z trajectories. In computing these curves, the sign of k_p has been

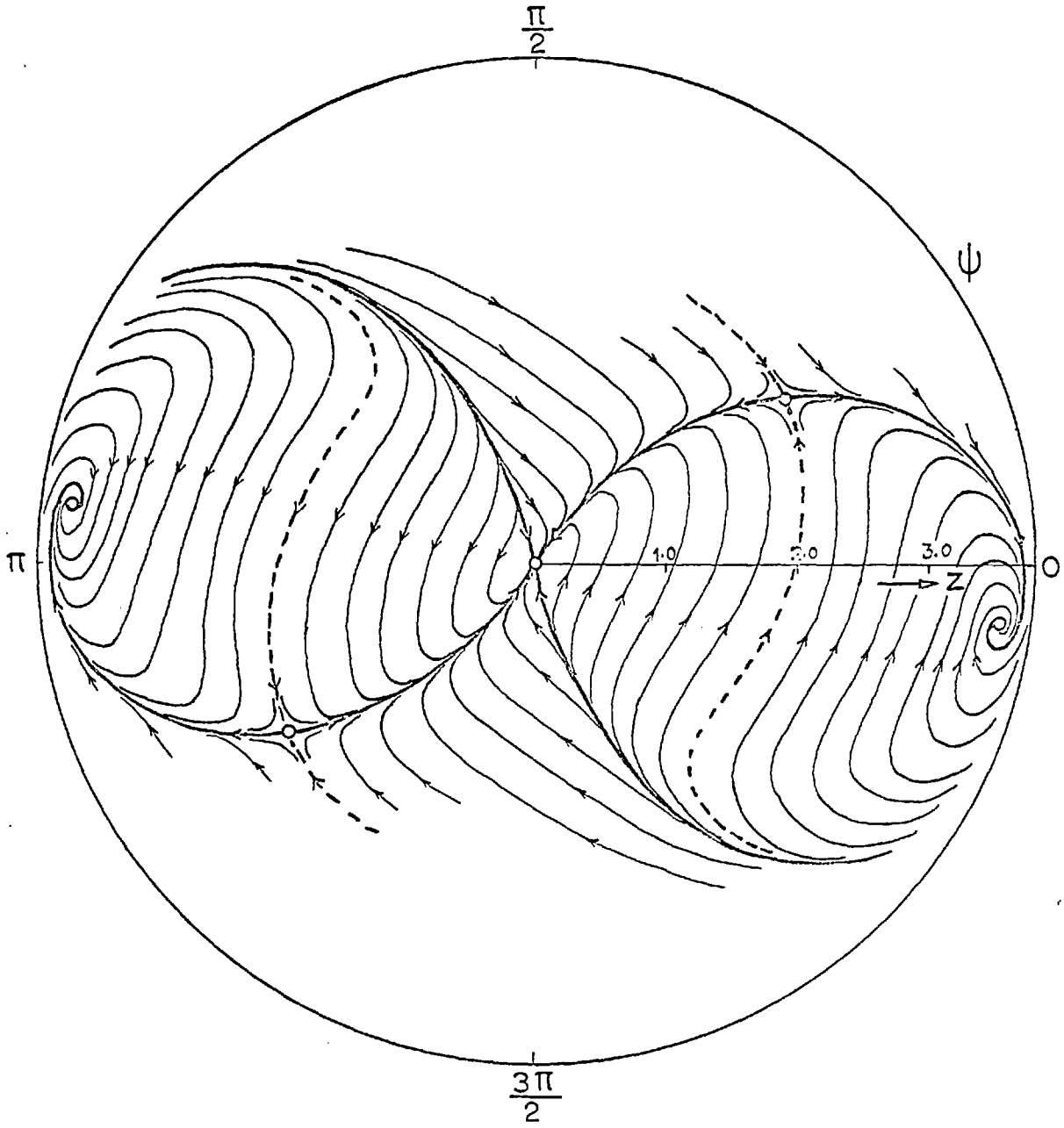


Figure 7.20 - Large-signal (Z,ψ)-trajectories calculated by the Isotan method for the case: $\nu = 0.9$, $X = 0.5$, $k_p = 0.28$, $B = 0.45$.

changed in accordance with the considerations of Sub-Section 7.4.6.1. There are now five singularities. The origin is a stable node; the two outer singularities are stable spirals. The remaining two singularities correspond to the points (u,u) on the trajectory diagram for the lossless case, Figure 7.9. As in that diagram, they are again unstable saddle-points.

The entire (Z,ψ)-plane is divided into three regions by the two broken lines. All initial conditions lying within the region containing the origin give rise to trajectories leading ultimately to the origin, but the amplitude does not necessarily decay monotonically That is, it may increase before it finally decreases. In the other two regions the trajectories eventually reach one of the stable outer singularities. The amplitude can now decrease before it increases.

As Z increases, the two arms of the separatrix form a double spiral expanding in a counter-clockwise direction. The broken lines passing through the unstable saddle-points each form a pair of spirals "interleaved" between the first double spiral. For sufficiently large values of Z, the (Z,ψ)-plane always contains a similar system of spirals, no matter what values of ν and X are selected. It is only relatively near the origin that the trajectory-diagrams become significantly different.

Finally, Figure 7.21 shows an example of (Z,ψ)-trajectories for a set of conditions under which no steady-state exists; in this case, above the resonant frequency. As might be expected, all the trajectories tend towards the origin.

7.4.7.1 Summary

The various relationships which can exist between the subharmonic

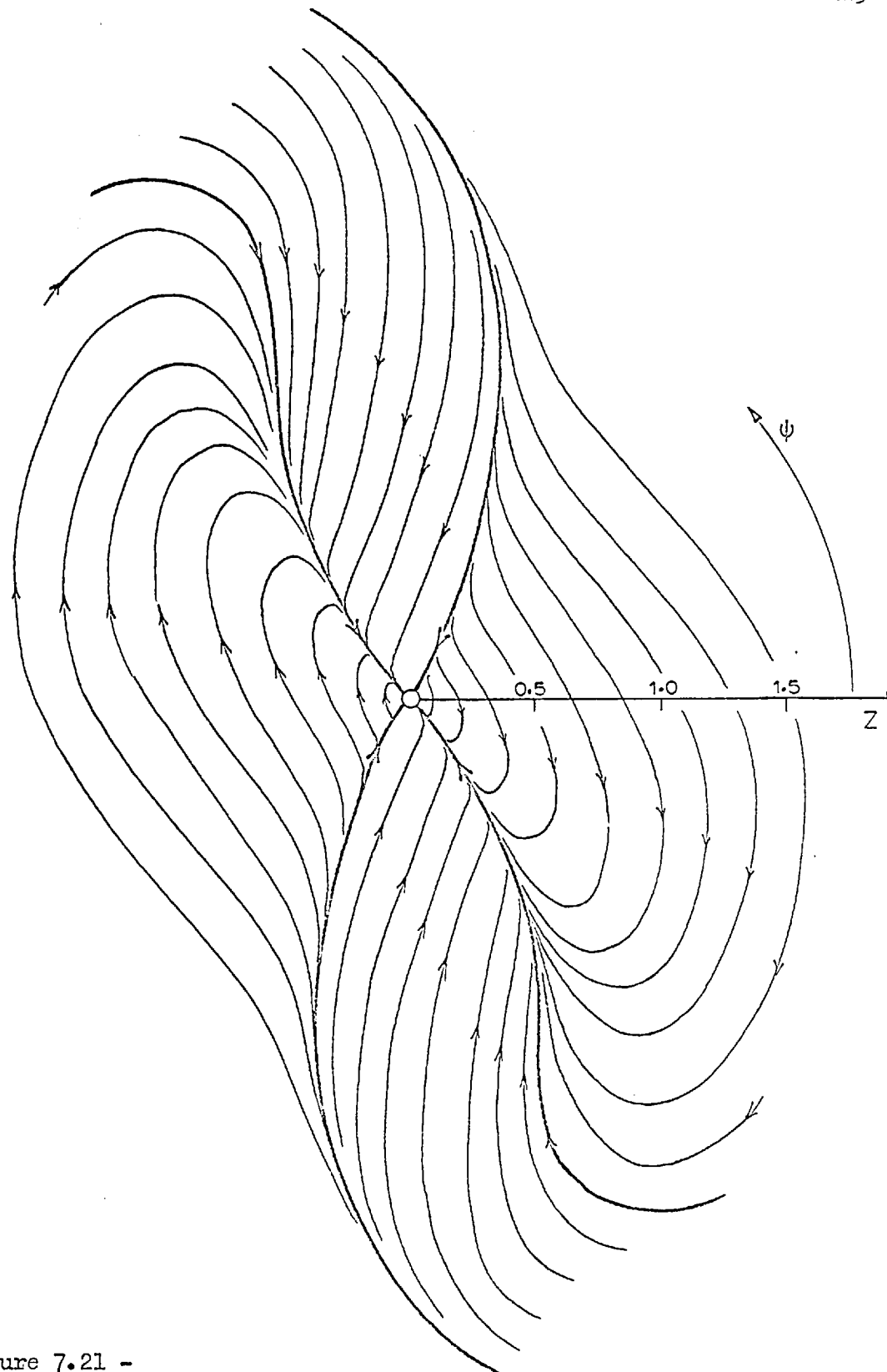


Figure 7.21 -

Large-signal (Z,ψ)-trajectories for detuning above resonance:a case in which no stable oscillation exists.

ν = 1.04, X = 0.5, k_p = 0.28, B = 0.45.

amplitude and phase under large-signal transient conditions have been investigated. The study has given certain insights into parametron behaviour and indicates how fast phase switching can be achieved:

(1) The device should be operated in the region of soft oscillation if large logical gain* is required. Thus it is desirable to choose an operating point at which a large-amplitude singularity can be selected by means of a very small-smplitude initial signal. In the region of hard oscillation, large-amplitude initiation is required if a stable singularity is to be reached.

(2) Operation in the "linear" mode is desirable if the fastest speed of operation is to be attained. This means that the Z,ψ -information content of the parametron is utilised to initiate a second device before the first has achieved its steady state. This kind of operation would also be possible in cases of hard oscillation if use were made of the "loop" trajectories which grow but ultimately converge on the origin.

7.4.8 Approximate treatment of transient behaviour

It was seen in the previous section that the exact trajectories cannot be found without recourse to numerical or graphical techniques for solving the relevant differential equations. The same will be true of the exact amplitude and phase transients. It will therefore be necessary to use the approximate method envisaged at the beginning of Sub-Section 7.4.6. On the basis of results already obtained, we shall now see what this involves.

---

* Logical gain is defined as the number of computer switching elements which can be controlled unambiguously by a single switching element of the same kind.

It has been remarked that in practice a parametron would be used only in the region of soft oscillation, otherwise the possibility of using a very small-amplitude signal to initiate the ultimate phase would be lost. It is therefore appropriate to consider transients occurring in this region. Refer, for example, to Figure 7.14, which shows typical small-signal trajectories. The proposed method allows the tip of the (Z,ψ)-vector to follow such a trajectory into the large-signal region. When the final steady-state amplitude $Z(\infty)$ (given by the large-signal steady-state analysis) is reached, the trajectory is to be constrained to follow a circular arc of radius $Z(\infty)$ until the phase reaches the value $\psi(\infty)$. The tip of the vector then remains stationary at the singularity $(Z(\infty), \psi(\infty))$. It is found in practice that the trajectories tend to lie near the S-curve. The approach should therefore give a reasonable approximation to the true amplitude transient, although it will tend to underestimate the actual risetime. A consequence of the method is that the phase will undergo a "jump", no matter what small-signal initial conditions are chosen. This is an unavoidable consequence of abruptly limiting the amplitude at its steady-state value. The initial part of the phase-transient, for which Z is sufficiently small, should, however, be adequately predicted.

It might be thought that an alternative approach would be to constrain the approximate trajectory in such a way that the phase is stopped at $\psi(\infty)$ and the amplitude is subsequently allowed to proceed to $Z(\infty)$. This possibility must be rejected for two reasons.

(1) A non-physical amplitude-jump would be involved.

(2) There is no guarantee that the phase-angle of a small-signal trajectory would ever reach $\psi(\infty)$. On the other hand, the amplitude must

always reach $Z(\infty)$, except, of course, for initiation at the critical angles ψ_c^-, in which case the amplitude decays monotonically to zero.

Figure 7.22 shows in diagrammatic form the kinds of transient response to be expected for three different $\psi(0)$ at a constant $Z(0)$. The transient response is shown for the trajectory diagram and for the amplitude and phase responses. The exact curves are indicated in heavy lines; the approximations are shown in broken lines. Diagrams 7.22(a_1), (a_2) and (a_3) are for a case in which the initial condition lies on the S-curve, while the diagrams (b) and (c) relate to initial conditions lying on one side and the other of the S-curve. The phase-jump is indicated in each case and is seen to take place from the critical angle ψ_c^+ to the final angle $\psi(\infty)$.

The real-time phase transient response will now be determined on the basis of this approximate approach.

7.4.8.1 The approximate transient phase solution in the presence of damping

The equations for the real-time phase and amplitude transients under the condition $Z \ll 1$ are (7.78) and (7.77) respectively. The equation (7.78) for $\dot{\psi}$ is homogeneous in ψ, whereas (7.77) for $\dot{Z}$ is inhomogeneous. The phase equation will therefore be solved first. In terms of the σ, ρ-notation established in Sub-Section 7.4.6. it is

$$\frac{4X}{3n} \cdot d\tau = \frac{-d(2\psi)}{\rho + \sigma.\cos 2\psi + \sin 2\psi} \qquad (7.90)$$

As in the case of the solution of the corresponding trajectory problem, the form of the integral of the right member of (7.90) depends on $\mathrm{sgn}(1+\sigma^2-\rho^2)$. If $\rho^2 < 1+\sigma^2$, a condition which encompasses the whole of the region of soft oscillation, $\rho^2 < 1$, (see Figure 7.24), then the real-time transient

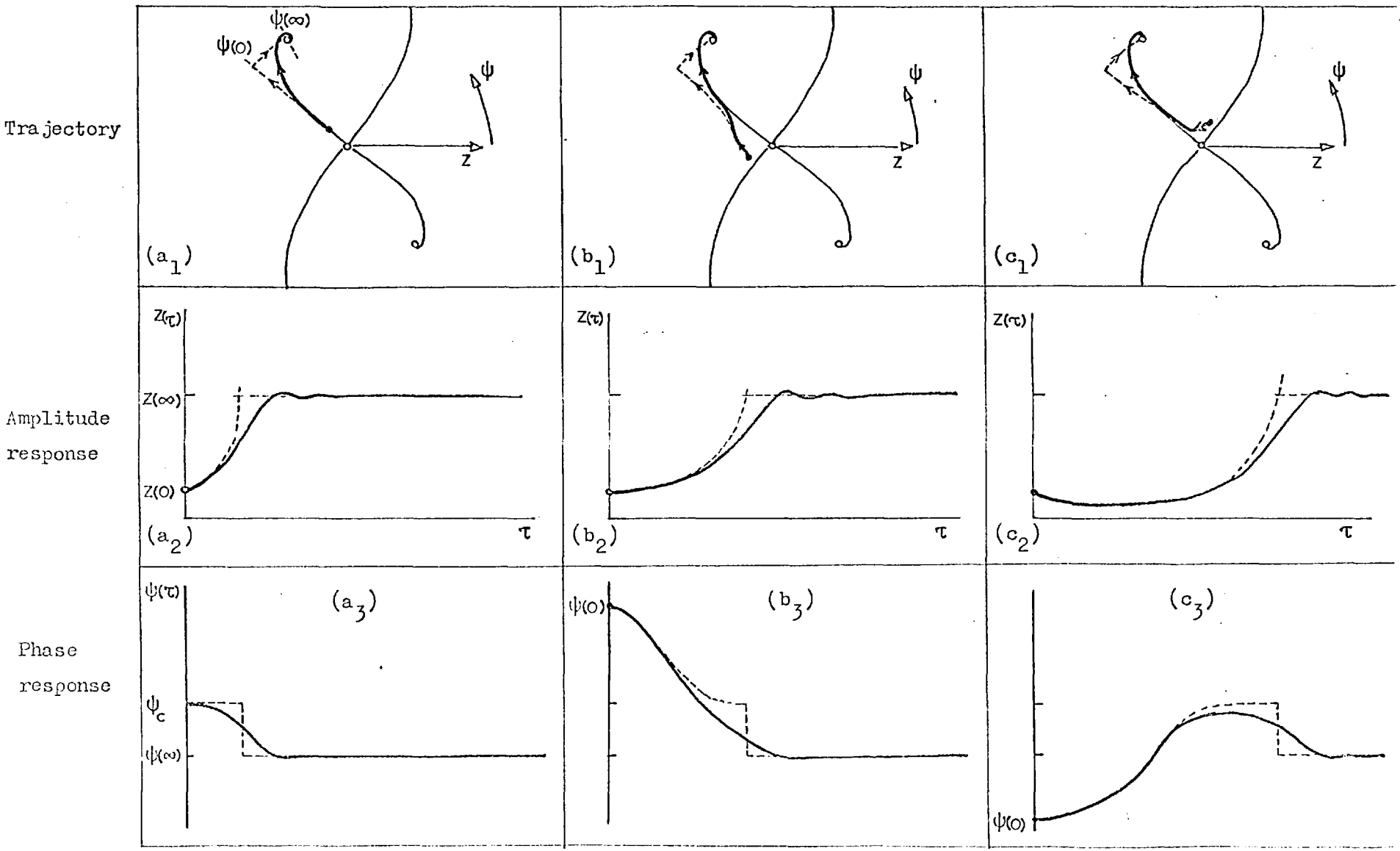


Figure 7.22 - The nature of the approximations to the trajectory and to the amplitude and phase responses for (a) initiation on the S-curve and (b) and (c) initiation off the S-curve.

phase solution is

$$A.e^{2S\tau} = \frac{\rho + \sqrt{1+\sigma^2}.\ \cos(2\psi - \xi)}{\sqrt{1+\sigma^2} + \rho.\cos(2\psi - \xi) + \sqrt{1+\sigma^2-\rho^2}.\sin(2\psi - \xi)}, \tag{7.91}$$

where

$$S = \frac{2X}{3n}\sqrt{1+\sigma^2-\rho^2},$$

$$\operatorname{tg}\xi = \frac{1}{\sigma}$$

and A is a constant of integration which can be expressed in terms of the initial phase angle by substituting into the expression $\psi = \psi(0)$ for $\tau = 0$. Only one initial condition appears because the nature of the phase transient is independent of the amplitude so long as $Z \ll 1$. Inclusion of the initial phase angle leads to an unwieldy expression, so that we shall use the solution in the form given above. This is satisfactory because the phase-transient curves are, in the present approximation, always of the same shape for given values of ν, X, k_p and B, so that a variation in the choice of $\psi(0)$ merely has the effect of shifting the entire (ψ,τ)-curve bodily along the τ-axis in such a way as to cut the ψ-axis in the value $\psi(0)$.

If this result (7.91) is compared with equation (7.83) for the trajectory under the same conditions, it will be seen that the right member of the phase expression appears imbedded in the trajectory expression also.

For the resonant condition $\nu = 1$ we have $\rho = 0$, so that (7.91) reduces to the simple result

$$Ae^{2S_\sigma\tau} = \operatorname{tg}\left(\frac{\pi}{4} + \frac{\xi}{2} - \psi\right), \tag{7.92}$$

where

$$S_\sigma = \frac{2X}{3n}\sqrt{1+\sigma^2}.$$

In this case the explicit phase solution can be written

$$\psi(\tau) = \text{arc tg } (Ae^{2S_\sigma \tau)} - \tfrac{1}{2} \text{ arc tg } \left(\frac{1}{\sigma}\right) - \frac{\pi}{4} . \qquad (7.93)$$

An example of the phase-transient curves for the typical practical case

$$\begin{aligned} \nu &= 1.0 \\ k_p &= 0.28 \\ B &= 0.45 \end{aligned}$$

is shown in Figure 7.23. The pump-amplitude parameter X appears only in the quantity S_σ and its sole effect is to alter the time-scale, i.e. an increase of X increases the rate at which ψ changes with time. For this resonant case the curves are symmetrical about the critical phase-angles, but this is no longer true for off-resonance tuning.

The general transient phase solution for $1 + \sigma^2 > \rho^2$ can be written in a variety of ways. Anticipating the requirements of the next section, we shall need an explicit solution for $\psi(\tau)$ from which it will be possible to calculate the transient amplitude under the condition $Z \ll 1$. For this purpose it is convenient to write the phase solution in the form

$$\left[\begin{matrix}\tanh \\ \text{ctnh}\end{matrix}\right] S(\tau - \tau_o) = \frac{(\rho - \sigma).\text{tg}\,\psi + 1}{\sqrt{1 + \sigma^2 - \rho^2}} , \qquad (7.94)$$

where the tanh is to be taken when the R.H.S. is < 1 and the ctnh when the R.H.S. is > 1, and in which the constant of integration now appears as an arbitrary time-origin τ_o. This solution can be expressed in terms of the initial phase-angle by putting $\psi = \psi(0)$ when $\tau = 0$ and eliminating τ_o. The same result is obtained for both the tanh and ctnh functions:

$$\text{tg}\,\psi = \frac{\sqrt{1 + \sigma^2 - \rho^2}.\text{tg}\,\psi(0) - [\sigma + \rho + \text{tg}\,\psi(0)].\tanh S\tau}{\sqrt{1 + \sigma^2 - \rho^2} + [1 + (\rho - \sigma).\text{tg}\,\psi(0)] . \tanh S\tau} . \qquad (7.95)$$

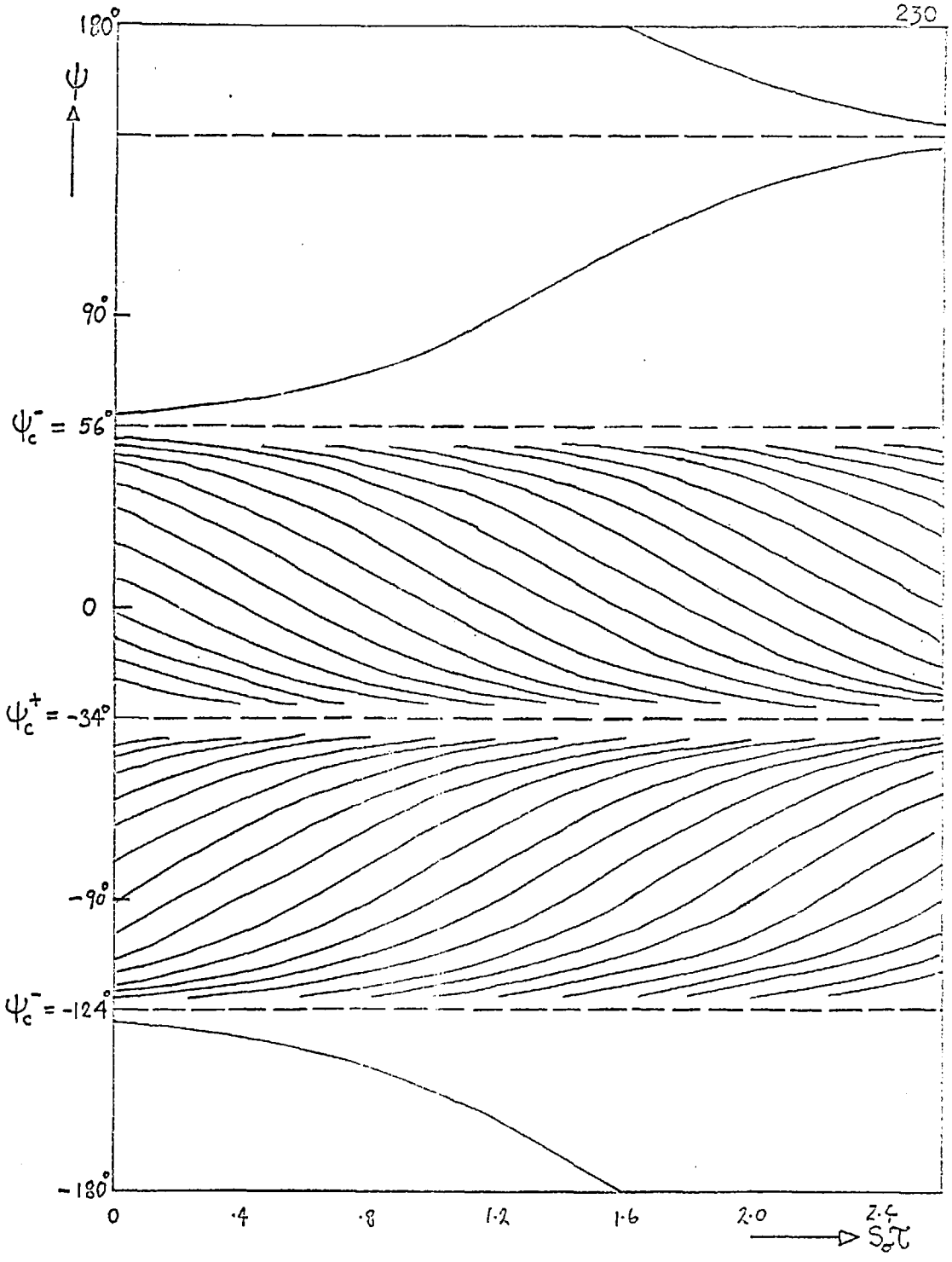


Figure 7.23 - Phase transient response curves calculated according to the small-amplitude approximation $Z \ll 1$. The parameters are

$$\nu = 1.0$$

$$k_p = 0.28$$

$$B = 0.45$$

and the curves are valid for any value of X.

7.4.8.2 The approximate real-time transient amplitude solution in the presence of damping

In order to find the real-time transient amplitude solution in the presence of damping and under the condition $Z \ll 1$, an expression is required for $\cos 2\psi$ in terms of the normalised time :

$$\cos 2\psi(\tau) = \mathcal{F}(\tau) . \qquad (7.96)$$

Such a function can be obtained from the general solution for the phase-transient. If this solution is substituted into equation (7.77) for the rate of change of amplitude with time, the resulting differential equation is separable and can be integrated:

$$\frac{dZ}{Z} = \frac{X}{n} . \mathcal{F}(\tau)\, d\tau . \qquad (7.97)$$

The expression for $\mathcal{F}(\tau)$, valid for any initial phase-angle $\psi(0)$ is, in its general form, a complicated function of τ. However, it becomes simple for the particular cases of the critical angles ψ_c^+ and ψ_c^- referred to in Sub-Sections 7.4.6.2 and 7.4.8. These critical angles are identical to the angles of the straight-line trajectories of the small-signal (Z, ψ)-diagrams. Phase-initiation at $\psi_c^{\pm}(0)$ leads to stationary phase during the initial part of the transient and the function $\mathcal{F}(\tau)$ degenerates into a constant. We shall therefore begin by considering the amplitude transients corresponding to these important special cases before going on to the general case of arbitrary $\psi(0)$.

7.4.8.3 Transient amplitude solutions for initiation at critical phase-angles

If the parametron is initiated at one of the critical phase angles $\psi_c^{\pm}(0)$, then the ensuing amplitude variation is given by

$$\frac{\dot{Z}}{Z} = \frac{X}{n} \cdot \cos 2\psi_c = \text{constant.} \qquad (7.98)$$

It follows that the transient amplitude solution is

$$Z(\tau)\Big|_{\psi_c} = Z(0).\exp\left(\frac{X\tau}{n} \cdot \cos 2\psi_c\right). \qquad (7.99)$$

An expression for $\cos 2\psi_c$ is now required. This can be obtained from the differential equation (7.78) for the phase transient. Let $\dot{\psi} = 0$, so that

$$\rho + \sigma \cdot \cos 2\psi_c + \sin 2\psi_c = 0 \qquad (7.100)$$

The solution of this for ψ_c is

$$\cos 2\psi_c = \frac{-\sigma\rho \pm \sqrt{1 + \sigma^2 - \rho^2}}{1 + \sigma^2}, \qquad (7.101)$$

which may be substituted into equation (7.99) to give for the critically-initiated amplitude transients:

$$\boxed{Z(\tau)\Big|_{\psi_c} = Z(0).\exp\left(\frac{X\tau}{n} \cdot \frac{-\sigma\rho \pm \sqrt{1 + \sigma^2 - \rho^2}}{1 + \sigma^2}\right).} \qquad (7.102)$$

This shows that for critical phase initiation the small-signal part of the amplitude transient is a <u>pure exponential</u>, which may grow or decay, according to the sign of the interior of the bracket in equation (7.102). Referring to the (Z, ψ)-trajectory diagrams, critical (straight-line) trajectories leading <u>to</u> the origin correspond to exponentially decaying oscillations. The critical trajectories leading <u>away</u> from the origin correspond to exponentially growing oscillations. Amplitude transients relating to other, non-critical, trajectories cannot be described in terms of simple exponentials. Because of the small-amplitude approximation $Z \ll 1$, a subharmonic transient initiated at these angles maintains a

constant phase-angle as time increases. An exact analysis would reveal that ψ changes with time to some extent even for the critical initiating phase-angles.

We shall now consider what types of amplitude-transient behaviour ensue upon critical-angle phase initiation for various values of pump amplitude X and subharmonic frequency ν. This can be done by determining

$$\text{sgn} \quad (-\sigma\rho \pm \sqrt{1 + \sigma^2 - \rho^2} \quad) \qquad (7.103)$$

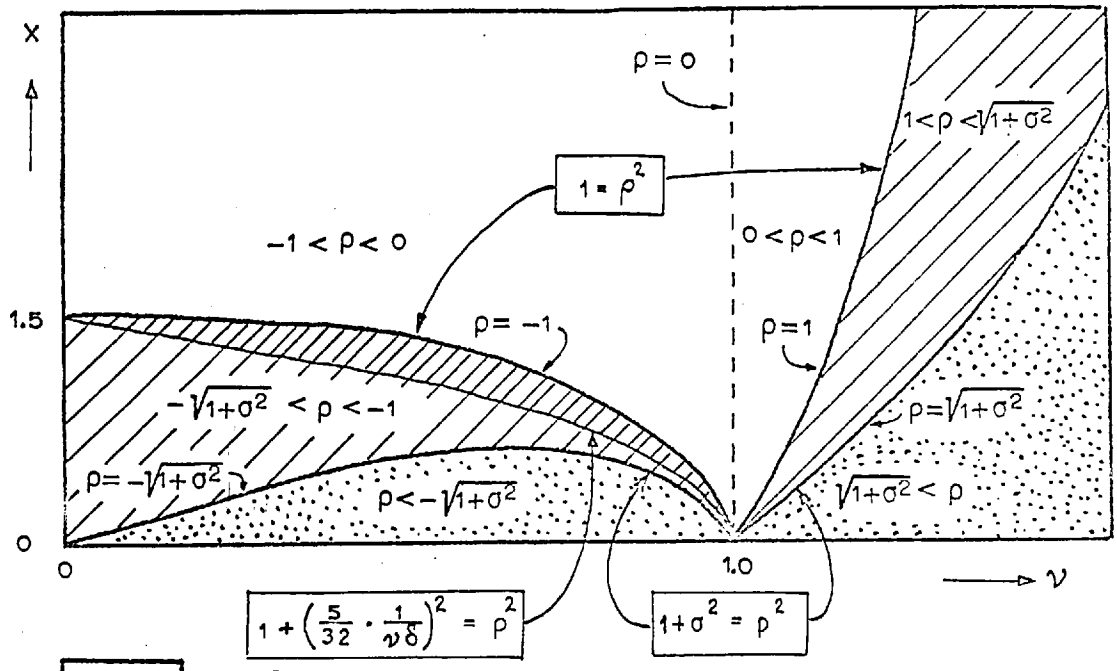
in the various regions of the (ν, X)-plane shown in Figure 7.24, taking into account the considerations of Sub-Section 7.4.6.1, which mean that the sign of σ must be reversed for $\nu < 1.0$. In this diagram the unshaded region $\rho^2 < 1$, in which soft oscillation occurs, is the only one of practical interest. This is because the full advantages of phase-initiation, such as the possibility of controlling the phase of a large-amplitude subharmonic oscillation by means of a determining signal of much smaller amplitude, can only be realised in this region. In the region of hard oscillation, the transient can lead to a stable non-zero oscillation only if the initial amplitude is sufficiently greater than zero. The minimum possible initial amplitude (for a given value of ν) progressively increases as the nose of the (ν, X, Y)-surface is approached.

The change in the sign of σ can be accounted for by writing $\sigma.\text{sgn}\ \rho$ instead of σ. Then the condition for exponentially growing oscillation is

$$\pm \sqrt{1 + \sigma^2 - \rho^2} > \sigma\rho.\text{sgn}\ \rho = \sigma|\rho| \quad , \qquad (7.104)$$

and the two signs attached to the root must be considered separately. Taking the positive root, the condition is

$$+ \sqrt{1 + \sigma^2 - \rho^2} > \sigma|\rho| \quad ,$$



$\rho^2 < 1$. Soft oscillation.

$1 < \rho^2 < 1+\sigma^2$. Temporary oscillation.

$1+\sigma^2 < \rho^2$. No oscillation.

$1 < \rho^2 < 1 + \left(\frac{5}{32} \cdot \frac{1}{\nu\delta}\right)^2$. Hard oscillation.

Figure 7.24 -

Regions of the (ν, X)-plane in which various types of amplitude transients can occur.

or, squaring both sides,

$$1 + \sigma^2 - \rho^2 > (\sigma\rho)^2$$

i.e.

$$1 + \sigma^2 > \rho^2(1+\sigma^2)$$

or

$$1 > \rho^2 .$$

Thus the positive root corresponds to growing oscillations in the region $\rho^2 < 1$. Note that this result is independent of σ, i.e. it is independent of the damping parameter k_p.

Taking the negative root, the condition for growing oscillation is

$$-\sqrt{1 + \sigma^2 - \rho^2} > \sigma|\rho|$$

which can only be fulfilled for $|\rho| < 0$. This condition cannot be satisfied, so that the negative root never gives rise to growing oscillations.

By means of similar calculations, the following table can be built up. Plus signs indicate growing oscillations and minus signs indicate decaying oscillations. The regions defined by $1 + \sigma^2 < \rho^2$ do not appear in the table because then the root is imaginary and exponential solutions do not exist.

Table of sign of $\pm\sqrt{1 + \sigma^2 - \rho^2} - \sigma|\rho|$:

Region of (ν, X)-plane	Positive root	Negative root
$-1 < \rho < 0$	+	-
$0 < \rho < +1$	+	-
$-\sqrt{1+\sigma^2} < \rho < -1$	-	-
$1 < \rho < +\sqrt{1+\sigma^2}$	-	-

This table confirms that oscillations grow from arbitrarily small initial amplitudes only in the region of soft oscillation. Elsewhere they decay towards zero.

It must be pointed out that the rates of rise and fall of the oscillation envelope for these critically-initiated transients are not necessarily maximum. It will be seen* that slightly greater rates are possible for initiation at phase-angles other than critical. However, the present theoretically-predicted rates should be in reasonable agreement with the experimentally-determined maximum rates of increase and decrease.

It has already been mentioned in Sub-Section 7.3.2 that the dimensionless risetime, the number of subharmonic cycles μ required for the amplitude to increase by a factor e, is a quantity of considerable interest. We shall also have occasion to refer to the dimensionless fall-time. This is defined here as the number of cycles of oscillation required for the amplitude to decrease by a factor e. In this latter case μ is negative.

The concept of dimensionless rise- and fall-times has meaning only for initiation at the critical phase-angles.

Curves of constant μ are given by

$$\mu = \frac{\nu}{2\pi} \cdot \frac{n}{X} \left(\frac{1 + \sigma^2}{\pm \sqrt{1 + \sigma^2 - \rho^2} - \sigma \left| \rho \right|} \right) . \qquad (7.105)$$

It is shown in Appendix 7.4 that this can be rearranged to give the following expression for the curves in terms of the independent variable X:

$$X^2 = \frac{1 + \left(\sigma + \frac{3\pi\mu}{n\nu} \left| \Gamma^2 - 1 \right| \right)^2}{\left(\frac{2\pi\mu}{n\nu} \right)} . \qquad (7.106)$$

The sign of the square root in (7.105) does not affect this result, so that it applies for both positive and negative values of μ, corresponding to

---

* In a subsequent section.

growing and decaying oscillations respectively.

In the idealised "skeletal" case in which both damping and stray capacitance are absent, equation (7.106) becomes simply

$$X^2 = \left(\frac{2}{\mu\pi} \right)^2 + \left(\frac{3}{2} \left[\nu^4 - 1 \right] \right)^2 . \qquad (7.107)$$

Curves of constant dimensionless rise- and fall-time for this case are shown in Figure 7.25. The curves for positive and negative μ coincide if there is no damping; the associated invariance with respect to $\mathrm{sgn}(\mu)$ is reflected in (7.107). The curves resemble a mirror-image of the corresponding results of the highly approximate treatment of Sub-Section 7.3.2, shown in Figure 7.6. The resemblance is largely fortuitous, and in any case does not apply for large values of X.

Figure 7.26 shows curves of constant dimensionless rise- and fall-time calculated from equation (7.106) for the typical practical case

$$k_p = 0.28,$$
$$B = 0.45.$$

The solid curves are for positive and the broken curve for negative values of μ. It can be seen that for a given magnitude of μ, the curves corresponding to the positive and negative signs now coincide at resonance only. Elsewhere they follow different paths. As in Figure 7.25 for the lossless case, μ is infinite on the Frequency Characteristic and decreases as the operating point (ν, X) moves into the interior of the region of soft oscillation. However, Figure 7.26 illustrates certain new phenomena which appear when damping is present.

(1) Except at resonance, for every point within the region of soft oscillation $\rho^2 < 1$, there is a positive and a negative value of μ, the

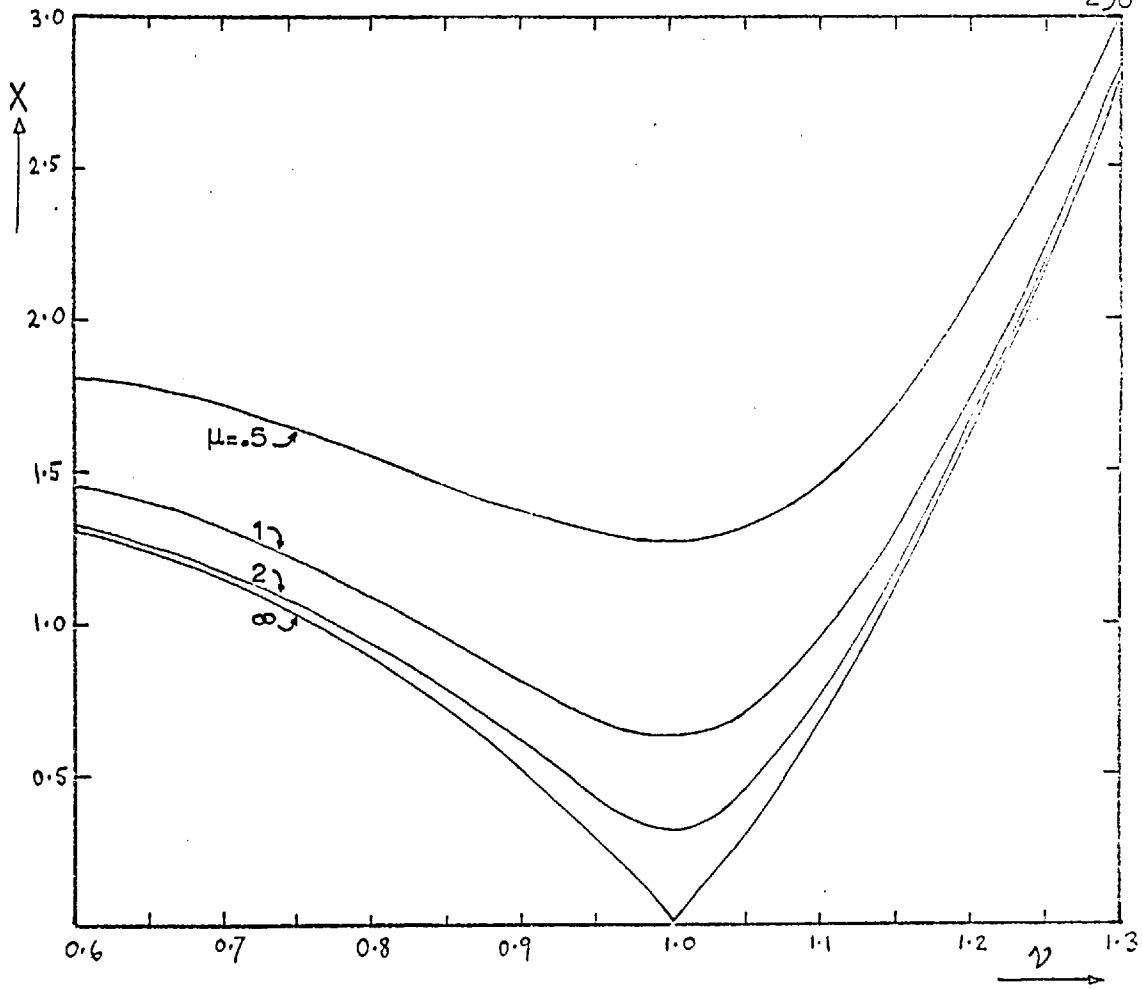


Figure 7.25 -

Curves of constant Dimensionless Risetime μ for zero damping and for no stray capacitance.

$k_p = 0,$

$B = 1.0.$

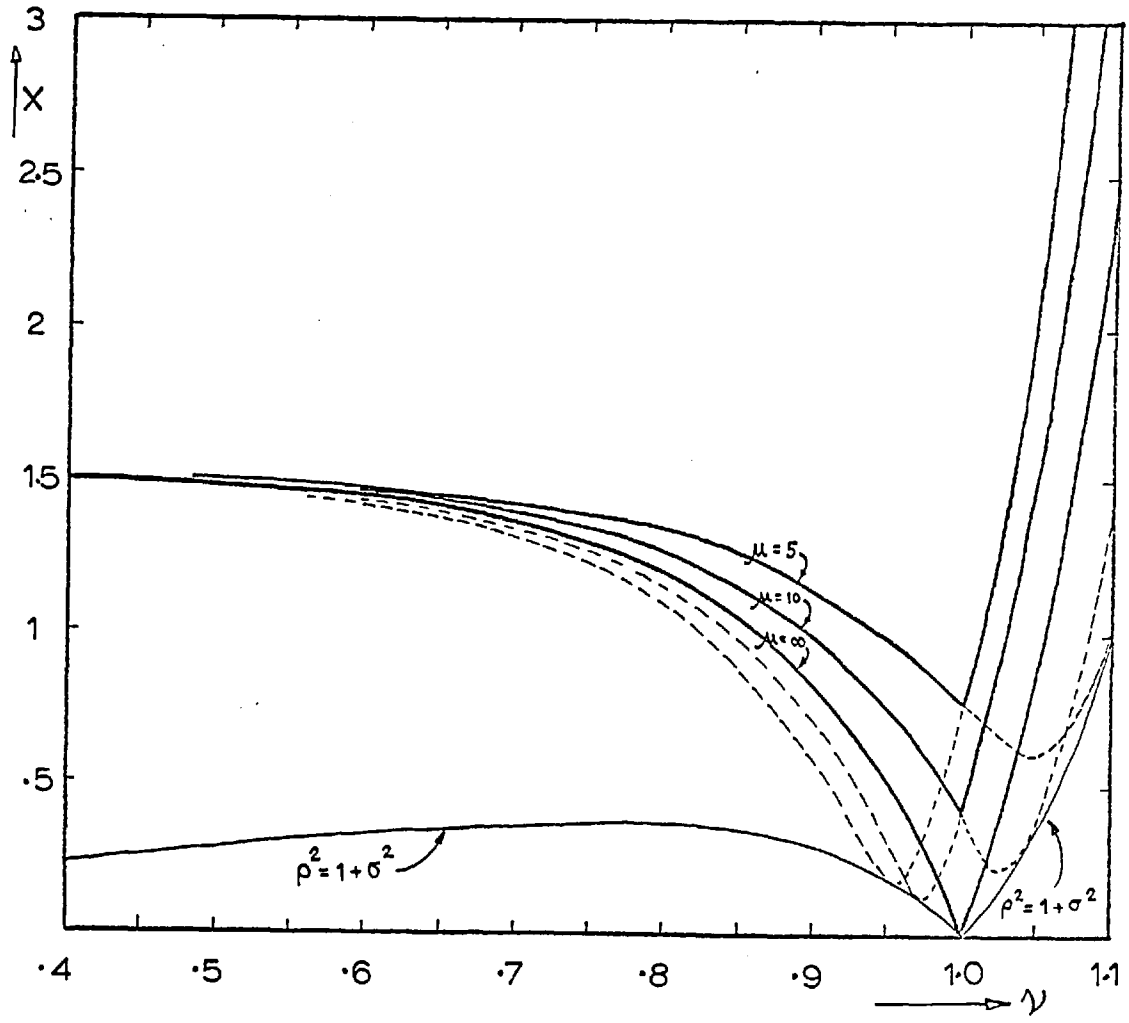


Figure 7.26 - Curves of constant dimensionless risetime and fall-time μ on the (ν,X)-plane for the case $k_p = 0.28$, $B = 0.45$.

magnitudes of which are different. In the lossless case, the magnitudes are the same.

(2) The magnitudes of μ are increased by the presence of stray capacitance and loss, consequently the rates of change of amplitude are decreased.

(3) For every point within the region of temporary oscillation $1 < \rho^2 < 1 + \sigma^2$ (which includes the region of hard oscillation, see Figure 7.24), there are two negative values of μ with different magnitudes. This region of temporary oscillation does not exist in the lossless case since then the only singularities are foci, whereas here the zero-amplitude singularities are nodes.

Experimental results will be given in Section 7.5.

7.4.8.4 Transient amplitude solutions for initiation at arbitrary phase-angles

It has been seen that in order to find the transient amplitude response for initiation at arbitrary non-critical phase-angles it is first necessary to find a general expression for cos 2ψ as a function of time. Such a function $\mathcal{F}(\tau)$ must be substituted into equation (7.97), which can then be integrated to yield the amplitude response. A convenient general relationship between ψ and τ is the form of the transient phase solution given by equation (7.95), Section 7.4.7., which for the present purpose may be written

$$\text{tg } \psi = \frac{C.\tanh S\tau + D}{A.\tanh S\tau + B}$$

where $A = 1 + (\rho - \sigma\rho)\,\mathrm{tg}\,\psi(0)$

$B = \sqrt{1 + \sigma^2 - \rho^2}$

$C = -(\sigma + \rho + \mathrm{tg}\,\psi(0))$

$D = \sqrt{1 + \sigma^2 - \rho^2}\cdot \mathrm{tg}\,\psi(0)$

and $\psi(0)$ is the initiating phase-angle at $\tau = 0$. Then, by making use of the identity

$$\cos 2\psi = \frac{1 - \mathrm{tg}^2\psi}{1 + \mathrm{tg}^2\psi} ,$$

the required time-function is

$$\mathcal{Y}(\tau) = \frac{(A.\tanh S\tau + B)^2 - (C.\tanh S\tau + D)^2}{(A.\tanh S\tau + B)^2 + (C.\tanh S\tau + D)^2} \qquad (7.108)$$

It is shown in Appendix 7.5 that when this is substituted into equation (7.97) and the integrations are performed, the complete amplitude solution for initiation at arbitrary phase angles $\psi(0)$ is

$$\boxed{\mathcal{A}.z^{\frac{4}{3}(1+\sigma^2)} = \mathcal{Y}_1(\tau, \psi(0)).\exp \mathcal{Y}_2(\tau, \psi(0)) ,} \qquad (7.109)$$

where

$$\mathcal{Y}_1(\tau, \psi(0)) = (A.\sinh S\tau + B.\cosh S\tau)^2 + (C.\sinh S\tau + D.\cosh S\tau)^2 ,$$

$$\mathcal{Y}_2(\tau, \psi(0)) = -2\sigma\left\{\frac{\rho}{B}.S\tau + \mathrm{arc\,tg}\left[\frac{\left(\frac{1-B}{\rho-\sigma} - \sigma\right)\left(\frac{B+A}{B-A}\right)e^{2S\tau} + \rho}{B}\right]\right\},$$

and $\mathcal{A}$ is a constant which can be determined from

$$\mathcal{A}.z(0)^{\frac{4}{3}(1+\sigma^2)} = \mathcal{Y}_1(0, \psi(0)).\exp \mathcal{Y}_2(0, \psi(0)).$$

Equation (7.109) is a rather complicated function for general use, but is given here for the sake of completeness. Fortunately, however, a simplification occurs at resonance, for then $\rho = 0$, and it is shown in Appendix 7.6 that in this case the amplitude solution can be written

$$\mathcal{A} \cdot Z^{\frac{4}{3}(1+\sigma^2)} \Big|_{\nu=1} = \cosh 2S_\sigma(\tau+\tau_o) \cdot \exp\left(\sigma \cdot gd\left[2S_\sigma(\tau+\tau_o)\right]\right) , \tag{7.110}$$

where $S_\sigma = \frac{2X}{3n}\sqrt{1+\sigma^2}$,

$\tau_o = \frac{1}{2S_\sigma} gd^{-1}(\xi - 2\psi(0))$,

$\xi = \text{arc tg } \frac{1}{\sigma}$,

$\mathcal{A} =$ a constant containing $Z(0)$,

and $gd(u) = \phi$ is the gudermannian of u defined by

$u = \ln . \text{tg} \left(\frac{\pi}{4} + \frac{\phi}{2}\right)$.

The above expression for $Z(\tau)\Big|_{\nu=1}$ is simple to use, but for detuned cases ($\nu \neq 1$) it is best to construct the amplitude solutions graphically from the appropriate (Z, ψ)-trajectories and the (ψ, τ)-curves of the phase solution.

The relationship between this solution and the corresponding one for critical-angle phase initiation can be seen by letting $\tau_o \to \pm \infty$, which makes $\cosh 2\, S_\sigma(\tau+\tau_o) \to \exp\left[\pm\ 2\, S_\sigma(\tau+\tau_o)\right]$, so that the amplitude solution tends to

$$\frac{Z}{Z(0)}\Big|_{\nu=1} = \exp\left[\pm\ \frac{3}{2} \cdot \frac{S_\sigma}{1+\sigma^2} \cdot \tau\right] = \exp\left[\pm\ \frac{X}{n} \cdot \frac{1}{\sqrt{1+\sigma^2}} \cdot \tau\right],$$

which is the same as the result obtained from equation (7.102), Section 7.4.8.1.

As an example, curves of Z versus τ have been computed from equation (7.109) for the typical practical case

$$\nu = 1.0$$

$$X = 1.15$$

$$k_p = 0.28$$

$$B = 0.45$$

From these quantities the parameters required for the solution are found to be

$$S_\sigma = 0.231,$$

$$\xi = 21.9^\circ,$$

$$\frac{3}{4(1+\sigma^2)} = 0.104.$$

Figure 7.27 shows amplitude response curves for certain initial phase-angles lying in the range

$$-34^\circ < \psi(0) < 56^\circ.$$

This quadrant contains half the possible amplitude solutions and is bounded by the critical angles ψ_c^+ and ψ_c^-. The same amplitude solutions are obtained for initial angles differing by 180° from those given in the diagram. The response curve for $\psi_c^-(0) = 56^\circ$ is a pure decaying exponential. A phase-shift of only -0.5° has a dramatic effect upon the response: the curve for $\psi(0) = 55.5^\circ$ decays at first, goes through a minimum and then grows indefinitely.

Further changes of $\psi(0)$ towards -34° have a less pronounced effect upon the response. However, a very interesting and unexpected result is that for a certain range of $\psi(0)$ near 42°, the response is (at least

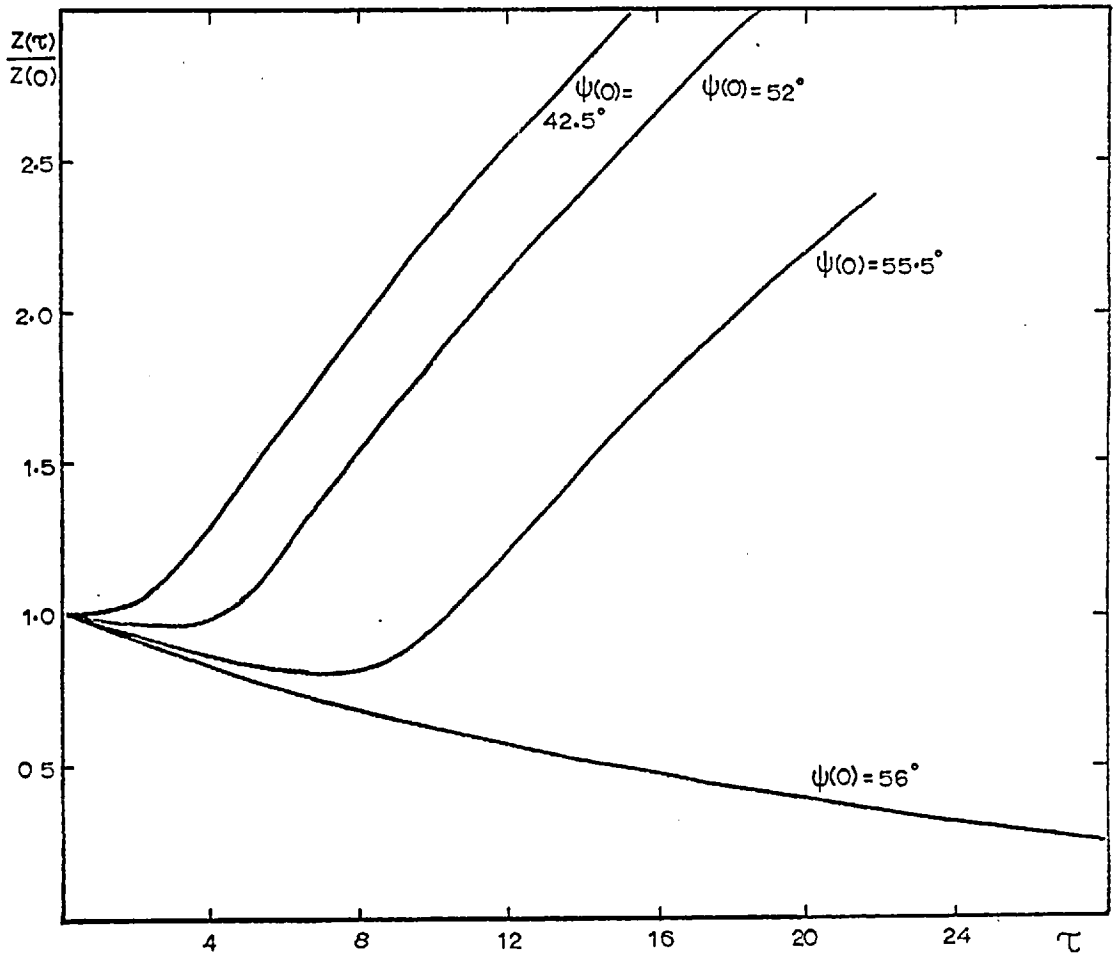


Figure 7.27 - Theoretical amplitude response curves for the typical practical case:

$\nu = 1.0,$

$X = 1.15,$

$k_p = 0.28,$

$B = 0.45,$

when the initial phase-angle $\psi(0)$ is varied.

initially) faster than the exponentially increasing envelope obtained for initiation at $\psi_c^+(0) = -34^\circ$. This point is brought out by presenting the amplitude transients on a logarithmic scale, as in Figure 7.28. The exponential solutions now appear as straight lines. All the other solutions, with the exception of the one for $\psi_c^-(0) = 56^\circ$, eventually acquire the slope of the rising exponential. The time taken for the solution to become nearly exponential depends on $\psi(0)$.

Since the present theory is for small signal levels, the initial amplitude $Z(0)$ is generally much less than unity. Therefore, by the time the large-signal amplitude $Z(\infty)$ is reached (in accordance with the approximate treatment described in Sub-Section 7.4.8.), the solution can be regarded as a virtually pure increasing exponential delayed by a time which depends on $\psi(0)$.

Figure 7.29 shows in three-dimensional form the calculated amplitude-time response as a function of the initial phase angle in the range

$$-34^\circ < \psi(0) < + 146^\circ.$$

The other 180° need not be shown since the response curves are repeated in that range. The amplitude $Z(\tau)$ is again normalised with respect to $Z(0)$ and plotted logarithmically. The marked sensitivity of the amplitude response to the initial angle in the vicinity of $\psi(0) = 56^\circ$ is evident. In accordance with our approximate approach, the response curves in Figure 7.29 have been limited at a steady-state amplitude $Z(\infty)$, here 6.3 db above $Z(0)$. Inspection of the diagram reveals that $Z(\infty)$ is reached in the least time for $\psi(0)$ about 42°. In this case the initial slope of the response-curve is actually zero, but rapidly becomes steeper than exponential. This suggests that for the set of conditions considered, initiation near this

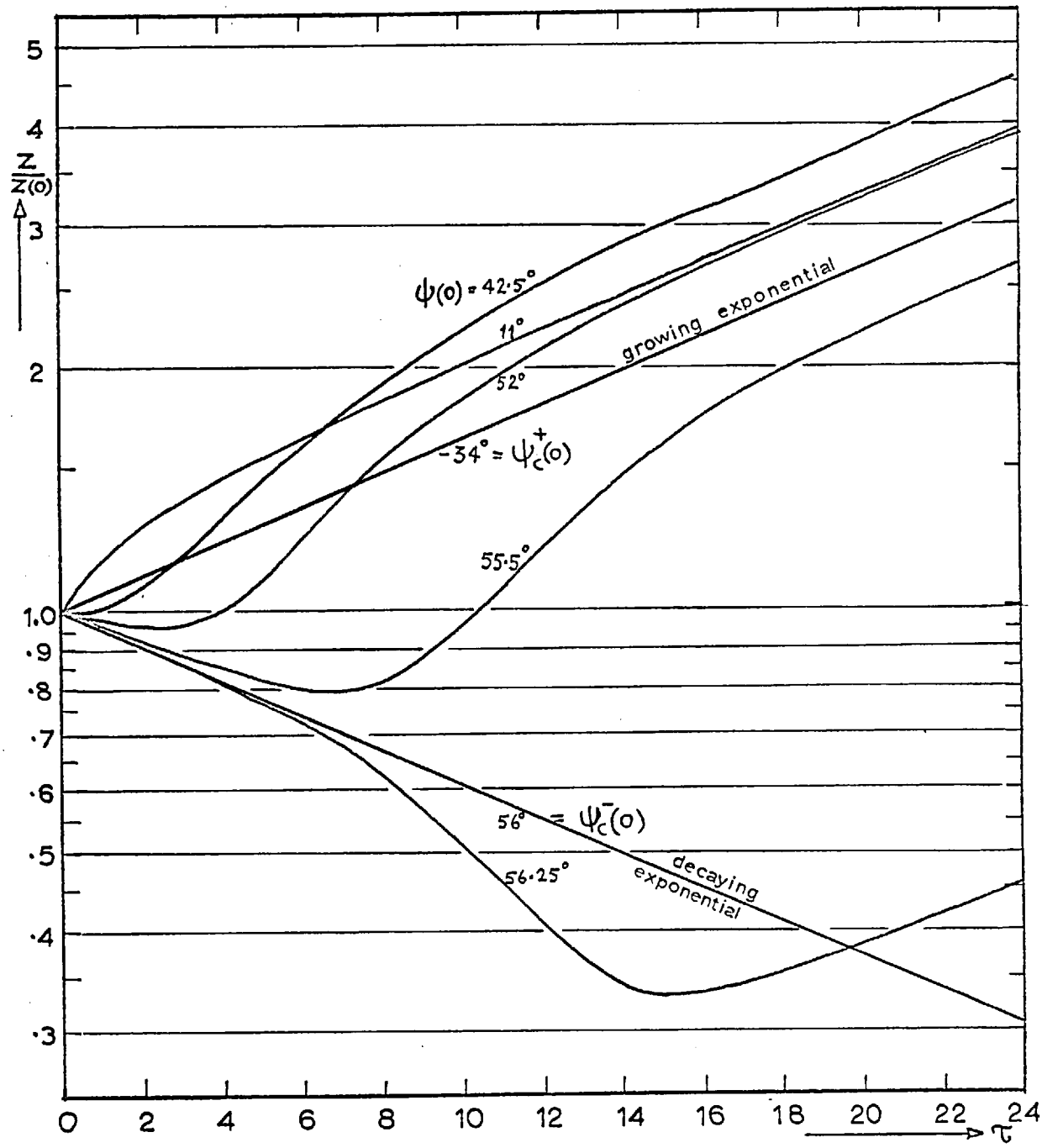


Figure 7.28 - Theoretical logarithmic amplitude response curves for various initial phase-angles. The conditions are as for Figure 7.27.

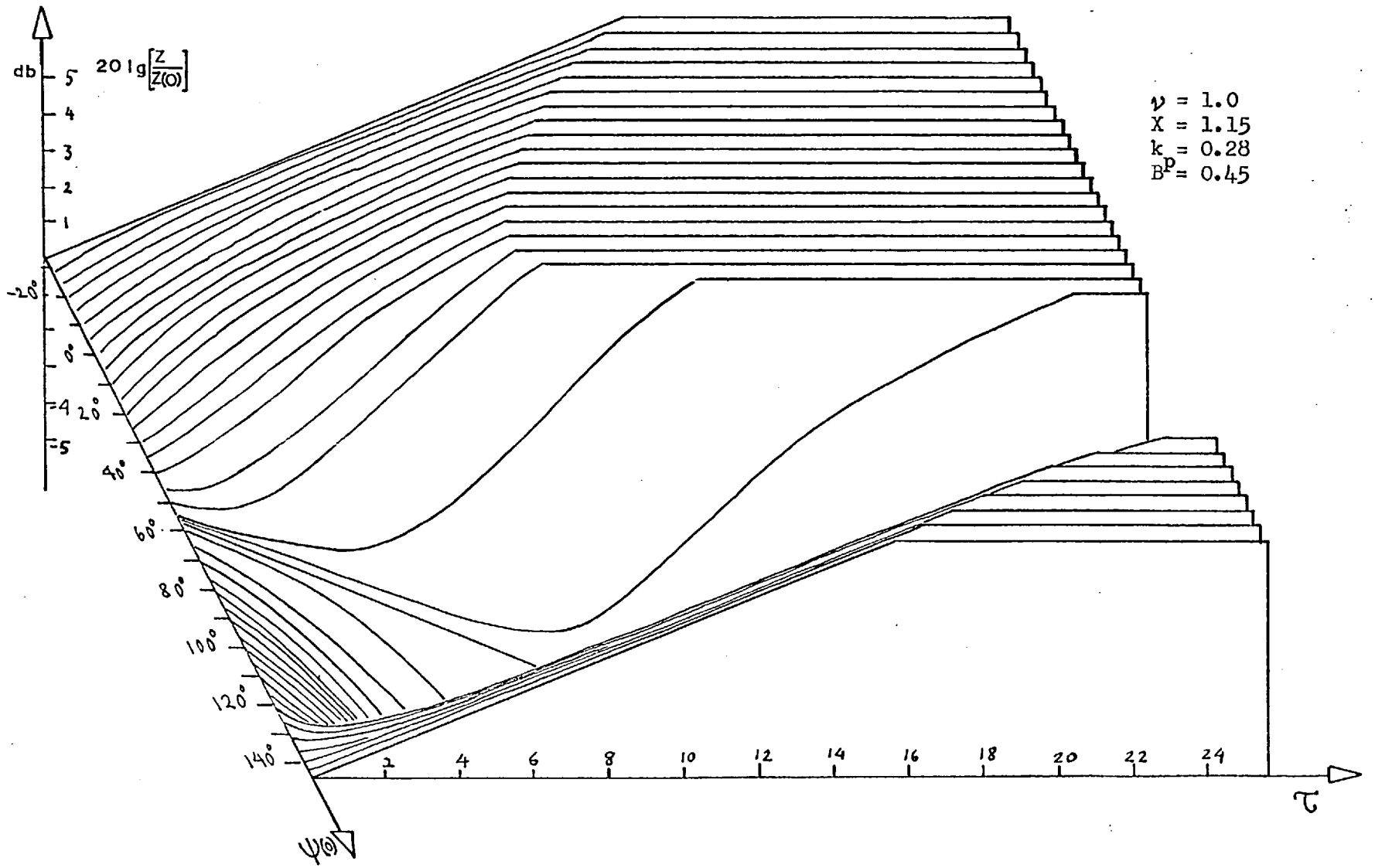


Figure 7.29 - Logarithmic amplitude transient solutions as a function of the initial phase angle.

angle is desirable if the maximum speed of parametron-switching is to be obtained.

Except for critical-angle initiation, the instantaneous phase angle changes continuously as the instantaneous amplitude varies. This happens in such a way that the minima of the response curves always occur at $\pm 45^{\circ}$ or $\pm 135^{\circ}$.

The diagram shows that some of the response curves dip below the straight line corresponding to the decaying exponential solution. It will be seen in the next section, which deals with experimental observations on transient phenomena, that this also occurs in practice.

7.5 Experimental investigation of transient phenomena

7.5.1 Introduction

The object of this section is to determine to what extent the preceding transient theory agrees with measurements on practical devices. The amplitude transients are relatively easy to measure, but observations on the phase transients require a special technique.

The first part of the section contains a description of the experimental arrangements used to obtain a stable and controllable oscilloscope display of the transient phenomena. Subsequently, possible methods of quenching the BSP and BPP are discussed. The techniques employed for measuring the amplitude and phase transients are then described. Finally, the results of some measurements are given in a form suitable for comparison with the theoretical predictions.

7.5.2 Experimental arrangements for measurements on phase-initiated transients

The arrangement of the equipment used in the experimental investigation of the transient phenomena is indicated in the block diagram of Figure 7.30. A pumping source of frequency 2f energies the parametron under test via a 50Ω attenuator which is used to set the pump amplitude V_p. The pump also energises a parametron which oscillates continuously at the frequency f. The latter parametron is used for three purposes:

(1) as a source of phase-initiation signals at the subharmonic frequency,

(2) in order to synchronise the oscilloscope and

(3) to provide an input signal to the electronic counter.

This device is needed because the phenomena to be investigated are extremely sensitive to small variations in the frequency, which must therefore be measured with accuracy. Since pump frequencies up to 20 Mc/s are used and the limit of the frequency meter is about 10 Mc/s, the subharmonic rather than the pump frequency is monitored. The continuously-oscillating parametron will be referred to as the Phaselock Parametron. It should be of a type similar to the one under investigation, but with a somewhat higher resonant frequency. This ensures that the parametron under test receives adequate phaselock amplitude up to its maximum frequency of operation.

A sampling oscilloscope was selected for several reasons.

(1) Its wide bandwidth and good amplitude calibration mean that instantaneous voltage amplitudes can be measured over a large range of frequencies without frequency-response corrections being required.

(2) It has good sensitivity and sufficiently high input impedance to avoid excessive circuit loading.

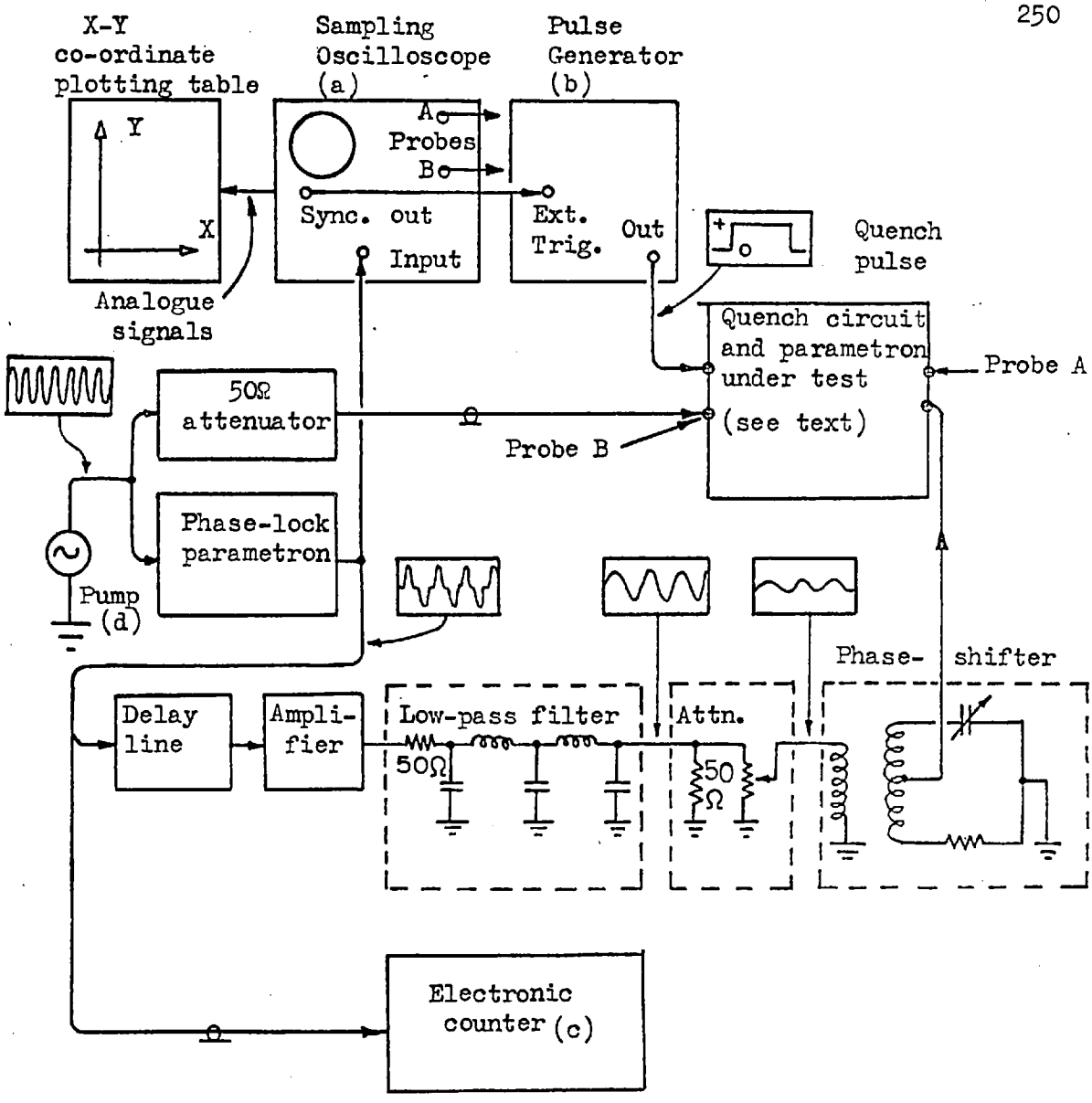


Figure 7.30 - Experimental Arrangement for Observation and Measurement of Phase-Initiated Transients.

(a) Hewlett-Packard Sampling Oscilloscope, Model 185B with dual-trace Vertical Amplifier Model 187B.

(b) Nagard Double Pulse Generator Type 5002 C.

(c) Hewlett-Packard Electronic Counter Model 524C with Video Amplifier Model 526A.

(d) General Radio Unit Oscillator, 0.5 - 50 Mc/s, Type 1211-C.

(3) There is provision for the connection of an X-Y coordinate pen recorder. This is possible because the sampling oscilloscope works in an "analogue" manner, the high-frequency input signals being translated to a very much lower frequency for display purposes. The traces of transient waveforms which can be obtained in this way are more accurate than those obtainable photographically since the pen has a better resolution than a C.R.T. trace.

The count-down circuits of the sampling oscilloscope produce synchronising pulses at a repetition rate of about 100 Kc/s, locked to a submultiple of the pump frequency f. These are used to trigger the Pulse Generator which in turn produces pulses of controlled delay, width and amplitude which are used (by means to be described below) to quench the subharmonic oscillations of the parametron under test.

For reference purposes, the instant at which the quenching-pulse is removed from the parametron is defined to be $t = 0$.

If it is assumed that the parametrons in a given practical computing system are all similar, then the phase-locking signal applied to one parametron is simply the nonsinusoidal output of another parametron of similar characteristics.

The theory developed in the preceding work, however, assumes that the phase-locking signal is a pure sinusoid of prescribed amplitude $V_s(0)$ and phase $\theta(0)$, so that it is desirable to use a signal of this kind in the present experimental investigations. In the system described here, the phase-locking signal is derived from the continuously-oscillating Phaselock Parametron, the output of which consists of the subharmonic frequency f and

odd-order harmonics 3f, 5f, 7f, etc., their relative amplitudes depending on the pump amplitude and frequency. In accordance with the above requirement, the unwanted harmonics are removed by a low-pass filter which is designed to cut off at about 2f. A disadvantage of this arrangement is that the derived phaselock-signal has an amplitude which is strongly dependent upon the amplitude and frequency of the pumping signal.

A possible solution to this problem would be to use a van der Pol-type oscillator entrained to the $\frac{1}{2}$th-subharmonic of the pump frequency; the output of this device should be sensibly constant in amplitude. A tunnel-diode balanced synchronised oscillation was tried for this purpose since it has satisfactory limiting, filtering and frequency-following properties. However, it was rejected because of its small output level, its noisiness and its tendency to oscillate at very high frequencies even in the presence of good decoupling arrangements.

The filter is followed by an attenuator of negligible phase-shift, the function of which is to set the initial subharmonic amplitude $V_s(0)$. This,in turn, is followed by an R-C phase-shifting network of fairly constant attenuation, the purpose of which is to set the initial phase-angle $\theta(0)$. Additional phase-shift can be introduced for special experimental purposes by inserting a 50 Ω delay line of suitable electrical length at the input to the filter, and large-amplitude phase-initiating signals can be obtained by inserting an amplifier as well.

Figure 7.31 is a photograph of the equipment used for the experimental investigation of the transient phenomena. The electronic counter and the X,Y-recorder have been omitted for clarity. The sampling oscilloscope displays a typical amplitude transient.

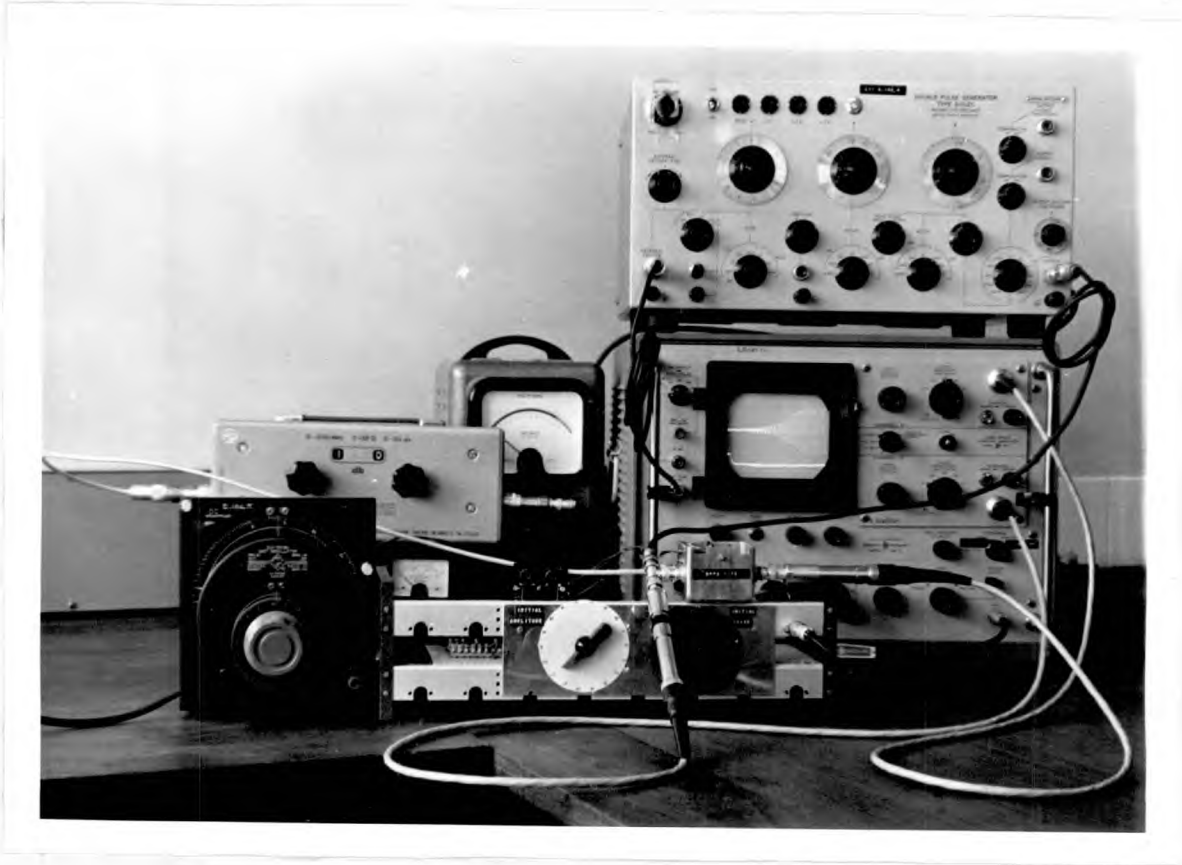


Figure 7.31 - Equipment used in the experimental investigation of transient phenomena .

The contents of the schematic block in Figure 7.30 designated "Quench circuit and parametron under test" can take several different forms depending both on the kind of parametron and the type of quenching to be employed. There are two ways in which the subharmonic oscillations can be quenched, by Pump Modulation and by Pulse-Biasssing the varactors.

First consider Pump Modulation. This involves the periodic "disconnection" of the pump source from the parametron, which may be of any type, balanced or unbalanced. In general, the amplitude of the subharmonic oscillation will decay slowly upon the application of the "disconnecting" quench-pulse. The rate of decay is governed by the effective Q of the parametron, and since this is fairly high, the turn-off is necessarily a slow process occupying many cycles of oscillation at the natural frequency of the device. This limits the rate at which phase-initiated switching can be accomplished.

As an example, the practical circuit of a BSP with pump modulator is shown in Figure 7.32. A simple balanced modulator employing fast diodes disconnects the pump from the BSP upon application of a positive-going quench pulse. Since the parametron and modulator are balanced, while the pump source is unbalanced, the effect of the interwinding capacitance in transformer T_1 must be neutralised by means of the adjustable trimmer C_T. Otherwise the output of the BSP will be contaminated with the pump frequency and its harmonics (4f, 8f etc).

Phase-switching in the BPP can also be accomplished by Pump Modulation. In this case the balance of the device is not affected by stray capacitances.

---

e.g. Qutronics Q5-100.

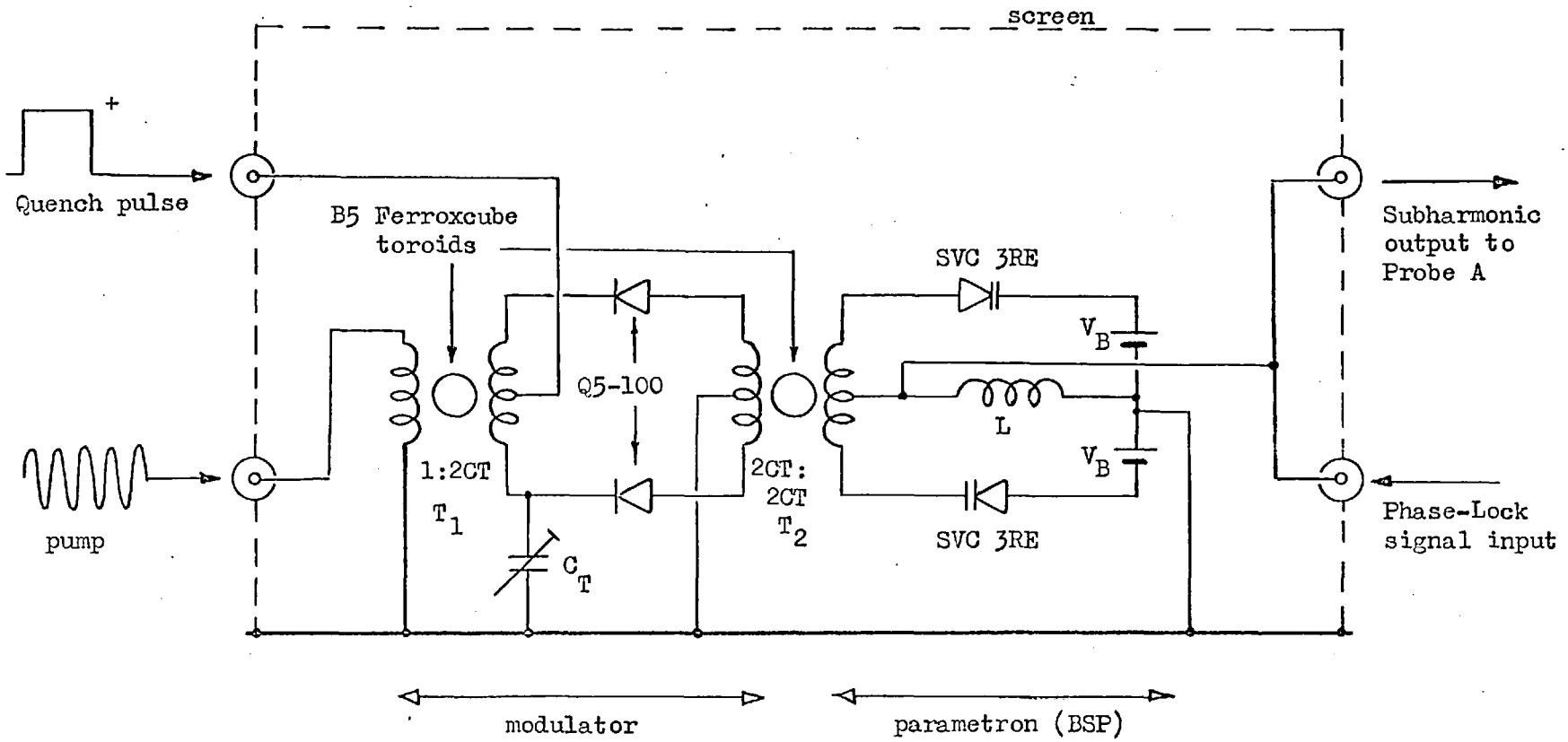


Figure 7.32 - Experimental BSP with quenching by pump modulation.

The interrupted pumping signal is applied directly to the centre-tap of the tuning inductor, which is a neutral point from the point of view of the sub-harmonic voltage. A diagram of a typical arrangement is shown in Figure 7.33(a).

The method of quenching by Pulse Biassing the varactors will now be considered. This attractive alternative possibility can be applied to the BPP very simply, but not to the BSP without undue complication (because of the orientation of its varactors). In the BPP both the varactors are oriented in the same polarity so that they can be simultaneously biassed into forward conduction, thus lowering the Q of the device to the point where oscillation ceases in a fraction of a cycle. This can be an extremely fast process because the BPP looks non-inductive from the point of view of a quench-pulse applied to the centre-tap of the tuning inductance. Since this input is a high-impedance point during the oscillatory régime the pump and quench signals can be added together by means of the resistors R_p and R_q, resulting in the simple arrangement of Figure 7.33(b).

The forward diode current used to quench the oscillations must be kept as small as possible, otherwise excessive storage of minority carriers in the junctions will lead to appreciable turn-on delay when the forward bias is removed (i.e. the full Q of the parametron will not be restored immediately).

Therefore, if this type of quenching is used, the initial part of the transient may not be explained by the present theory. If, however, the time-origin is transferred to a later instant at which the minority carriers have leaked away, the transient will be predicted adequately.

It is found in practice that complete quenching can be accomplished in

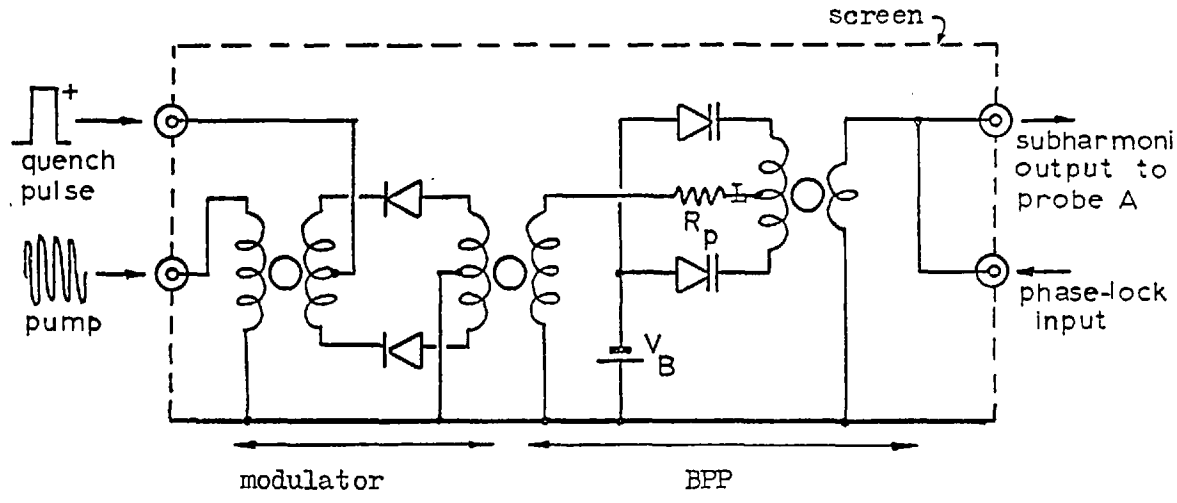


Figure 7.33(a) Experimental BPP with quenching by pump modulation.

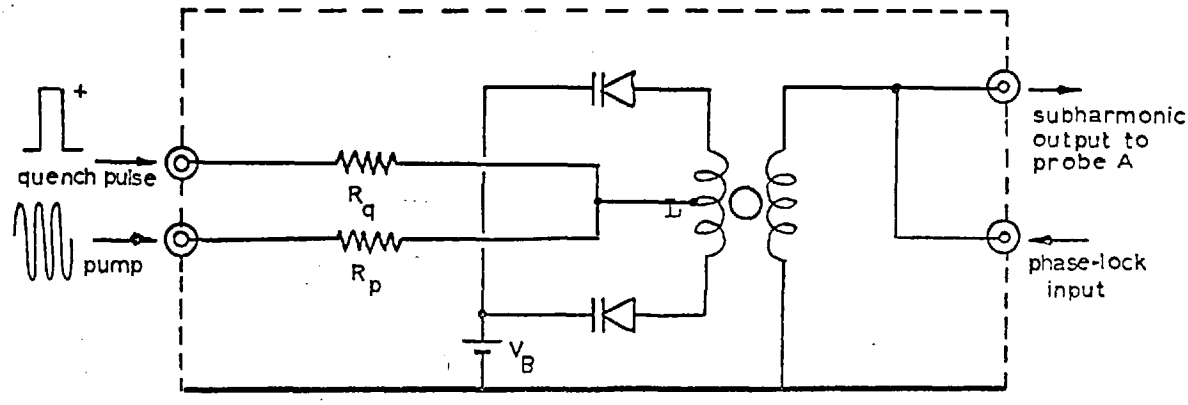


Figure 7.33(b) Experimental BPP with quenching by varactor biassing.

less than one subharmonic cycle by the method of Pulse Biassing. An example is shown in the photograph of Figure 7.34.

7.5.3 Method of measuring instantaneous amplitude and phase

The instantaneous amplitude of the subharmonic oscillation is measured by observing the heights of successive peaks as displayed on an oscilloscope. $V_s(t)$ is found by multiplying the readings by the turns-ratio of the output transformer (if any).

Measurement of the steady-state phase angle is not easy at the frequencies of interest. The cycle-by-cycle measurement of time-varying phase angles presents even more severe difficulties. The instantaneous phase, unlike the instantaneous amplitude, is an elusive and ill-defined quantity. Various ad hoc definitions are possible. Thus one could superimpose the pump and subharmonic waveforms and measure the time-displacement of the peaks. This displacement expressed as a fraction of one subharmonic cycle would give the phase angle in radians. An alternative method, and one which has been adopted here, is to measure the displacement of the zero-crossings of the two waveforms. In general, the two methods give different results for the same transient. This is particularly true when the phase is changing quickly or when the subharmonic waveform contains a large proportion of harmonics, the phases of which change at different rates. The second method was selected because a zero-crossing is a more precisely-defined instant than a peak, leading to improved reproducibility of measurements.

It is worth mentioning that measurement of the transient phase angle would not have been possible without the use of a sampling oscilloscope. Only a very small amount of time-jitter could be tolerated. In the early

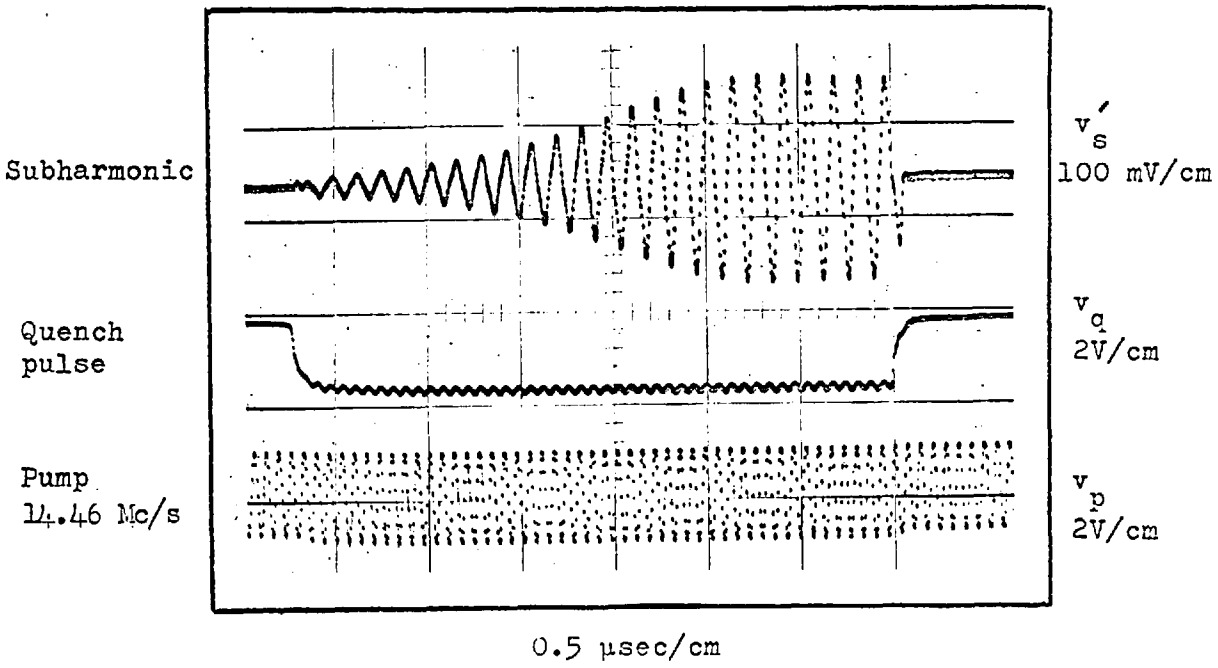


Figure 7.34 -

Example of Fast Quenching by Varactor Biassing.

Parameters:

$\nu = 1.0$
$X = 1.4$
$k_p = 0.28$
$B = 0.45$

$$\begin{bmatrix} f_o = 7.23 \text{ Mc/s} \\ \varphi = 0.7 \text{ V} \\ V_p = 1.0 \text{ V} \\ V_q = 1.6 \text{ V} \\ R_p = 330 \ \Omega \\ R_q = 330 \ \Omega \end{bmatrix}$$

Note that v_s' is measured at the secondary of the BPP transformer. It is approximately $\frac{1}{15} v_s$.

stages of the work many attempts at transient phase measurement were made using conventional oscilloscopes with auxiliary count-down circuits. In no case could a sufficiently stable display be obtained.

For a given set of operating conditions, the amplitude and phase measurements were repeated for successive cycles until ultimately both became constant and steady-state conditions were reached.

The short-term stability of the experimental system was such that instantaneous phase-angles could be measured to a self-consistent accuracy of about $\pm 2^{\circ}$. The long-term stability was not sufficient for reliable phase measurements to be taken from the X-Y "analogue" pen recordings. These took about 30 seconds per trace.

In the resonant case, the measurement technique described above is accurate even when the harmonic content of the signal is quite large due to forward diode conduction at large pump amplitudes. This is because the zero-crossings of all the harmonics are coincident at resonance. It is possible to explain why this should be so as follows. At resonance the impedance seen by the "fundamental" subharmonic frequency is purely resistive. The harmonics of the fundamental are due to the nonlinearity of this resistive impedance. However, there is no fundamental voltage at the zero-crossings, so that there can be no harmonic voltage at the corresponding instants either.

In detuned cases, on the other hand, the impedance becomes reactive. The relative phases of the harmonics are now such that the zero-crossings of the total waveform are displaced relative to those of the fundamental. Such displacement tends to lead to a systematic error in the phase measurements; the magnitude of the error will in general increase with detuning.

Thus the phase definition used is not ideal but it is convenient for experimental purposes.

7.5.4 Transient measurements

The major part of the transient theory has been based on the consideration of the Balanced Parallel Parametron (BPP), although the reasoning in the case of the Balanced Series Parametron follows very similar lines. Most of the transient experiments have therefore been conducted on a typical BPP, the relevant parameters of which are summarised below.

Small-signal resonant frequency: f_o = 7.226 Mc/s.

Pump-circuit damping parameter: k_p = 0.28.

Stray capacitance parameter: B = 0.45.

Nonlinear capacitance-law exponent: n = 0.4.

The damping parameter k_L depends on the value of the load R_L. This load was intentionally kept as small as possible in the transient experiments so that the theoretical assumption that k_L is negligible might be fulfilled. The parameter k_p was made relatively large by using a high value for R_p(350 Ω).

Figure 7.35 consists of a set of pen-recordings of amplitude transients for the resonant case ν = 1. The (X,Y) "analogue" signals were obtained from the sampling oscilloscope. The subharmonic signal actually recorded is v_s', the transformer secondary voltage, which is approximately $\frac{1}{15} v_s$. In order to avoid initial delays due to charge-storage effects, the quenching was accomplished by pump modulation. The modulated pump waveform appears at the foot of the Figure. The transient recordings were made for different values of the initial phase-angle $\theta(0)$; in each case the initial amplitude $V_s'(0)$ was kept constant at 65 mV. It can be seen that as the initial phase angle increases, the time taken to reach the limiting amplitude $V_s'(\infty)$=125 mV becomes progressively longer. When $\theta(0)$ reaches approximately 65°, the transient becomes "infinitely" long. In practice, however, there is always

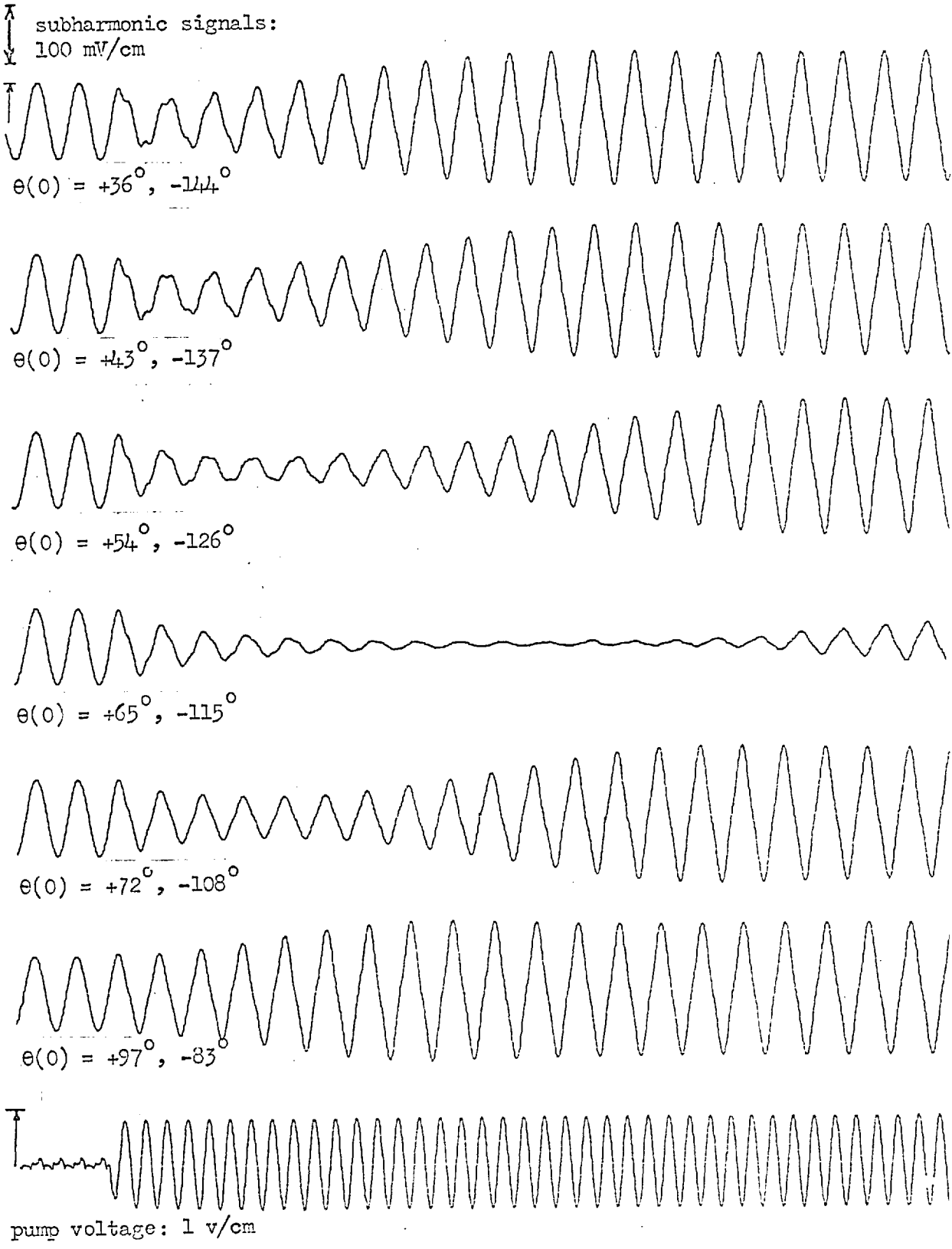


Figure 7.35 - "Analogue" pen-recordings of amplitude transients for the resonant case. Parameters: $\nu = 1.0$, $X = 1.15$, $k_p = 0.28$, $B = 0.45$

sufficient residual noise to trigger eventual oscillation. If $\theta(0)$ is increased beyond this critical value, the time taken to rise to full amplitude becomes progressively shorter again, but the phase of the final steady-state oscillation is now shifted through 180°.

If the amplitude-response recordings of Figure 7.35 are compared with the theoretical curves of Figure 7.27, it will be seen that the dependence of the rate-of-rise upon the initial phase-angle is predicted with remarkable accuracy. The only significant error is that the actual and theoretical critical phase-angles leading to the "worst" response differ by 9°.

Figure 7.36 shows measured (Y,θ)-trajectories for the same set of conditions. The points were obtained by direct measurement of waveforms and not from the pen-recordings. These curves should be compared with the theoretical (Z,ψ)-trajectories of Figure 7.18, calculated for similar conditions. The agreement is again excellent, even to the predicted "kinks" in the non-critical trajectories in the neighbourhood of the origin, which also occur in the small-signal trajectory diagram of Figure 7.14.

Some measured amplitude-transients for initiation at various phase angles $\theta(0)$ and a constant initial amplitude $V_s'(0)$ are plotted logarithmically in Figure 7.37. These curves should be compared with the theoretically-predicted transients of Figure 7.29, (for which the logarithmic amplitude scale is different). The types of response for various initial phase-angles are very similar in the two cases. In particular, it may be pointed out that the measured amplitude response curve for $\theta(0) \cong 65^{\circ}$ actually does dip below a decaying exponential, in agreement with the theoretical prediction concerning $\psi(0)$.

Figure 7.38 shows the effect of increasing the initial amplitude $V_s'(0)$

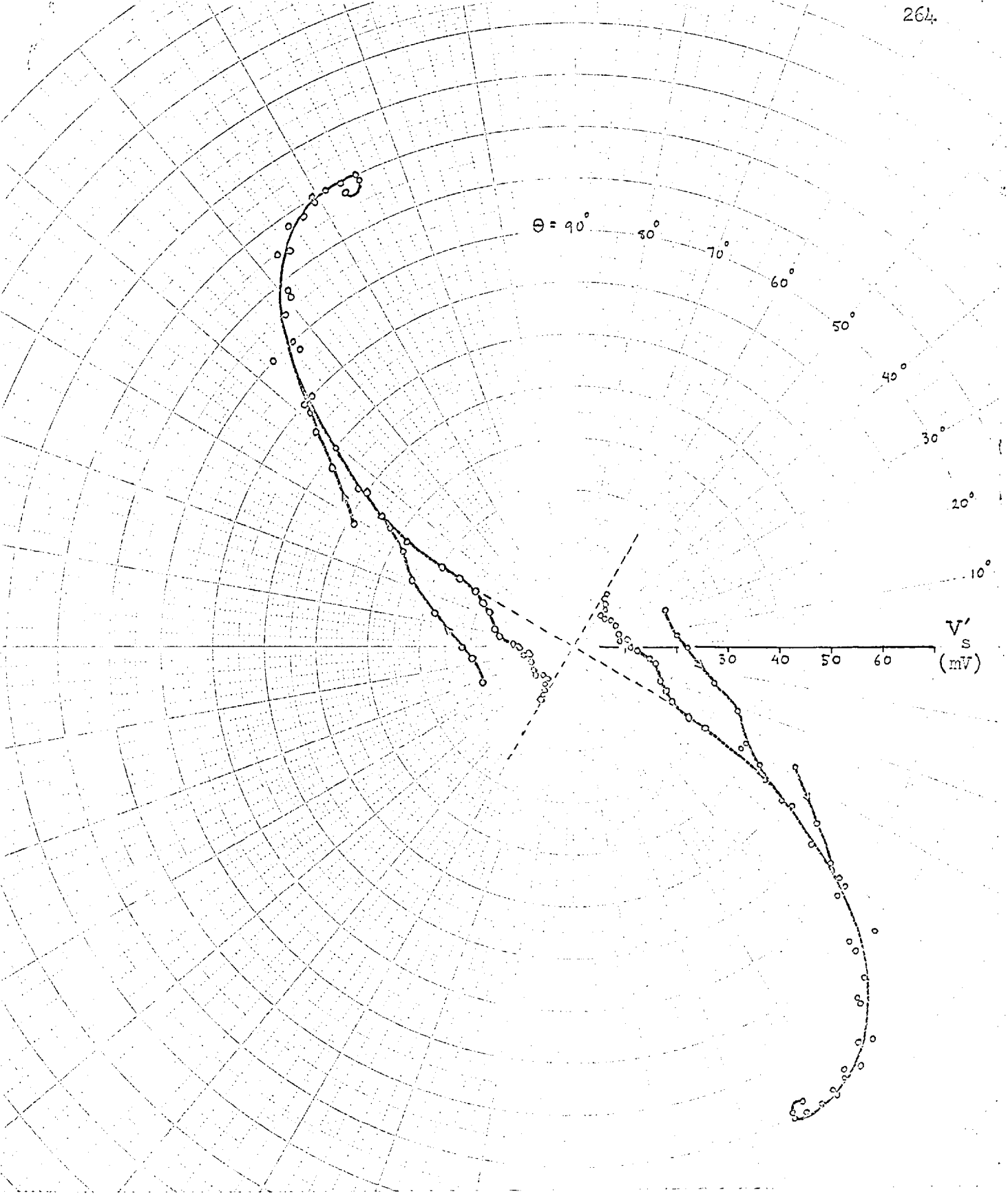


Figure 7.36 - Measured (Y,Θ)-trajectories for an experimental EPP with the parameters $k_p = 0.28$, B = 0.45. The operating conditions are $\nu = 1.0$, X = 1.15.

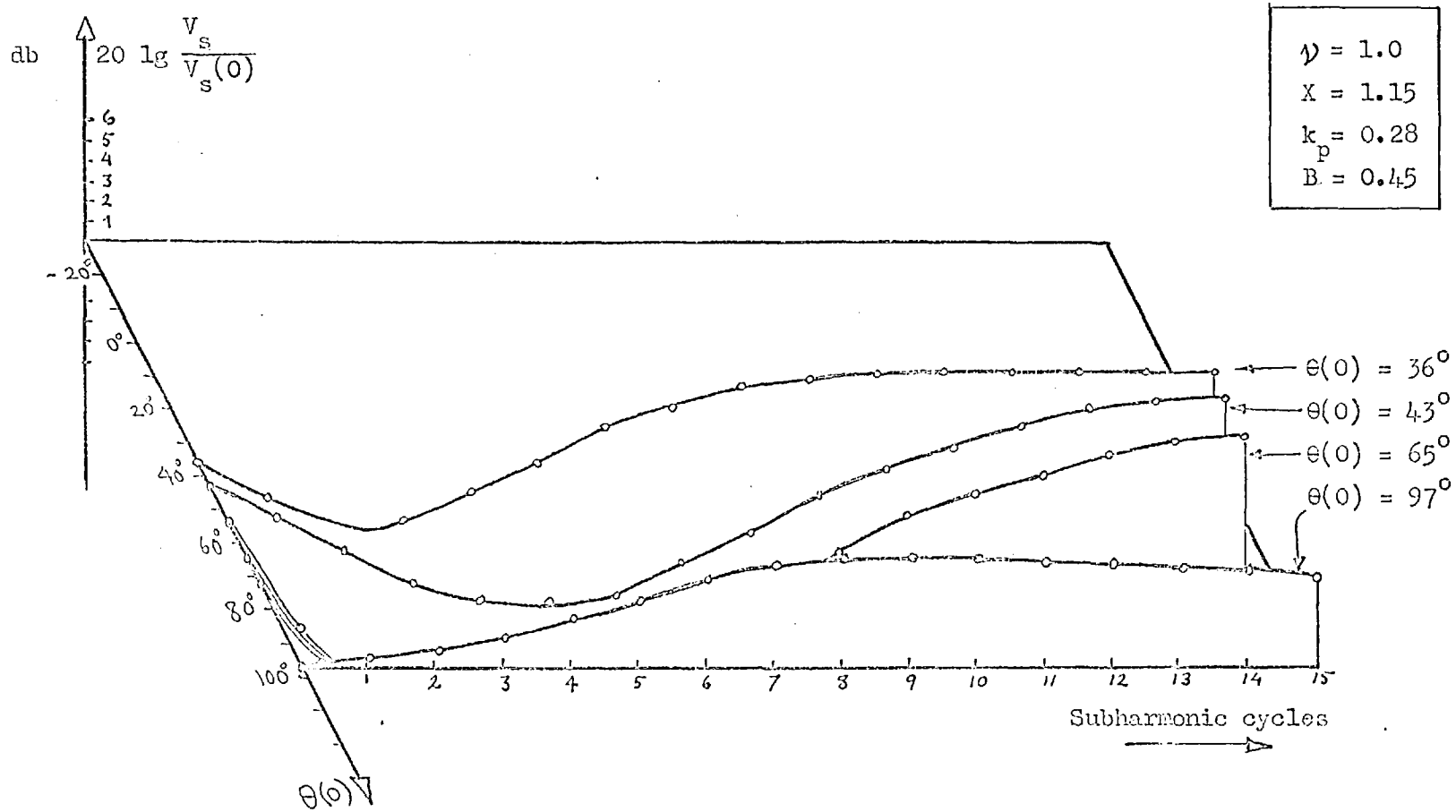


Figure 7.37 - Measured logarithmic amplitude transients for various initial phase-angles θ(0).

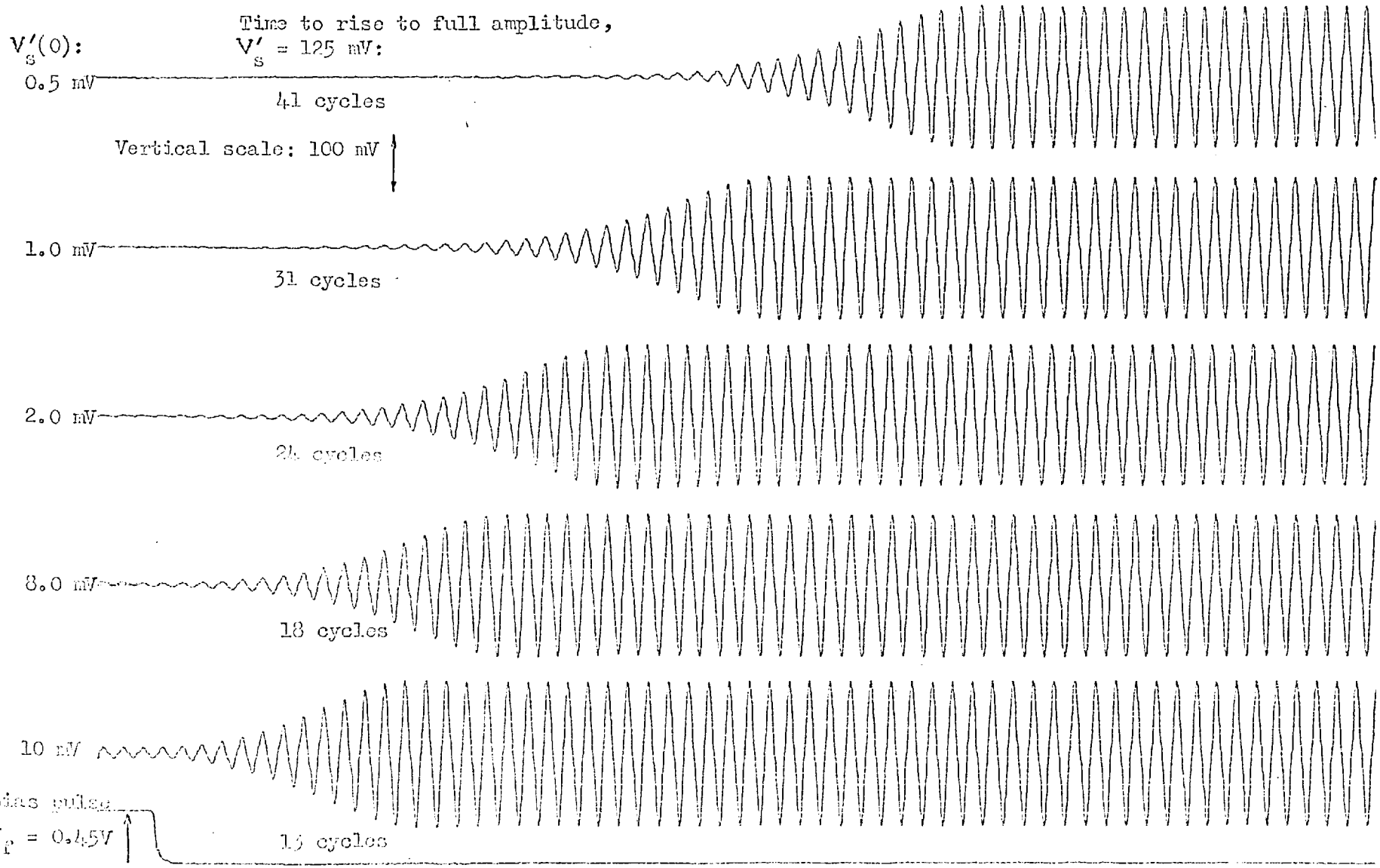


Figure 7.3 8 - Effect of varying the initial amplitude $V_s(0)$, the initial phase $\theta(0)$ being held constant at 104°.
Conditions: k_p= 0.28, B= 0.45, ν = 1.0, X = 1.57.

while the initial phase $\theta(0)$ is kept constant. The parametron now behaves in a manner reminiscent of the superregenerative oscillator operated in the so-called logarithmic mode[40]: the time taken for the amplitude to reach its steady-state value is an approximately logarithmic function of the initial amplitude. This is exactly what would be expected on theoretical grounds for initiation near a critical phase-angle.

Measured phase-transients for the resonant case are given in Figure 7.39. The curves are difficult to measure accurately, but for those ranges of phase-angle which correspond to small amplitudes, agree quite well with the theoretical phase-response curves of Figure 7.23. Figure 7.40 shows theoretical phase transients calculated according to the approximate method of Sub-Section 7.4.8: the curves given by the small-signal theory either "stop at" or "jump to" the steady-state phase-angles given by the large-signal theory. These transients differ in several respects from the actual ones, but the general agreement is satisfactory.

In order to make clear the manner in which the actual instantaneous phase and amplitude change with time, Figure 7.41 shows a drawing of a pair of typical transients in (Y,θ,τ)-space for initiation at phase angles $\theta(0)$ close to the separatrix and for $Y(0)$ about $\frac{1}{2}\,Y(\infty)$. The arrows represent positions of the $\underline{Y}$-vector at equal increments of time. The two curves, which are always 180° apart, pass close to the τ-axis, but ultimately spiral around the broken lines (parallel to the τ-axis) which represent the positions of the stable singularities.

Figures 7.42 to 7.45 inclusive show the measured phase-initiated amplitude transients and trajectories for two values of detuning away from resonance: $\nu = 0.9$ and $\nu = 0.8$. The amplitude-response curves are similar

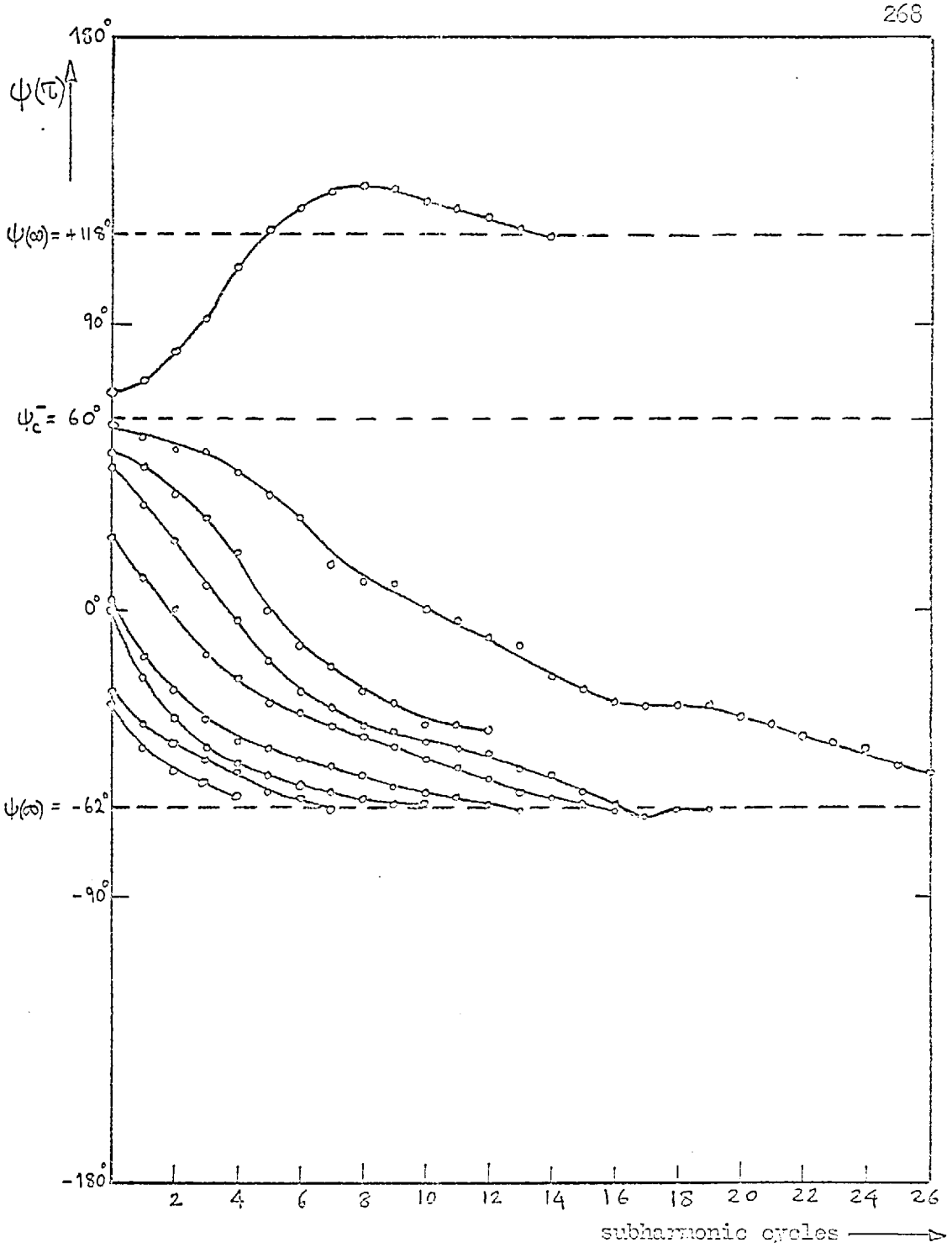


Figure 7.39 - Measured phase transients for the resonant case.
$\nu = 1.0$, $K = 1.07$, $k_p = 0.28$, $B = 0.45$.

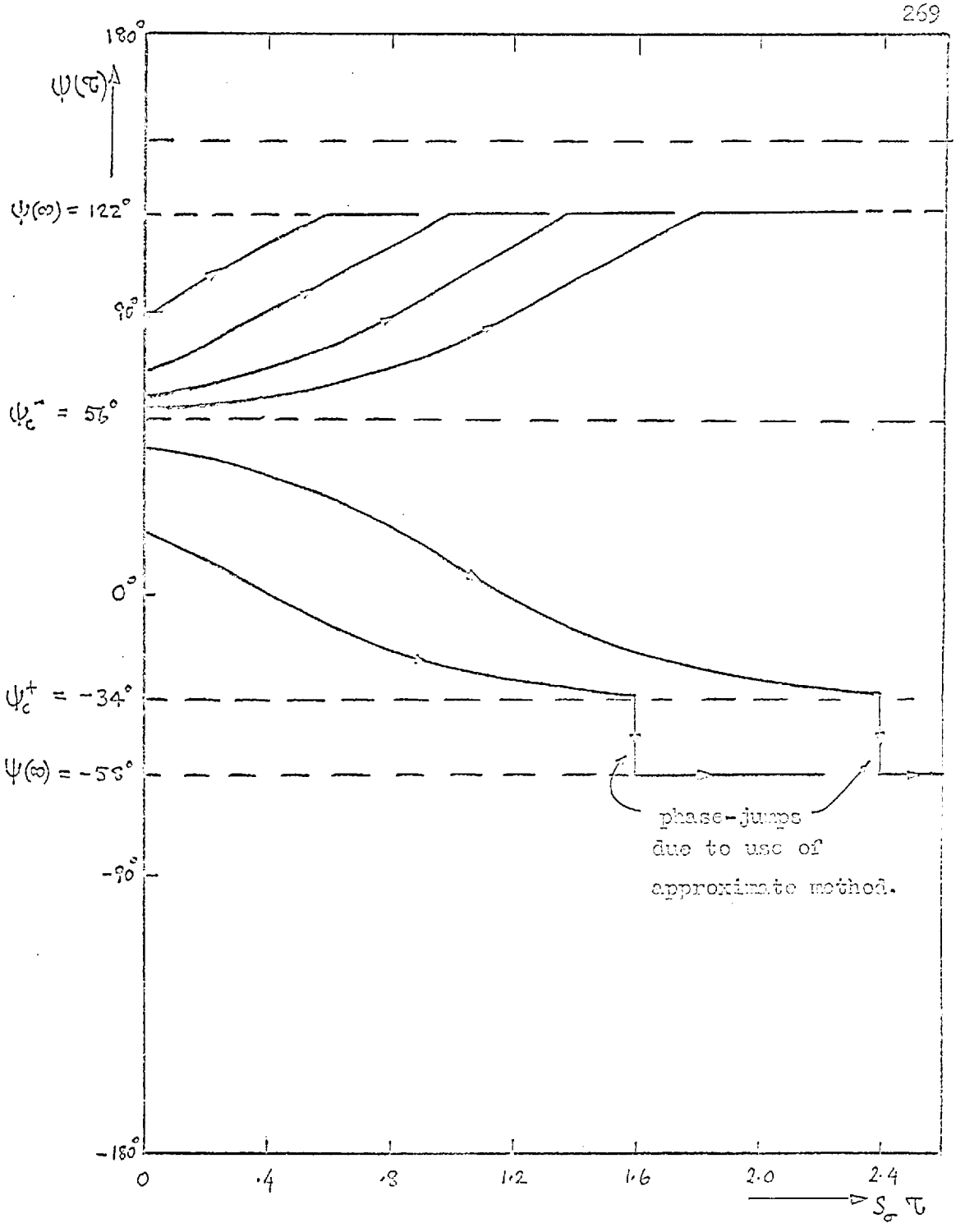


Figure 7.40 - Theoretical phase transients calculated according to the approximate method of Sub-Section 7.4.3.
$\nu = 1.0$, $k_p = 0.20$, $B = 0.45$.

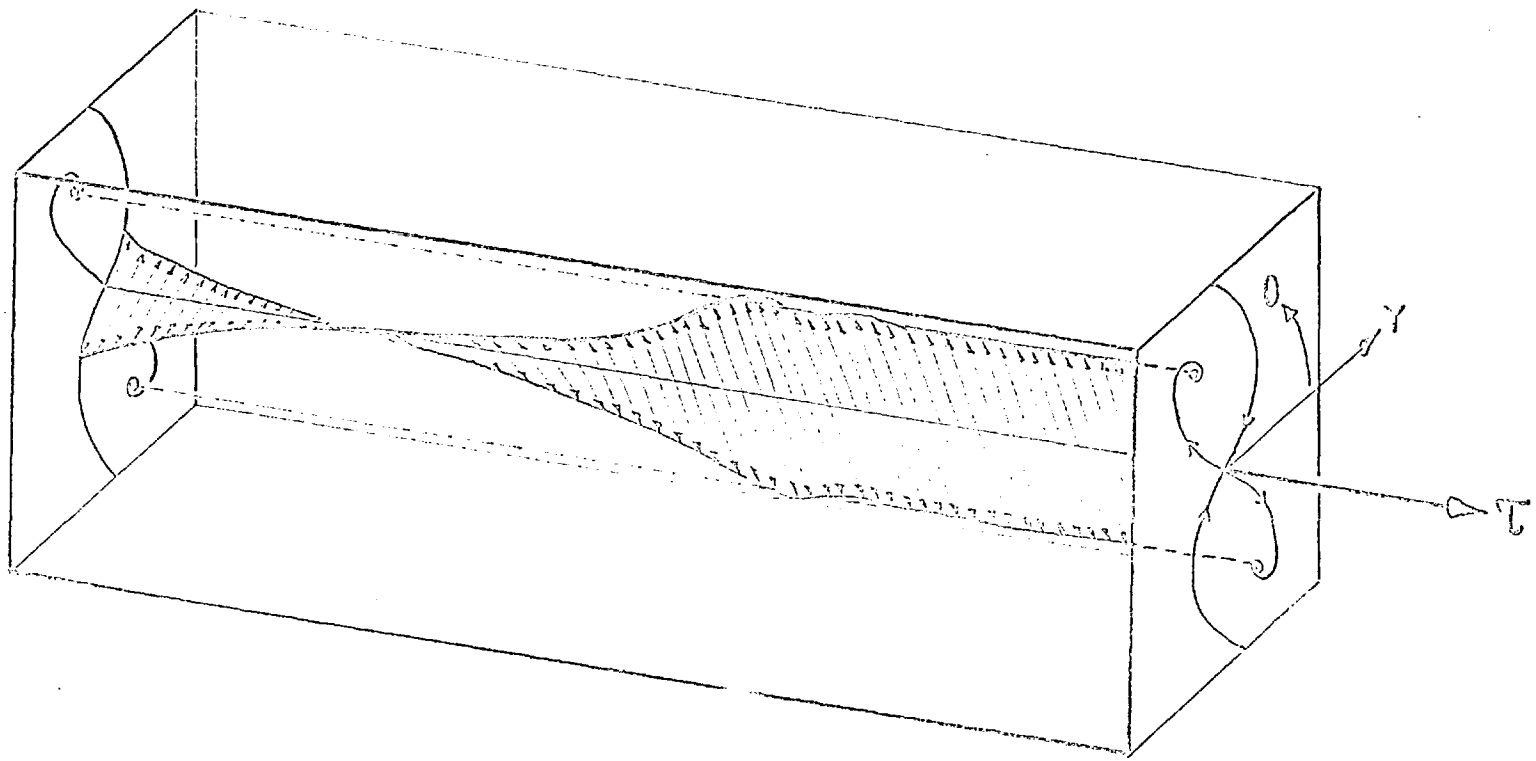


Figure 7.41 - Drawing of a typical pair of transients in (γ,θ,τ)-space for initiation near the separatrix.

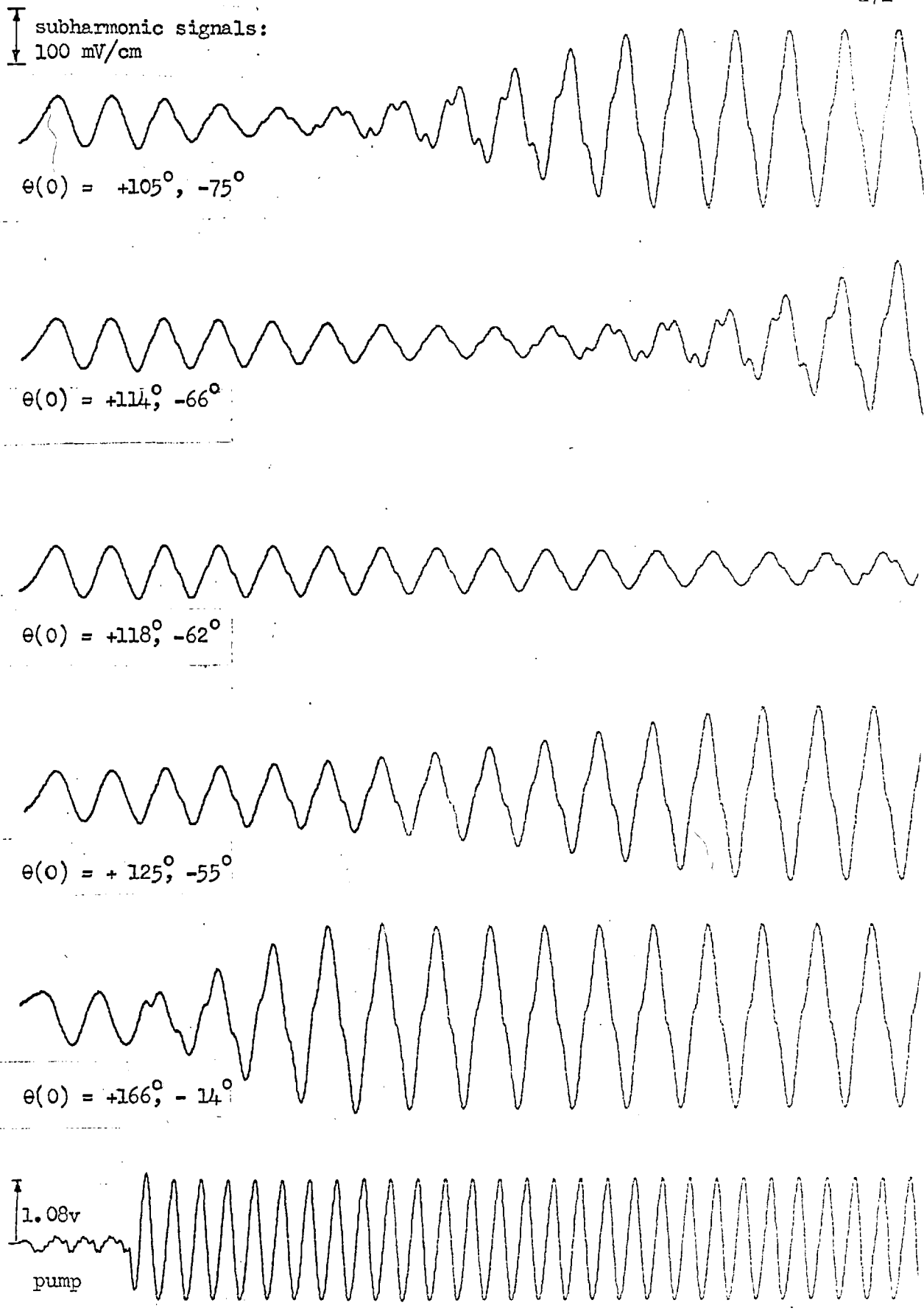


Figure 7.42 - Recordings of amplitude transients for a case of detuning below resonance: ν = 0.9, X = 1.55, k_p = 0.28, B = 0.45.

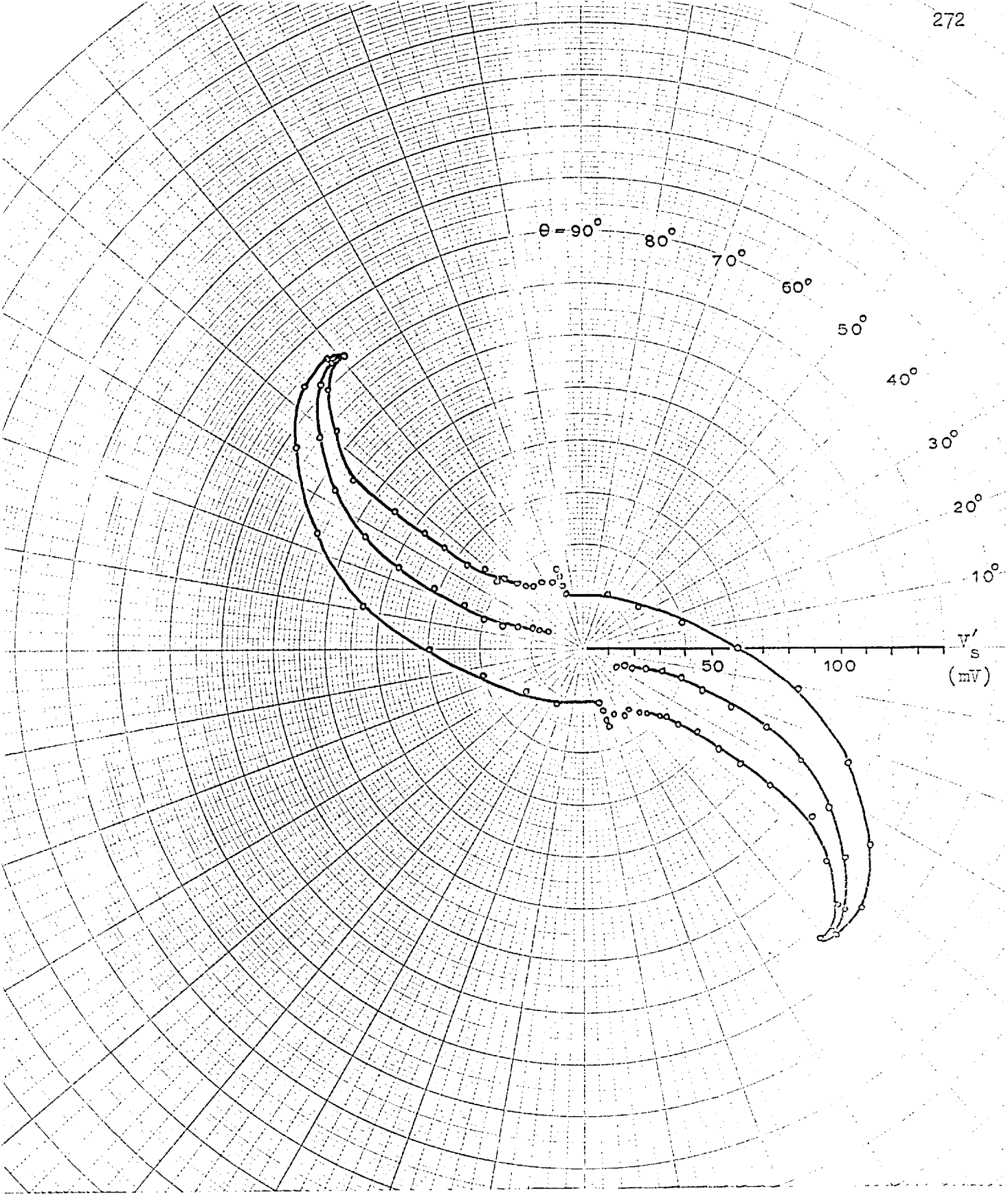


Figure 7.43 - Measured (Y,θ)-trajectories for detuning below resonance: $\nu = 0.9$, $X = 1.55$, $k_p = 0.28$, $B = 0.45$.

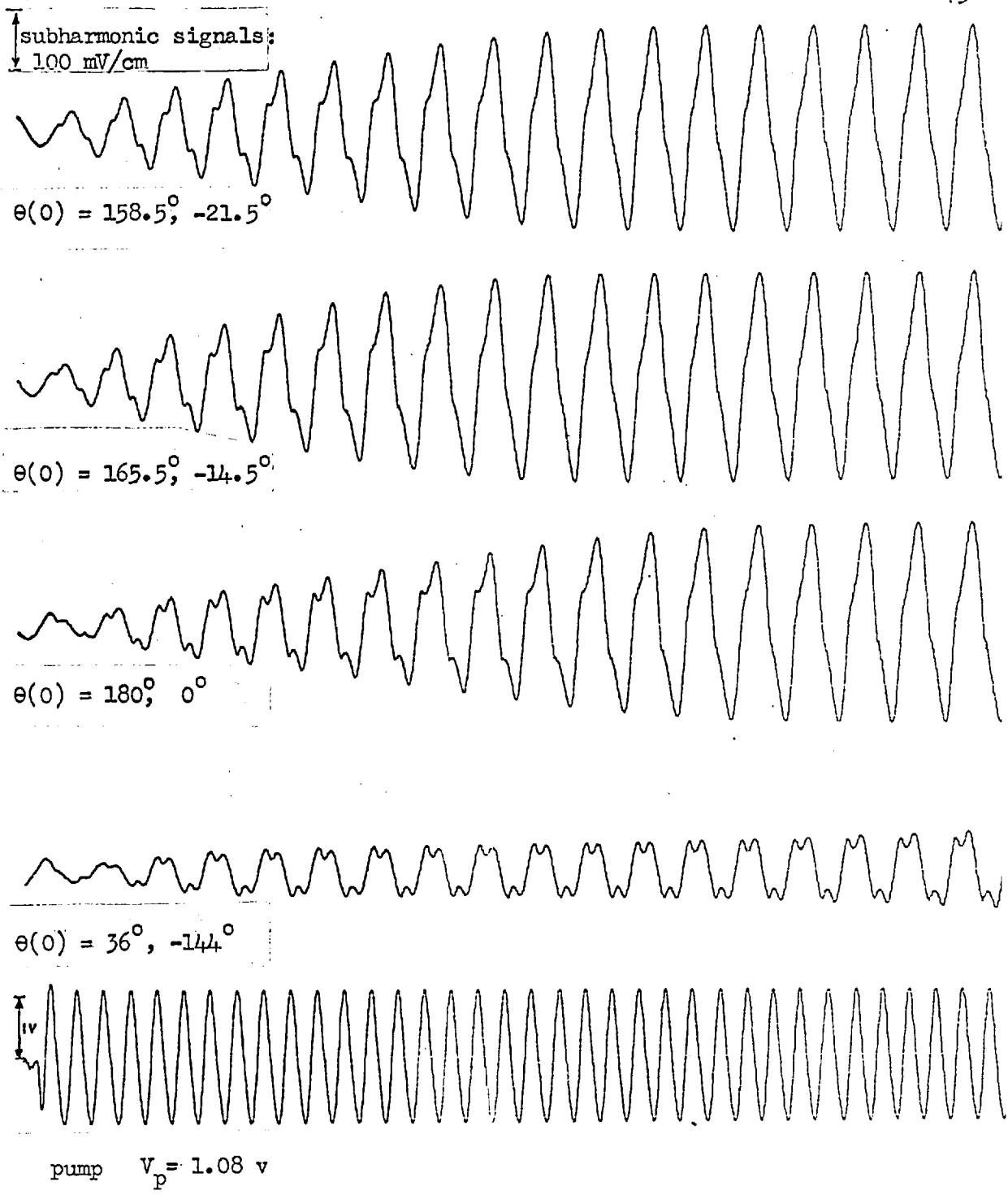


Figure 7.44 - Recordings of amplitude transients for a case of increased detuning below resonance:

ν = 0.8, X = 1.55, k_p= 0.28, B = 0.45.

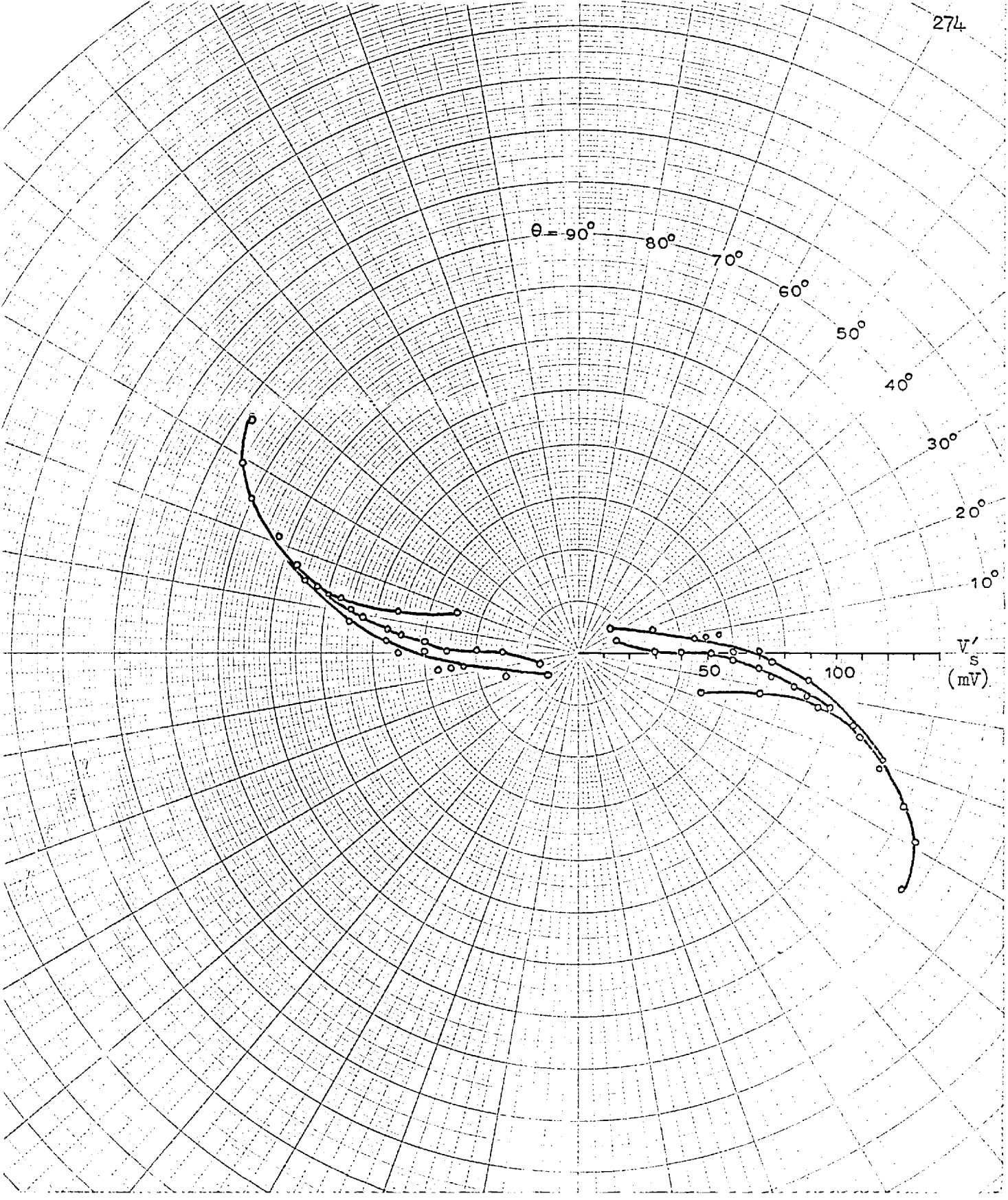


Figure 7.45 - Measured (Y,θ)-trajectories for increased detuning below resonance: ν = 0.80, X = 1.55, k_p = 0.28, B = 0.45.

to those of the resonant case, but the initial phase-angles for which the various kinds of response occur are now different. The trajectory diagrams show the typical counter-clockwise rotation of the outer stable singularities as the detuning is increased.

Finally, Figure 7.46 shows some experimentally-determined curves of constant "dimensionless risetime" μ. In order to obtain these curves, an extremely small phase-locking signal was applied, so that the initial part of each transient might be truly small-signal. The quantity μ was determined in each case by counting the number of subharmonic cycles required for the amplitude to increase by a factor 2.7. These curves should be compared with the theoretical predictions of Figure 7.26 for the same circuit parameters. Apart from the expected differences near $\nu = 1.0$, which are due to the neglect of k_L in the theoretical case, and the differences at large pump amplitudes, which are due to the neglect of nonlinear diode conduction, the agreement is highly satisfactory.

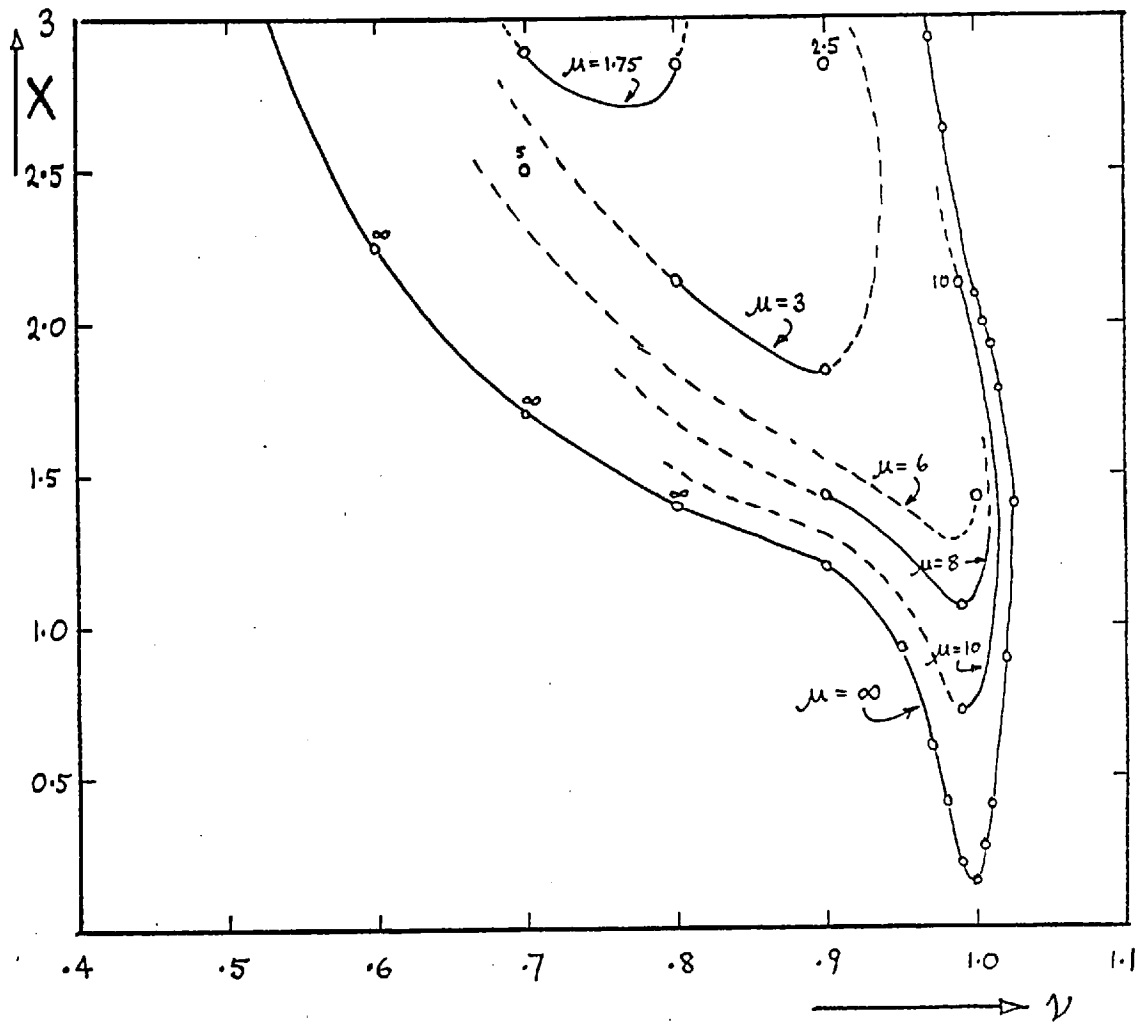


Figure 7.46 - Measured curves of constant dimensionless risetime μ for a BPP characterised by k_p= 0.28, B = 0.45. Compare with the theoretical curves of Figure 7.26.

CONCLUSIONS

A large part of the problem proposed at the outset has been solved. In the early chapters of the thesis an attempt has been made to bring order to the hitherto disparate theoretical and experimental work previously published on the subject. The mathematical and physical relationships between the possible types of lumped-element parametric subharmonic oscillator have been elucidated with the aid of an 'evolution' chart. On the basis of these considerations and experimental evidence, the types most suitable for use as fast-phase-switching parametrons in digital computers have been selected. These devices have been treated by several different mathematical approaches with varying degrees of success. These are summarised below.

(1) The first-order quasi-static theory developed in Chapter 4, Section 4.2, gave perhaps the simplest and most easily apprehended insights into the nature of parametron behaviour. In particular, the strong inter-relationships between the amplitude and phase phenomena were brought out. The theory suffered, however, from lack of rigour and its inability to account for any but extremely small-signal phenomena.

(2) Under certain conditions the piecewise-linear theory of Section 4.3 gave rise to a satisfactory explanation of the very large signal steady-state phenomena, but offered no prospect of extension to the analytical (rather than numerical) treatment of the transient phenomena.

(3) The limitations of these two approaches led, in Chapter 5, to the investigation of the possibilities of differential-equation models. These models were of two kinds: the simpler were based on the representation of

varactor capacitance as a nonlinear function of voltage. Owing to the nature of the nonlinear functions, the differential equations of these "voltage" models could be solved approximately only under small-signal conditions. Nevertheless, they gave accurate steady-state results for such conditions. Accurate prediction of transient phenomena by the use of "voltage" models was found to be impracticable. The second and somewhat more complicated kind of model made use of the representation of the varactor voltage as a nonlinear function of charge. The advantage of this model was that under certain conditions the nonlinear function reduced to a sum of integral powers. This made it possible to find solutions having large-signal validity.

Chapter 6 was concerned with the prediction of steady-state phenomena using both "voltage" and "charge" models. Transients were treated in Chapter 7, initially by the simplified "voltage" approach. The remainder of this final chapter was devoted to a detailed "charge" investigation of transient phenomena. The results obtained were in excellent agreement with experimental observations and for the first time the detailed quantitative mechanism of the hitherto poorly-understood transient phenomena has been given.

The analyses given in this thesis necessarily lack generality: in the class of nonlinear devices treated, exact results can only be obtained if specific nonlinear laws are considered. A more general theory would have wider application but poorer accuracy.

Suggestions for further work are indicated below.

(1) It is desirable to generalise the "charge" theory to cover the operation of both BSP and BPP and to include in it the effects of those

parasitic elements which only become important at very high frequencies. These elements include the series inductance and resistance of the varactor diodes.

(2) At the highest frequencies of operation, the lumped-element approximation becomes inadequate. It is therefore necessary to extend the theory to cover distributed parametrons. Such a theory might perhaps be valid for hypothetical parametrons operating at optical frequencies.

(3) Finally, for the maximisation of switching speeds, it would be of interest to determine how phase-switching might be accomplished without alteration of energy-levels. Such an optimisation procedure, however, would probably involve the use of a digital computer and lies outside the scope of the present work.

Appendix 4.1

Piecewise-linear mode-equations for the BSP: the case of finite damping

The behaviour of the BSP is governed by equations (4.5), (4.23) and (4.24). If we make use of the normalisations

$$x = \frac{v_p}{V_o} ,$$

$$y = \frac{v_s}{V_o} ,$$

$$\tau' = \frac{R_p t}{L} , \text{ the dimensionless time,}$$

$$\xi' = \frac{R_p \dot{q}}{V_o} , \text{ the dimensionless inductor current,}$$

the last two of which are peculiar to the problem in hand, the three equations become

$$y = \dot{\xi}'_2 - \dot{\xi}'_1 \qquad (A4.1)$$

$$y_1 = x + y - \xi'_1 \geqslant -1 \qquad (A4.2)$$

$$y_2 = x - y - \xi'_2 \geqslant -1 \qquad (A4.3)$$

respectively. The circles above quantities in (A4.1) signify differentiation with respect to τ'.

A4.1.1 The Z_1I_2- mode

The Z_1I_2- mode is defined by constraining equations (A4.2) and (A4.3) with the conditions $v_2 = -V_o$ and $\dot{q}_1 = 0$. The result is the following set

of equations for the varactor voltages and currents:

$$y_1 = x + y > -1 , \tag{A4.4}$$

$$y_2 = -1 , \tag{A4.5}$$

$$\xi'_1 = 0 , \tag{A4.6}$$

$$\xi'_2 = x - y + 1 . \tag{A4.7}$$

A differential equation for the subharmonic current y can be found by substituting (A4.6) and (A4.7) into (A4.1). The result is

$$\overset{\circ}{y} + y = \overset{\circ}{x} . \tag{A4.8}$$

As before, the pumping function will be defined by

$$x = X.\sin 2\nu'\tau', \tag{A4.9}$$

where $\nu' = \omega L/R_p$.

The solution of (A4.8) with this value of x is

$$y(\tau') = \frac{2\nu' X}{1+4\nu'^2}\left[2\nu'.\sin 2\nu'\tau' + \cos 2\nu'\tau'\right] + \left[y(0) - \frac{2\nu' X}{1+4\nu'^2}\right] e^{-\tau'}, \tag{A4.10}$$

where y(0) is the value of y at $\tau' = 0$. Equation (A4.4) indicates that this result is subject to the condition

$$y(\tau') \qquad -1 - X.\sin 2\nu'\tau' . \tag{A4.11}$$

The normalised subharmonic current flowing in L during this mode is given by equation (A4.7):

$$\xi' = \xi'_2 = x - y + 1 \tag{A4.12}$$

where y is the solution (A4.10).

A4.1.2 The I_1Z_2- mode

As in the lossless case, the rôles of the two varactors are reversed during the Z_1I_2- mode. The differential equation for y is now

$$\dot{y} + y = -\dot{x}, \tag{A4.13}$$

so that

$$y(\tau') = -\frac{2\nu' X}{1+4\nu'^2}\left[2\nu' \sin 2\nu'\tau' + \cos 2\nu'\tau'\right] + \left[y(0) + \frac{2\nu' X}{1+4\nu'^2}\right] e^{-\tau'}, \tag{A4.14}$$

subject to the condition

$$y(\tau') < 1 + X \sin 2\nu'\tau'. \tag{A4.15}$$

The subharmonic current is

$$\xi' = -\xi_1' = -(x + y + 1). \tag{A4.16}$$

A4.1.3 The I_1I_2- mode

In this case the varactor voltages and currents are

$$y_1 = -1 \tag{A4.17}$$

$$y_2 = -1 \tag{A4.18}$$

$$\xi_1' = x + y + 1 \tag{A4.19}$$

$$\xi_2' = x - y + 1 . \tag{A4.20}$$

Substitution of (A4.19) and (A4.20) into (A4.1) gives

$$2\dot{y} + y = 0 . \tag{A4.21}$$

The solution of this is

$$y = y(0)\, e^{-\tau'/2}, \tag{A4.22}$$

where $y(0)$ is the voltage at the beginning of the mode. The subharmonic current is

$$\xi_s' = -2y. \tag{A4.23}$$

Appendix 5.1

Derivation of the differential equation of the BSP using the $C = \mathcal{F}(v)$ representation of the capacitive nonlinearity

Referring to Figure 5.1(b), Section 5.2, the following nine equations describe the equivalent circuit:

$$v_1 = v_p + v_s \,, \tag{A5.1}$$

$$v_2 = v_p - v_s \,, \tag{A5.2}$$

$$i_1 = C_o\left(1 + \frac{v_1}{V_o}\right)^{-n} \frac{dv_1}{dt} \,, \tag{A5.3}$$

$$i_6 = C_o\left(1 + \frac{v_2}{V_o}\right)^{-n} \frac{dv_2}{dt} \,, \tag{A5.4}$$

$$v_s = L \frac{d}{dt}(i_4 - i_3) \,, \tag{A5.5}$$

$$i_1 - i_2 = I_s\left(e^{-\Lambda(V_B + v_1)} - 1\right) \,, \tag{A5.6}$$

$$i_6 - i_5 = I_s\left(e^{-\Lambda(V_B + v_2)} - 1\right) \,, \tag{A5.7}$$

$$i_3 - i_2 = C_s \frac{dv_s}{dt} \,, \tag{A5.8}$$

$$i_5 - i_4 = G_L v_s \,. \tag{A5.9}$$

Elimination of i_1, i_2, i_3, i_4, i_5, i_6 from equations (A5.3) to (A5.9) inclusive results in

$$L C_s \ddot{v}_s + L G_L \dot{v}_s + v_s + L C_o \frac{d}{dt}\left[\left(1 + \frac{v_1}{V_o}\right)^{-n} \dot{v}_1 - \left(1 + \frac{v_2}{V_o}\right)^{-n} \dot{v}_2\right] + \\ + L I_s e^{-\Lambda V_B} \frac{d}{dt}\left(e^{-\Lambda v_2} - e^{-\Lambda v_1}\right) = 0. \tag{A5.10}$$

Introduction of the normalisations

$$y = \frac{v_s}{V_o}, \quad x = \frac{v_p}{V_o} \quad \text{and} \quad \tau = \omega_o t ,$$

where ω_o is the small-signal angular resonant frequency, together with the use of equations (A5.1), (A5.2) and the identity

$$\frac{d}{d\tau}\left[(1+y)^{-n}\ \frac{dy}{d\tau}\right] \equiv \frac{1}{1-n} \cdot \frac{d^2}{d\tau^2}\left[(1+y)^{1-n}\right] , \qquad (A5.11)$$

effects the simplification

$$\omega_o^2 L C_s \overset{oo}{y} + \omega_o L G_L \overset{o}{y} + y + \frac{\omega_o^2 L C_o}{1-n} \cdot \frac{d^2}{d\tau^2}\left[(1+x+y)^{1-n} - (1+x-y)^{1-n}\right] +$$

$$+ \frac{2\omega_o L I_s e^{-\Lambda V_B}}{V_o} \cdot \frac{d}{d\tau}\left[e^{-\Lambda V_o x} \sinh \Lambda V_o . y\right] = 0 \qquad (A5.12)$$

The small-signal angular resonant frequency ω_o may be determined by setting n equal to zero (thus linearising the reactances) and neglecting all the damping, which gives

$$\omega_o^2 L C_s \overset{oo}{y} + 2\omega_o^2 L C_o \overset{oo}{y} + y = 0 , \qquad (A5.13)$$

so that

$$\omega_o^2 = \frac{1}{L(2C_o + C_s)} . \qquad (5.7)$$

If we define a "stray capacitance parameter"

$$B = \frac{2C_o}{2C_o + C_s} , \qquad (5.8)$$

which gives

$$\omega_o^2 L C_s = 1-B , \qquad (A5.14)$$

$$\omega_o^2 L C_o = \tfrac{1}{2} B , \qquad (A5.15)$$

and write

$$k_v = \frac{\omega_o L I_s}{V_o} e^{-\Lambda V_B} , \tag{5.9}$$

$$k_L = \omega_o L G_L , \tag{5.10}$$

$$c = \Lambda V_o , \tag{5.11}$$

then the complete differential equation becomes

$$(1-B)\,\overset{\circ\circ}{y} + k_L \cdot \overset{\circ}{y} + y + \frac{B}{2(1-n)} \cdot \frac{d^2}{d\tau^2}\left[(1+x+y)^{1-n} - (1+x-y)^{1-n} \right] + 2k_v \cdot \frac{d}{d\tau}\left[e^{-cx} \sinh cy \right] = 0$$

which is the required result, equation (5.6).

Appendix 5.2

Derivation of the differential equation of the BPP using the $C = \mathcal{F}(v)$ representation of the capacitive nonlinearity

The thirteen equations describing the equivalent circuit of Figure 5.2(b), Section 5.3, are

$$v_p = -v_4 - v_2 \tag{A5.16}$$

$$v_p = v_3 - v_1 \tag{A5.17}$$

$$v_s = v_3 + v_4 \tag{A5.18}$$

$$v_s = v_1 - v_2 \tag{A5.19}$$

$$i_1 - i_2 = C_o\left(1 + \frac{v_1}{V_o}\right)^{-n} \frac{dv_1}{dt} \tag{A5.20}$$

$$i_5 - i_6 = C_o\left(1 + \frac{v_2}{V_o}\right)^{-n} \frac{dv_2}{dt} \tag{A5.21}$$

$$i_1 = -\tfrac{1}{2} C_s \frac{dv_1}{dt} \tag{A5.22}$$

$$i_6 = \tfrac{1}{2} C_s \frac{dv_2}{dt} \tag{A5.23}$$

$$i_3 - i_2 = I_s\left(e^{-\lambda(V_B+v_1)} - 1\right) \tag{A5.24}$$

$$i_5 - i_4 = I_s\left(e^{-\lambda(V_B+v_2)} - 1\right) \tag{A5.25}$$

$$v_3 = \tfrac{1}{4} L \frac{d}{dt}(i_3 - i_7) + M \frac{d}{dt}(i_4 - i_7) \tag{A5.26}$$

$$v_4 = \tfrac{1}{4} L \frac{d}{dt}(i_4 - i_7) + M \frac{d}{dt}(i_3 - i_7) \tag{A5.27}$$

$$v_s = i_7 R_L \tag{A5.28}$$

Elimination of the currents i_1, i_2, i_3, i_4, i_5, i_6, i_7 yields

$$v_s + (\tfrac{1}{4}L + M)\frac{d}{dt}\left[C_o\left\{\left(1+\frac{v_1}{V_o}\right)^{-n}\dot{v}_1 - \left(1+\frac{v_2}{V_o}\right)^{-n}\dot{v}_2\right\} + I_s e^{-\Lambda V_B}\left\{e^{-\Lambda v_2} - e^{-\Lambda v_1}\right\} + \right.$$

$$\left. + \tfrac{1}{2}C_s(\dot{v}_1 - \dot{v}_2) + 2\,G_L\,v_s\right] = 0. \qquad (A5.29)$$

This equation can be expressed in terms of the two variables v_p and v_s only if the two halves of the tuning inductor L are closely coupled. In that case $M = \frac{1}{4}L$, so that from equations (A5.26) and (A5.27),

$$v_3 = v_4 , \qquad (A5.30)$$

and consequently from (A5.16), (A5.17), (A5.18) and (A5.19):

$$v_1 = \tfrac{1}{2}v_s - v_p \qquad (A5.31)$$

$$v_2 = -\tfrac{1}{2}v_s - v_p \qquad (A5.32)$$

This pair of equations, together with the normalisations of Appendix 5.1, converts (A5.29) into

$$\tfrac{1}{4}\omega_o^2 L C_s \ddot{y} + \omega_o L G_L \dot{y} + y +$$

$$+ \frac{\tfrac{1}{2}\omega_o^2 L C_o}{1-n}\cdot\frac{d^2}{d\tau^2}\left[(1-x+\tfrac{1}{2}y)^{1-n} - (1-x-\tfrac{1}{2}y)^{1-n}\right] +$$

$$+ \frac{\omega_o L I_s}{V_o}\cdot e^{-\Lambda V_B}\frac{d}{d\tau}\left[e^{\Lambda V_o x}\sinh\Lambda V_o\frac{Y}{2}\right] = 0 . \qquad (A5.33)$$

We can again determine ω_o, the small-signal angular frequency of resonance by putting n = 0 and neglecting all damping:

$$\tfrac{1}{4}\omega_o^2 L C_s \ddot{y} + \tfrac{1}{2}\omega_o^2 L C_o \ddot{y} + y = 0 , \qquad (A5.34)$$

whence

$$\omega_o^2 = \frac{4}{L(2C_o + C_s)} . \qquad (A5.35)$$

The resonant frequency of the BPP is thus twice that of a BSP constructed with the same varactors and with the same value of L. This is because the varactors are now effectively in series at the subharmonic frequency.

In terms of the previously-defined quantities B, k_v, k_L and c, the differential equation becomes, with a reversal of the sign of x to conform with its sign in the equation for the BSP,

$$(1-B)\ddot{y} + k_L \cdot \dot{y} + y + \frac{B}{1-n} \cdot \frac{d^2}{d\tau^2}\left[(1+x+\tfrac{1}{2}y)^{1-n} - (1+x-\tfrac{1}{2}y)^{1-n}\right] +$$

$$+ k_v \cdot \frac{d}{d\tau}\left[e^{-cx} \sinh \tfrac{1}{2} cy \right] = 0 \qquad (A5.36)$$

which is equation (5.12).

Appendix 5.3.

Derivation of the differential equations of the BPP using the $v = \mathcal{F}(q)$ representation of the capacitive nonlinearity: the case $n = \frac{1}{2}$

The fourteen equations for the equivalent circuit of Figure 5.3 are:

$$v_5 G_p = \dot{q}_5 - \dot{q}_3 , \tag{A5.37}$$

$$v_p + v_5 = -v_2 - v_4 , \tag{A5.38}$$

$$v_p + v_5 = v_3 - v_1 , \tag{A5.39}$$

$$v_s = v_3 + v_4 , \tag{A5.40}$$

$$v_s = v_1 - v_2, \tag{A5.41}$$

$$v_1 = V_o \left[\left\{ 1-(1-n) \frac{q_1}{C_o V_o} \right\}^{\frac{1}{1-n}} - 1 \right] , \tag{A5.42}$$

$$v_2 = V_o \left[\left\{ 1+(1-n) \frac{q_7}{C_o V_o} \right\}^{\frac{1}{1-n}} - 1 \right] , \tag{A5.43}$$

$$\dot{q}_1 - \dot{q}_2 = \tfrac{1}{2} C_s \dot{v}_1 , \tag{A5.44}$$

$$\dot{q}_6 - \dot{q}_7 = \tfrac{1}{2} C_s \dot{v}_2 , \tag{A5.45}$$

$$\dot{q}_2 - \dot{q}_3 = G_v v_1 , \tag{A5.46}$$

$$\dot{q}_5 - \dot{q}_6 = G_v v_2 , \tag{A5.47}$$

$$v_3 = \tfrac{1}{4} L (\ddot{q}_3 - \ddot{q}_8) + M(\ddot{q}_5 - \ddot{q}_8) , \tag{A5.48}$$

$$v_4 = \tfrac{1}{4} L (\ddot{q}_5 - \ddot{q}_8) + M(\ddot{q}_3 - \ddot{q}_8) , \tag{A5.49}$$

$$v_s = \dot{q}_8 R_L . \tag{A5.50}$$

If n is set equal to $\frac{1}{2}$ and if the usual normalisations

$$y = \frac{v}{V_o},$$

$$z = \frac{q}{C_o V_o},$$

are made, then equations (A5.42) and (A5.43) become

$$y_1 = z_1(\tfrac{1}{4} z_1 - 1) \tag{5.14}$$

and $$y_2 = z_7(\tfrac{1}{4} z_7 + 1) \tag{5.15}$$

respectively. If the pumping voltage is also normalised:

$$x = \frac{v_p}{V_o},$$

and the quantities

$$y_3, y_4, y_5, z_2, z_3, z_4, z_5, z_6$$

are eliminated, and if in addition it is assumed that perfect coupling exists between the two inductors, so that

$$M = \tfrac{1}{4} L,$$

then the following four equations are obtained:

$$y_1 + y_2 = \tfrac{1}{4}(z_1^2 + z_7^2) - (z_1 - z_7) = \tfrac{1}{8}\left[(z_1^2 + z_7^2) + (z_1^2 - z_7^2)\right] - (z_1 - z_7), \tag{A5.51}$$

$$y_1 - y_2 = y = \tfrac{1}{4}(z_1^2 - z_7^2) - (z_1 + z_7) = (z_1 + z_7)\left[\tfrac{1}{4}(z_1 - z_7) - 1\right], \tag{A5.52}$$

$$y + (\omega_o L G_L + \tfrac{1}{2}\omega_o L G_v)\dot{y} + \tfrac{1}{4}\omega_o^2 L C_s \ddot{y} = \tfrac{1}{2}\omega_o^2 L C_o(\ddot{z}_1 + \ddot{z}_7), \tag{A5.53}$$

and

$$x + \omega_o C_o R_p\left[(\dot{z}_7 - \dot{z}_1) + \frac{C_s}{2C_o}(\dot{y}_1 + \dot{y}_2) + \frac{G_v}{\omega_o C_o}(y_1 + y_2)\right] + \tfrac{1}{2}(y_1 + y_2) = 0. \tag{A5.54}$$

The sum of the varactor charges will be defined by

$$z_7 - z_1 = u \,, \tag{5.16}$$

and the difference between them by

$$z_7 + z_1 = z \,. \tag{5.17}$$

Then from equation (A5.51)

$$y_1 + y_2 = \tfrac{1}{8}(z^2 + u^2) + u \,, \tag{A5.55}$$

and from equation (A5.52),

$$\boxed{u = -4\left(1 + \frac{y}{z}\right)} \,. \tag{5.18}$$

Substitution of (5.17) into (A5.53) gives

$$\tfrac{1}{4}\omega_o^2 L\, C_s \ddot{y} + \omega_o L(G_L + \tfrac{1}{2}G_v)\dot{y} + y = \tfrac{1}{2}\omega_o^2 L\, C_o \ddot{z} \tag{A5.56}$$

and substitution of (5.16) and (A5.55) into (A5.54) gives

$$\omega_o C_o R_p \dot{u} + x + \tfrac{1}{2}\omega_o C_s R_p \frac{d}{d\tau}\left[\tfrac{1}{8}(z^2 + u^2) + u\right] + \left(\tfrac{1}{2} + G_v R_p\right)\left[\tfrac{1}{8}(z^2 + u^2) + u\right] = 0. \tag{A5.57}$$

If the following quantities:

$$B = \tfrac{1}{2}\omega_o^2 L\, C_o \,,$$

$$k_p = \omega_o C_o R_p \,,$$

$$k_v = \omega_o L\, G_v \,,$$

$$k_L = \omega_o L\, G_L$$

(which are identified in Sub-Section 5.5.1) are used to simplify (A5.56) and (A5.57), there results

$$\boxed{(1-B)\ddot{y} + (\tfrac{1}{2}k_v + k_L)\dot{y} + y = B\ddot{z}} \,, \tag{5.19}$$

and

$$k_p \dot{u} + B x + \tfrac{1}{8}k_p(1-B)\frac{d}{d\tau}(z^2 + u^2) + \tfrac{1}{2}(B + k_v k_p)\left[\tfrac{1}{8}(z^2 + u^2) + u\right] = 0, \tag{5.20}$$

as required.

Appendix 6.1

Approximate solution of the generalised "voltage" differential equation

By using the assumed value of y given in (6.8):

$$\tilde{y} = - j\, Y(\tau)\, (\alpha - \alpha^*),$$

where $\alpha = \frac{1}{2} e^{j(\nu\tau + \theta(\tau))}$,

and the value of x given by (6.9):

$$x = - j2X(\alpha^2 e^{-j2\theta} - \alpha^{*2} e^{j2\theta}),$$

it is possible to express all the quantities (6.7) in the form

$$\lambda_1(\alpha + \alpha^*) - j\,\lambda_2(\alpha - \alpha^*)$$

if the powers of α and α^*, corresponding to the harmonics of ν, are neglected. In the following Table, the expression for λ_1 and λ_2 for each of the required nine quantities (6.7) is given, with the omission of the second-order-small derivatives indicated in the fourth column. The fifth column contains the neglected harmonic terms.

Substitution of these quantities into (6.4) and separation of the coefficients of $(\alpha + \alpha^*)$ and $j(\alpha - \alpha^*)$ gives the pair of equations (6.10) and (6.11).

Quantity	λ_1	λ_2	Neglected 2nd-order small derivatives.	Neglected harmonic terms.
$\tilde{y}$	0	Y	-	-
$\overset{o}{\tilde{y}}$	$Y(\nu + \overset{o}{\theta})$	$\overset{o}{Y}$	-	-
$\overset{oo}{\tilde{y}}$	$2\nu\overset{o}{Y}$	$-Y\nu(\nu + 2\overset{o}{\theta})$	$\overset{o}{Y}\overset{o}{\theta}$, $\overset{oo}{\theta}$, $\overset{oo}{Y}$, $\overset{o}{\theta}^2$	-
$(x\tilde{y})^o$	$\frac{1}{2}X\left[\overset{o}{Y}\cos 2\theta + Y(\nu - \overset{o}{\theta})\sin 2\theta\right]$	$\frac{1}{2}X\left[\overset{o}{Y}\sin 2\theta - Y(\nu - \overset{o}{\theta})\cos 2\theta\right]$	-	α^3, α^{*3}
$(x\tilde{y})^{oo}$	$\frac{1}{2}\nu X\left[Y(2\overset{o}{\theta} - \nu)\cos 2\theta + 2\overset{o}{Y}\sin 2\theta\right]$	$\frac{1}{2}\nu X\left[Y(2\overset{o}{\theta} - \nu)\sin 2\theta - 2\overset{o}{Y}\cos 2\theta\right]$	$\overset{o}{Y}\overset{o}{\theta}$, $\overset{oo}{\theta}$, $\overset{oo}{Y}$, $\overset{o}{\theta}^2$	α^3, α^{*3}
$(x^2\tilde{y})^o$	$\frac{1}{2}X^2Y(\nu + \overset{o}{\theta})$	$\frac{1}{2}X^2\overset{o}{Y}$	-	$\alpha^3, \alpha^{*3}, \alpha^5, \alpha^{*5}$
$(x^2\tilde{y})^{oo}$	$\nu X^2\overset{o}{Y}$	$-\frac{1}{2}\nu X^2Y(\nu + 2\overset{o}{\theta})$	$\overset{o}{Y}\overset{o}{\theta}$, $\overset{oo}{\theta}$, $\overset{oo}{Y}$, $\overset{o}{\theta}^2$	$\alpha^3, \alpha^{*3}, \alpha^5, \alpha^{*5}$
$(\tilde{y}^3)^o$	$\frac{3}{4}Y^3(\nu + \overset{o}{\theta})$	$\frac{9}{4}Y^2\overset{o}{Y}$	-	α^3, α^{*3}
$(\tilde{y}^3)^{oo}$	$\frac{18}{4}\nu Y^2\overset{o}{Y}$	$-\frac{3}{4}\nu Y^3(\nu + 2\overset{o}{\theta})$	$\overset{o}{Y}\overset{o}{\theta}$, $\overset{oo}{\theta}$, $\overset{oo}{Y}$, $\overset{o}{\theta}^2$, $\overset{o}{Y}^2$	α^3, α^{*3}

Appendix 7.1

Expression of $\tilde{y}(\tau)$ in terms of charge coordinates for the case in which R_p dominates the device behaviour

A relation between $Y(\tau)$ and $Z(\tau)$, valid under conditions of slowly-varying amplitude and phase, is given by equations (7.32) and (7.33). They are

$$Y_s = a \overset{\circ}{Z}_c - \Gamma Z_s,$$

$$Y_c = -a \overset{\circ}{Z}_s - \Gamma Z_c,$$

where

$$a = \frac{2\Gamma^2}{B\nu^3} .$$

Now

$$\tilde{y} = Y_s.\cos\nu\tau + Y_c.\sin\nu\tau ,$$

so that substituting for Y_s and Y_c,

$$\tilde{y} = (a \overset{\circ}{Z}_c - \Gamma Z_s).\cos\nu\tau - (a \overset{\circ}{Z}_s + \Gamma Z_c).\sin\nu\tau,$$

$$= a \overset{\circ}{Z}.\cos(\nu\tau+\psi) - Z(a\overset{\circ}{\psi}+\Gamma).\sin(\nu\tau+\psi),$$

or in terms of the complex notation $\gamma = \frac{1}{2} e^{j(\nu\tau+\psi)}$,

$$\boxed{\tilde{y} = a \overset{\circ}{Z}(\gamma + \gamma^*) + jZ(a\overset{\circ}{\psi}+\Gamma)(\gamma - \gamma^*)} .$$

Appendix 7.2

Derivation of the intermediate differential equations for the case in which R_p dominates the device behaviour

The construction of the approximate form (7.39) of equation (7.26) involves the expression of the following nine instantaneous quantities in terms of the charge amplitude Z and phase :

$\tilde{z}^4\,\dot{\tilde{z}}$	$\tilde{y}\,\tilde{z}\,\dot{\tilde{y}}$	$\tilde{y}^2\,\dot{\tilde{z}}$
$\tilde{z}^2\,\dot{\tilde{y}}$	$\tilde{z}\,\tilde{y}\,\dot{\tilde{z}}$	$\tilde{z}^3$
$\tilde{z}^3$ x	$\tilde{z}^5$	$\tilde{y}^2\,\tilde{z}$

This can be done by substituting in them equations (7.38), (7.37) and (7.36) for x, $\tilde{y}$ and $\tilde{z}$ respectively. The assumption that y and z are pure sinusoids means that the harmonic terms in γ^3 and γ^5 must be neglected. Following the slowly-varying amplitude and phase assumption, the second-order small derivative products

$$\dot{Z}\dot{\psi}\ ,\quad \dot{Z}^2\ ,\quad \dot{\psi}^2$$

must also be neglected. (The quantities $\overset{\infty}{Z}$ and $\overset{\infty}{\psi}$ have already been omitted in arriving at the expression for $\tilde{y}$ in charge coordinates). If the quantities in the above table are written in the form

$$f(\tilde{y},\tilde{z}) = \lambda_1(\gamma + \gamma^*) - j\lambda_2(\gamma - \gamma^*)\ ,$$

then the coefficients λ_1 and λ_2 are given in the following table. The neglected terms are also indicated. Substitution of the resultant expressions into (7.26), followed by separation of the terms in $(\gamma + \gamma^*)$ and $-j(\gamma - \gamma^*)$ at once gives the required equations (7.40) and (7.41).

Quantity	λ_1	λ_2	Neglected 2nd-order small derivatives	Neglected harmonic terms
$\tilde{z}^4\mathring{\tilde{z}}$	$\frac{1}{8}(\nu+\mathring{\psi})\,z^5$	$\frac{5}{8}\,z^4\mathring{z}$	-	r^3, r^{*3}, r^5, r^{*5}
$\tilde{y}\,\tilde{z}\,\mathring{\tilde{y}}$	$\frac{1}{4}\Gamma(\nu\Gamma+[2a\nu+\Gamma]\mathring{\psi})\,z^3$	$\frac{1}{4}\Gamma(2a\nu+3\Gamma)\,z^2z$	$\mathring{z}\mathring{\psi}, \mathring{z}^2, \mathring{\psi}^2$	r^3, r^{*3}
$\tilde{y}^2\mathring{\tilde{z}}$	$\frac{1}{4}\Gamma(\nu\Gamma+[2a\nu+\Gamma]\mathring{\psi})\,z^3$	$\frac{1}{4}\Gamma(-2a\nu+3\Gamma)\,z^2z$	$\mathring{z}\mathring{\psi}, \mathring{z}^2, \mathring{\psi}^2$	r^3, r^{*3}
$\tilde{z}^2\mathring{\tilde{y}}$	$-\frac{1}{4}\cdot(\nu\Gamma+[a\nu+\Gamma]\mathring{\psi})\,z^3$	$-\frac{3}{4}(a\nu+\Gamma)\,z^2z$	-	r^3, r^{*3}
$\tilde{z}\,\tilde{y}\,\mathring{\tilde{z}}$	$-\frac{1}{4}\cdot(\nu\Gamma+[a\nu+\Gamma]\mathring{\psi})\,z^3$	$\frac{1}{4}(a\nu-3\Gamma)\,z^2z$	$\mathring{z}\mathring{\psi}, \mathring{z}^2, \mathring{\psi}^2$	r^3, r^{*3}
$\tilde{z}^3$	0	$\frac{3}{4}\,z^3$	-	r^3, r^{*3}, r^5, r^{*5}
$\tilde{z}^3x$	$\frac{1}{4}\,z^3X.\cos 2\psi$	$\frac{1}{2}\,z^3X.\sin 2\psi$	-	r^3, r^{*3}, r^5, r^{*5}
$\tilde{z}^5$	0	$\frac{5}{8}\,z^5$	-	r^3, r^{*3}, r^5, r^{*5}
$\tilde{y}^2\tilde{z}$	$-\frac{1}{2}a\Gamma z^2\mathring{z}$	$\frac{3}{4}\Gamma(\Gamma+2a\mathring{\psi})\,z^3$	$\mathring{z}\mathring{\psi}, \mathring{z}^2, \mathring{\psi}^2$	r^3, r^{*3}

Appendix 7.3

Derivation of approximate expression for $\tilde{y}(\tau)$ in charge coordinates for the case in which R_L dominates

Write $\tilde{y}$ and $\tilde{z}$ in Cartesian coordinates:

$$\tilde{y} = Y_s.\cos\nu\tau + Y_c.\sin\nu\tau, \quad \text{where } Y_s = Y.\sin\theta,\ Y_c = Y.\cos\theta; \tag{A7.1}$$

$$\tilde{z} = Z_s.\cos\nu\tau + Z_c.\sin\nu\tau, \quad \text{where } Z_s = Z.\sin\psi,\ Z_c = Z.\cos\psi. \tag{A7.2}$$

Substitute these approximations into equation (7.48), separate out coefficients of $\cos\nu\tau$ and $\sin\nu\tau$ and neglect second derivatives of the amplitudes, and obtain

$$\begin{aligned}(1-B)(2\nu\dot{Y}_c - \nu^2 Y_s) + k_L(\dot{Y}_s + \nu Y_c) + Y_s &= B\nu(2\dot{Z}_c - \nu Z_s),\\ (1-B)(-2\nu\dot{Y}_s - \nu^2 Y_c) + k_L(\dot{Y}_c - \nu Y_s) + Y_c &= B\nu(-2\dot{Z}_s - \nu Z_c).\end{aligned} \tag{A7.3}$$

Differentiate and again neglect second derivatives:

$$\begin{aligned}L\,\dot{Y}_s + M\,\dot{Y}_c &= -\dot{Z}_s,\\ L\,\dot{Y}_c - M\,\dot{Y}_s &= -\dot{Z}_c;\end{aligned} \tag{A7.4}$$

hence

$$\begin{aligned}(L^2+M^2)\dot{Y}_c &= -L\,\dot{Z}_c - M\,\dot{Z}_s,\\ (L^2+M^2)\dot{Y}_s &= -L\,\dot{Z}_c + M\,\dot{Z}_c\end{aligned} \tag{A7.5}$$

where

$$L = \frac{1-\nu^2(1-B)}{B\nu^2},$$

$$M = \frac{k_L}{B\nu}.$$

Eliminate $\dot{Y}_c$ and $\dot{Y}_s$ between (A7.3) and (A7.5) and rearrange to obtain expressions for Y_c and Y_s:

$$Y_c = a\,\overset{\circ}{Z}_c + b\,\overset{\circ}{Z}_s - c\,Z_s - d\,Z_c,$$
$$Y_s = a\,\overset{\circ}{Z}_s - b\,\overset{\circ}{Z}_c + c\,Z_c - d\,Z_s, \qquad \text{(A7.6)}$$

where
$$a = \frac{1}{\nu(L^2+M^2)^2}\left[\, 4\left(\frac{1-B}{B}\right) LM + M(3L^2+M^2)\,\right],$$
$$b = \frac{1}{\nu(L^2+M^2)^2}\left[\, 2\left(\frac{1-B}{B}\right)(M^2-L^2) - 2L^3\,\right],$$
$$c = \frac{M}{L^2+M^2},$$
$$d = \frac{L}{L^2+M^2}.$$

It remains to express equations (A7.6) in a concise complex form. To do this, replace (A7.6) into (A7.1) and put

$$\sin(\nu\tau+\psi) = -j(\gamma - \gamma^*),$$
$$\cos(\nu\tau+\psi) = (\gamma + \gamma^*),$$

where
$$\gamma = \tfrac{1}{2}\, e^{j(\nu\tau+\psi)}.$$

The result is

$$\boxed{\tilde{y} = (\gamma + \gamma^*)(aZ\overset{\circ}{\psi} - b\overset{\circ}{Z} + cZ) - j(\gamma - \gamma^*)(a\overset{\circ}{Z} + bZ\overset{\circ}{\psi} - dZ)}$$

From (A7.6) ignoring $\overset{\circ}{Z}_c$ and $\overset{\circ}{Z}_s$: $(L^2+M^2)Y^2 = Z^2$.

Appendix 7.4

Calculation of expression for curves of constant dimensionless rise- and fall-time on the (ν,X)-plane

Write equation (7.105) in the following form

$$A = \text{constant} = \frac{2\pi\mu X}{n} = \frac{1+\sigma^2}{\pm\sqrt{1+\sigma^2-\rho^2}-\sigma|\rho|} .$$

Then

$$A^2(1+\sigma^2-\rho^2) = (1+\sigma^2+A\sigma|\rho|)^2,$$

so that putting in the expression for A and writing ρ in full,

$$\left[\sigma + \frac{3\pi\mu}{n\nu}\cdot\left|\Gamma^2-1\right|\right]^2 + 1 - \left[\frac{2\pi\mu X}{n\nu}\right]^2 = 0.$$

Therefore the required expression for $X(\nu,\mu)$ is

$$X^2 = \frac{1+\left[\sigma+\frac{3\pi\mu}{n\nu}\left|\Gamma^2-1\right|\right]^2}{\left[\frac{2\pi\mu}{n\nu}\right]^2} .$$

Appendix 7.5

Transient amplitude solution in detuned case

The solution is given by equations (7.97) and (7.108):

$$\int \frac{dZ}{Z} = \frac{X}{n} \int \mathcal{Y}(\tau)\, d\tau,$$

and $$\mathcal{Y}(\tau) = \frac{(A \tanh S\tau + B)^2 - (C \tanh S\tau + D)^2}{(A \tanh S\tau + B)^2 + (C \tanh S\tau + D)^2} .$$

The latter can be written in the form

$$\mathcal{Y}(\tau) = \frac{fe^{4S\tau} + ge^{2S\tau} + h}{ae^{4S\tau} + be^{2S\tau} + d}$$

where

$$a = (A + B)^2 + (C + D)^2 = \left[T^2 + (B-1)^2 \right](B + A)^2,$$

$$b = 2(B^2 - A^2 + D^2 - C^2) = 2\left[T^2 - B^2 + 1 \right](B^2 - A^2),$$

$$c = (A - B)^2 + (C - D)^2 = \left[T^2 + (B + 1)^2 \right](B - A)^2,$$

$$f = (A + B)^2 - (C + D)^2 = \left[T^2 - (B - 1)^2 \right](B + A)^2,$$

$$g = 2(B^2 - A^2 - D^2 + C^2) = 2\left[T^2 + B^2 - 1 \right](B^2 - A^2),$$

$$h = (A - B)^2 - (C - D)^2 = \left[T^2 - (B + 1)^2 \right](B - A)^2,$$

and $T = \rho - \sigma$.

Therefore, if the variable of integration is changed to $u = e^{2S\tau}$,

$$\int \mathcal{Y}(\tau) d\tau = \frac{1}{2S} \int \frac{1}{u} \cdot \left(\frac{fu^2 + gu + h}{au^2 + bu + c} \right) \cdot du,$$

and the form of the integral depends on sgn(q), where

$$q = b^2 - 4ac$$

$$= -16(BC - AD)^2$$

$$= -16(BT)^2(B^2 - A^2)^2$$

which is always < 0, so that the complete solution is

$$\frac{2nS}{X}\ \ln Z + \text{const} = \frac{1}{\sqrt{-q}}\left[\ 2g - b\left(\frac{f}{a} + \frac{h}{c}\right)\right].\arctan\left[\ \frac{2au + b}{\sqrt{-q}}\ \right] +$$

$$+\ \frac{1}{2}\left(\frac{f}{a} - \frac{h}{c}\right)\ln\left(au^2 + bu + c\right) + \frac{h}{c}\ln u.$$

The constant terms are

$$\frac{2nS}{X} = \frac{4}{3}B,$$

$$\frac{1}{\sqrt{-q}}\left[\ 2g - b\left(\frac{f}{a} + \frac{h}{c}\right)\ \right] = \frac{-2\sigma B}{1+\sigma^2}\ ,$$

$$\frac{2a}{\sqrt{-q}} = \frac{1 - B - \sigma T}{BT}\left(\frac{B + A}{B - A}\right),$$

$$\frac{b}{\sqrt{-q}} = \frac{\rho}{B}\ ,$$

$$\frac{1}{2}\left(\frac{f}{a} - \frac{h}{c}\right) = \frac{B}{1+\sigma^2}\ ,$$

$$\frac{h}{c} = -\frac{(B + \sigma\rho)}{1+\sigma^2},$$

so that some rearrangement results in

$$\frac{4}{3}(1+\sigma^2)\ln Z + \text{constant} =$$

$$= \ln(au + b + cu^{-1}) - \sigma\left\{\frac{\rho}{B}\ln u + 2\ \text{arc tan}\left[\ \frac{\left(\frac{1-B}{T}\right) - \sigma\left(\frac{B+A}{B-A}\right)u + \rho}{B}\ \right]\right\},$$

where

$$au + b + cu^{-1} = 4T^2\left[\ (A.\sinh S\tau + B.\cosh S\tau)^2 + (C.\sinh S\tau + D.\cosh S\tau)^2\right]$$

Finally we obtain

$$\boxed{\mathcal{A}.Z^{\frac{4}{3}(1+\sigma^2)} = \mathcal{F}_1(\tau, \psi(0))\ \exp\ \mathcal{F}_2(\tau, \psi(0))\ ,}$$

where

$$\mathcal{J}_1(\tau, \psi(0)) = (A.\sinh S\tau + B.\cosh S\tau)^2 + (C.\sinh S\tau + D.\cosh S\tau)^2,$$

and

$$\mathcal{J}_2(\tau, \psi(0)) = -2\sigma\left\{ \frac{\rho}{B} S\tau + \arctan\left[\frac{(\frac{1-B}{T} - \sigma)(\frac{B+A}{B-A})\, e^{2S\tau} + \rho}{B} \right] \right\},$$

which is the required general amplitude solution.

Appendix 7.6

Transient amplitude solution in the resonant case

In the resonant case the transient amplitude solution can be found most simply from the appropriate transient phase solution (7.92) and the trajectory equation (7.84). These are respectively

$$e^{2S_\sigma(\tau+\tau_o)} = \left| tg\left(\frac{\pi}{4}+\frac{\xi}{2}-\psi\right)\right| ,$$

where $e^{2S_\sigma\tau_o} = |A| = \left| tg\left(\frac{\pi}{4}+\frac{\xi}{2}-\psi(0)\right)\right|$, and

$$\mathcal{A}.Z^{\frac{4}{3}(1+\sigma^2)} = \frac{e^{\sigma(\xi-2\psi)}}{\cos(\xi-2\psi)} .$$

The phase equation (7.92) gives

$$2S_\sigma(\tau+\tau_o) = \ln\left| tg\left(\frac{\pi}{4}+\frac{\xi}{2}-\psi\right)\right|$$

or

$$\xi - 2\psi = \text{gudermannian}\,(2S_\sigma(\tau+\tau_o)),$$

so that using the relation

$$\sec(\text{gd } x) = \cosh x$$

the required solution is

$$\left.\mathcal{A}.Z^{\frac{4}{3}(1+\sigma^2)}\right|_{\nu=1} = \cosh 2S_\sigma(\tau+\tau_o).\exp\left[\sigma.\text{gd } 2S_\sigma(\tau+\tau_o)\right] ,$$

with

$$\tau_o = \frac{1}{2S_\sigma}\ \text{gd}^{-1}(\xi-2\psi(0)).$$

LIST OF REFERENCES

1. F.Melde, "Ueber die Erregung stehender Wellen eines fadenförmigen Körpers", Annalen der Physik (Poggendorff's Annalen), vol.109, no.2, 1860, pp. 193-215

2. Lord Rayleigh, "On Maintained Vibrations", Phil. Mag., vol. 15, Series 5, no.94, April 1883, pp. 229-235.

3. J.Fallou, "Sur un demultiplicateur de fréquence statique", Rev. Gén. Élect., no.25, vol. 19, June 1926, pp. 987-991.

4. E.Rouelle, "Les characteristiques et la stabilite des circuits ferro-resonants", Compt. Rend. Acad. Sci., vol.118, May 1929, pp. 1392-1394.

5. E.Rouelle, "Quelques nouvelles experiences de demultiplication de fréquence dans un circuit oscillant dont la bobine est a noyau de fer", Rev. Gén. Élect., vol. 40, no.26, Dec.1936, pp.811-819.

6. P.O.Pederson, "Subharmonics in forced oscillations of dissipative systems", J. Acoust. Soc., Amer., vol.6, no.4, April 1935, pp. 227-238.

7. J.D.McCrumm, "An Experimental Investigation of Subharmonic Currents", Trans. AIEE, vol.60, 1941, pp. 533-540.

8. C.F.Spitzer, "Sustained Subharmonic Response in a Nonlinear Series Circuit", J. Appl. Phys., vol.16, no.2, February 1945, pp. 105-111.

9. G.Duffing, "Erzwungene Schwingungen bei veränderlicher Eigenfrequenz und ihre technische Bedeutung", F.Vieweg und Sohn,Braunschweig, 1918, (book).

10. E.T.Whittaker, G.N.Watson, "Modern Analysis", book, Cambridge University Press, 1935.

11. N.W.McLachlan, "Theory and Applications of Mathieu Functions", book, Oxford, Clarendon Press, 1947.

12. N.W.McLachlan, "Ordinary Nonlinear Differential Equations in Engineering and Physical Science",book, Oxford, Clarendon Press, 1950.

13. A.Lavi, L.A.Finzi, "An Analysis of the Magnetic Second-Subharmonic Oscillator", Proc. IRE, vol.49, no.4, April 1961, pp. 779-787.

14. M.E.Levenson, "Harmonic and Subharmonic Response for the Duffing Equation $\ddot{x} + \alpha x + \beta x^3 = F\cos\omega t$ $(\alpha > 0)$," J. Appl. Phys., vol.20, no.11, November 1949, pp.1045-1051.

15. C.A.Ludeke, " Predominantly Subharmonic Oscillations", J. Appl. Phys., vol.22, no.11, November 1951, pp.1321-1326.

16. C.Hayashi, "Subharmonic Oscillations in Nonlinear Systems", J.Appl. Phys., vol.24, no.5, May 1953, pp.521-529.

17. J. von Neumann, "Nonlinear Capacitance or Inductance Switching, Amplifying and Memory Organs", U.S. Patent no. 2,815,488, filed 28 April 1954, issued 3 December 1957, assigned to IBM.

18. E.Goto, "On the Application of Parametrically Excited Non-linear Resonators", K.D.D. Kenkyu Shiryo, vol.52, November 1954.

19. E.Goto, "The Parametron, a New Circuit Component using Non-linear Reactors", paper given before the Electronic Computer Technical Committee, J.I.E.C.E.J., 1954.

20. E.Goto, "On the Application of Parametrically Excited Nonlinear Resonators", J.I.E.C.E.J., vol.38, October 1955, pp.770-775.

21. C.Hayashi, "Initial Conditions for Certain Types of Nonlinear Oscillators", Proceedings of the Symposium on Nonlinear Circuit Analysis, Polytechnic Institute of Brooklyn, April 1956, pp.63-92.

22. C.Hayashi, Y.Nishikawa, M.Abe, "Subharmonic Oscillations of Order $\frac{1}{2}$", I.R.E.Trans.Circuit Theory, vol.CT-7, no.2, June 1960, pp.102-111.

23. Takahashi, E.Goto, "The Memory for Parametron Computer", meeting of P.G.E.C., Tokyo, Japan, February 1956.

24. S.Muroga, "On Logical Elements with Majority Decision Principle and the Complexity of their Circuits", Nat.Conv.Elec.Commun.Engrs., Fukuoka, Japan, May 1958.

25. S.Muroga, K.Takashima, "System and Logic Design of the Parametron Digital Computer MUSASINO-1", J.I.E.C.E.J., vol.41, no.41, Nov. 1958, pp.1132-1141.
(See also: same authors, "The Parametron Digital Computer MUSASINO-1", IRE Trans.Electronic Computers, vol.EC-8, no.3, September 1959, pp.308-316.)

26. E.Goto, "The Parametron, a Digital Computing Element which Utilises Parametric Oscillation", Proc.IRE, vol.47, no.8, August 1959, pp.1304-1316.

27. Kiyasu Zen'iti, S.Sekiguti, M.Takasima, "Parametric Excitation Using Variable Capacitance of Ferroelectric Materials", J.I.E.C.E.J., vol.41, no.3, March 1958, pp.239-244.

28. Kiyasu Zen'iti, K.Fusimi, K.Kataoka, K.Yamanaka, "Parametric Excitation Using Barrier Capacitance of Semiconductor", J.I.E.C.E.J., vol.40, no.2, February 1957, pp.162-169.

29. Kiyasu Zen'iti, "Parametron", J.I.E.C.E.J., vol.41, no.4, April 1958, pp.397-403.

30. F.Sterzer, W.R.Beam, "Parametric Subharmonic Oscillators", paper given at IRE-AIEE Solid-State Circuits Conference, Philadelphia, Pa., February 1959.

31. J.Hilibrand, W.R.Beam, "Semi-conductor Diodes in Parametric Subharmonic Oscillators", RCA Rev., vol.20, no.2, June 1959, pp.229-253.

32. F.Sterzer, "Microwave Parametric Subharmonic Oscillator for Digital Computing", Proc.IRE, vol.47, no.8, August 1959, pp.1317-1324.

33. L.S.Onyshkevych, W.F.Kosonocky, A.W.Lo, "Parametric Phase-Looked Oscillator - Characteristics and Applications to Digital Systems", IRE Trans. Electronic Computers, vol.EC-8, no.3, September 1959, pp.277-286.

34. I.Abeyta, F.Borgini, D.R.Crosby, "A Computer Subsystem Using Kilomegacycle Subharmonic Oscillators", Proc.IRE, vol.49, no.1, January 1961, pp.128-135.

35. S.Bloom, K.K.N.Chang, "Theory of Parametric Amplification Using Nonlinear Reactances", RCA Rev., vol.18, no.4, December 1957, pp.578-593.

36. J.Hilibrand, C.W.Mueller, C.F.Stocker, R.D.Gold, "Semi-conductor Parametric Diodes in Microwave Computers", IRE Trans. Electronic Computers, vol.EC-8, no.3, September 1959, pp.287-297.

37. A.H.Nethercot, "On the Switching Time of Subharmonic Oscillators", IBM J.Res. & Dev., vol.4, no.4, October 1960, pp.402-406.

38. N.Rouche, "Steady Oscillations of Parametric Subharmonic Oscillator", IRE Trans. Circuit Theory, vol.CT-9, no.1, March 1962, pp.7-12.

39. D.F.Page, "Instability in Transistor Circuits with Passive Feedback, with Special Reference to Tuned Oscillator and Superregenerative Applications", Ph.D.Thesis, University of London, April 1959.

40. J.R.Whitehead, "Superregenerative Receivers", book, Cambridge University Press, 1950.

41. C.Hayashi, "Stability Investigation of Nonlinear Periodic Oscillations", J.Appl.Phys., vol.24, no.3, March 1953, pp.344-348, (see p.346).

42. C.Hayashi, H.Shibayama, Y.Nishikawa, "Frequency Entrainment in a Self-Oscillatory System with External Force", IRE Trans. Circuit Theory, vol.CT-7, no.4, December 1960, pp.413-422.

43. L.Mandelstam, M.Papalexi, "Über Resonanzerscheinungen bei Frequenzteilung", Z.Physik, vol.73, 1932, pp.223-248.

44. D.J.Roulston, "Frequency Multiplication Using Non-Linear Capacitance Effects of p-n Junction Diodes", Ph.D.Thesis, University of London, August 1962.

45. B.A.Kaufman, W.Pfeiffer, "On the Characteristics of Cylindrical Thin-Film Parametrons Pumped to Saturation", Proc.IEEE, vol.51, no.5, May 1963, pp.855-856, (correspondence).

46. Kiyasu Zen'iti, K.Husimi, Y.Hiyama, K.Yamanaka, "Parametric Excitation Using Selenium Rectifier", J.I.E.C.E.J., vol.41, no.8, August 1958, pp.786-791.

47. W.Shockley, "The Theory of p-n Junctions in Semi-conductors and p-n Junction Transistors", B.S.T.J., vol.28, no.3, July 1949, pp.435-489.

48. L.J.Giacoletto, J.O'Connell,"A Variable Capacitance Germanium Junction Diode for UHF", RCA Rev.,vol.17, no.1, March 1956, pp.68-85.

49. J.J.Chang, J.H.Forster, R.M.Ryder, "Semiconductor Junction Varactors with High Voltage Sensitivity", IEEE Trans. Electron Devices, vol.ED-10, no.4, July 1963, pp.281-287.

50. J.M.Manley, H.E.Rowe, "Some General Properties of Nonlinear Elements - Part I. General Energy Relations", Proc.IRE, vol.44,no.4, July 1956, pp.904-913.

51 H.E.Rowe, "Some General Properties of Nonlinear Elements. II. Small-Signal Theory", Proc.IRE, vol.46, no.5, May 1958, pp.850-860.

52. R.T.Aiken, L.A.Finzi, "Large-Signal Analysis of a Parametric Second-Subharmonic Oscillator", IEEE Trans. Circuit Theory, vol.CT-10, no.4, December 1963, pp.476-486.

53. D.L.Hedderley, "An Exact Analysis of a Parametric Subharmonic Oscillator", IEEE Trans. Electron Devices, vol.ED-10, no.3, May 1963, pp.134-142.

54. W.J.Cunningham, "Introduction to Nonlinear Analysis",book, McGraw-Hill, 1958.

55. J.H.Poincaré, "Sur les courbes définies par une équation différentielle", Jour.de Math., vol.8, 1882, p.251.

57. L.V.Kantorovich, V.I.Krylov, "Approximate Methods of Higher Analysis", book, P.Noordhof, 1958, see p.258.